



AFRL-RX-WP-TR-2015-0192

**TECHNICAL AND ASSOCIATED R&D
LABORATORY/PROJECT SUPPORT TO AFRL/RXQL
AIRBASE SCIENCES BRANCH**

Brian Heimbuch, Robert McDonald, John Hearn, and Bruce Salter

Applied Research Associates, Inc.

**OCTOBER 2011
Final Report**

Distribution Statement A. Approved for public release: distribution unlimited.

STINFO COPY

**AIR FORCE RESEARCH LABORATORY
MATERIALS AND MANUFACTURING DIRECTORATE
WRIGHT-PATTERSON AIR FORCE BASE, OH 45433-7750
AIR FORCE MATERIEL COMMAND
UNITED STATES AIR FORCE**

NOTICE AND SIGNATURE PAGE

Using Government drawings, specifications, or other data included in this document for any purpose other than Government procurement does not in any way obligate the U.S. Government. The fact that the Government formulated or supplied the drawings, specifications, or other data does not license the holder or any other person or corporation; or convey any rights or permission to manufacture, use, or sell any patented invention that may relate to them.

This report was cleared for public release by the USAF 88th Air Base Wing (88 ABW) Public Affairs Office (PAO) and is available to the general public, including foreign nationals.

Copies may be obtained from the Defense Technical Information Center (DTIC)
(<http://www.dtic.mil>).

AFRL-RX-WP-TR-2015-0192 HAS BEEN REVIEWED AND IS APPROVED FOR
PUBLICATION IN ACCORDANCE WITH ASSIGNED DISTRIBUTION STATEMENT.

//SIGNATURE//

Joseph Wander
Work Unit Manager
Materials and Manufacturing Directorate

//SIGNATURE//

Andrew Jeffers
Branch Chief
Materials and Manufacturing Directorate

//SIGNATURE//

Pamela Schaeffer
Deputy Division Chief
Materials and Manufacturing Directorate

This report is published in the interest of scientific and technical information exchange, and its publication does not constitute the Government's approval or disapproval of its ideas or findings.

REPORT DOCUMENTATION PAGE				Form Approved OMB No. 0704-0188	
<p>The public reporting burden for this collection of information is estimated to average 1 hour per response, including the time for reviewing instructions, searching existing data sources, gathering and maintaining the data needed, and completing and reviewing the collection of information. Send comments regarding this burden estimate or any other aspect of this collection of information, including suggestions for reducing this burden, to Department of Defense, Washington Headquarters Services, Directorate for Information Operations and Reports (0704-0188), 1215 Jefferson Davis Highway, Suite 1204, Arlington, VA 22202-4302. Respondents should be aware that notwithstanding any other provision of law, no person shall be subject to any penalty for failing to comply with a collection of information if it does not display a currently valid OMB control number. PLEASE DO NOT RETURN YOUR FORM TO THE ABOVE ADDRESS.</p>					
1. REPORT DATE (DD-MM-YY) October 2011		2. REPORT TYPE Final		3. DATES COVERED (From - To) 1 December 2009– 30 September 2011	
4. TITLE AND SUBTITLE TECHNICAL AND ASSOCIATED R&D LABORATORY/PROJECT SUPPORT TO AFRL/RXQL AIRBASE SCIENCES BRANCH				5a. CONTRACT NUMBER In-House (FA4819-10-C-0012)	
				5b. GRANT NUMBER	
				5c. PROGRAM ELEMENT NUMBER	
6. AUTHOR(S) Brian Heimbuch, Robert McDonald, John Hearn, and Bruce Salter				5d. PROJECT NUMBER	
				5e. TASK NUMBER	
				5f. WORK UNIT NUMBER X0B6	
7. PERFORMING ORGANIZATION NAME(S) AND ADDRESS(ES) Applied Research Associates, Inc. 421 Oak Avenue Panama City, FL 32401-2737				8. PERFORMING ORGANIZATION REPORT NUMBER	
9. SPONSORING/MONITORING AGENCY NAME(S) AND ADDRESS(ES) Air Force Research Laboratory Materials and Manufacturing Directorate Wright-Patterson Air Force Base, OH 45433-7750 Air Force Materiel Command United States Air Force				10. SPONSORING/MONITORING AGENCY ACRONYM(S) AFRL/RXQO	
				11. SPONSORING/MONITORING AGENCY REPORT NUMBER(S) AFRL-RX-WP-TR-2015-0192	
12. DISTRIBUTION/AVAILABILITY STATEMENT Distribution Statement A. Approved for public release: distribution unlimited.					
13. SUPPLEMENTARY NOTES Public Affairs Case Number: 88ABW-2015-5415, dated 04Nov2015. Report contains color.					
14. ABSTRACT (<i>Maximum 200 words</i>) ARA supported three RXQL technical programs. Chemical Dynamics: measurements and modeling of large atmospheric releases of chlorine and of ammonia across samples of several soil types; measurements of adsorption of two chemical agent surrogates (dimethyl methylphosphonate and diisopropyl fluorophosphate) on cellulose and silica gel surfaces by inverse gas chromatography, to infer enthalpies of adsorption. Reactive Materials: assembly of textile application apparatus to microwave-cure surface treatments on textiles; development of water-based formulations for surface treatments, application to a variety of materials; identification of polyphenolic biocides active against Gram-positive and -negative bacteria, development of laundry-stable process for attaching the biocides to textiles/other surfaces; preparation and testing of highly repellent aircraft topcoats, including agent tests at a surety laboratory; effort to decontaminate aircraft coatings with microwave power from radar systems; concept realized at small scale inside microwave reactor, but initial tests with aircraft radar system failed. Toxic/Pathogenic Bioaerosols: experimental demonstration that biological particles interact with filters the same as inerts of the same size and density, development of protocols for preparation and analysis of anthrax spore surrogates, design and construction of a chamber to achieve reproducible dispersion of individual spores onto surfaces, and a cleaning study in support of respirator reuse during crises.					
15. SUBJECT TERMS ammonia, bacteria, bioaerosols, chemical agents, chlorine, decontamination, microwave, protection					
16. SECURITY CLASSIFICATION OF:			17. LIMITATION OF ABSTRACT: SAR	18. NUMBER OF PAGES 162	19a. NAME OF RESPONSIBLE PERSON (Monitor) Joseph Wander 19b. TELEPHONE NUMBER (Include Area Code) (850) 283-6240
a. REPORT Unclassified	b. ABSTRACT Unclassified	c. THIS PAGE Unclassified			

TABLE OF CONTENTS

LIST OF FIGURES	iii
LIST OF TABLES	vi
1. EXECUTIVE SUMMARY	1
2. PROGRAM INTRODUCTION	4
3. CHEMICAL DYNAMICS	5
3.1. Introduction.....	5
3.2. Atmospheric Chemistry of Chemical Agents for HPAC (WUN # DODT0040).....	5
3.2.1. Technical Introduction	5
3.2.2. Methods.....	7
3.2.3. Results and Discussion	10
3.2.4. Conclusions.....	30
3.3. Material and Surface Phenomena (WUN # Q220L8A2).....	31
3.3.1. Technical Introduction	31
3.3.2. Methods.....	31
3.3.3. Results and Discussion	32
3.3.4. Conclusions.....	40
3.4. Summary/Intangibles	41
3.4.1. Proposals	41
3.4.2. Meetings/Presentations	42
3.4.3. Publications	42
4. REACTIVE/RESPONSIVE MATERIALS	43
4.1. Introduction.....	43
4.2. Individual Protection.....	43
4.2.1. Technical Introduction	43
4.2.2. Methods.....	44
4.2.3. Results and Discussion	45
4.2.4. Conclusions.....	66
4.2.5. Follow-on Work.....	67
4.3. Chemical Agent Resistant Coating	67
4.3.1. Technical Introduction	67
4.3.2. Methods.....	68
4.3.3. Results and Discussion	69
4.3.4. Conclusions.....	79
4.3.5. Follow-on Work.....	81
4.4. Directed Energy Enhanced Coatings	81
4.4.1. Introduction.....	81
4.4.2. Methods.....	82
4.4.3. Results and Discussion	84
4.4.4. Conclusions.....	95
4.4.5. Follow-on Work.....	96
4.5. Summary	96
5. TOXIC AND PATHOGENIC AEROSOLS	99
5.1. Introduction.....	99
5.2. H1N1 Filtration and Total Inward Leakage Study	99
5.2.1. Technical Introduction	99

5.2.2. Methods.....	99
5.2.3. Data Analysis	103
5.2.4. Results.....	104
5.2.5. Discussion.....	107
5.2.6. Conclusions.....	108
5.3. Biological Aerosol Test Method Study.....	109
5.3.1. Technical Introduction.....	109
5.3.2. Results and Discussion	111
5.3.3. Conclusions.....	122
5.4. FFR Hospital FFR Wear Assessment and Cleaning Study.....	124
5.4.1. Technical Introduction.....	124
5.4.2. Materials and Methods.....	125
5.4.4. Discussion.....	129
5.4.5. Study Limitations.....	135
5.4.6. Summary.....	136
5.5. Summary/Intangibles	136
5.5.1. Proposals.....	137
5.5.2. Meetings/Presentations	137
5.5.3. Publications and Standards	138
6. PROGRAM SUPPORT	139
6.1. Background/Overview	139
6.2. Laboratory/Logistics Support	139
6.3. Program/Financial Management, Reporting and Administrative Support	140
6.4. Notable Achievements.....	141
6.4.1. Laboratory Management Review (LMR)	141
6.4.2. Equipment Account Management.....	142
7. Report Summary	143
8. REFERENCES	144
LIST OF SYMBOLS, ABBREVIATIONS, AND ACRONYMS	149

LIST OF FIGURES

Figure	Page
Figure 1. AFRL/RXQL Support Staff (1 January–30 December 2010)	4
Figure 2. Ammonia Loss from Soil for Various Depths of Application and Soil Moisture	7
Figure 3. Design of Radial Chamber for Deposition Experiments	10
Figure 4. Breakthrough Curves for Cl ₂ on Silt Loam	11
Figure 5. Normalized Uptake of Cl ₂ on Silt Loam as a Function of Humidity	12
Figure 6. Breakthrough Curves for Cl ₂ as a Function of Soil Type at 0% Humidity	13
Figure 7. Normalized Cl ₂ Uptake as a Function of Humidity	13
Figure 8. Normalized Cl ₂ Uptake as a Function of Soil Organic Fraction	14
Figure 9. Relative Rate Measurements of AsH ₃ Reaction with OH	15
Figure 10. Cl ⁻ Concentrations in Core Samples from Cl ₂ Release #1, Site 3	16
Figure 11. Cl ⁻ Concentrations in Core Samples from Cl ₂ Release #1, Site 2	17
Figure 12. Cl ⁻ Concentrations in Core Samples from Cl ₂ Release #1, Site 1	17
Figure 13. Soil Temperature during Cl ₂ Release #1	18
Figure 14. Cl ⁻ Concentrations in Soil Cores from Cl ₂ Release #3, Site 3	19
Figure 15. Cl ⁻ Concentrations in Soil Cores from Cl ₂ Release #3, Sites 2 and 4	20
Figure 16. Cl ⁻ Concentrations in Soil Cores from Cl ₂ Release #3, Sites 1 and 5	20
Figure 17. Cl ⁻ Concentrations in Concrete Samples Exposed During Cl ₂ Release #3	21
Figure 18. Chloroform Signals from Soil Headspace	23
Figure 19. Chlorinated Organic Signal from Soil Headspace	24
Figure 20. NH ₄ ⁺ Concentrations in Core Fractions from NH ₃ Release #1	25
Figure 21. Soil Temperature during NH ₃ Release #1	26
Figure 22. NH ₄ ⁺ Concentrations in Core Fractions during NH ₃ Release #2	27
Figure 23. Soil Temperature during NH ₃ Release #2	28
Figure 24. Data Used for Scaling up Cl ₂ Deposition from Release #1	29
Figure 25. Interpolated Cl ₂ Deposition within 20 m from Release	30
Figure 26. XRD Patterns of Cellulose I α and I β	33
Figure 27. Enthalpy Measurements for DMMP on Silica Gel	34
Figure 28. Isotherm of DMMP Adsorption on Cellulose at 313 K	35
Figure 29. Enthalpy of Adsorption for DMMP on Cellulose 1 α and 1 β	35
Figure 30. Comparison of DMMP Retention on Cellulose with Various Solvents	36
Figure 31. Elution Profile for DMMP and Ethyl Acetate on Cellulose at 98 °C	37
Figure 32. Temperature-dependent V_g for Dilute DMMP on Cellulose	37
Figure 33. Comparison of Enthalpy Measurements for DMMP on Cellulose for the Indicated Injection Strategies	38
Figure 34. Elution Profile for DIFP/Hexane on Cellulose	39
Figure 35. Temperature Dependence of DIFP Retention on Cellulose	40
Figure 36. Comparison of DIFP and DMMP Enthalpy (ΔH) Measurements	40
Figure 37. [3-(Trimethoxysilyl)propyl]octadecyldimethylammonium Chloride (Quat)	44
Figure 38. 2-(3-Triethoxysilylpropyl)-5,5-dimethylhydantoin (BA-1)	44
Figure 39. (Heptadecafluoro-1, 1, 2, 2,-tetrahydrodecyl)trimethoxysilane (FS)	44
Figure 40. Waveguide Connecting Magnetron to Applicator	45
Figure 41. Water-Catalyzed FS Coating on Nanoparticle-Coated Fabrics	54
Figure 42. Base-Catalyzed FS Coating on Nanoparticle-Coated Fabrics	55
Figure 43. Contact Angle of Water on FS-Treated Nylon	55

Figure 44. Contact Angle of <i>n</i> -Hexadecane on FS-Treated Nylon.....	55
Figure 45. Samples Taken from the Tech Demo at NCSU Demonstrating Repellency against Hydraulic Fluid and Kerosene	57
Figure 46. Repellency Data for Several Materials Treated with FS (Data Are Given As Percent Improvement Versus the Untreated Controls)	58
Figure 47. Resveratrol Powder Plated with <i>B. atrophaeus</i> Showing a Zone of Inhibition.....	59
Figure 48. Resveratrol Plated with <i>Ps. fluorescens</i> Showing No Zone of Inhibition	59
Figure 49. 8-Hydroxyquinoline Crosslinked to Fabric by (3-Glycidoxypopyl) trimethoxy- silane Plated with <i>B. atrophaeus</i> Showing a Strong Zone of Inhibition.....	60
Figure 50. Same Sample Plated with <i>Ps. fluorescens</i> Showing Zone of Inhibition	60
Figure 51. 8-(2,3-Dihydroxypropoxy)quinoline, a Derivative of 8HQ Prepared from Glycidol ...	62
Figure 52. Reaction of Pyridoxal with APTS to Form a Schiff Base	63
Figure 53. Reaction of Salicylaldehyde with APTS to Form a Schiff Base	63
Figure 54. Proposed Reaction of Sodium Hydroxide and Cotton with Diiodo-8HQ	63
Figure 55. Cotton Treated with APTS, Then 8-Hydroxyquinoline-2-carboxaldehyde	64
Figure 56. <i>B. atrophaeus</i> Killed by 8-Hydroxyquinoline-2-carboxaldimine-treated Cotton ...	64
Figure 57. Laccase Enzyme Assay Showing Absorbance at 2 Min and Slope of Absorbance between 0.07 and 0.14 s	66
Figure 58. Surface Energies for 11 Modified Coatings	73
Figure 59. Average Contact Angle for Methyl Salicylate (<i>n</i> =5)	74
Figure 60. Average Contact Angle for 3-Hepten-2-one (<i>n</i> =5)	74
Figure 61. Average Contact Angle for Tributyl Phosphate (<i>n</i> =5)	74
Figure 62. Comparison of Average Water Contact Angles (<i>n</i> =5)	75
Figure 64. Comparison of Average Tributyl Phosphate Contact Angles (<i>n</i> =5);	75
Figure 63. Comparison of Average Contact <i>n</i> -Hexadecane Contact Angles (<i>n</i> =5);.....	76
Figure 65. Average Contact Angles (<i>n</i> =5); for Methyl Salicylate on Al Membrane, AFRL Data, and 60-min Data, (<i>n</i> =1)	77
Figure 66. Average Contact Angles (<i>n</i> =5); for 3-Hepten-2-one; Cellulose and Nickel 60-min Data and Al Membrane Data, (<i>n</i> =1); Al Coupon 60-min Data and Nickel AFRL Data (<i>n</i> =4); Si Wafer Data (<i>n</i> =3)	77
Figure 67. Average Immediate and 60-min Contact Angles for DMSO on Cellulose (<i>n</i> =5), Nickel (<i>n</i> =3), Si Wafer (<i>n</i> =4), and Al Membrane (<i>n</i> =1).....	77
Figure 68. Average Roll-Off Angle (<i>n</i> =3)	78
Figure 69. Step-Growth Polymerization to Form Polyurethane from Aliphatic Diisocyanates and Polyols	82
Figure 70. Synthesis of Polypyrrole from Pyrrole by Ferric Chloride Oxidation	83
Figure 71. Polyaniline Chemical Structure	83
Figure 72. Variable-power Microwave Test System	84
Figure 73. Ceramic with 85285 control (left) and Teflon (right) sample holders	85
Figure 74. Schematic for the Ceramic and Teflon Sample Holders	85
Figure 75. A Comparison of the Temperature Profiles of Various Coatings	88
Figure 76. Comparison of the Power Absorption by a Control (85285)	88
Figure 77. Heating rate to 140 °C for Four 1% PPy Samples of Differing Masses.....	90
Figure 78. Time for Microwave Heating to Warm 11 Coating Samples to 200 °C;	91
Figure 79. Energy per Gram of 85285 PPy Coating Necessary to Reach Various Temperatures in the Coating–Mineral Oil–Quartz Calorimeter (<i>n</i> =3)	92

Figure 80. Energy Per Gram of Mineral Oil Necessary to Reach Temperatures in the Mineral Oil–Quartz Calorimeter ($n=3$).....	93
Figure 81. Temperature of Mineral Oil in Quartz Tubes vs. Energy per Gram ($n=1$)	93
Figure 82. Laboratory-Scale Aerosol Tunnel (LSAT).....	101
Figure 83. Comparison of Mucin PSD to 0.8- μ m PSL Bead PSD	102
Figure 84. <i>Bacillus</i> Spore Aerosol Project Overview	110
Figure 85. Spore Preparations Using Difco Sporulation Medium. (a) Bg Spores (Phase-dark Bodies Are Out-of-focus Phase-bright Spores), (b) Bt Spores	113
Figure 86. Spore Preparations Using Blood Agar Plates. (a) <i>B. thuringiensis</i> Al Hakam, (b) <i>B. anthracis</i> Δ Sterne	113
Figure 87. Preparations of <i>B. anthracis</i> Δ Sterne Spores from (a) Nutrient Agar	114
Figure 88. Preparation of <i>B. anthracis</i> Δ Sterne Spores (a) before Treatment with Histodenz, (b) after Treatment with Histodenz.....	114
Figure 89. Biological Aerosol Dispersing System (BDS): (a) Chamber (b) Sample Access Door, (c) Optically Clear Glass Panels, (d) Rotating Table, (e) Rolling Cart, (f) Air Exit Manifold, (g) Air Compressor, (h) Air Buffer Tank, (i) Type I Biological Safety Cabinet, (j) Pitt-3 Powdered Aerosol Dispenser, (k) Six-Way Diffuser, (l) Large Access Door, (m) Biological Dispersing System, (n) Malvern Spraytec	116
Figure 90. Plumbing Schematic Detailing Airflow in the Biological Dispersing System.....	117
Figure 91. Test Setup for Analyzing Pitt-3 Aerosol Generator	118
Figure 92. Particle Quantities as Functions of Speaker Amplitude and Flow	119
Figure 93. Particle Size as a Function of Amplitude and Flow	119
Figure 94. Particle Concentration Produced in the Pitt-3 Aerosol Generator Using Different Starting Weights of Dipel® Dust: (a) 50 mg, (b) 100 mg, (c) 250 mg.....	120
Figure 95. Particle Size as a Function of Amplitude and Flow	121
Figure 96. Sample Loading Pattern in the Biological Dispersing System.....	122
Figure 97. Cleaning Efficiency for the 3M 1860 FFR.....	128
Figure 98. Cleaning Efficiency for the 3M 1870 FFR.....	128
Figure 99. Supply “Checkbook”	140
Figure 100. Obligation/Expenditure Tracking Tool.....	140
Figure 101. LMR Products	142

LIST OF TABLES

Table	Page
Table 1. Synthetic Soil Sample Blends for Breakthrough Measurements.....	8
Table 2. Soil Mixture Compositions for Field Experiment	8
Table 3. Sample Site Locations for Field Measurements	8
Table 4. Experimental Matrix for Capacity Measurements.....	11
Table 5. Experimental Results for AsH ₃ + OH Relative Rate Measurements.....	15
Table 6. Water Samples Exposed at Site 4, Cl ₂ Release #1.....	18
Table 7. pH Measurements for Cl ₂ Release #3	21
Table 8. Fresh Water Samples at Site 2, NH ₃ Release #1.....	26
Table 9. Water Samples at Site 2, NH ₃ Release #2	27
Table 10. Extrapolated NH ₃ Deposition within a 5-m Liquid Spread	29
Table 11. Summary of Binding Enthalpies (kcal/mol) from Theory and Experiment	41
Table 12. Summary of Parallel Streak Tests for One and Three Immersions in 1% BA-1 and 1% Quat in a Water-Acetone Solution	46
Table 13. Parallel Streak Tests of NyCo Swatches Treated with Quat or BA-1 in Water	47
Table 14. Summary of <i>B. atrophaeus</i> Parallel Streak Tests Using Quat and BA-1	48
Table 15. Summary of the Average Concentration (ppth) of Chlorine Available on Kermel® and NKA Materials	48
Table 16. Preliminary Surfactant Tests	49
Table 17. Surfactants Used in KMS20100204- FS Compatibility Tests on NyCo	49
Table 18. Treatments Used in KMS20100208- Fabric Tests on NyCo and Kermel®	50
Table 19. Contact Angles of Materials KMS20100301- Treated with FS and 1–4% Concentrations of Surfactant	52
Table 20. Effect of Method of Removing Surfactant from Fabrics on Contact Angles	53
Table 21. Biocidal Properties of Candidate Phenols; “Yes” Indicates a Zone of Inhibition.....	58
Table 22. Biocidal Properties of Phenols Attached to NyCo with (3-Glycidoxypropyl)trimethoxysilane; “Yes” Indicates a Zone of Inhibition.....	60
Table 23. Durability Test Results for Candidate Biocidal Textiles after Five Washes;	61
Table 24. Biocidal Tests Results for Phenols Attached to NyCo via TEOS	61
Table 25. Biocidal Efficacy of 8-Hydroxyquinoline and Derivatives	62
Table 26. Biocidal Efficacy of 8-Hydroxyquinoline Derivatives	62
Table 27. Biocidal Efficacy of Cotton Fabric Treated with Either Schiff Base or Phenol, and Complexed with CuSO ₄	65
Table 28. Two-hour Reactivity Data	69
Table 29. Twenty-four-hour Reactivity Data	70
Table 30. Average Repellency Study using TBP (<i>n</i> =3).....	70
Table 31. Average Repellency Study MeS (<i>n</i> =3)	70
Table 32. Aircraft Protective Coatings Modified by ARL	71
Table 33. Average Repellency of Weathered Coatings on Al Coupons (<i>n</i> =1*).....	71
Table 34. Average Contact Angle (<i>n</i> =5)	72
Table 35. Surface Energy (mN/m)	72
Table 36. Average Contact Angle (<i>n</i> =5)	73
Table 37. Average Contact Angles (<i>n</i> =5)	75
Table 38. Average Contact Angles (<i>n</i> =5)	76
Table 39. Average Roll-Off Angles for 50-μL Droplets, (<i>n</i> =3)	78

Table 40. Average Contact Angle ($n=5$)	79
Table 41. Calculated Surface Energies (mN/m)	79
Table 42. Candidate Dopants for Incorporation into DEECs	86
Table 43. Conditions for Challenging FFRs with H1N1	100
Table 44. Challenge of N95 Filtering Facepiece Respirators with PSL Beads	104
Table 45. Challenge of N95 Filtering Facepiece Respirators with H1N1 Influenza—	105
Table 46. Average Removal Efficiencies for Condition #1 (85 LPM, 0.8- μ m particles)	105
Table 47. Challenge of N95 Filtering Facepiece Respirators with PSL Beads—Percent Reduction Using Condition #2 (170 LPM, 0.8- μ m Particles)	106
Table 48. Challenge of N95 Filtering Facepiece Respirators with H1N1 Influenza	106
Table 49. Average Removal Efficiencies of 0.8- μ m Particles at 85 LPM and at 170 LPM.....	107
Table 50. Filtration Efficiencies of 3M 1860S and 3M 1870 Challenged with Different Beads	107
Table 51. Critical Method Elements	110
Table 52. Reviewers for the Method Justification	111
Table 53. Comparison of Titers of <i>B. anthracis</i> Δ Sterne Grown on Blood Agar Plates with Spores Grown in Liquid Medium	113
Table 54. Material List and Dimensions of Sample Used to Evaluate	121
Table 55. Data Compiled from the <i>Bacillus atrophaeus</i> Spore Aerosol	122
Table 56. Filtering Facepiece Respirators (FFRs) Selected for the Study.....	126
Table 57. API Analysis of Bacterial Isolates from FFRs 3M 1860 and 3M 1870.....	131
Table 58. Growth Properties of Bacterial Isolates on Differential and Selective Media.....	132
Table 59. Vancomycin and Oxaicillin Resistance of Bacterial Isolates from FFRs.....	133

1. EXECUTIVE SUMMARY

Applied Research Associates, Inc. (ARA) supported the Air Force Research Laboratory, Airbase Sciences Branch (AFRL/RXQL) for contract (FA4819-10-C-0012), for the period of performance from 1 January 2010–31 December 2010. The three major technical programs supported for AFRL/RXQL were 1) Chemical Dynamics, 2) Reactive/Responsive Materials, and 3) Toxic and Pathogenic Biological Aerosols. Each technical program was composed of discrete projects in support of varied U.S. Department of Defense (DoD) or U.S. Department of Health and Human Services requirements and each is described separately in this document. ARA also provided program and laboratory support as required by AFRL.

CHEMICAL DYNAMICS

Atmospheric Chemistry of Chemical Agents for HPAC

- Laboratory and field experiments demonstrated that deposition to terrestrial surfaces can be a significant loss term for modeling dense Cl_2 plumes. The reactive capacity of a variety of soil types was high enough to remove a significant mass of Cl_2 from a concentrated cloud, and field experiments showed that under real-world conditions, deposition does account for significant losses to a Cl_2 plume. Another significant finding of this research was that deposition rates for modeling trace pollutants are not directly applicable to dense toxic industrial chemical (TIC) releases. Otherwise, NH_3 deposition would have been much more significant in the field experiments.
- In addition to deposition of Cl_2 and NH_3 , gas-phase measurements of AsH_3 reacting with OH radicals were made to expand the current database for atmospheric degradation of TICs for the Hazard Prediction and Assessment Capability (HPAC) model. Other AFRL contractors are now incorporating AsH_3 degradation into the HPAC software package.

Material and Surface Phenomenon

- Adsorption of dimethyl methylphosphonate (DMMP) on silica and cellulose was investigated using a variety of injection strategies. The results from these measurements indicated that solvent dilution is a valid and appropriate injection strategy for live agent measurements. This was tested with a reactive simulant (diisopropyl fluorophosphate, DIFP), for which no breakthrough was observed on silica. DIFP adsorption on cellulose was measured and—for the same injection amount—exhibited a similar adsorption enthalpy as DMMP. These results were delivered to collaborators who are predicting binding enthalpies and structures using quantum chemistry.

REACTIVE/ RESPONSIVE MATERIALS

Individual Protection

- Assembled a textile applicator to treat medium-to-large-scale quantities of textile via microwave-promoted (MP) addition reactions. Evaluated the system for safety and performance. Performed two technology demonstrations using this system to produce several hundred yd of treated textiles.
- Developed new repellent and multifunctional textile formulations that made use of aqueous emulsions instead of flammable organic solvents.

- Applied repellent treatments to leather and cloth portions of Airman Battle Uniform (ABU) boots and evaluated hydro- and oleophobicity. Successfully treated some non-textile materials (glass, steel, and plastics) with repellent formulations.
- Researched novel and known polyphenolic biocidal compounds and tested their efficacies against Gram-positive and Gram-negative bacteria. Attached the most-successful candidates to textiles and evaluated their durability for up to 20 wash cycles. Performed enzyme assays in an attempt to determine the compounds' mechanism of biocidal activity.

Chemical Agent Resistant Coatings

- Evaluated contact angle (CA) and surface energies of MIL-PRF-85285 type repellent coatings formulated at the Army Research Laboratory.
- Evaluated reactivity of Naval Research Laboratory coatings against simulants for chemical warfare agents HD and VX.
- Synthesized PPG, Inc., and Deft, Inc., polyurethane coatings containing reactive and repellent additives. Compared the efficacy of the additives when formulated into the two manufacturers' products.
- Measured CAs and surface energies for a polyurethane and five other coating types provided by collaborators at Clemson University.
- Contributed to the development of four MIL-PRF-85285 type coatings that can repel a challenge of VX or HD for over two weeks.

Directed-Energy Enhanced Coatings

- Developed a system and test protocols for materials research using a variable-power, 3.5-kW microwave reactor. Worked on system designs with a specialty provider to provide AFRL with the state-of-the-art in experimental microwave testing capabilities.
- Formulated MIL-PRF-85285 type coatings doped with additives to enhance material susceptibility to microwave and RF radiation. Synthesized conductive polymers at AFRL for use as additives.
- Coordinated and ran a demonstration/proof-of-concept experiment using currently fielded attack radar systems.
- Conducted experiments to determine the time and power required to heat various coating formulations to 200 °C.

TOXIC AND PATHOGENIC BIOLOGICAL AEROSOLS

H1N1 Filtration And Total Inward Leakage Study

- Five N95 filtering facepiece respirator (FFR) models—3M 1860, 3M 1870, Kimberly Clark PFR, Triosyn T5000 and Glaxo-Smith-Kline Actiprotect—were evaluated in triplicate for their filtration efficiencies under two separate conditions. Condition #1 required a NIOSH standard flow rate of 85 LPM and the count median diameter (CMD) of both inert and viable aerosol challenges to be ~0.8 µm. For Condition #2, the flow rate was increased to 170 LPM, while maintaining the same particle size.
- All FFRs demonstrated filtration efficiencies exceeding the N95 benchmark rating of both inert polystyrene latex (PSL) bead and viable H1N1 influenza aerosols. No statistically significant difference was found between the two populations, except for the

Kimberly Clark FFR in Conditions #1 ($P = 0.026$) and #2 ($P = 0.005$). Although this difference is statistically significant, it is not considered to be of practical importance.

Biological Aerosol Test Method Study

- A method justification was developed based on a SME panel review of the literature and DoD technical reports. This review served as the foundation for the entire method development project. The document was reviewed by spore experts within the DoD, providing further clarity on the direction of the method. The method identified several Data Quality Objectives (DQOs) that drove the experimental program.
- The Biological Dispersing System (BDS) was conceived and developed, and two copies were constructed and delivered to AFRL and Natick. Tests using non-fluidized *Bacillus atrophaeus* spores determined the system meets the DQOs for aerosol properties and loading density and distribution.
- Spore production, purification, and quality control procedures were finalized for *B. anthracis* Δ Sterne spores.

Filtering Facepiece Respirator (FFR) Hospital Wear Assessment and Cleaning Study

- Examination of 3M 1860S and the 3M 1870 FFRs worn by the Bay Medical Center environmental staff showed that $> 96\%$ of the contamination deposited on the external surface of the FFR; the remainder of contamination was caught on the filtering layer. Some microorganisms identified on the external surface of the FFR are representative of skin flora, indicating the FFR user may unknowingly contribute to contamination on the exterior of the FFR during normal wear.
- To meet FDA regulatory standards for reuse of a FFR, contamination must be removed from the FFR. A commercial wipe product was used to clean the exterior of the FFRs, resulting in 40–50% removal efficiency of microorganisms. The low removal efficiency may be due to the FFRs porous outer surface and a new FFR may need to be developed that is suitable for cleaning and reuse.
- Analysis of microbial flora on the respirators was performed using visual identification, Gram stains, differential/selective media, API bacterial identification strips, and 16S ribosomal RNA sequencing. Additionally, antibiotic resistance testing was performed, with results showing oxacillin- and vancomycin-resistant strains. Because healthcare workers may be exposed to antibiotic-resistant bacteria on a daily basis, these results are concerning. Healthcare providers may need to consider protective measures for their staff.

2. PROGRAM INTRODUCTION

ARA's contract (FA4819-10-C-0012) with AFRL/RXQL called for broad technical, program and laboratory support to help sustain the AFRL/RXQL research mission. ARA provided support for the contract period of performance (1 January–31 December 2010) with a staff of 23 highly skilled individuals (Fig. 1). Nine of those individuals supported AFRL for a fraction of the contract period due to either being hired or leaving midway through the contract period of performance (Fig. 1). The three major technical programs supported by AFRL were 1) Chemical Dynamics, 2) Reactive/Responsive Materials, and 3) Toxic and Pathogenic Biological Aerosols. Each technical program was composed of discrete projects that will be described separately in this report. What follows is a comprehensive dissertation of the technical, program, and laboratory support provided by ARA. The report is organized by technical area and then by discrete project. An overview and summary of each technical area are also provided, as are intangibles that demonstrate where ARA went above and beyond contract deliverables to provide exemplary support for AFRL/RXQL.

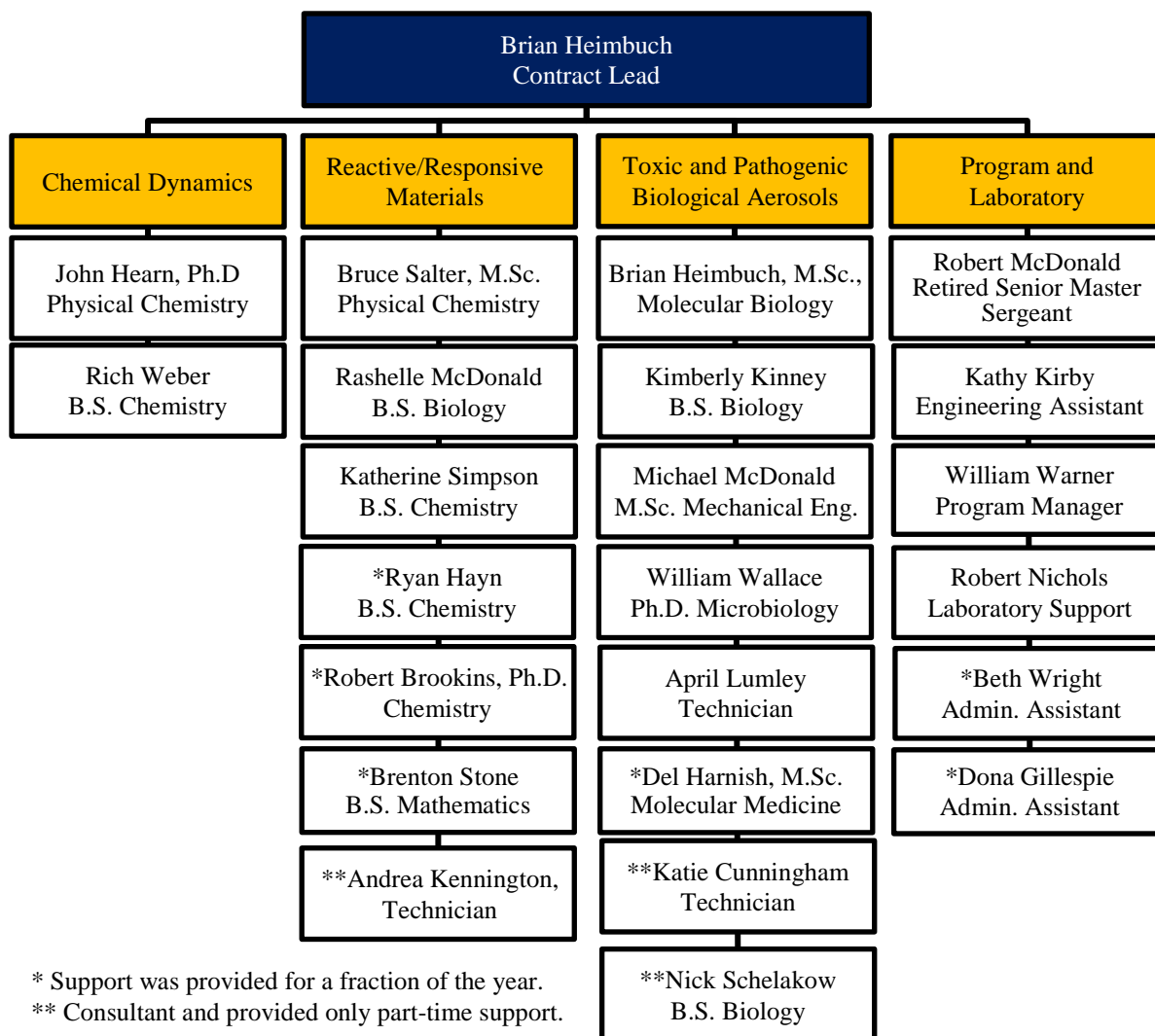


Figure 1. AFRL/RXQL Support Staff (1 January–30 December 2010)

3. CHEMICAL DYNAMICS

3.1. Introduction

This task area is broken down into two primary projects: Atmospheric Chemistry of Chemical Agents for Hazard Prediction and Assessment Capability (WUN # DODT0040) and Material and Surface Phenomena (WUN # Q220L8A2). Accomplishments for these projects are described separately below. Separate external customers funded two efforts under “Atmospheric Chemistry of Agents for HPAC” but, as the objectives of these two efforts closely paralleled each other, they are combined into one coherent section in this report. Accomplishments for Material and Surface Phenomena will be described only for the experimental support to AFRL/RXQL. This project was part of a larger project involving computational chemistry. The theoretical portion of this work will not be discussed. The common theme in this task area is the role chemical reactions/interactions in the environmental effects and fate and transport of hazardous chemicals.

3.2. Atmospheric Chemistry of Chemical Agents for HPAC (WUN # DODT0040)

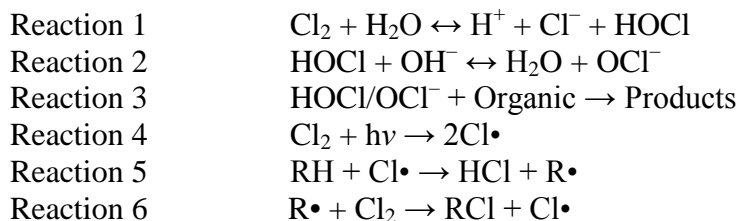
3.2.1. Technical Introduction

Accidental and intentional releases of TICs pose a significant threat to populated areas. To have an appropriate response plan for TIC releases, city planners and emergency response personnel need accurate predictions of TIC transport, diffusion and chemical evolution to effectively allocate resources to affected areas. When compared to data from actual releases of chlorine (Hanna and Chang 2008) current models overestimate the number of casualties and it is unclear where the predictions fail (Hanna 2007). Modeling a TIC release is broken down into several parts, including (1) source description, (2) plume transport, diffusion and dispersion, (3) chemical degradation in the atmosphere and on environmental surfaces (soil, vegetation, concrete, etc.), and (4) health risk estimations (Hanna et al. 2008). Each piece to the model requires careful consideration to maximize accuracy, minimize uncertainty, and maintain low computational cost. Currently, dry deposition is excluded from such predictions primarily because insufficient experimental data exist to assign accurate rate terms. Including heterogeneous loss terms will decrease the TIC concentration and potentially provide more accurate hazard predictions. Some transport-and-diffusion models (e.g., SCIPUFF) contain algorithms for including both first-order gas-phase loss and deposition velocities, so only accurate deposition velocities are needed to populate the appropriate inputs (Sykes et al. 1998).

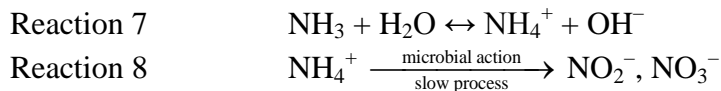
Approximate deposition velocities for several TICs (e.g., SO_2 , NH_3 , HNO_3) are known because of their importance in atmospheric chemistry (Finlayson-Pitts and Pitts 2000), but it is not clear that these values are directly applicable to dense-TIC releases (Renard, et al. 2004). Chlorine (Cl_2) and ammonia (NH_3) are TICs of emerging concern to the defense community because their ubiquity in industry and quantities transported make them convenient targets for intentional releases. Common transport and dispersion models compare with one another within about a factor of two for Cl_2 releases, and the differences among the predictions are largely attributed to descriptions in the source term (Hanna et al. 2008). While there was good agreement among the models, they may all be biased, as neither gas-phase nor heterogeneous chemistry was included in those simulations. The only publication (to our knowledge) that investigated Cl_2 deposition observed a deposition velocity of between 0.7 and 3.3 cm/s on alfalfa, depending on the height of the grass (Hill 1971). Other publications have investigated uptake of Cl_2 into wet and dry salt

particles, yielding uptake coefficients on the order of 10^{-2} (Hu et al. 1995, Mochida et al. 1998). All these measurements were made at very low mixing ratios and indicate that deposition is primarily transport limited. For a high-concentration Cl_2 plume, gravitational settling may increase deposition velocity, as the density of Cl_2 is 2.5 times higher than that of air (Pohanish 2008).

Whereas the kinetics of deposition for highly-concentrated gases is the appropriate input for transport and dispersion models, a valid first step is to verify that the quantity of deposited chemical is significant enough to matter in a large-scale release. Therefore, for the experiments here, deposition velocities were not measured; rather, products from deposition were measured. This provides an integrated picture of deposition during the release and can answer the question “can deposition attenuate a highly concentrated plume?” As chlorine chemistry oxidizes organic molecules, the smaller—often chlorinated—organic products evaporate. Thus these do not provide quantitative chemical markers for Cl_2 deposition. Cl_2 chemistry is complex, yielding a variety of chlorinated products, and one of the more prominent products is the chloride ion (in Reactions 1 and 5). Assuming the $p\text{H}$ is high enough that $\text{HCl}(\text{g})$ does not evolve from the surface, the molar Cl^- yield will be equivalent to the Cl_2 loss. Regardless of whether water-mediation (Reactions 1–3) or photoinitiation (Reactions 4–6) facilitates Cl_2 deposition, Cl^- is a good marker.



NH_3 is less dense than air, and unlike Cl_2 , which chemically reacts with environmental surfaces, it primarily dissolves into water or adsorbs to acidic surface sites. Microbial processes slowly convert NH_3 into nitrates and nitrites (Reaction 8), but this will not be important during the time-scale of hazard predictions for large-scale releases. Therefore, the reversible dissolution of NH_3 in water (Reaction 7—a $p\text{H}$ -dependent process) is expected to be the primary mechanism for NH_3 deposition.



Regarding atmospheric chemistry, NH_3 deposition is a very important loss process for dilute NH_3 plumes. Deposition velocities of 0.3–3.6 cm/s have been observed for NH_3 on vegetation for concentrations ranging from 0.1–500 $\mu\text{g}/\text{m}^3$ (Renard et al. 2004). While these rates are fast enough to attenuate NH_3 toxicity in a large-scale release, it may not be applicable to high-concentration NH_3 plumes ($> 200 \text{ mg}/\text{m}^3$). In addition to atmospheric chemistry, anhydrous NH_3 has been used in agriculture as a fertilizer. The efficiency of retaining anhydrous NH_3 in soils depends on a number of factors, including injection depth and soil moisture. Figure 2 shows the effects of injection depth and soil moisture on NH_3 loss, and for hazardous NH_3 releases the application depth will be zero (i.e., the surface). It is safe to conclude that long-term retention of

NH₃ in soil requires significant penetration of NH₃ into the soil (several in), so the critical question to answer is “Does NH₃ in a large-scale release penetrate deep enough into the soil to be retained?”

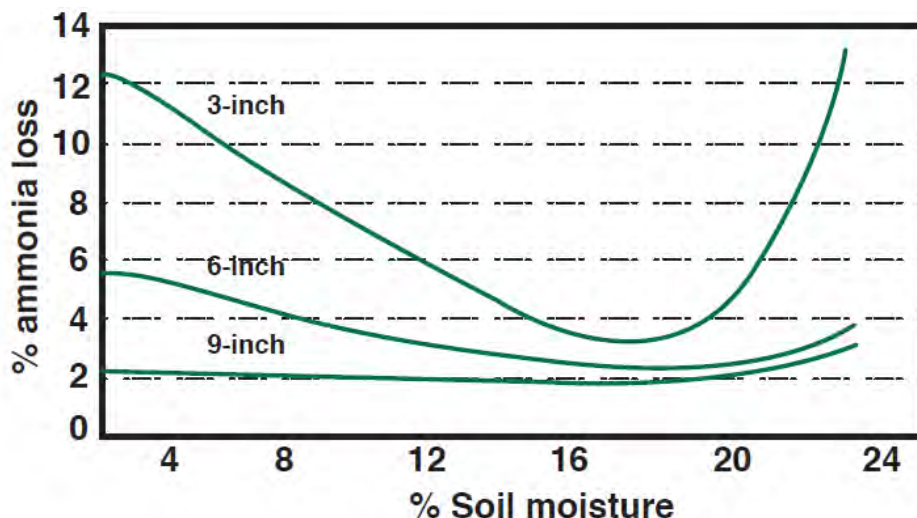


Figure 2. Ammonia Loss from Soil for Various Depths of Application and Soil Moisture

The purpose of this work was to measure integrated deposition onto soils and other terrestrial materials for Cl₂ and NH₃ in field experiments and Cl₂ in laboratory experiments. These measurements provide critical data for estimating the magnitude of dry deposition as a loss term for dense plumes. Of particular interest is the capacity of the terrestrial material—because deposition is expected to be transport limited—and how variables such as water content and organic content affect the saturation point.

In addition to heterogeneous deposition, gas-phase chemistry has the potential to alter the toxicity of a chemical plume if the reaction rate constants with atmospheric oxidants are fast enough and if the ambient steady-state oxidant concentration is not depleted by the plume. One priority TIC—AsH₃—is expected to have an appreciable reaction rate with OH, the primary oxidant in the troposphere, because it reacts quickly with Cl radicals (Schlyer, Wolf, and Gaspar 1978). However, no measurements of its reactivity toward OH radicals have appeared in the open literature.

3.2.2. Methods

3.2.2.1. Breakthrough Measurements

To investigate the saturation point for environmental materials, breakthrough measurements were made on packed columns. Samples were packed into a glass tube and a flow of N₂ with variable humidity containing Cl₂ was passed through the column until the normalized Cl₂ signal recovered to approximately 0.70 (or higher if feasible). Cl₂ was detected with chemical ionization mass spectrometry by electron capture from SF₆⁻. SF₆ anions were generated by passing a small flow of SF₆/N₂ through a radioactive ²¹⁰Po source (model P-2031, NRD, LLC), and ions were analyzed with a magnetic sector mass spectrometer. Numerical integrations were calculated according to Equation (1) in which S_t is the signal at time t , S_0 is the unreacted signal, f is the volumetric flow rate of gas, m is the column mass, n_{Cl_2} is the moles of Cl₂ exposed to the column (5 μmol), and $n_{\text{Cl}_2(\text{reacted})}$ is the moles of Cl₂ reacted.

$$\frac{n_{\text{Cl}_2(\text{reacted})}}{g} = \frac{\int_0^{n_{\text{Cl}_2}} [\text{Cl}_2]_0 \left(1 - \frac{S_t}{S_0}\right) f dn_{\text{Cl}_2}}{m} \quad (1)$$

Columns were packed with synthetic soil samples made from kaolin (Sigma) or basalt clay as the fine particulate source, Ottowah river sand as the coarse grain source, and humic acid (Sigma) as the organic source. Relative amounts of the source materials were mixed thoroughly before packing in the column. Table 1 shows the relative masses used in the synthetic soil blends.

Table 1. Synthetic Soil Sample Blends for Breakthrough Measurements

Soil Type	% clay	% sand	% organic
Silt Loam	15	15	70
Clay Loam	33	33	34
Sandy Loam	15	70	15
Basalt Clay	100	0	0

3.2.2.2. Deposition Measurements

Deposition measurements were carried out in both laboratory- and field-scale experiments. Field experiments were performed at Dugway Proving Grounds during 2,000-kg releases of Cl_2 and NH_3 , and laboratory experiments were performed at AFRL/RXQL in a small deposition chamber. A variety of terrestrial samples were included in the field measurements (e.g., soil, water, concrete, grass) with most of the emphasis on soils of varying composition. Soil samples were made by mixing various organic ("top soil," Home Depot), clay (indigenous soil excavated 5 km SE from the release point), and sand ("construction sand," Home Depot) fractions according to Table 2 and subsequently packing into 2-gal buckets. Samples were exposed at varying distances from the release point as detailed in Table 3.

Table 2. Soil Mixture Compositions for Field Experiment

Name	% Clay ^a	% Sand ^a	% Top soil ^a	% Moisture ^b	% Organic ^b
Sandy loam	15	70	15	7.37	3.54
Silt loam	15	15	70	14.91	16.91
Clay loam	33	33	33	10.27	8.10
Clay loam wet	33	33	33	16.16	8.10
Clay	70	15	15	6.79	7.50
Sand	0	100	0	5.29	0.80
Top soil	0	0	100	29.47	43.33
Dugway soil	100	0	0	3.40	7.37

^aPercentages are based on volume measurements.

^bMoisture and organic contents measured gravimetrically.

Table 3. Sample Site Locations for Field Measurements

Site Number	Distance from release point, m	Direction
1	15	NNW
2	9	NNW
3	2.5	NNE
4	9	SSE
5	15	SSE

After exposure, soil samples were cored and fractionated vertically. Duplicate soil cores (nominally 6 in long and 2 in diameter) were obtained by pounding a 6-in split core sampler into the sample buckets using a slide hammer. The split core assembly was then disassembled and the resulting soil core was fractionated vertically from the top into 0.5-, 0.5-, 1-, 2-, and 2-in fractions. Concrete cores were sealed in plastic wrap, placed in plastic bags, and shipped back in a cooler. The concrete cores were sampled after exposure by drilling 1/4-in holes to different depths. The resulting powder was extracted and analyzed. Water samples were immediately transferred into 200-mL plastic sample containers.

Ion-specific probes were used in the field to measure H^+ and NH_4^+ concentrations for the water samples. A small amount of salt was added to the fresh water samples just prior to analysis to obtain accurate pH measurements. NH_4^+ measurements were made by adding 2 mL of ionic strength adjuster (Cat. No. 951211, Thermo Scientific) to 100 mL of sample and reading the ammonia-ion-specific-electrode (Thermo Scientific Orion) response using a voltmeter. The probe response was calibrated with solutions of known NH_4Cl concentration.

Samples were extracted and analyzed by ion chromatography to measure Cl^- and NH_4^+ concentrations. Cl_2 -exposed samples (~ 1 g) were extracted into 10 mL deionized (18 MΩ/cm) water in 20-mL scintillation vials for a minimum of 24 h (longer extraction times did not affect the results). NH_3 -exposed samples were treated identically except the extract was slightly acidic (250 mM H_2SO_4). The resulting extract was analyzed with ion chromatography, and in some cases it was necessary to dilute the extract to stay within the linear response of the detector.

For the Cl_2 -exposed samples, 100 μL of extract was injected onto an anion exchange column (4×250 mm IonPac[®] AS9–HC, Dionex[®]) (EPA Method 9056A). The mobile phase was 1.0 mL/min 9.0 mM Na_2CO_3 at a pressure of ~2000 psi (pump model GP40, Dionex[®]). A small flow of 25 mM H_2SO_4 was used to regenerate the suppressor (model ASRS[®]–ULTRA II 4mm, Dionex[®]). Chloride was detected by a change in conductivity (detector model ED50, Dionex[®]). Standard solutions of NaCl (0.0178 to 1.7836 mM) were analyzed to generate a calibration curve. For the NH_3 -exposed samples, 50 μL of extract was injected onto a cation exchange column (5×250 mm IonPac[®] CS16, Dionex[®]) with a 1.5-mL/min mobile phase (26 mM methane-sulfonic acid, Sigma–Aldrich) (ASTM D6919-09). A suppressor (4-mm CRS[®] 300, Dionex[®]) was used to reduce the mobile phase signal and was regenerated with the waste stream. Cations were detected by a change in conductivity (detector model CD20, Dionex[®]). Standard solutions of NH_4Cl (0.094 to 1.869 mM) were analyzed to generate a calibration curve.

Water and organic fractions were quantified gravimetrically. Moisture content was determined by heating samples in glass beakers to 90 °C for three days and measuring mass loss. Organic fractions were determined by heating samples in ceramic crucibles to 600 °C for 6 h and measuring mass loss. Higher temperatures were avoided to prevent additional mass loss through decomposition of $CaCO_3$ present in the soil.

Headspace vials were filled and sealed in the field and shipped back for analysis by gas chromatography–mass spectrometry (GC/MS). Vial headspaces were adsorbed at 60 °C onto solid-phase microextraction (SPME) fibers and subsequently desorbed in the GC injection port. Organics were then separated on a GC column (Restek Rtx[®]-5; 0.25-mm diameter, 30-m length, 0.25-μm film thickness) and detected using mass spectrometry with electron impact ionization. Each vial was sampled in duplicate.

Laboratory-scale deposition measurements were initiated with most of the emphasis on chamber design. The chamber (Figure 3) houses six samples and allows samples to be removed from the bottom without interfering with other samples so that three different time points can be sampled in duplicate. A radial design ensures equivalent exposures for the various sample positions. The strategy for these laboratory-scale deposition measurements is to efficiently explore the parameter space for Cl_2 penetration and reaction with soils and other terrestrial material. For soil, an I-optimal experimental design was produced that probes Cl_2 penetration as a function of soil composition (clay, sand, and loam fractions), moisture content, packing density and chlorine concentration.

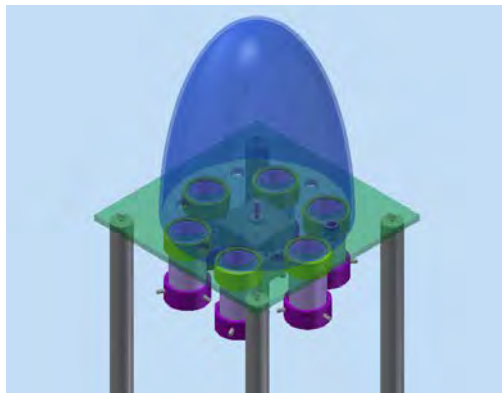


Figure 3. Design of Radial Chamber for Deposition Experiments
(Colors Are Used to Distinguish the Separate Components.)

3.2.2.3. Gas-phase Kinetics

The gas-phase reaction rate of AsH_3 with OH radicals was measured using a relative rates approach that is well documented in the open literature (Finlayson–Pitts and Pitts 2000). Detection of AsH_3 and the organic reference compounds was accomplished with cryotrap collection followed by GC/MS (AsH_3) and GC with flame ionization detection (GC/FID) (organic reference compounds). AsH_3 was collected at -167°C , and the organic reference compounds were collected at -80°C because collection of the organic reference compounds at -167°C caused unwanted artifacts in the analysis. Reference compounds were separated on a RTX 5 column (30-m length, 0.53-mm diameter) with a GC temperature-ramp program of $\sim 10^\circ\text{C}/\text{min}$ from 30 – 200°C . AsH_3 was analyzed on a volatiles column (90-m length, 0.15-mm diameter) with a GC temperature program of -80°C for 5 min, ramp at $10^\circ\text{C}/\text{min}$ to 30°C , and ramp at $20^\circ\text{C}/\text{min}$ to 200°C .

3.2.3. Results and Discussion

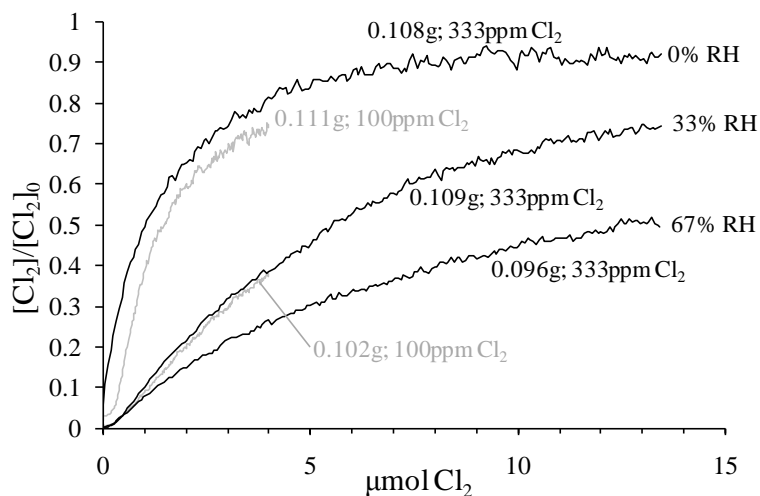
3.2.3.1. Breakthrough Measurements

The experimental matrix for each soil type is shown in Table 4, for which there is a high and low Cl_2 concentration, flow rate, soil mass, and a high, middle, and low relative humidity. Adding humidity to the gas flow generated additional losses for the Cl_2 flow through reactions with metal-fitting surfaces. This was circumvented by coating the inner surfaces of metal fittings with halocarbon wax 600 (Halocarbon[®] Products Corp.). No Cl_2 losses to the Teflon[®], glass, or glass-wool surfaces were observed at the highest humidity investigated (67 %).

Table 4. Experimental Matrix for Capacity Measurements

Experimental parameter	High Value	Middle Value	Low Value
[Cl ₂], ppm	333	none	100
Flow Rate, sccm	100	none	60
Relative Humidity	67%	33%	0%
Mass, g	Varies by sample	none	Varies by Sample

Figure 4 shows breakthrough on silt loam for the low and high Cl₂ concentrations and all relative humidities for a column with a nominal mass of 0.1 g. The dry breakthrough curves exhibit significantly faster recovery of the Cl₂ signal than the 33 and 67% RH flows. Qualitatively, this is consistent with what is expected, because the irreversible deposition of Cl₂ is water mediated. There is an insignificant difference between the low (gray lines) and high (black lines) Cl₂ concentrations. This is also consistent with expectations, as the amount of recovery should be dependent on the absolute exposure (moles of Cl₂) and not the gas-phase concentration (note the x-axis units are μmol).

**Figure 4. Breakthrough Curves for Cl₂ on Silt Loam**

Measurements Were Made with a Total Column Flow Rate of 100 sccm, and Column Masses, Cl₂ Concentrations, and Relative Humidities Are Indicated in the Figure.

Figure 5 shows the integrated Cl₂ uptake normalized to the silt loam column mass (Eq. 1) as a function of humidity and column flow rate. The faster volumetric flow rate exhibited less Cl₂ uptake than the slower flow rate. While this difference is not outside the uncertainty of the measurement, the consistent lower uptake measurements at the higher flow rate suggests that the apparent difference is real. This indicates that mass accommodation or condensed-phase reaction chemistry is limiting the deposition in these breakthrough experiments. Based on previous work accomplished in this laboratory, mass accommodation is rapid and does not limit the deposition rate, suggesting that condensed-phase chemistry limits the uptake of Cl₂ at these high exposures. Also, in Figure 5, there is a relatively large increase in the moles of Cl₂ reacted moving from the dry (0 % RH) to 33 % RH condition, and a much smaller increase at higher humidity (66 % RH).

Figure 6 shows a comparison among the different soil types with a 100-sccm column flow rate and a Cl_2 concentration of 333 ppm. Silt loam, with the highest organic fraction (67 %), exhibits the slowest breakthrough. An equivalent column mass of clay loam (33 % organic) exhibits slower breakthrough. Cl_2 uptake on sandy loam (15 % organic) is approximately the same as basalt clay (0 % organic). Qualitatively, Cl_2 uptake is consistent with what is expected from the chemistry (i.e., soil with more organic content generally reacts more Cl_2). Figure 7 shows a more comprehensive comparison of Cl_2 uptake on the various soil types in which integrated Cl_2 reacted was calculated from the data using Equation 1. Within the uncertainty of the measurement silt loam and clay loam exhibit the same Cl_2 uptake over the full humidity range studied. Sandy loam reacted the smallest amount of Cl_2 under dry conditions, but at elevated humidity basalt clay reacted the least. Interestingly, Cl_2 deposition decreased slightly on basalt clay at higher humidity.

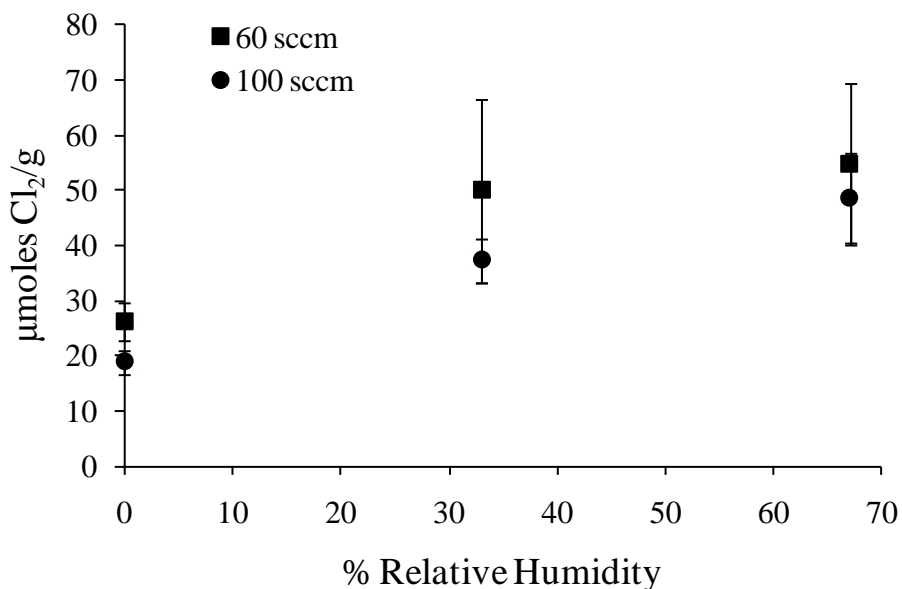


Figure 5. Normalized Uptake of Cl_2 on Silt Loam as a Function of Humidity
 Cl_2 Deposition Was Calculated by Equation (1) to an Exposure of 5 μmol Cl_2 . Measurements Were Made at 333-ppm Cl_2 Concentration and the Column Flow Rate Indicated in the Figure Legend; Error Bars Represent the Standard Deviation of the Averaged Measurements.

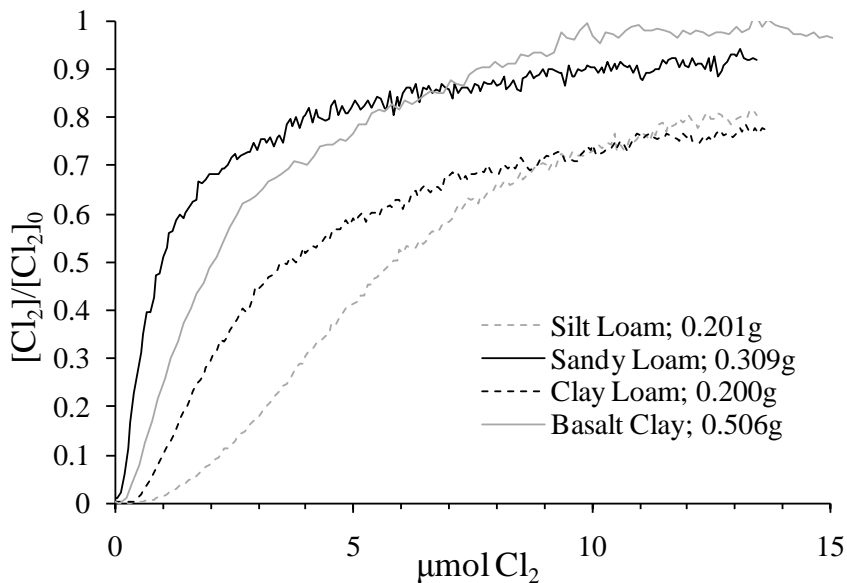


Figure 6. Breakthrough Curves for Cl_2 as a Function of Soil Type at 0% Humidity
Measurements Were Made with a 100-sccm Column Flow and 333 ppm Cl_2 .

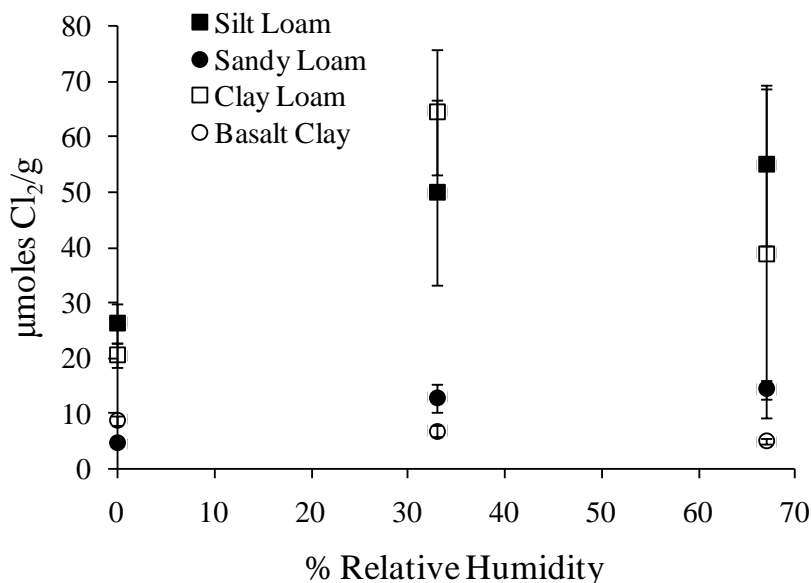


Figure 7. Normalized Cl_2 Uptake as a Function of Humidity
 Cl_2 deposition was calculated according to Equation (1) to an exposure of 5 $\mu\text{mol Cl}_2$.
Measurements were made with a 60-sccm column flow rate.

Figure 8 plots the data of Figure 7 against the organic mass fraction. This reinforces the conclusion that the organic fraction is a significant parameter for Cl_2 deposition. It is not clear what caused the outlier point (33 % organic and RH), so breakthrough curves for these conditions need to be reinvestigated.

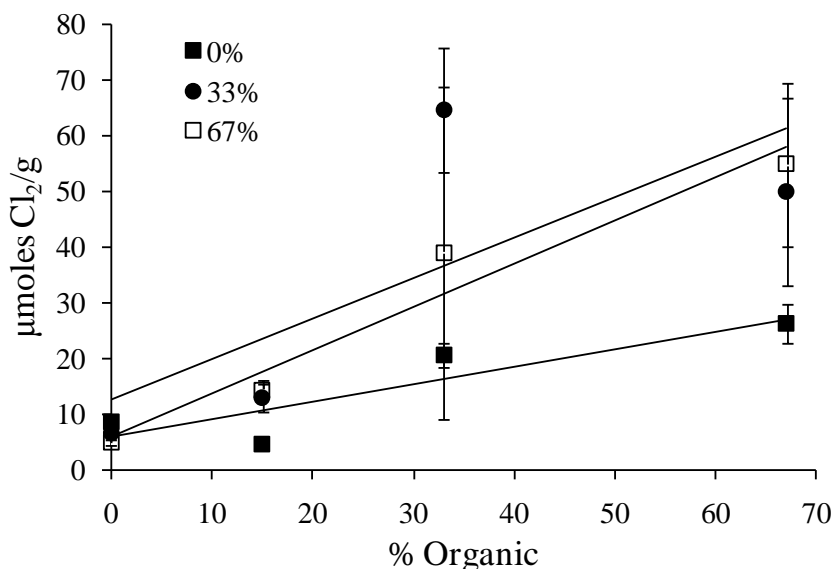


Figure 8. Normalized Cl₂ Uptake as a Function of Soil Organic Fraction

Cl₂ deposition was calculated according to Equation (1) to an exposure of 5 μmol Cl₂.

Measurements were made with a 60-sccm column flow rate at the humidity indicated in the legend; error bars represent the standard deviation of the averaged measurements and lines are guides for the eye and do not represent fits to the data.

3.2.3.2. Gas-phase Kinetics

Measurements of the reaction of AsH₃ with OH were made using the relative rates approach. A separate GC was used to collect the organic reference compounds at a higher temperature. The low temperature required for AsH₃ collection was causing artifacts in the reference compounds results. Figure 9 shows the results using both 2-methyl-2-butene and 1-hexene as reference compounds. The plots are linear, showing agreement between the two different reference compounds within 20%. Measurements using 2-methyl-2-butene were fit only to a $\ln([AsH_3]/[AsH_3]_0)$ value of 0.5 due to a product interference (note the deviation between the data and the linear fit). Additional AsH₃ relative rate measurements were completed with two additional reference compounds (1-heptene and *trans*-4-octene), and the results agreed well among all reference compounds. All measurements were fit to a line on a \ln - \ln scale with a floating intercept. The average measured OH rate constant was 8.65×10^{-11} cm³/molecule/s yielding a 1/*e* lifetime of 3 h (at [OH] = 10⁶ cm⁻³). Table 5 shows the final results.

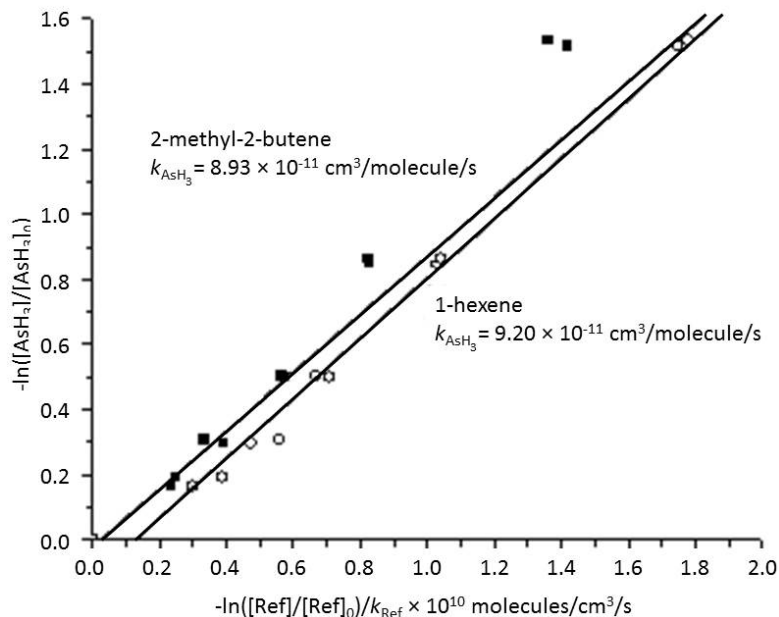


Figure 9. Relative Rate Measurements of AsH₃ Reaction with OH

Table 5. Experimental Results for AsH₃ + OH Relative Rate Measurements

Reference	$k_{\text{ref}} \times 10^{11}$, molecules/cm ³ /s ^a	Slope	$k_{\text{AsH}_3} \times 10^{11}$, molecules/cm ³ /s
2-methyl-2-butene	8.69	0.931	8.09
1-hexene	3.70	2.33	8.62
cyclohexane	0.72	11.5	8.26
2-methyl-2-butene	8.69	1.03	8.93
1-hexene	3.70	2.49	9.20
1-heptene	4.0	2.26	9.02
<i>trans</i> -4-octene	6.9	1.22	8.45
Average			8.65
St. Dev.			0.41

^aReference rate constants obtained from Atkinson, 1997.

3.2.3.3. Cl₂ Deposition on Soils

During the first Cl₂ release, silt loam, clay loam, and sandy loam were exposed at sites 1, 2 and 3 (Table 3) in addition to samples outside the berm. Figure 10–Figure 12 show the results for chloride measurements in the soil fractions in which the largest concentrations were observed for samples closest to the release point. Figure 10 shows chloride measurements for samples exposed to the liquid Cl₂ pool, and results show significant penetration of Cl₂. Some penetration may be caused by packing densities that are lower than normal and, qualitatively, liquid Cl₂ should penetrate much deeper than the vapor. Whether Cl₂ will penetrate 12 cm into undisturbed indigenous soil is a question that still needs to be answered. For some reason the clay loam exhibits the highest chloride content in the bottom fraction, but this sample appears to be an anomaly.

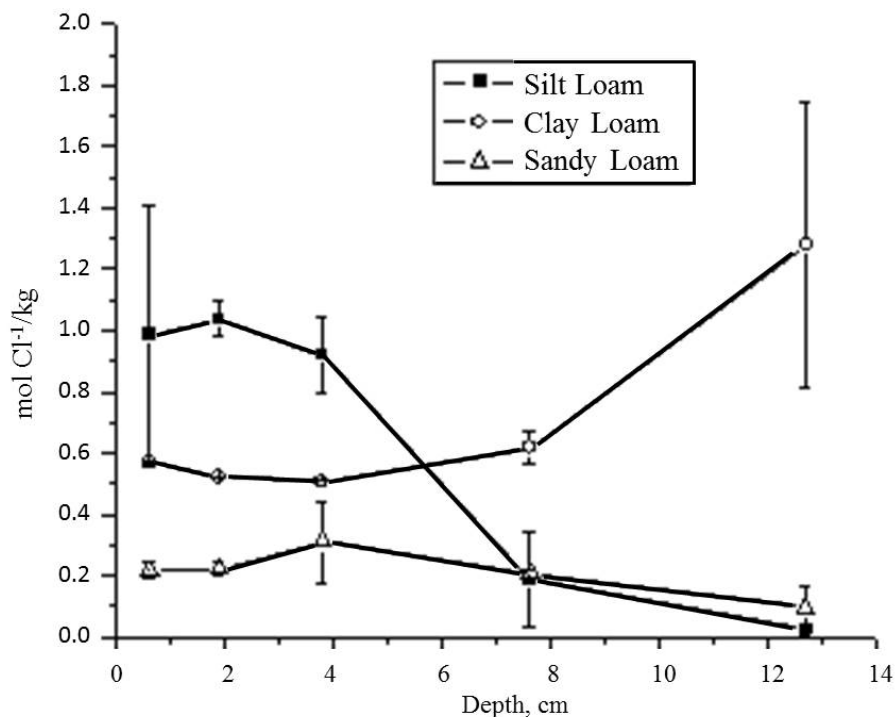


Figure 10. Cl^- Concentrations in Core Samples from Cl_2 Release #1, Site 3
 Samples exposed 3 m from release. Error bars are the range of concentrations in duplicate cores.

Figure 11 and Figure 12 show samples exposed to vapor chlorine at sites 2 and 1, respectively. Samples at site 1—farther from the release and elevated 1 m relative to the base of the depression—exhibited significantly less chloride than those at site 2. In fact, the only measurement that was significantly above the background chloride levels from samples at site 1 was the top fraction for silt loam. This is somewhat surprising considering the amount of chlorine these samples were exposed to. This may indicate that chloride ions are not appropriate tracers for Cl_2 deposition downwind from a release. Upon further examination of Figure 11 and Figure 12, it is clear that the magnitudes of the chloride concentrations in the top fractions always decrease from silt loam to clay loam to sandy loam. This is also in decreasing order of the organic volume fraction. This has implications for deposition of Cl_2 because reaction between HOCl and organic molecules is the irreversible step and, typically, the top layer of soil contains the largest organic fraction.

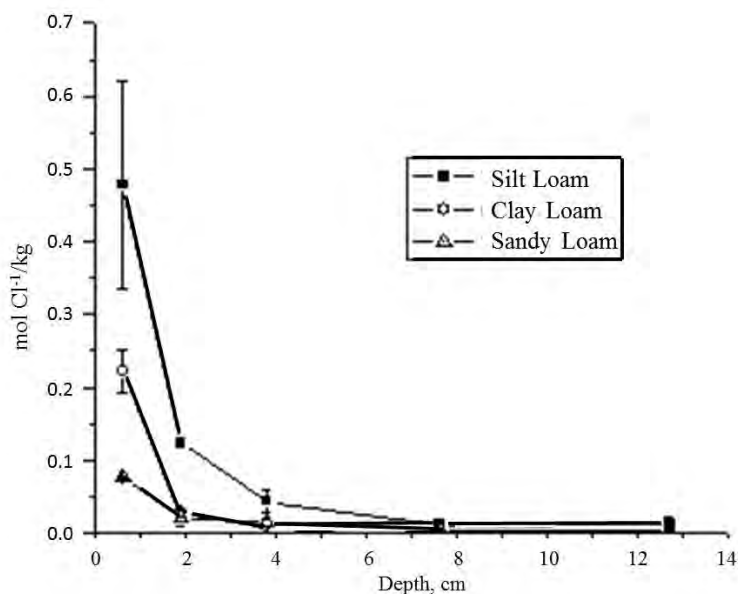


Figure 11. Cl^- Concentrations in Core Samples from Cl_2 Release #1, Site 2
Samples were exposed 10 m from release. Error bars are the range of concentrations in the duplicate cores.

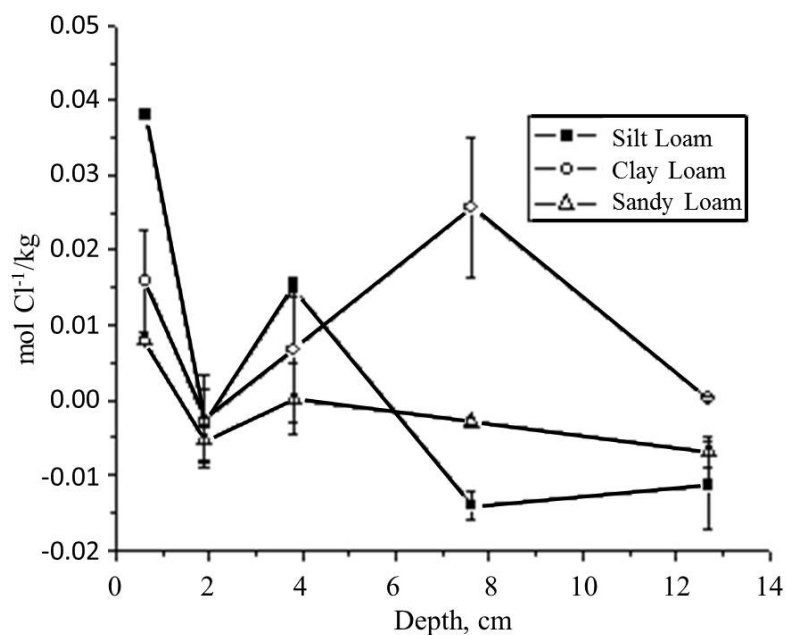


Figure 12. Cl^- Concentrations in Core Samples from Cl_2 Release #1, Site 1
Samples were exposed 15 m from release. Error bars are the range of concentrations in the duplicate cores.

Figure 13 shows the temperature results for thermocouples placed in silt loam at site 4 (exposed to Cl_2 vapor). The only thermocouple that recorded a significant temperature change was at the surface. Buried probes were not affected by the Cl_2 plume. The surface temperature, like the NH_3 results (see below), shows a significant drop due to the cold vapor from the adiabatic expansion and phase change of the compressed, liquefied Cl_2 released. However, in contrast to the NH_3 release, there is a subsequent 40°C increase in temperature, and ambient temperature is not reached until 20 min after the release. The enthalpy of dissolution ($\Delta H_{\text{sol}} = -19.8 \text{ kJ/mol}$) (Alkan et al. 2005) for Cl_2 in water is less than that for NH_3 ($\Delta H_{\text{sol}} = -30.5 \text{ kJ/mol}$) (Lide 1995), so the temperature rise is clearly not caused by physical dissolution. This temperature rise is, therefore, attributed to chemical reactions of the resulting HOCl/OCl^- with the organics in the soil. After this release, the thermocouple readout stopped working, so no additional data were collected during subsequent releases.

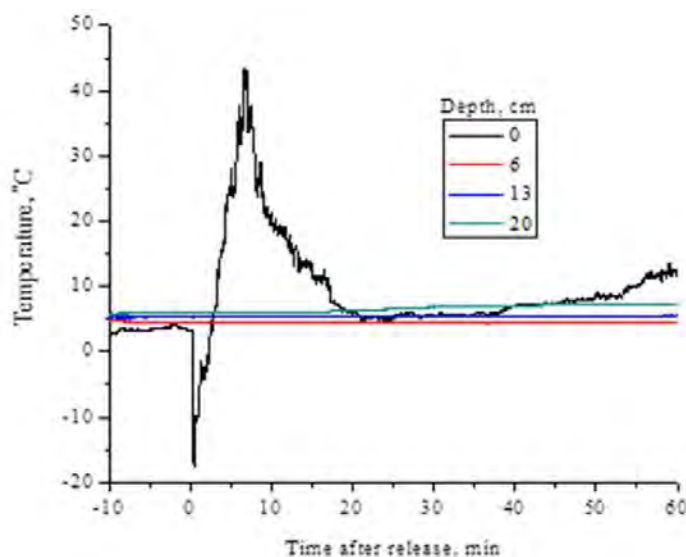


Figure 13. Soil Temperature during Cl_2 Release #1

Thermocouples were placed at the indicated depth in silt loam at site 4 (10 m from release). Fresh- and salt-water samples were placed at site 4 in 250-mL cups. The results in Table 6 show an acidic pH , consistent with dissolution of Cl_2 in the water. Interestingly, the fresh water exhibited significantly lower pH than salt water, and a colorimetric assay—which produces a pink color when active chlorine is present—showed active chlorine present in only the fresh-water sample. These differences were probably caused by a visible soil contamination in the salt water. The release apparently kicked up loose soil which fell in the salt water container partially neutralizing the HCl generated and consuming the active chlorine species present (HOCl). The pH measured in the freshwater sample is near the pK_a of 3.3 for Reaction 1 (White 1972).

Table 6. Water Samples Exposed at Site 4, Cl_2 Release #1

Sample	pH	Colorimetric HOCl assay	Notes
Salt water	5.43	No color	Contaminated with soil
Fresh water	2.73	Bright pink	none

The second Cl_2 release was performed under high wind conditions (SSW at ~ 5.5 m/s). Video footage from this release showed the visible portion of Cl_2 being swept out of the berm with less than 1 m spreading upwind. Subsequent analysis of water samples at site 2 showed no evidence of Cl_2 deposition. The closest soil samples were located 2–3 m upwind and did not exhibit any Cl_2 odor after the release. Therefore, all soil samples from this release were covered with plastic wrap and left for the next release. No data were collected from this release.

In addition to soil samples placed during release #2 (clay loam wet and clay at sites 1, 2, and 3), sand, silt, and Dugway soil were placed at sites 4 and 5 for release #3. Figures 14–16 show the chloride measurements for the fractions in each sample. The samples exposed to the liquid Cl_2 pool (Figure 14), again, show deeper penetration of Cl_2 ; however, in comparison with the top fraction, the deeper fractions do not exhibit as much Cl^- as those exposed during the first release (Figure 10). This may be a result of better packing of the clay and wet clay loam samples or a difference in exposures during the first and third Cl_2 releases. Samples exposed to Cl_2 vapor 9 m (Figure 15) or 15 m (Figure 16) from the release point exhibit qualitatively the same results as those exposed in release #1. Samples 15 m from the release showed Cl^- levels near background, and those 9 m from the release showed significant Cl^- levels in the top fraction, in which the Cl^- concentration is related to the organic fraction in the samples.

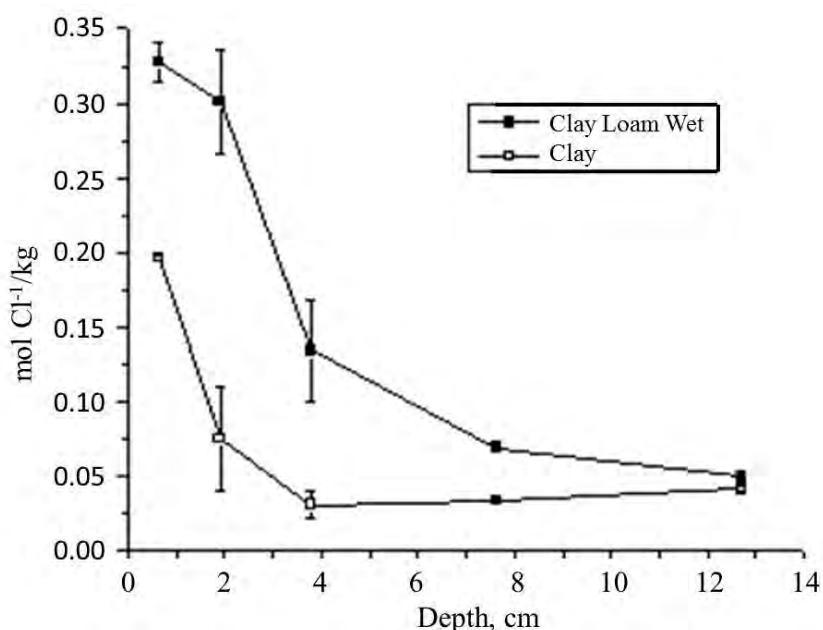


Figure 14. Cl^- Concentrations in Soil Cores from Cl_2 Release #3, Site 3
 Samples exposed 3 m from release. Error bars are the range of concentrations in duplicate cores.

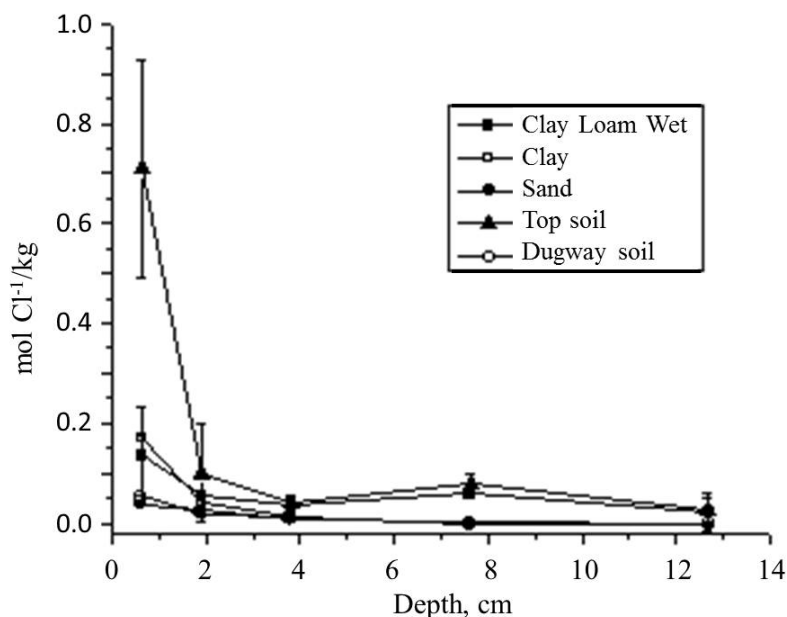


Figure 15. Cl^- Concentrations in Soil Cores from Cl_2 Release #3, Sites 2 and 4

Samples exposed 10 m from release; clay loam wet and clay exposed at site 2; sand, top soil, and Dugway soil exposed at site 4. Error bars are the range of concentrations in the duplicate cores.

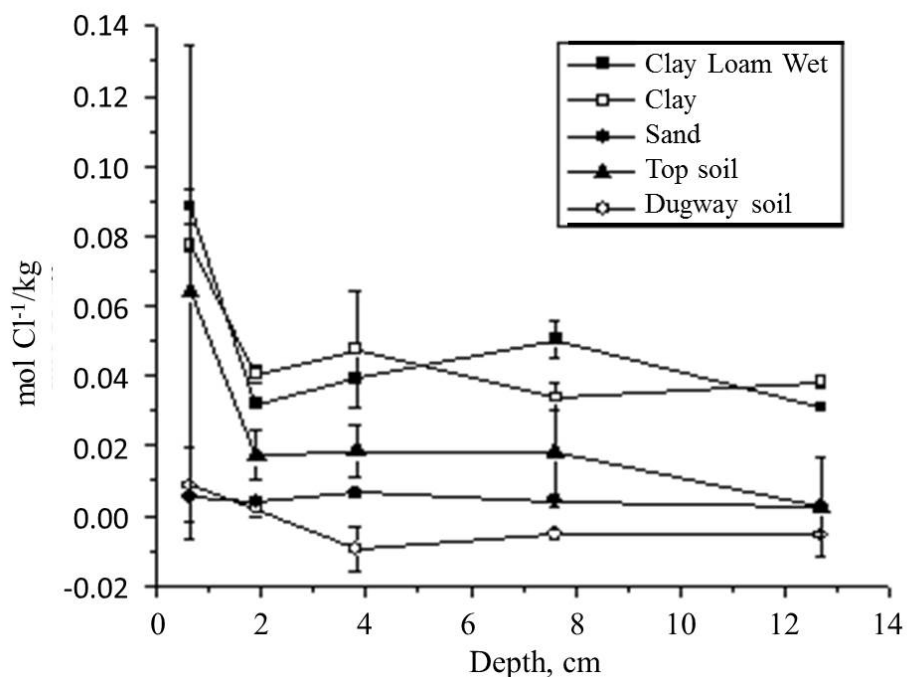


Figure 16. Cl^- Concentrations in Soil Cores from Cl_2 Release #3, Sites 1 and 5

Samples were exposed 15 m from release; clay loam wet and clay were exposed at site 1, and sand, top soil, and Dugway soil were exposed at site 5. Error bars are the range of concentrations in the duplicate cores.

Salt- and fresh-water samples were placed at sites 2 and 4 in 250-mL plastic cups. Table 7 shows pH measurements, and there is very good agreement among the samples at each site. When tested for active chlorine with the colorimetric assay, all samples exhibited a pink (positive) color. The color change for salt water exposed at site 2 exhibited a less intense color change than the other samples, and it had some visible soil sediment. Similar to the salt water in release #1, the soil consumed part of the active chlorine.

Table 7. pH Measurements for Cl₂ Release #3

Site	Salt water	Fresh water
#2 (9 m NNW)	2.64	2.60
#4 (9 m SSE)	3.01	3.01

In addition to the soil and water samples, concrete samples were placed at sites 3, 4, and 5. As mentioned above, each core had a unique composition, so there was no “blank” core to compare with. The strategy was to simply compare the Cl⁻ concentration–depth profile, which would be higher near the surface. Figure 17 shows the results which were inconclusive. Cl⁻ concentration did not show the expected decreasing trend with depth. Instead, internal fractions exhibited higher Cl⁻ concentrations than surface fractions. The core sample at site 4 was sampled from both the top (closed circles) and bottom (open circles), and the bottom surface exhibited significantly less Cl⁻ than the top surface. This difference might be attributable to Cl₂ deposition, but such a conclusion is speculative at this point. These results do show that a more controlled experiment needs to be done using laboratory-prepared mortar cores. This would eliminate inhomogeneities observed in cores pulled from the field, and the mortar cores could be artificially aged to different degrees.

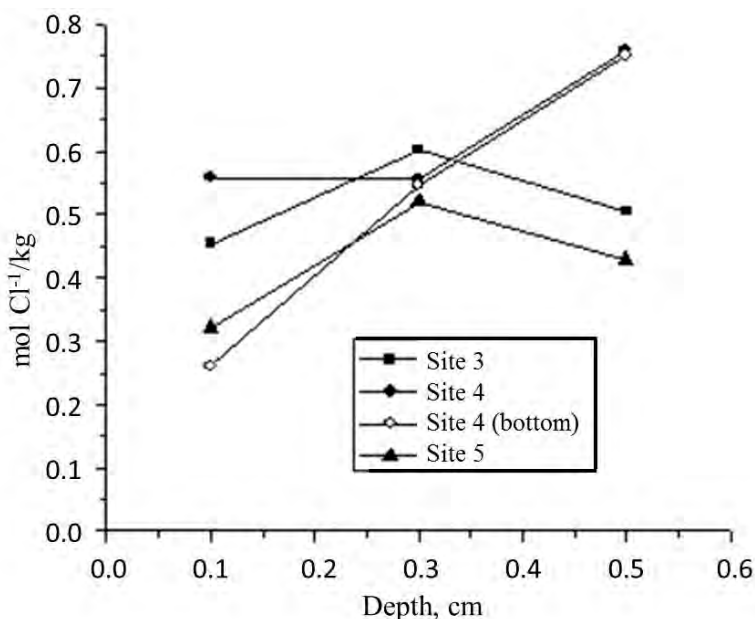


Figure 17. Cl⁻ Concentrations in Concrete Samples Exposed During Cl₂ Release #3
 Samples were exposed at the indicated site, and the depth profile from the bottom side of the concrete core is shown in the open symbols. No error bars are shown because these are measurements of single extractions.

Headspace vials were filled with 1–2 g of soil in the field after fractionating soil cores and sealed with a Teflon-lined cap, so escape of volatile organics was minimized. As active chlorine was not quenched additional chemical degradation of the organic mass in the samples likely continued during sample shipment and storage. Therefore, this analysis is qualitative rather than quantitative. Figure 18 shows the resulting chloroform signals (retention time = 2.2 min) obtained from the soil fractions, and Figure 19 shows the integrated signals from all chlorinated organics in the chromatograms. Chlorinated-organic peaks in the chromatogram were identified by characteristic isotopic abundances attributable to chlorine, and by library searches. Both figures exhibit qualitatively the same results, chloroform and chlorinated organics appearing in higher concentrations near the surface, and samples exposed to the liquid Cl_2 pool exhibiting significant chlorinated signals in deeper fractions. The chloroform signals for top fractions in the silt, clay and sandy-loam samples were similar for samples 3 m and 10 m from the release. Samples 15 m from the release exhibited roughly an order of magnitude less chloroform signal in the top fraction. The distance dependence for the integrated signals from all chlorinated organics is more apparent. Interestingly, there were detectable amounts of chlorinated organics in the bottom fractions of the clay loam samples at both 10 and 15 m from the release. This is somewhat surprising, as there were background levels of chloride in those fractions. This may indicate either a small amount of cross contamination or a lower detection limit for volatile chlorinated organics. There was no headspace analysis for the bottom fractions of the silt and sandy loam samples because these samples were not collected in the field.

Although these measurements are only qualitative, they do bring up an important question: do volatile products from Cl_2 deposition pose an acute hazard during a large-scale release? The Permissible Exposure Limit for chloroform—one of the primary chlorinated organics detected—is 50 ppm (240 mg/m^3) according to the Occupational Safety and Health Administration (OSHA). The concentration of chloroform that is immediately dangerous to life and health (IDLH) is 500 ppm whereas the IDLH for Cl_2 is 10 ppm (Ludwig et al. 1994). This suggests that although volatile chlorinated organics will certainly be present in a Cl_2 plume, they are unlikely to be the primary hazard, as Cl_2 is $\sim 50\times$ more toxic based on IDLH values.

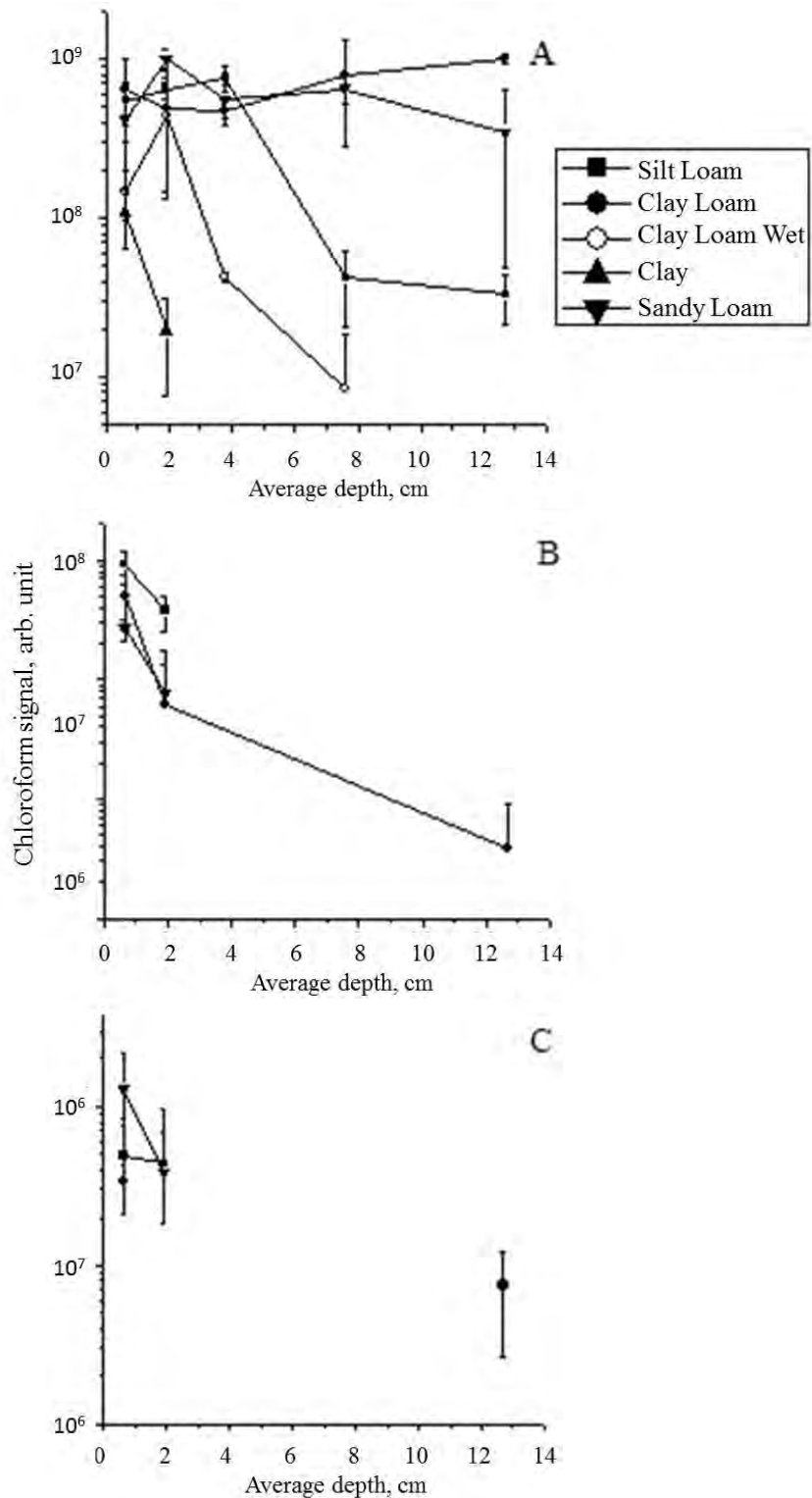


Figure 18. Chloroform Signals from Soil Headspace

Soil samples exposed at (A) site 3 (3 m from release), (B) site 2 (10 m from release) and (C) site 1 (15 m from release). Clay loam wet and clay samples were exposed during Cl_2 release #3; all other samples were exposed during Cl_2 release #1. Error bars are the standard deviation of the averaged signals from duplicate cores and duplicate injections.

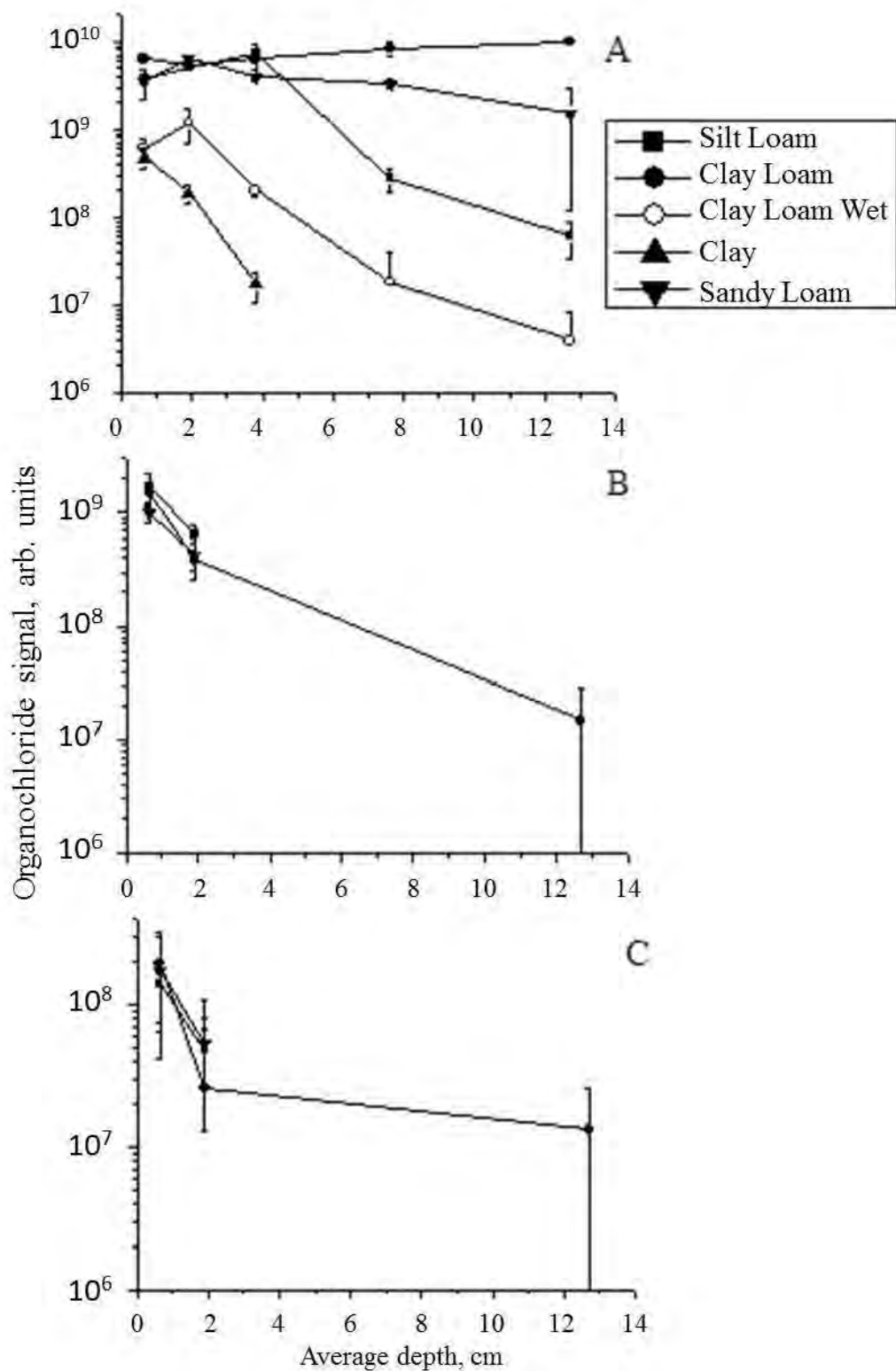


Figure 19. Chlorinated Organic Signal from Soil Headspace
(See notes under Figure 18.)

3.2.3.4. NH_3 Deposition on Soils

For the first NH_3 full-scale release (2,000 kg) soil samples of sandy loam and silt loam were exposed. Extracts from samples exposed only to the vapor cloud (> 9 m from source) exhibited no detectable amounts of NH_4^+ . The minimum detectable NH_4^+ concentration in the soil samples was $0.001 \text{ mol NH}_4^+/\text{kg}$, assuming a 10-mL extraction volume and 1-g soil sample. Samples exposed to liquid NH_3 (site 3 in Table 3) did exhibit detectable amounts of NH_4^+ as shown in Figure 20. The top fractions exhibited very similar NH_4^+ concentrations, and both show higher concentrations in deeper fractions. Deeper penetration of NH_3 in sandy loam may be a result of the porous nature of sandy soils, but this must be confirmed through more-rigorous experiments.

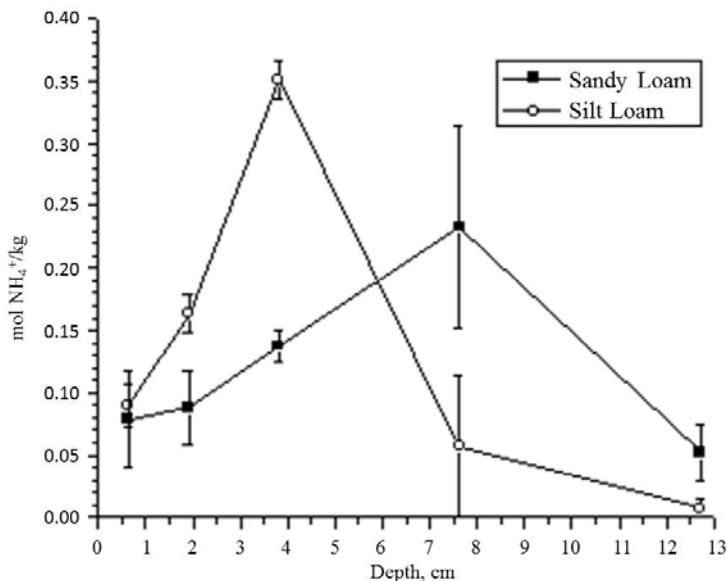


Figure 20. NH_4^+ Concentrations in Core Fractions from NH_3 Release #1

Samples at site 3 (3 m from release). Error bars are the range of concentrations in duplicate cores.

Thermocouples were placed in a bucket of sandy loam at the depths indicated in Figure 21 and show the temperature profiles measured. The only thermocouple that exhibited a significant temperature change was at the surface caused by the cold vapor front from the release. A slight temperature increase might be expected from dissolution of NH_3 in the soil moisture ($\Delta H_{\text{sol}} = -30.5 \text{ kJ/mol}$) (Lide 1995), but apparently this was not large enough to cause a measurable temperature change.

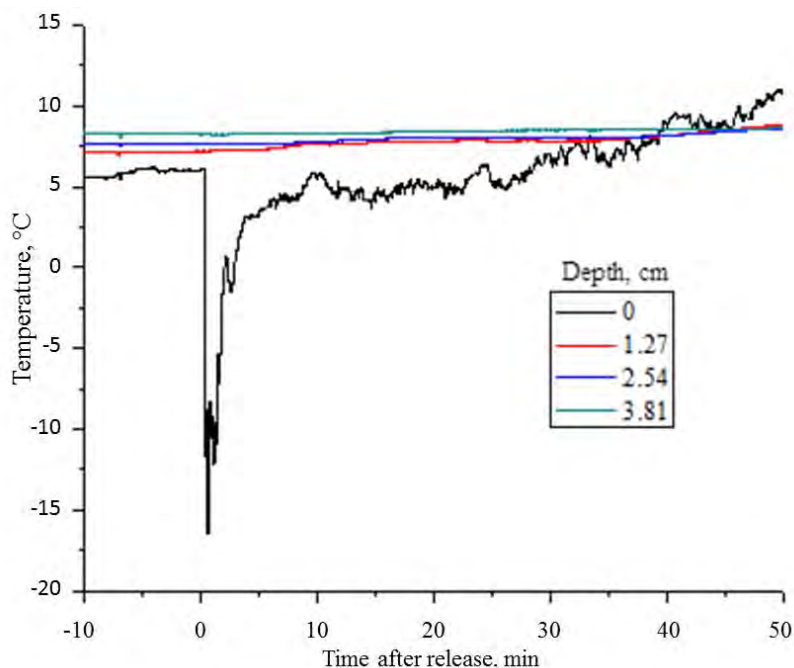


Figure 21. Soil Temperature during NH₃ Release #1

Thermocouples were placed at the indicated depth in sandy loam at site 4 (10 m from release).

Fresh water samples were placed at site 2 (exposed to vapor cloud only) in 250-mL cups and a 2-gal bucket. Measurements were made the afternoon of the day of the release, and results are shown in Table 8. NH₄⁺ probe measurements were calibrated onsite using NH₄Cl standard solutions. The *pH* measurements are all equivalent to the nearest tenth of a *pH* unit indicating that similar concentrations of NH₃ dissolved in the samples. This is corroborated by the NH₄⁺ measurements showing agreement within 30% (within the uncertainty of the measurement) among the three samples. Error bars for NH₄⁺ concentrations were propagated from the uncertainty on the fit to the calibration curve. The same concentrations measured in the 2-gal bucket and the cups indicate that equilibrium is achieved in water to at least the depth of the bucket (20 cm). All samples had neutral *pH* before exposure.

Table 8. Fresh Water Samples at Site 2, NH₃ Release #1

Sample	<i>pH</i>	NH ₄ ⁺ probe	
		mV	[NH ₄ ⁺], mM
2-gal bucket	10.24	46	9.3 (± 2.8)
Cup 1	10.15	44	10.3 (± 3.1)
Cup 2	10.18	36	15.7 (± 4.2)

All remaining soil types were exposed during NH₃ release #2 because weather delays prevented participation in the final two releases. Clay, clay loam, and clay loam wet were exposed at sites 1, 2, and 3, and the three source materials (sand, silt, and clay 100) were exposed at sites 4 and 5. As in release #1, samples exposed only to the vapor cloud did not exhibit any detectable amount of NH₄⁺. Figure 22 shows the NH₄⁺ concentrations for soil samples exposed to the liquid pool (site 3) in which the clay loam and clay samples show depth profiles very similar to those in Figure 20—higher concentrations of NH₄⁺ detected in deeper fractions. Clay loam wet,

however, shows a different depth profile, with the highest NH_4^+ concentration in the top fraction. This may be a result of better retention in soil with optimal moisture content.

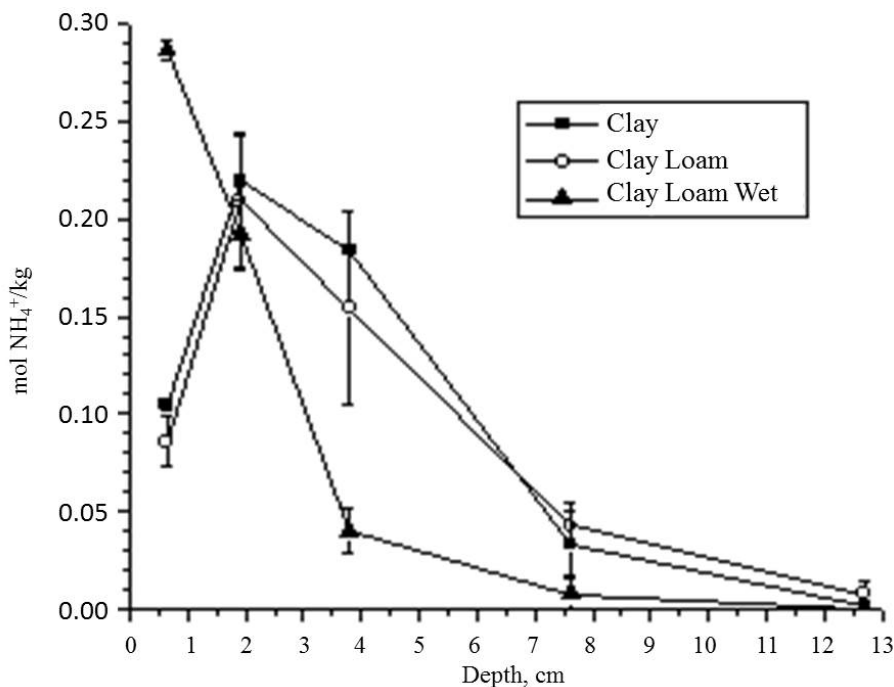


Figure 22. NH_4^+ Concentrations in Core Fractions during NH_3 Release #2

Samples at site 3 (3 m from release). Error bars are the range of concentrations in duplicate cores.

Thermocouples for NH_3 release 2 were placed in clay loam within the liquid pool (site 3), and results are shown in Figure 23. As in the previous release, the thermocouple placed at the soil surface measured a significant decrease in temperature due to the adiabatic release of compressed, liquefied NH_3 . The sub-ambient temperature lasted for more than one hour with some cooling observed for the 6- and 13-cm deep thermocouples. However, the buried thermocouples all exhibited small temperature increases, consistent with dissolution of NH_3 in the soil moisture. The deepest thermocouple (21 cm) measured the largest temperature increase (1.5°C) presumably because it was insulated from the cryogenic surface conditions. Data were not collected beyond 70 min, because the data logger memory was full.

Fresh- and saltwater samples were placed 9 m from the release point (site 2) in 250-mL plastic cups. Results are shown in Table 9 in which there is no significant difference between the samples. This is expected since the saturation of NH_3 in water is $p\text{H}$ dependent and the ionic strength will not significantly affect this. Both samples had neutral $p\text{H}$ before exposure.

Table 9. Water Samples at Site 2, NH_3 Release #2			
Sample	$p\text{H}$	NH_4^+ probe	
		mV	$[\text{NH}_4^+]$, mM
Fresh water	10.1	46	$9.0 (\pm 3.6)$
Salt water	10.2	39	$11.7 (\pm 4.4)$

Headspace analysis of soil samples exposed to NH_3 did not yield any volatile organic compounds that were different from what was present in unexposed soil samples. This is not surprising, as NH_3 is unreactive toward organic compounds. It does dissolve in water to make a basic solution, so NH_3 could initiate base-catalyzed chemistry. However, there was no evidence for any significant chemical changes to volatile organic compounds.

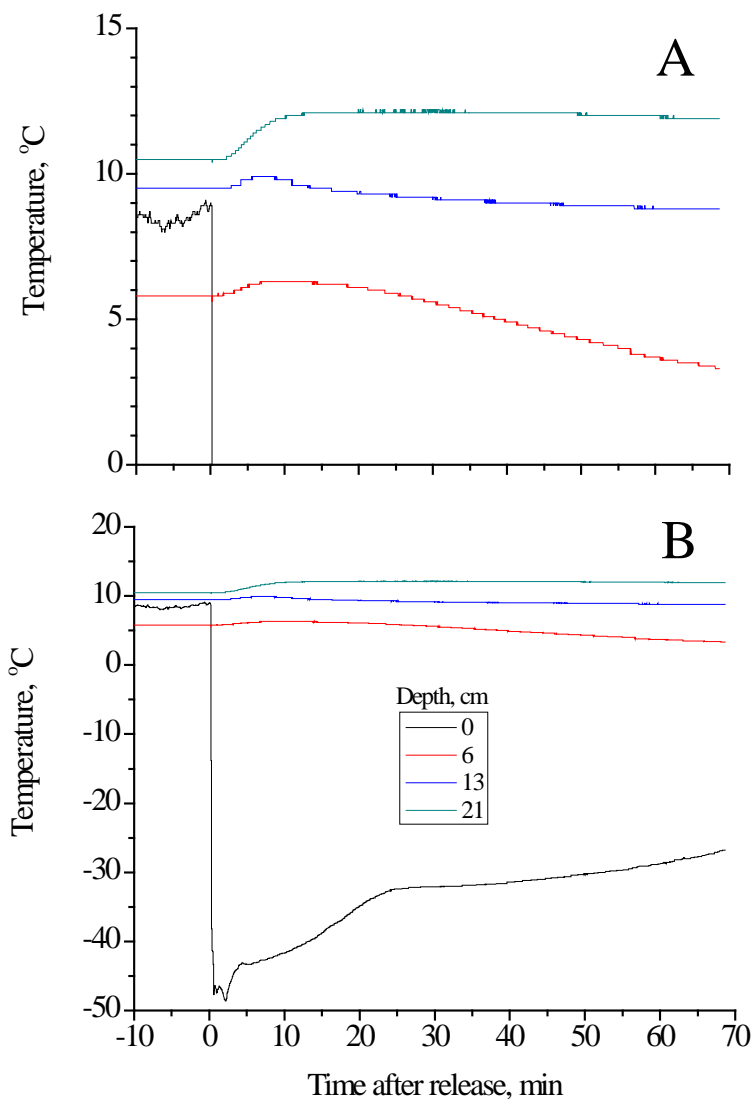


Figure 23. Soil Temperature during NH_3 Release #2
Thermocouples were placed at the indicated depth in clay loam at site 3 (3 m from release) with an expanded y-scale (A) and full y-scale (B).

3.2.3.5. Implications for Modeling

The NH_3 results overwhelmingly show that deposition will not irreversibly impact a highly concentrated plume. NH_4^+ was observed only in samples exposed to the liquid NH_3 pool, so soil at the surface exposed to $\text{NH}_3(\text{g})$ contained less than 0.001 mol NH_4^+/kg (the detection limit). Part of the reason for this observation is that NH_3 deposition is an equilibrium reaction, so its

retention in the soil depends on the $\text{NH}_3(\text{g})$ concentration above it, the soil pH and the kinetics of desorption. As samples were stored for many days after the releases before they were extracted, it is conceivable that NH_3 desorbed during shipment and sample storage. In any case, it is safe to conclude that deposition will slow the propagation of the plume, but it will do little to chemically attenuate it. The total NH_3 expected to be lost in the liquid pool area for the various soil types is shown in Table 10, which includes the following assumptions: (1) NH_3 penetrates 13 cm deep, (2) the liquid pool spreads uniformly to a 5-m radius, (3) the density of soil is 1.5 g/cm^3 , and (4) the results from site 3 represent long-term NH_3 deposition (Figure 20 and Figure 22). This provides an upper bound for the NH_3 lost due to deposition, and none of the soil types are expected to sorb more than 2% of the 2,000-kg release.

Table 10. Extrapolated NH_3 Deposition within a 5-m Liquid Spread

Soil	NH_3 sorbed (kg)	Percent of release
Clay	20.8	1.0%
Clay loam	20.2	1.0%
Clay loam wet	14.7	0.7%
Sandy loam	39.6	2.0%
Silt loam	26.7	1.3%

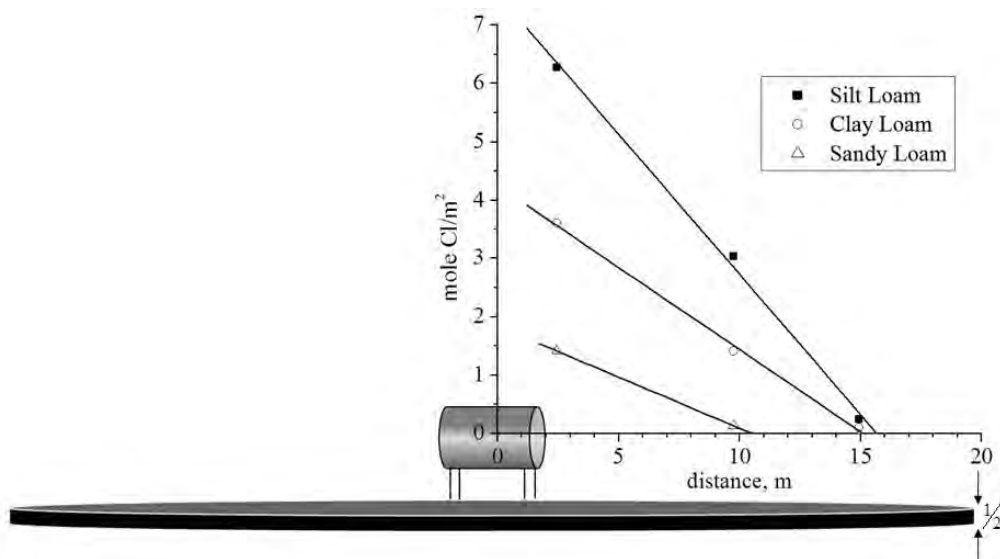


Figure 24. Data Used for Scaling up Cl_2 Deposition from Release #1

Cl_2 deposition, on the other hand, is expected to be an important loss term for dense plumes. While penetration into the soil is difficult to apply to undisturbed soils, it is safe to assume that the top layer of soil (1.27 cm) is loose enough to be available for reaction, so only results from the top fraction will be used to predict the impact of deposition on these 2,000-kg releases. Figure 24 shows the data used for this prediction, in which the y-scale is displayed in units of moles/ m^2 , assuming a penetration of 1.27 cm and a soil density of 1.5 g/cm^3 . The linear fits are assumed to adequately describe deposition as a function of the distance from the release, and these linear fits were integrated using Equation 2 in which C is the Cl_2 deposited per area, r is the distance from the release, and m and b are the slope and intercept of the linear fit, respectively.

$$\text{mass Cl}_2 = \int_0^r \frac{dC}{dr} dr = \pi r^2 \left\{ \frac{2}{3} mr + b \right\} \quad (2)$$

In Figure 25 the integration results show strong correlation between the topsoil volume fraction and the total amount of Cl_2 deposition for releases 1 and 3. As mentioned above, this is not surprising because the irreversible loss of Cl_2 requires a chemical reaction, and most soil mineral components are not reactive toward HOCl/OCl^- , whereas many organic molecules are reactive. The total amount of Cl_2 lost due to deposition is very large. Were the depression made of a high-organic-content soil, 20–30 % of the plume would have been irreversibly lost in the first 15 m. This indicates both that deposition is fast enough to significantly attenuate a Cl_2 plume and that soil has the capacity to react with significant quantities of Cl_2 . Typically, the top layer of soil has high organic content, so high-organic soils may be the most appropriate for modeling.

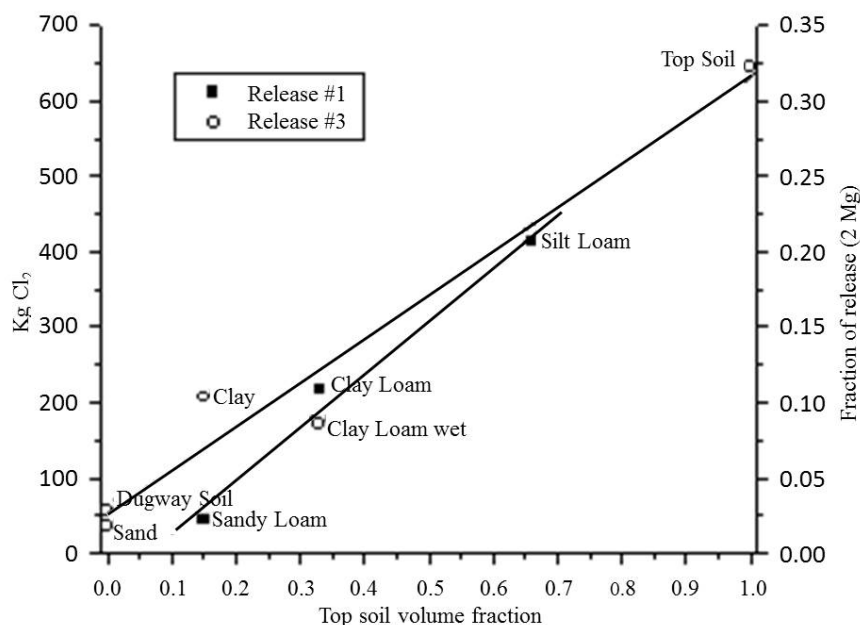


Figure 25. Interpolated Cl_2 Deposition within 20 m from Release
Values calculated from chloride concentrations as described in the text. This calculation is based on a Cl_2 penetration depth of 1.27 cm.

3.2.4. Conclusions

It is clear from the laboratory and field experiments that deposition to terrestrial surfaces can be a significant loss term for modeling dense Cl_2 plumes. It was shown through laboratory experiments that the reactive capacity of a variety of soil types was high enough to react a significant mass of Cl_2 from a concentrated cloud. The field experiments showed that under real-world conditions, deposition does account for significant losses to a Cl_2 plume. This research also demonstrated that deposition rates for modeling trace pollutants are not directly applicable to dense-TIC releases. Otherwise, NH_3 deposition would have been much more significant in the field experiments. Additionally, gas-phase measurements of AsH_3 's reaction with OH radicals were made to expand the current database for atmospheric degradation of TICs for HPAC. AsH_3 degradation is now being incorporated into the HPAC software package.

3.3. Material and Surface Phenomena (WUN # Q220L8A2)

3.3.1. Technical Introduction

The chemical/biological defense (CBD) community has the requirement to obtain the best technology for decontamination, detection and protection of people and assets in potential chemical/ biological warfare agent (CBWA) environments. An understanding of the fundamental interactions between chemical warfare agents (CWAs) and operationally relevant surfaces is critical to selecting and applying the best (most appropriate) technology for each of these capability areas. This understanding can be obtained only by conducting carefully designed experiments in each domain. As an infinite number of scenarios and situations face the CB defense community, it is impossible to experimentally examine all possible cases. This project supported a larger effort aimed at developing a methodology for theoretically predicting the interactions between selected molecules and silica. Work accomplished under this project provided experimental validation of theoretical predictions. The validated theoretical/experimental methodology will ultimately be applied to CWA–surface interactions for operationally relevant conditions—useful for predicting and evaluating fundamental interactions related to (a) evaluating new materials and barriers used in individual and collective protection; (b) identifying new/proposed decontamination approaches (e.g., understanding physical removal of agents from various materials such as painted surfaces); (c) expanding the knowledge base for simulant selection; and (d) understanding agent fate in the environment.

A variety of techniques have been used to experimentally measure enthalpies of adsorption (ΔH_{ads}), including spectroscopy (Hair 1977), isotherm measurements (Lee et al. 2002), calorimetry (Smith and Shirazi 2000) and inverse gas chromatography (IGC) (Conder and Young 1979). Of these techniques, IGC provides a robust method for making the measurement in the linear part of the isotherm. The other techniques are often not sensitive enough to measure ΔH_{ads} approaching zero surface coverage. The problem with measuring ΔH_{ads} at high surface coverage is that the measurement can be affected by adsorbate–adsorbate interactions (e.g., condensation in the pores). As the theoretical predictions are only for adsorbate–surface site interactions, the measurements must reflect the same physical phenomenon. IGC, because of the sensitivity of available detectors, is capable of making measurements that approach zero surface coverage. Furthermore, IGC measurements—like some of the other techniques—can be made with environmentally relevant humidity.

3.3.2. Methods

3.3.2.1. Inverse Gas Chromatography

Experimental measurements of the enthalpies of adsorption for the various probes on silica gel were made with IGC, a well-established method for investigating physicochemical properties of heterogeneous interactions (Conder and Young 1979). Detailed descriptions of experimental IGC methods can be found in the open literature (Thielmann 2004), so only a brief description is provided here. In a typical IGC experiment, a dilute gas-phase probe molecule (e.g., H_2O , NH_3 , DMMP) is passed over a stationary phase (silica gel) and the elution profile is measured. The net retention volume (V_n , volume of gas needed to elute the probe molecule) is directly proportional to the partition coefficient (K): $V_n = KA$, where A is the surface area (or mass) of the stationary phase (Katz and Gray 1981). The van't Hoff relation yields the enthalpy of adsorption (ΔH) by relating V_g (the net retention volume normalized to the stationary-phase mass) to the

column temperature (T_c). Equation 3 shows the relationship between V_g and ΔH , in which R is the universal gas constant (8.31415 J/K/mol) and C is a constant.

$$\ln \frac{V_g}{T_c} = -\frac{\Delta H}{RT_c} + C \quad (3)$$

Column flow rates were measured and maintained with a mass flow controller (MKS Instruments) or electronic pressure control in the gas chromatograph. V_g was determined from Equation 4, in which F is the flow rate, t_r and t_0 are the retention times of the retained and unretained probes, respectively, m is the mass of stationary phase, and j is the James–Martin correction factor, defined in Equation 5. For the conditions in these experiments where the inlet and outlet pressures (P_{in} and P_{out} , respectively) are almost equivalent, j is a negligible correction (i.e., $j \approx 1$).

$$V_g = jF \frac{(t_r - t_0)}{m} \frac{T_c}{273.15} \quad (4)$$

$$j = \frac{3}{2} \left(\frac{(P_{in}/P_{out})^2 - 1}{(P_{in}/P_{out})^3 - 1} \right) \quad (5)$$

3.3.2.2. Powder X-ray Diffraction

X-ray diffraction measurements were made using a Panalytical X-ray diffraction (XRD) system scanning 2θ from 10° to 70° . The cellulose crystalline phases (1α and 1β) were separated based on solubility. Cellulose 1β was dissolved in a 17.5% NaOH solution, insoluble cellulose 1α was filtered off, and cellulose 1β was finally precipitated by neutralizing the solution with H_2SO_4 . Cellulose was pressed into pellets and analyzed at room temperature ($\sim 20^\circ C$) and ambient humidity ($\sim 50\%$).

3.3.2.3. Chemicals and Gases

All chemicals were purchased from the indicated vendor and used without further purification unless indicated otherwise. Reverse osmosis water was generated in house. Dimethyl methylphosphonate (DMMP) was purchased from Sigma–Aldrich. Gases (He, N_2 , H_2 , Ar, UHP grade) were purchased from Airgas. Compressed air was made and purified in house with an Aadco pure air generator model 737. Ammonia was purchased from Union Carbide Corporation.

3.3.3. Results and Discussion

3.3.3.1. Cellulose Characterization

Cellulose was characterized with powder XRD and atomic force microscopy (AFM). However, AFM images of purified cellulose 1α and 1β exhibited no clear microcrystalline character and were inconclusive respecting surface composition. Conversely, XRD patterns showed clear differences between cellulose 1α and 1β . Figure 26 shows XRD patterns in which the results are in agreement with those in the literature (Zhao et al. 2007, Yan et al. 2008). The 002 planes yield peaks at 22.42° and 21.93° for the 1α and 1β cellulose samples, respectively. An additional peak in the cellulose 1β spectrum at 20.02° may be caused by acid- or base-catalyzed hydrolysis (Xiang et al. 2003). This should be further examined, if necessary, to determine potential artifacts in the adsorption measurements.

3.3.3.2. Adsorption on Silica

Further experimental characterization of DMMP adsorption on silica was characterized for method development purposes. Both sarin (GB) and DIFP pose significant hazards to laboratory technicians and researchers, so minimizing the concentrations and volumes needed is an important safety consideration. Additionally, smaller quantities ensure measurements will be made in the linear part of the isotherm so that interactions measured are not affected by probe molecules already adsorbed (e.g., condensation). The two primary injection strategies investigated were (a) sample loop injection and (b) liquid injection of a dilute solution.

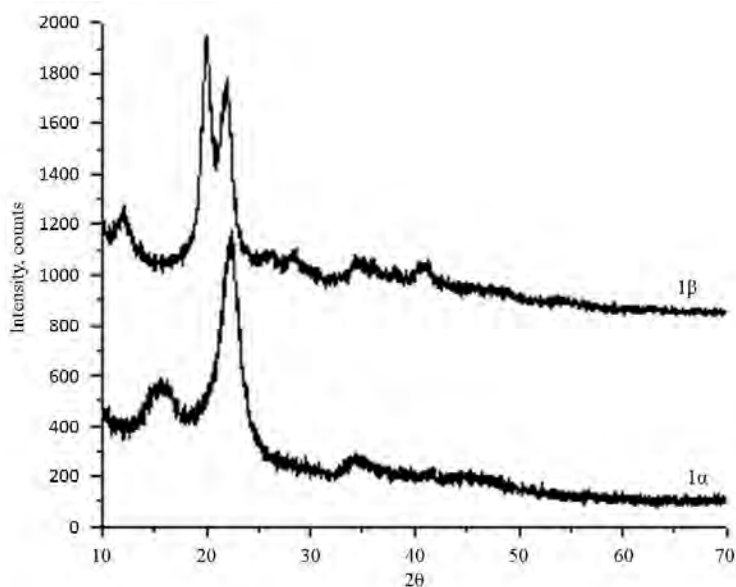


Figure 26. XRD Patterns of Cellulose I α and I β

Sample loop injections were made by bubbling a small flow of He through a reservoir containing liquid DMMP at $\sim 35^\circ\text{C}$ and further diluting this saturated flow with another He flow. This resulting DMMP/He flow filled a 90- μL Teflon sample loop held at $50\text{--}60^\circ\text{C}$, which was injected onto a silica gel column using a six-port Valco valve. An optional flow of methane was added to the DMMP/He flow to measure the dead time of the column. The column flow (10–15 mL/min) was sent to an FID to measure DMMP retention. The sample loop strategy allows small quantities of probe molecule to be injected on the column without a solvent; however, it does require working with neat material and carefully controlling the exhaust flow. Previous attempts at sample loop injection using the commercial IGC (Surface Measurement Systems) system failed presumably because there was too much “cold” tubing between the sample loop and the column. The results presented below were obtained using a commercial GC (HP6890N) fitted with a packed silica or cellulose column. This setup allowed heating all tubing after the DMMP reservoir to $50\text{--}60^\circ\text{C}$.

The second strategy, solvent dilution, was achieved by diluting a small amount of DMMP in a selected solvent and injecting 0.1 to 0.3 μL of the mixture onto the column using a GC autosampler. Injector pressures (and therefore column flows) were calibrated for each column over the range of column temperatures relevant for the experiment. This strategy minimized the risk of handling neat material, but it did introduce the possibility of solvent interference with the

measurement. Additionally, the quantity injected using this technique was known whereas in the sample loop injection method, the quantity injected must be calculated from the flow rates and reservoir temperature or the detector signal. For the experiments here, sample loop injection quantities were calculated from the signal using a calibration curve obtained from direct injection of diluted DMMP.

These two injection strategies, along with liquid injection of neat DMMP, were used to investigate adsorption on silica gel. Results in Figure 27 show the results, in which there is no significant difference between the solvent and sample loop injection strategies. Sample loop injections were placed on the x-axis using the integrated DMMP signals, but in this case, considerable error does not affect the conclusion because the same ΔH measurements indicate the solvent does not interfere. Liquid injections of neat DMMP exhibit slightly lower ΔH , but within the uncertainty of the measurement, this may not be significant. Additional experiments are required to reconcile any apparent discrepancies.

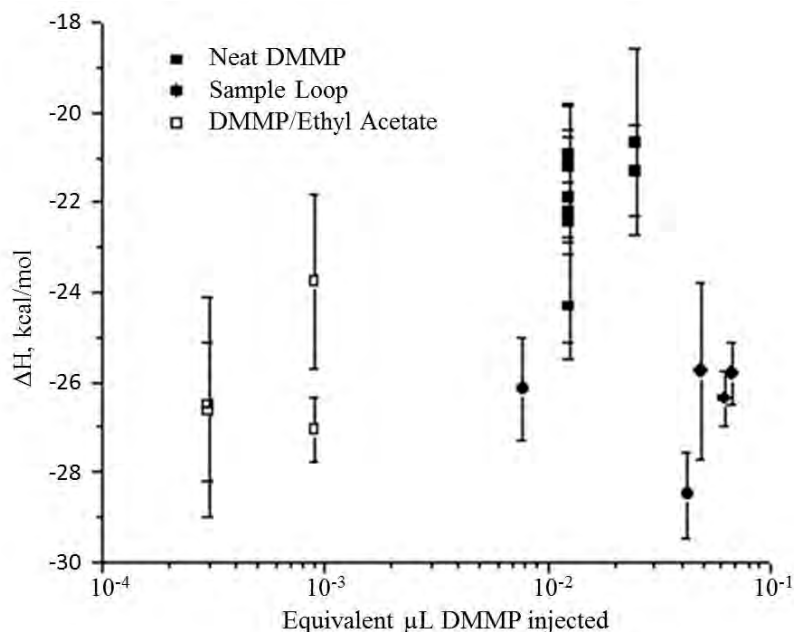


Figure 27. Enthalpy Measurements for DMMP on Silica Gel for the Indicated Injection Strategies

3.3.3.3. Adsorption on Cellulose

Initial experiments were performed using IGC to measure both the isotherm and the enthalpy of adsorption of DMMP on cellulose. During these initial experiments it was discovered that the cellulose needed to be conditioned at 100 °C for at least one hour. If the cellulose was not conditioned the DMMP injected did not desorb from the cellulose surface. In addition, heating the column to temperatures over 120 °C caused oxidation of the cellulose column (detected visually by a color change). These results are drastically different from adsorption of DMMP on silica. Silica columns were maintained above 180 °C for DMMP adsorption measurements. The adsorption isotherm for DMMP on cellulose (Figure 28) was measured on the conditioned surface at 40 °C. The isotherm was determined from the elution profile using the elution by characteristic point (ECP) analysis (Conder and Young 1979).

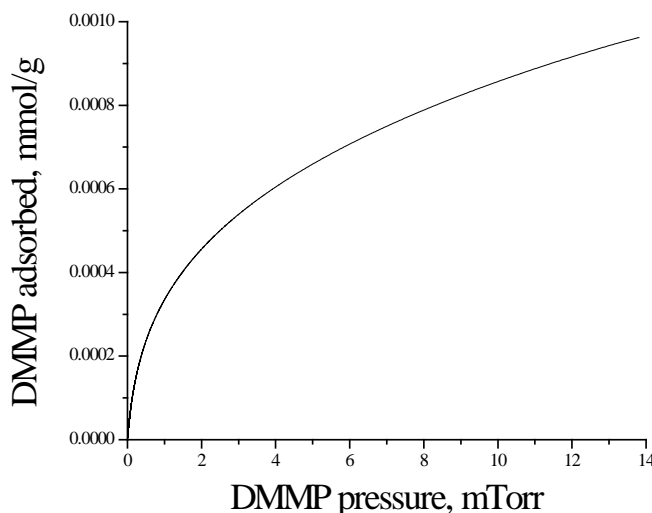


Figure 28. Isotherm of DMMP Adsorption on Cellulose at 313 K

ΔH for DMMP adsorbing on celluloses 1 α and 1 β were measured to determine whether the crystalline phases affect the measured interaction energies. Cellulose 1 α and 1 β were separated based on acid/base solubilities (described above), and results are shown in Figure 29, in which $\Delta H_{1\alpha}$ is -13.08 kcal/mol and $\Delta H_{1\beta}$ is -13.07 kcal/mol. There is no statistical difference between these measured enthalpies, indicating that surface functionality of celluloses 1 α and 1 β is the same, as expected. The increased retention volume (V_n) for cellulose 1 β compared with 1 α suggests that 1 β may contain a higher density of adsorption sites, but this needs to be confirmed through additional experiments. These measurements were made using liquid injections of neat DMMP and were not in the linear part of the isotherm. However, the agreement between these measurements does indicate that the crystalline phase does not affect surface composition.

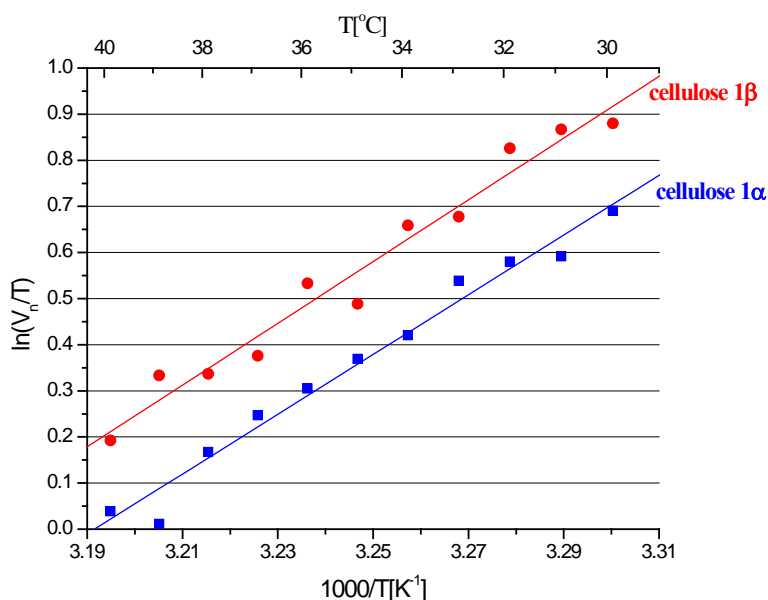


Figure 29. Enthalpy of Adsorption for DMMP on Cellulose 1 α and 1 β

As mentioned above, liquid and sample loop injection strategies were investigated to facilitate method development for agent experiments. Figure 30 shows results obtained for liquid injections of either neat (100%) DMMP or a 25% DMMP solution in the indicated solvent. A fourfold larger volume of liquid was injected for the diluted sample to achieve the same DMMP injection volume. These injections were not in the linear part of the isotherm for DMMP on cellulose, but the results clearly show that at these DMMP injection volumes, the presence of a solvent does little to affect the measurement. However, solvent effects in the linear part of the isotherm may be significant. To investigate this, sample loop injections were compared with liquid injections of diluted DMMP.

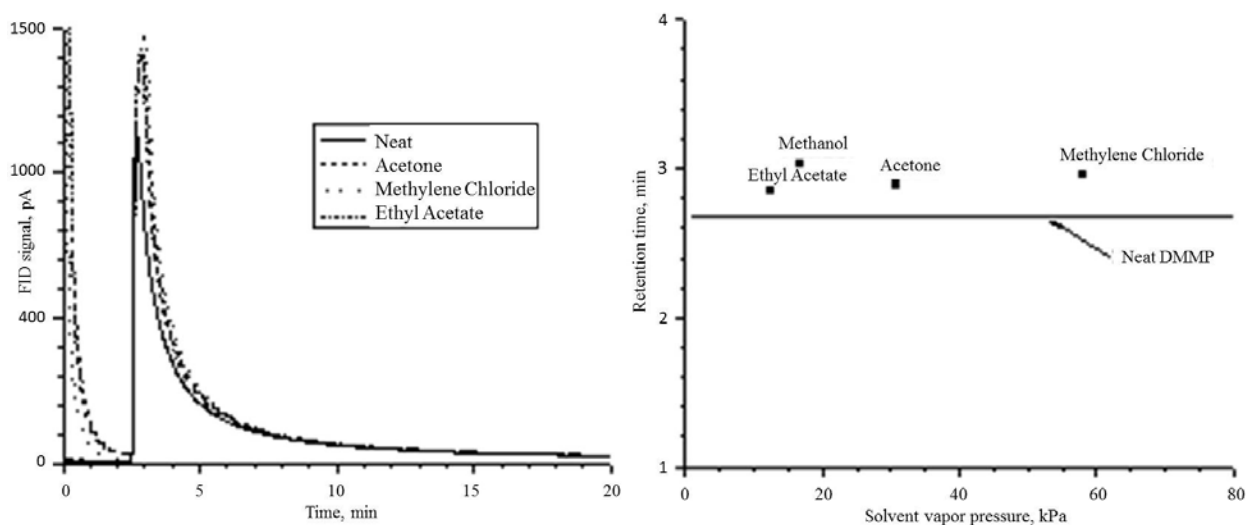


Figure 30. Comparison of DMMP Retention on Cellulose with Various Solvents
Left: elution profiles; Right: peak retention time vs. solvent vapor pressure.

Injection of more-dilute DMMP solutions on the cellulose column required increasing column temperatures (up to 100 °C). There was also less separation between the DMMP and solvent peaks (Figure 31). This was remedied by empirically fitting the tail of the solvent peak to a double exponential function and subtracting this interpolated baseline from the DMMP signal. This resulted in a very symmetric DMMP peak (inset Figure 31). The peak in Figure 31 is one of the less resolved; lower temperatures yielded better separation of solvent from DMMP peaks.

Figure 32 shows the temperature-dependent measurements for DMMP adsorption on cellulose using liquid injection with ethyl acetate and hexanes as solvents. The different solvents show excellent agreement between each other, and the vertical offset for the different DMMP injection volumes indicates that this may not be in the linear part of the isotherm. However, the symmetric peak shown in the inset of Figure 31 suggests the opposite. It is unclear, at this point, that these measurements represent adsorption in the “Henry” region.

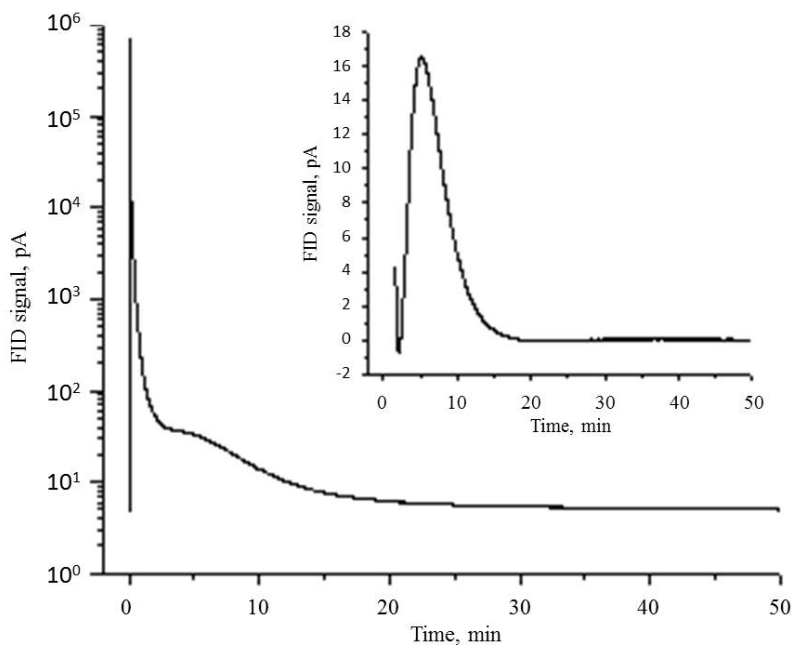


Figure 31. Elution Profile for DMMP and Ethyl Acetate on Cellulose at 98 °C
DMMP in ethyl acetate was injected at a 1/250 (v/v) dilution. Inset shows the DMMP elution after the interpolated ethyl acetate signal was subtracted.

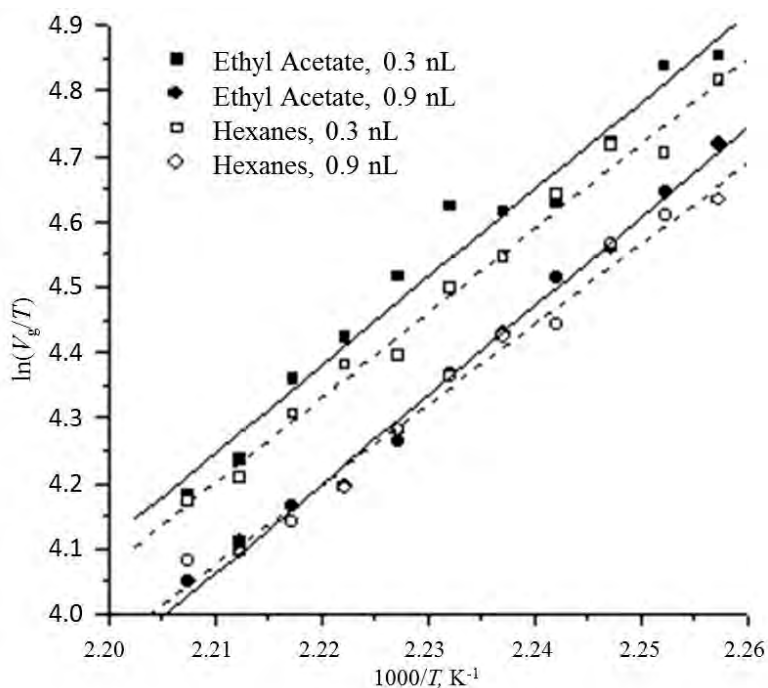


Figure 32. Temperature-dependent V_g for Dilute DMMP on Cellulose

Figure 33 shows ΔH measurements for all three injection strategies. Liquid injections of neat DMMP (closed squares) were able to achieve only a minimum injection volume of 7 nL, which was still in the nonlinear part of the isotherm. Sample loop injections (closed triangles) were able to achieve much lower DMMP injection quantities. The purpose of these experiments was

to determine the effect of solvents on the measurement in the linear part of the isotherm, and it is clear the DMMP–ethyl acetate injections follow a similar trend as the injection quantity is lowered, but the sample loop injection data shift to the left. This may not be significant since the sample loop measurements were placed on the x-axis by using the integrated DMMP signal. There may be considerable error in this scaling, so additional experiments need to be performed to obtain more-reliable values of DMMP injection volume for sample loop injection.

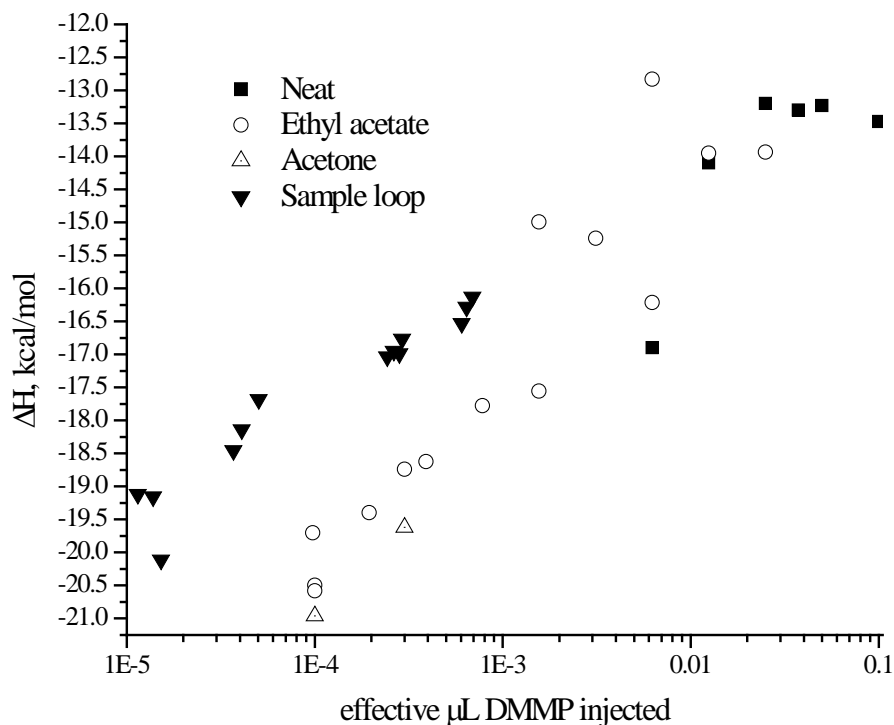


Figure 33. Comparison of Enthalpy Measurements for DMMP on Cellulose for the Indicated Injection Strategies

An additional point of concern regarding these measurements is that no asymptote is approached as the DMMP injection volume is reduced. This would be indicative of approaching the linear part of the isotherm, but the detection limit of the experiment precludes examining even smaller injection volumes. Elution peaks are much more symmetrical at low DMMP injection volumes, suggesting that adsorption is linear. Additional experiments are required to resolve this apparent discrepancy and determine the most appropriate enthalpy measurement for comparison with theoretical predictions.

DIFP was diluted into hexane to 10%, 2% and 1% by volume to facilitate injection of small quantities of DIFP on the column. Two different detection strategies were investigated for DIFP: GC/FID and GC/MS. Initially, DIFP–hexane mixtures were injected on an analytical GC column and detected with MS and FID. FID sensitivity for DIFP was significantly poorer than the MS detection based on signal-to-noise ratios. Therefore, MS was chosen as the detector. In addition, MS detection allows identification of products that form from surface reactions (if present).

Figure 34 shows an elution profile of 0.2 μL of 2% DIFP in hexane injected on a cellulose column (11.2 mg) held at 40 $^{\circ}\text{C}$. The elution profile was collected using multiple ion detection at m/z 58, 101 and 127. Injections scanning the full mass spectrum were also collected and revealed no evidence for surface reactions of DIFP on cellulose (data not shown). The peak at 0.12 min was from hexane (m/z 58) and the peak at 1.1 min was from DIFP (m/z 101 and 127). The solvent peak was taken as the column dead time for retention volume calculations. The DIFP peak for this and the other injections exhibited tailing, which suggests that these measurements were not in the linear part of the isotherm. Following each injection, the cellulose column was reconditioned at 50 $^{\circ}\text{C}$ for 3 min.

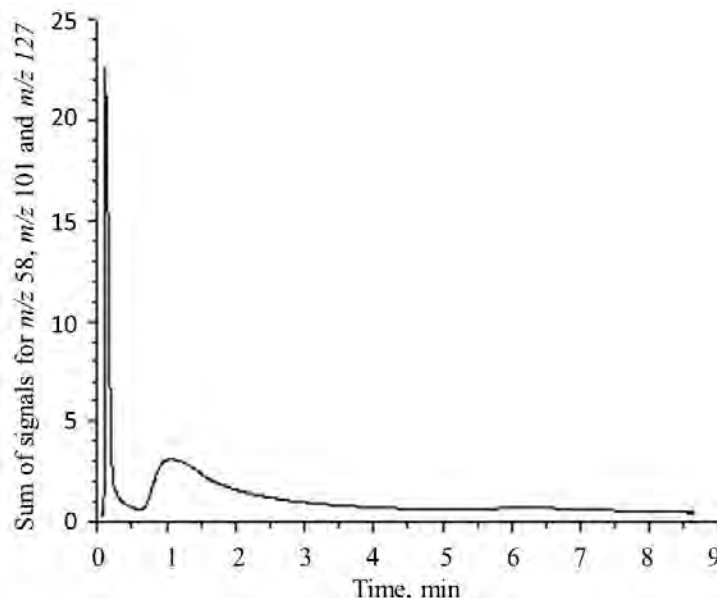


Figure 34. Elution Profile for DIFP/Hexane on Cellulose

Injections were repeated for column temperatures from 30 to 50 $^{\circ}\text{C}$, and the results are shown in Figure 35. The data fit a linear regression well, but it is unclear what caused the poorer fit at higher T . A duplicate measurement at 40 $^{\circ}\text{C}$ ($1000/T \approx 3.2$) at the beginning and end of the experiment show excellent agreement (the individual data points are not resolved in the figure).

From the slope of the linear fit, the enthalpy of adsorption of DIFP on cellulose is -13.4 kcal/mol. Additional measurements will be required at lower DIFP injection volumes to determine how the surface coverage affects the measurement. Figure 36 compares this measurement with measurements of DMMP on cellulose. DIFP shows a very similar result compared with DMMP at the same injection volume. Additional measurements of DIFP will be made to determine the dependence on injection volume.

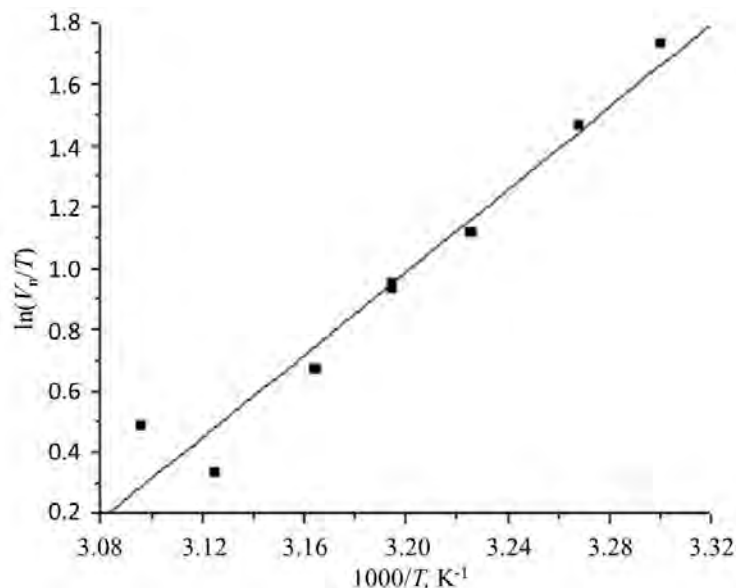


Figure 35. Temperature Dependence of DIFP Retention on Cellulose

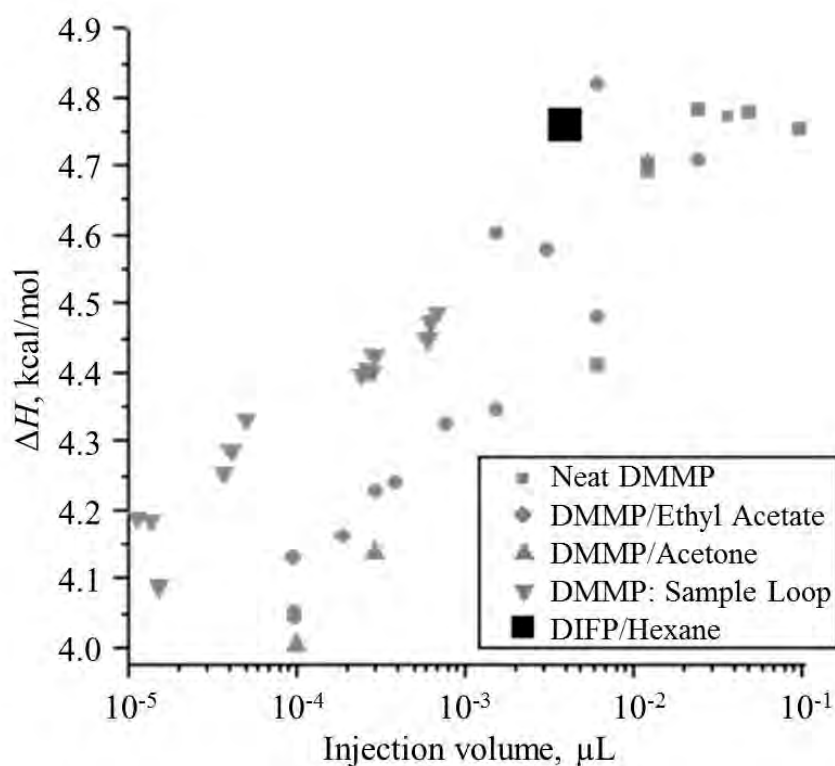


Figure 36. Comparison of DIFP and DMMP Enthalpy (ΔH) Measurements

3.3.4. Conclusions

At the conclusion of this contract, the theoretical predictions for adsorption enthalpies on cellulose had not been determined. However, Table 11 shows results from prior work on this project, in which there is excellent agreement among the theoretical and experimental adsorption

enthalpies for all studied probe molecule–silica interactions. This validates the theoretical approach and indicates that the IGC measurements were made in the linear part of the isotherm (i.e., the measurements predominantly represent interactions with the surface sites and not with other adsorbed molecules). Of particular interest is the excellent agreement among the adsorptions of dissimilar molecules. NH₃ (a base), NO (weakly interacting), and H₂O (a polar molecule) all show excellent agreement among experimental and theoretical results, which adds to the robustness of the methodology.

Table 11. Summary of Binding Enthalpies (kcal/mol) from Theory and Experiment

System	H₂O	NH₃	NO	DMS	DMMP
Theory Ensemble Average ^a	-13.48	-15.23	-3.94	-15.13	-19.67
Experimental	-13.6	-12.7	-4.03	-13.9	-22.4
(uncertainty)	(±2.8)	(±2.9)	(±0.35)	(±1.1)	(±0.9)
Expt'l Temp range [K]	330 – 370	323 – 383	243 – 263	340 – 375	453 – 473

^aEnsemble averages calculated at the midpoint of the experimental temperature range.

3.4. Summary/Intangibles

Significant technical accomplishments were realized in this task area regarding the effects of irreversible and reversible heterogeneous processes have on fate and transport of toxic chemicals. Measurements of Cl₂ deposition clearly show that heterogeneous loss to terrestrial materials can significantly attenuate a dense plume. Additional measurements are forthcoming that will examine in more detail the dependence of deposition on a variety of environmental conditions (light, humidity, water content, etc.). Measurements of reversible adsorption of small molecules to silica and cellulose surfaces provided critical data for validating a developing theoretical methodology for predicting the fate of chemical warfare agents on environmental substrates. In addition to these technical accomplishments, ARA also provided support for proposals, presentations, and publications. Those are summarized in the sections below in a list-style format.

3.4.1. Proposals

- Wrote a full proposal titled “Degradation of Perfluoroalkyl Compounds on Iron Using Microwave Activation.” The proposal was submitted to SERDP in response to their statement of need but was rejected for funding.
- Provided input and edited a proposal titled “In Situ Treatment of Fluorochemical Contaminated Soils and Groundwater.” The proposal was submitted through the EPA to SERDP and was a collaboration among several laboratories. The proposal was not funded.
- Submitted two white papers to the Defense Threat Reduction Agency (DTRA) in response to the services call titled “Binding of Chemical Agents to Complex Environmental Surfaces” and “Relating the Effects of Water on Heterogeneous Parameters to Bulk-Scale CWA Transport.” Both white papers were not invited for phase 2 submissions.

3.4.2. Meetings/Presentations

- Attended a workshop in Arlington, VA, on modeling dense-TIC plumes. The workshop primarily focused on potential chemical evolution of TICs, with some discussion of gas-phase and photochemical processes. It was concluded that (for the TICs discussed) heterogeneous deposition on terrestrial surfaces is a significant loss term that must be included. However, data are insufficient for one to predict the magnitude of this loss term.
- Prepared a poster presentation titled “Surface Diffusion of Dimethyl Sulfide on Silica Gel.” The poster was presented by Mike Henley at the Fundamentals of Adsorption Conference in Japan at the end of May 2010.
- Presented an oral talk titled “Deposition of Chlorine on Terrestrial Material as a Loss Mechanism for Dense Plumes” at the George Mason University Conference, 14 July 2010, covering a portion of the results from the Cl₂ releases.
- Attended a one-day workshop at Edgewood Chemical and Biological Center (ECBC) on nontraditional agents. The workshop focused on target compounds and experimental work that chemists at ECBC have accomplished regarding their interaction with a variety of materials. The workshop was classified.
- Presented a poster at the CBD conference in Orlando, FL, in November 2010 titled “Deposition of Chlorine on Terrestrial Material as a Loss Mechanism for Dense Plumes.”
- Presented a poster at the CBD conference in Orlando, FL, in November 2010 titled “Adsorption/Reaction of Diisopropyl Fluorophosphate and Dimethyl Methylphosphonate on Silica and Cellulose Surfaces.”

3.4.3. Publications

- Submitted a manuscript titled “Deposition of Chlorine as an Attenuation Mechanism for Dense Plumes” to the *Journal of Hazardous Materials*. The manuscript was rejected for publication and one referee suggested adding results regarding the effect of humidity on deposition before recommending it for publication. The other referee recommended only minor changes.
- A manuscript titled “Formation of Active Chlorine Oxidants in Saline–Ozone Aerosol” was published in *Aerosol Science and Technology*. This was a project performed in collaboration with Prof. Myoseon Jang of the Department of Environmental Engineering Sciences, University of Florida.
- A manuscript titled “The Effects of Active Chlorines on Photooxidation of 2-Methyl-2-butene” has been submitted for publication in *Atmospheric Environment*. This was a project performed in collaboration with Prof. Myoseon Jang of the Department of Environmental Engineering Sciences, University of Florida.

4. REACTIVE/RESPONSIVE MATERIALS

4.1. Introduction

Work done for the Reactive/Responsive Materials effort consisted of technical support for three DTRA-funded projects. These were Individual Protection, which focused on the development of a multifunctional material to replace the warfighter's current uniform; Chemical Agent Resistant Coatings (CARCs), which aimed to formulate a variation of a currently fielded military paint to improve resistance to CWAs; and Directed-Energy Enhanced Coatings, an attempt to use microwave or radio frequency sources in military radar to decontaminate CWAs absorbed into modified military paints. These three areas are outlined in separate sections below.

4.2. Individual Protection

The DTRA individual protection (IP or INDP) effort is an ongoing project to support multiple DoD requirements for enhanced protection of the warfighter. The project, which began in 2001, is striving to make improvements upon the currently fielded military uniforms such as the ABU used by the Air Force, the Navy Working Uniform (NWU) used by the Navy, or the Army Combat Uniform (ACU) used by the Army. In this report any and all are referred to by the designation Battle Dress Uniform (BDU) and typically consist of a 50/50 nylon–cotton fabric (NyCo) unless otherwise stated. Several improvements in BDUs were sought: 1) lowering the thermal burden of the garment, which has been criticized as an overwhelming encumbrance in some environments; 2) improved moisture transport—the material has to breathe; 3) mitigation of CBWA and toxic industrial compound threats; thus, alleviating the need for some of the MOPP (Mission Oriented Protective Posture) gear with which the warfighter is burdened, and 4) reducing the mass of the garment. The fourth factor is not necessarily required if the material can improve upon the first three. The focus of the work done for AFRL was on the third item, mitigation of CBWAs.

4.2.1. Technical Introduction

DTRA's requirement for IP is that the garment protect the wearer from permeation of a CWA challenge of 10 g/m² and reduce a biological threat by 99.99% ("4-log reduction"). Generally speaking, our work involved testing and down-selection of various compounds that could be used to create textiles that are biocidal and self-decontaminating. Eventually this spawned into multifunctional materials that are also hydro- and oleophobic. Flame-retardant (FR) treatments were also investigated; however, this avenue was eventually abandoned when a company that makes inherently FR textiles began to supply materials. AFRL was also supported in their task to identify methods necessary to treat the textiles. All textile treatments reported here require curing to form covalent bonds to the substrate. Through research conducted at AFRL, it was determined that the most efficient way to do this on a large or small scale was by MP attachment. Therefore, development of microwave treatments and specialty cavities and reactors was a significant part of this endeavor.

During the 2010 fiscal year, AFRL/RXQL was assigned several tasks to perform for the IP effort. The largest portion of the work involved the assembly, calibration, and demonstration of a production-scale microwave applicator, designed to treat amounts of textile from 15–500 yd by ~5 ft. Some of this work also included basic research to develop formulations that did not use

flammable organic solvents, but instead used aqueous-based emulsions coupled with surfactants. The purpose was to demonstrate feasibility of a large-scale microwave treatment of textiles, which could then be contracted to a textile mill to provide quantities of material to meet DoD requirements. This effort occupied roughly nine months of the fiscal year and was completed in early June 2010. The remainder of the year was spent either attempting to apply repellent treatments to non-textile surfaces or in the development and evaluation of novel biocidal textile treatments. Another area supported for IP, “Standard Method for Applying Spores to Surfaces,” will be discussed in the toxic and pathogenic biological aerosols section of this report.

4.2.2. Methods

For reference, the primary treatments used were Quat (a quaternary amine biocide, Figure 37), BA-1 (Figure 38, a hydantoin capable of storing Cl^-), and fluorosilane (FS, Figure 39). Each is attachable to substrates via covalent linkage by a siloxane tether.

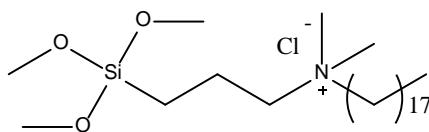


Figure 37. [3-(Trimethoxysilyl)propyl]octadecyldimethylammonium Chloride (Quat)

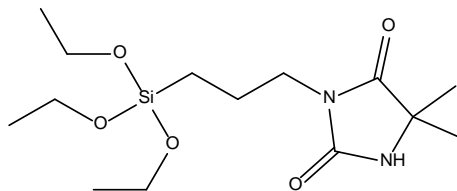


Figure 38. 2-(3-Triethoxysilylpropyl)-5,5-dimethylhydantoin (BA-1)

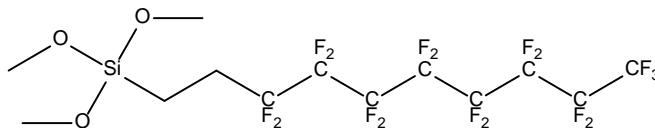


Figure 39. (Heptadecafluoro-1, 1, 2, 2-tetrahydrodecyl)trimethoxysilane (FS)

Static CAs were measured on a Krüss DSA 100 CA goniometer using water, *n*-hexadecane, diiodomethane, ethylene glycol, methyl salicylate (MeS), and tributyl phosphate (TBP). Full-scale microwave processing was carried out using a variable-power, 12-kW industrial system bought from Microdry, Inc., and modified for use on site. A WR-430 custom-built waveguide switch (Logus, Inc.) was used to connect the magnetron to a flat textile applicator containing an eight-pass meandering WR-430 waveguide. Certain chemical formulations for the treatments not included in previous reports per the wishes of AFRL and are not included here.

Microbiological assays were performed using one of two American Association of Textile Chemists and Colorists (AATCC) standard test methods; either AATCC 147, a parallel streak method, or AATCC 100, the liquid deposition method. Antimicrobial testing was performed using standard bacterial representative organisms. For Gram-positive evaluations, *B. atrophaeus* was used. For Gram-negative evaluations, either *Pseudomonas fluorescens* or *Escherichia coli* was used.

4.2.3. Results and Discussion

The first task performed for this effort was a live demonstration of a medium-scale treatment of materials for INDP principal investigator, Dr. Heidi Schreuder-Gibson. Waveguide components required to connect the industrial-scale microwave textile applicator to the 12-kW magnetron were designed and then purchased from a custom supplier, Gerling Applied Engineering, Inc (Figure 40). Upon arrival, the waveguide was used to connect the magnetron to the applicator. This required the support of three cantilevers, primarily because the waveguide switch weighed ~10 kg. Next, the applicator was energized and leak tested at power levels from 0.5–5 kW. Two problematic leaks measuring 5–15 mW/cm² were detected at flanges on the flexible portions of the waveguide. Because the leaks sometimes exceeded the exposure limit(s)¹ for microwave radiation, both areas of the waveguide were covered with aluminum foil to temporarily contain the field until the components could be returned to the manufacturer for repair. Results from the demonstration will be discussed in another section.

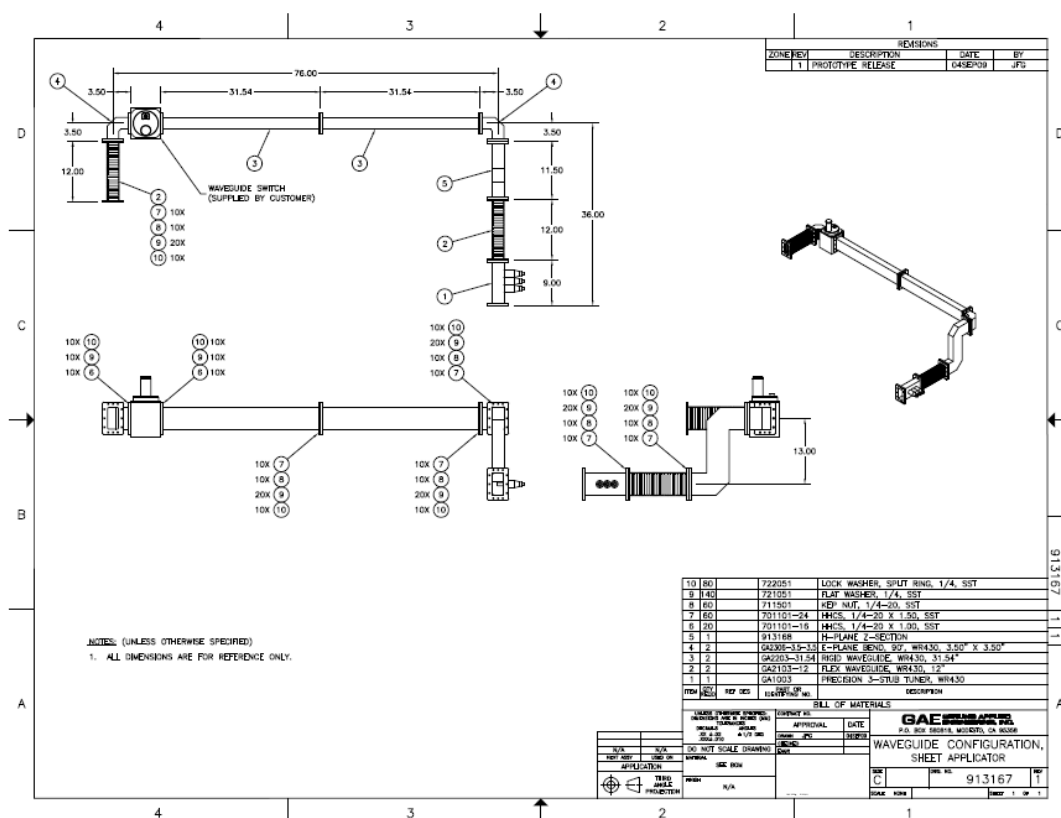


Figure 40. Waveguide Connecting Magnetron to Applicator

Meanwhile, parallel streak tests were performed on BA-1/Quat-treated Kermel® and Nomex/Kevlar antistatic (NKA) fabrics (Tencate, Inc.) in an acetone–water solvent system. These tests are metrics to qualitatively determine the biocidal efficacy of treated materials, and were done as preliminary examinations of treatments that could be used in the demonstration. Treatments

¹There is a debate over setting the permissible exposure limit for microwave radiation at 5 or 10 mW/cm². The historical value of 10 mW/cm² is based upon the level of heat flux of the human body in a normal sedentary state, and is roughly one-third of the flux density that can be detected as a sensation of warmth.

incorporating either one or three solution immersions were evaluated. Difficulties arose with BA-1/Quat combo fabrics because the oxidative potential due to the chloramide changes in the presence of Quat, rendering the test for oxidative chlorine unreliable. Parallel streak tests were more useful for determining the biocidal efficacy of samples and provided information required to down-select treatments. The samples listed in Table 12 are from a study of one immersion vs. three immersions in a 1% BA-1, 1% Quat, and 20% H₂O solution in acetone, cured in the microwave for 30 s at 100% power. All samples were left unchlorinated. Samples A and B were Defender-M® fabrics that received one or three dips respectively. Samples E and F both received three dips and were Kermel/spandex and NKA respectively. The samples did not kill the Gram-positive *B. atrophaeus* or Gram-negative *Ps. fluorescens* bacteria. The concentration of Quat was likely insufficient.

Table 12. Summary of Parallel Streak Tests for One and Three Immersions in 1% BA-1 and 1% Quat in a Water–Acetone Solution

Sample	Organism	Trial 1	Trial 2	Trial 3
Control Defender-M®	<i>B. atrophaeus</i>	+ ^a	+	+
RAH20100111A1		+	+	+
RAH20100111B1		+	+	+
RAH20100111F1		+	+	+
Control Defender-M®	<i>Ps. fluorescens</i>	+	+	+
RAH20100111A1		+	+	+
RAH20100111B1		+	+	+
RAH20100111F1		+	+	+
Control Kermel®	<i>B. atrophaeus</i>	+	+	+
RAH20100111E1		+	+	-
Control Kermel®	<i>Ps. fluorescens</i>	+	+	+
RAH20100111E1		+	+	+

^a For all parallel bacteria streak tests - denotes biocidal activity on the sample (no bacterial growth underneath the fabric), “zone” denotes biocidal activity underneath sample plus a zone of inhibition, and + denotes no biocidal activity underneath sample.

Table 13 below shows the results of the NyCo treated in Quat–water emulsions. These emulsions are of interest because they eliminate the need for high concentrations of a flammable solvent in the treatment process. Industrial textile mills are reluctant to work with flammable solvents in microwave processors due to the increased hazards associated with the treatment. Separate 5% and 10% solutions of Quat and of BA-1 were used to treat NyCo in single- and three-saturation series. The BA-1 treated samples were chlorinated using a 30-min exposure to a 10% solution of commercial bleach, which had a final concentration of ~0.5% sodium hypochlorite. For the Quat-treated samples, the three-immersion series revealed larger zones of inhibition. All BA-1-treated samples showed a zone of inhibition against *B. atrophaeus*. The sample treated with three immersions in 5% BA-1 showed no efficacy against *Ps. fluorescens*. This was an unexpected finding, and it is possible that this result could be erroneous.

Table 13. Parallel Streak Tests of NyCo Swatches Treated with Quat or BA-1 in Water

Quat	BA-1	Dips	Organism	Trial 1	Trial 2	Trial 3
Control Detergent		1	<i>B. atrophaeus</i>	+ ^a	+	+
5		1		-	-	-
		3		zone	zone	zone
10		1		-	-	-
		3		zone	zone	zone
	5	1		zone	zone	zone
		3		zone	zone	zone
	10	1		zone	zone	zone
		3		zone	zone	zone
Control Detergent		1	<i>E. coli</i>	+	+	+
	10	1		zone	zone	zone
Control Detergent		1	<i>Ps. fluorescens</i>	+	+	+
	5	1		zone	zone	zone
		3		+	+	+
	10	1		zone	zone	-
		3		zone	zone	-

^a See Table 12 for key

Table 14 below lists the results of parallel streak tests performed on fabrics treated using three immersions in either 10 or 20% BA-1 (RAH20091209A and B, respectively). The 20% outperformed the 10% fabric, as was expected due to the higher available chlorine content. The results of the RAH20091216A–E series are reported in Table 14. This series used 5%, 10% and 20% Quat treatments in a water–acetone solution and either one or three immersions. All samples showed some efficacy against *B. atrophaeus*, though none showed a clear zone of inhibition and none was decisively better than any of the others. A liquid deposition test was suggested to give a more definitive identification of the concentration of Quat that is most efficient as a biocide.

Table 14. Summary of *B. atrophaeus* Parallel Streak Tests Using Quat and BA-1

Quat	BA-1	Dips	Trial 1	Trial 2	Trial 3
0	0	0	+ ^a	+	+
	10%	3	-	-	-
	20%	3	zone	zone	zone
20% Quat		1	-	-	-
		1	-	-	-
10%		3	-	-	-
		1	-	-	-
5%		3	-	-	-

^a See Table 12 for key

Quantitative analysis of oxidative chlorine in the treated textiles was performed via iodometric back titration (Sun, 2003). Average concentrations of available chlorine are reported in Table 15.

Table 15. Summary of the Average Concentration (ppth) of Chlorine Available on Kermel® and NKA Materials

Fabric	Kermel®				NKA			
Sample	Control	RAH20091216G			Control	RAH20091216F		
Washes		1	10	20		1	10	20
Avg Cl (ppth)	0.409	3.410	3.563	3.923	0.696	3.423	4.222	4.228

A solution of approximately 0.5% sodium hypochlorite was added to each wash load for 1, 10 and 20 washes, and then the fabrics were allowed to air dry before being evaluated. Available chlorine increased on the Kermel® fabrics and was constant on NKA samples over the course of the washings. The durability of these fabrics was maintained throughout the 20-wash cycle.

Experiments were also conducted to determine the possibility of solubilizing FS in a water-surfactant mixture. Application of FS to fabric by microwave radiation previously required dissolving the FS in isopropyl alcohol (IPA). Because of its flammability, industrial textile providers will not work with IPA for large-scale applications. Several different surfactants were explored (Table 16) as possible components to improve the solubility of FS in water without increasing the overall microwave susceptibility of the solution.

Table 16. Preliminary Surfactant Tests

Surfactant	Failure Mode
Pluronic L-81	Too microwave active
Pluronic L-64	Too microwave active
Tergitol	Did not solubilize FS
Poly(ethylene glycol)	Too microwave active
Poly(propylene glycol)	Too microwave active
Palmolive	Did not solubilize FS
Aliquat 336	Not water miscible
Quat ([3-(trimethoxysilyl)propyl]octadecyldimethylammonium chloride)	Did not solubilize FS
Hexadecyltrimethylammonium chloride (HDTA)	Did not solubilize FS

Because no single surfactant from this list worked well enough on its own, three were chosen for further evaluation to look for a combination of surfactants that produces a beneficial synergistic effect. HDTA, Tergitol and Palmolive® were combined in a small percent-volume of IPA as a test formulation to be used on NyCo fabric.

NyCo fabric samples (10 cm × 10 cm) were moistened with the formulations in Table 17 and microwaved for three intervals of 5 s. After washing with copious amounts of water, samples were dried in a vacuum oven and challenged with droplets of water and brake fluid. Samples A–C were made with a single surfactant and repelled water but not brake fluid. Samples D–F, which were made with two surfactants, repelled both water and brake fluid. Durability studies were conducted on these three fabric swatches to evaluate their ability to retain their repellent characteristics. After 10 washes the water–substrate CA was 125.6° for D, 119.6° for E, and 123.4° for F, with standard deviation less than 4% for each sample.

Table 17. Surfactants Used in KMS20100204- FS Compatibility Tests on NyCo

Sample Suffix	Surfactants ^a		
	Tergitol (mg)	HDTA (mL)	Aliquat (mL)
A	600		
B		2.4	
C			1.2
D	300	0.3	
E	300		0.3
F		0.3	0.3

^a The surfactant(s) was/were dissolved in a final volume of 6.0 mL of water. Of this, 600 µL was added to a mixture containing 300 µL of FS and 600 µL of concentrated NH₄OH, before dilution with water to a final volume of 6.0 mL, application to a NyCo swatch, and microwaving for three 5-s-on-5-s-off cycles.

NyCo swatches of the same dimensions (A–I in Table 18) and swatches of Kermel® (J–R in Table 18) were used in tests to determine compatibility of BA-1 and of Quat with the attachment of FS. In step 1, BA-1 and/or Quat were dissolved in a final volume of 24 mL water; 2 mL was applied to a fabric swatch, which was microwaved for 30 s; the swatch was turned over and another 2 mL was applied and the swatch was microwaved for another 30 s. In step 2, 360 µL of FS, 1.2 mL of 0.1M NH₄OH solution and

indicated amounts of two surfactants were combined in a final volume of 12 mL water; a cycle of applying 2 mL to the swatch, microwaving for 30 s, and turning the swatch over was performed three times.

Table 18. Treatments Used in KMS20100208- Fabric Tests on NyCo and Kermel®

Sample Suffix	10% BA-1 (mL)	5% Quat (mL)	Surfactants		
			Tergitol (mg)	HDTA (mL)	Aliquat (mL)
A,J ^a	2.4 ^b		600 ^c	2.4 ^c	
B,K	2.4		600		1.2 ^c
C,L	2.4			2.4	1.2
D,M		1.2 ^b	600	2.4	
E,N		1.2	600		1.2
F,O		1.2		2.4	1.2
G,P	2.4	1.2	600	2.4	
H,Q	2.4	1.2	600		1.2
I,R	2.4	1.2		2.4	1.2

For Table 18 (a) A–I indicate NyCo; J–R indicate Kermel®; for (b) in step 1, BA-1 and/or Quat were dissolved in a final volume of 24 mL water; 2 mL was applied to a fabric swatch, which was microwaved for 30 s; the swatch was turned over, another 2 mL was applied and the swatch was microwaved for another 30 s. For (c), in step 2, 360 µL of FS, 1.2 mL of ~1.0 M NH₄OH solution, and indicated amounts of two surfactants were combined in a final volume of 12 mL water; a cycle of applying 2 mL to the swatch, microwaving for 30 s, and turning the swatch over was performed three times.

All of the above samples were washed nine times with Tide® laundry detergent. Clorox® was used instead of Tide® in a 10th wash cycle to chlorinate the BA-1. CA measurements on the dried swatches were taken with *n*-hexadecane. Analyzing these data made it clear that samples prepared with either BA-1 or Quat were not performing as well as fabrics prepared with both. Samples to which FS was attached with HDTA and Aliquat showed the best repellency.

Several swatches were submitted to AATCC 147 biocidal testing against *B. atrophaeus* to measure the efficacy of Quat loaded on the fabric. Control samples were tested with uncharged BA-1 (not chlorinated) so that it would not skew the results by acting as a secondary biocide. None of the fabrics tested showed biocidal activity. The chlorinated fabrics were evaluated by iodometric back-titration. None of the fabrics contained measurable quantities of chlorine, suggesting that BA-1 might not have attached to the fabric in these preparations.

Before using the textile applicator to treat large fabrics for demonstration, we evaluated the homogeneity of the microwave field, first with thermal paper and then with a 2-m piece of NyCo treated with poly(ethylene glycol) (PEG). The thermal paper was inserted into slots in the waveguide so that it lay perpendicular to the propagation of incident radiation. The magnetron was engaged at various power levels from 0.5–4.5 kW for durations of no longer than 90 s. At the lowest power levels, heating—seen as burns—occurred only at the ends of the first two passes of the waveguide. As power was increased, the paper began to burn along the entire length of the

waveguide; however, only the first four meandering passes were heated. The PEG-treated NyCo was inserted into the applicator as a single piece spanning all eight passes of the waveguide. PEG was selected because it absorbs microwave radiation very well; therefore, it provides good baseline information about how well the cavity heats materials that couple well to the induced field. The fabric did not burn, but dried in an intermittent pattern similar to what was observed on the thermal paper. This characteristic standing wave occurred at 9-cm intervals or roughly $\frac{3}{4}$ λ ($\lambda=12.2$ cm). This revealed that the standing waves were experiencing some degree of interference as they traveled through the waveguide. Whether this is caused by an impedance mismatch of the load or some intrinsic property of the waveguide was not determined. The burn pattern was consistent across each pass of the waveguide, but was observed to stagger slightly from one pass to the next.

Representatives from the Army Research, Development and Engineering Center (Natick), Stedfast, Inc., and Alexium, Inc., visited AFRL to observe the initial demonstration of the textile applicator. Approximately 15 m of Defender-M® and of Kermel® were submerged in a solution of 10% BA-1 and 5% Quat in water and pulled through the waveguide applicator by hand. The textiles passed through the applicator several times at a maximum power of 10 kW. They were then washed with Tide® and dried before the repellent treatment was applied as 5% HDTA, 5% Aliquat, 3% FS, and 10% NH₄OH. This formulation was consistent with those that were most successful on a small scale. However, the FS solution absorbed too much microwave radiation. The fabric was wet on one side and dry on the side nearer to the magnetron. Small samples were taken from both the Kermel® and the Defender-M® and chlorinated. A qualitative iodide test was used to show that the BA-1 had successfully adhered. Both materials tested positive, indicating the attachment and subsequent chlorination of BA-1.

Experiments were performed to determine a formulation for applying FS to fabrics, for which less surfactant is needed than previously used in large-scale tests. Large-scale tests conducted on Kermel® and Defender-M® fabrics found that energy absorbed by surfactants is regioselective, and that the radiation is not absorbed evenly across the textile. The original FS formulation contained 8% total surfactant. Other formulations tested after the initial large-scale demonstration included 1, 2 and 4% surfactant with and without a basic catalyst (Table 19). Swatches of Defender-M® and Kermel® used for this experiment were taken from the 15-m sheets that were treated with BA-1 and Quat during the large-scale demonstration.

Table 19. Contact Angles of Materials KMS20100301- Treated with FS and 1–4% Concentrations of Surfactant

Sample Suffix	Material	% Surfactant	Base	Contact Angle	
				Water	<i>n</i> -Hexadecane
A	Defender-M®	1%	10%	90.77°	0.00 °
B			---	93.00°	95.60°
C		2%	10%	85.83°	0.00°
D			---	74.23°	0.00°
E		4%	10%	84.37°	0.00°
F			---	81.33°	0.00°
G	Kermel®	1%	10%	148.82°	0.00°
H			---	145.96°	0.00°
I		2%	10%	148.99°	112.30°
J			---	157.38°	119.23°
K		4%	10%	152.41°	134.35°
L			---	146.15°	125.56°
M	Nomex	1%	10%	150.06°	141.59°
N			---	147.70°	146.96°
O		2%	10%	143.53°	134.39°
P			---	149.76°	138.48°
Q		4%	10%	147.54°	131.92°
R			---	152.10°	136.70°

Hydrophobicity of untreated Defender-M® (data not shown) was better than that of the treated fabric by about 32%. This may be due to remaining surfactant that was not rinsed out. Defender-M® displayed poor CAs for both water and hexadecane because the material had a permappress treatment, which does not allow siloxanes to polymerize on the surface.

As the Defender-M® and Kermel® fabrics were treated with BA-1 and Quat before the surfactant/FS treatment, biocidal efficacy of Quat-treated samples was tested against *B. atrophaeus* by AATCC Method 147. Samples taken from these swatches were not chlorinated before testing so BA-1 would not skew the results by acting as a secondary biocide. Defender-M® samples were effective against the *Bacillus* but the Kermel® samples were not. Samples were also taken from the same swatches and chlorinated to test against *Ps. fluorescens*. All of the samples tested failed to demonstrate biocidal activity. All of the chlorinated fabrics were quantitatively evaluated by iodometric back-titration. The Defender-M® and Kermel® tested positive for chlorination, affirming that the BA-1 attachment in the large-scale demonstration was successful.

A medium-scale test using 800-thread count bed sheets was conducted to test the feasibility of using a multi-mode microwave cavity to cure treated materials. For this test, a new bench-top textile applicator system was constructed from a commercial microwave oven. Narrow slots (~0.25 × 14 in) were cut along the top and bottom of the microwave's casing to allow for the passage of fabric through the body of the oven. These slots were lined with aluminum *L*-brackets

to smooth the sharp edges of the opening, preventing arcing in the system, and also to act as attenuators for the radiation. A mode mixer was built and installed to provide a more homogeneous electromagnetic field for uniform treatment of the fabric. Additionally, a reel system with a variable-speed motor was purchased, and was installed on a cart with the microwave to allow the fabric to be drawn through the applicator at a constant speed. This textile applicator can handle widths of fabric up to 1 yd depending on the thickness of the fabric as it must be folded into 12-in widths.

The 800-thread count sheets were cut into 1-yd widths, folded into thirds, submerged in an aqueous solution of FS and surfactant without a base catalyst, and irradiated in the bench-top textile applicator four times. After washing in a conventional household washing machine with water, the fabric from this experiment failed to repel water. We speculate that the surfactant used in the formulation may not have washed out of the cotton fibers since the fabric was partially dried during the treatment. Once the surfactant has dried on cotton it is nearly impossible to rinse. An experiment was conducted to determine if washing the fabric swatches in IPA immediately after microwaving would promote full removal of the surfactant before it becomes embedded in the textile. The samples were treated with FS in either 4% or 2% surfactant, with and without a base catalyst, and washed with 100% IPA, 50% IPA in water, or 30% IPA in water (Table 20).

Table 20. Effect of Method of Removing Surfactant from Fabrics on Contact Angles

Sample Number KMS20100322-	Surfactant	Base	% IPA in Wash	Contact Angle	
				Water	<i>n</i> -Hexadecane
A	4%	10%	100	140.38°	125.55°
B			50	138.55°	129.68°
C			30	140.63°	134.73°
D		0%	100	138.97°	0.00°
E			50	143.64°	0.00°
F			30	142.06°	111.77°
G	2%	10%	100	130.68°	120.02°
H			50	138.07°	123.28°
I			30	128.25°	125.10°
J		0%	100	131.87°	0.00°
K			50	132.99°	0.00°
L			30	150.69°	0.00°

The samples that were washed in 50% IPA and 30% IPA turned the solution cloudy. Samples were then rinsed with copious amounts of water until foaming subsided. The most significant effects on repellency involved whether or not the base was used—not the wash method.

When nanoparticle (NP)-modified fabrics (provided by Massachusetts Institute of Technology) were treated with FS without the basic catalyst it was noted that adding surfactants caused no observable differences in hydro- or oleophobicity. Further studies were done to determine whether the base-catalyzed reaction confers better durability than the reaction in water. Fabrics

received from Army Research, Development and Engineering Center (Natick) had been treated zero, one, two, three or four times with NPs. All fabric swatches were treated with FS; even the ones that were not treated with NPs. The NP-treated materials did not show appreciable improvement over the blank material when treated with FS (Figures 41 and Figure 42). A durability study gave mixed results. All of the materials demonstrated lower CAs after five washes, but there was no correlation between the number of NP coatings and the water or oil repellency. NyCo performed better than Defender-M®, possibly because the NyCo samples have a tighter weave. There was a trend in the oleophobicity of the base-treated NyCo after five washes; that is, the fewer treatments of NPs the higher the CA of *n*-hexadecane.

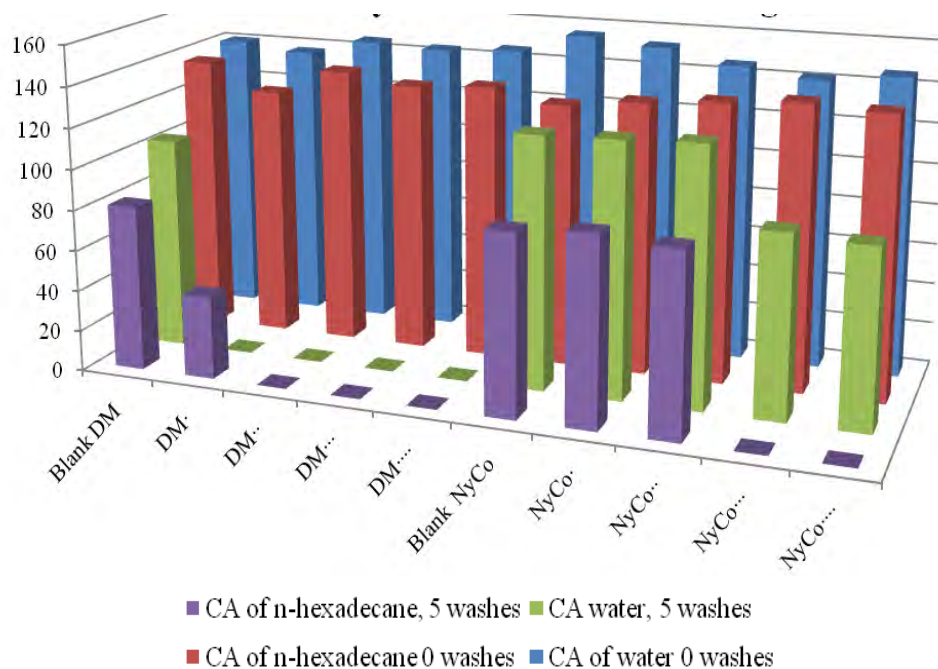


Figure 41. Water-Catalyzed FS Coating on Nanoparticle-Coated Fabrics

North Carolina State University (NCSU) sent samples of Nylon ripstop camo, a Nylon felt, and a Nylon film to AFRL for FS treatment. This was used as an opportunity to compare the effectiveness of the aqueous FS treatment to the previous method of treating fabrics in IPA. Formula one consisted of 3% FS, 10% base, and 87% IPA. Formula two consisted of 3% FS, 4% surfactant, 10% base and 83% water. There was no appreciable difference in performance between formula one and formula two except with the Nylon film, which displayed poor CAs over all, but improved water repellency after being treated with formula one. (Figure 43 and Figure 44)

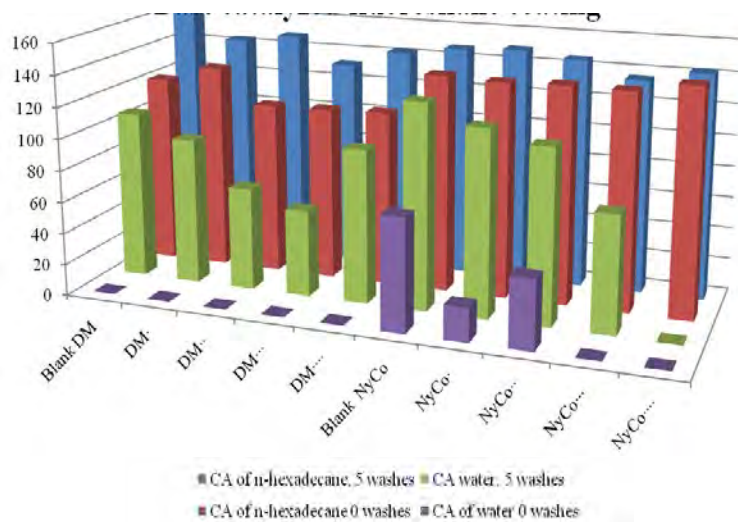


Figure 42. Base-Catalyzed FS Coating on Nanoparticle-Coated Fabrics

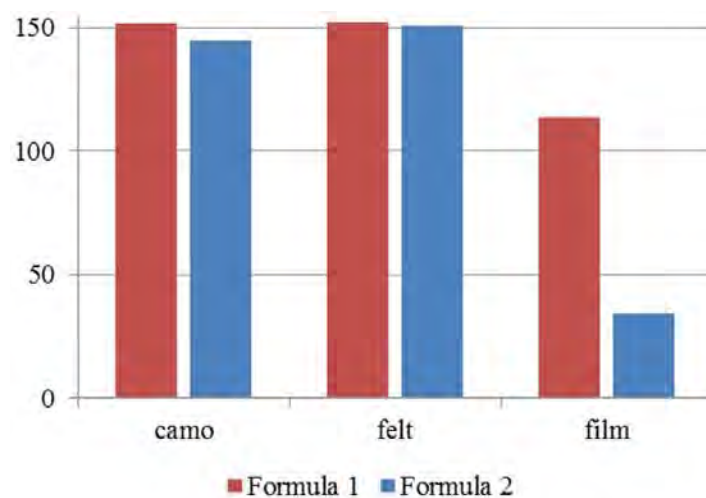


Figure 43. Contact Angle of Water on FS-Treated Nylon

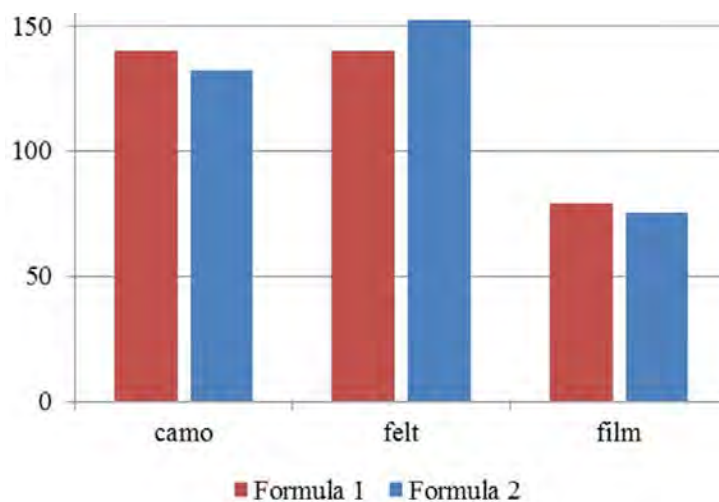


Figure 44. Contact Angle of *n*-Hexadecane on FS-Treated Nylon

Following the initial demonstration of the large-scale textile applicator, a second demonstration with this applicator was scheduled for May/June. This demo was conducted at the NCSU College of Textiles, in collaboration with members from Alexium, Inc. Before the tech demo at NCSU, our efforts focused on refining the chemistry to be used on a much larger scale (~100 yd). In previous experiments, an aqueous-based formulation was identified; however, this formulation did not perform as well as the organic solvent-based formulations. Two key differences of the aqueous-based formulations were 1) *n*-hexadecane drops began to absorb into the fabrics after extended exposure time and 2) dimethyl sulfoxide and jet fuel were absorbed much more readily.

To resolve this problem, previous data were analyzed and a revised approach was taken. A wide range of surfactants were tested including anionic, cationic, and nonionic surfactants of different HLB (hydrophilic-lipophilic balance) values. Additionally, emulsifying agents were considered, e.g., alcohols that are partially soluble in water. From this battery of experiments, approximately five combinations were identified (including the previous aqueous formulation). Refined compositions of these formulations were then analyzed and a newly optimized aqueous formulation was selected. This formulation produced materials with properties that were as beneficial as the previously used organic solvent-based materials. For example, the new formulation repelled water, jet fuel and hydraulic fluid for over 24 h, and *n*-hexadecane drops did not absorb into the fabric for over 72 h.

Previously, the surfactant/FS formula used a combination of surfactants that dissolved the FS extremely well and produced a clear solution. However, an emulsion is more desirable, as this produces a lower-surface-energy material and, thus, higher CAs with *n*-hexadecane. Several formulations were tested, and all yielded textiles with higher CAs than were observed using the original recipe. The final formulation we decided to use in the second technology demonstration held the FS in suspension with minimal precipitation of the FS or surfactant. However, the surfactant left the fabric feeling stiff and waxy with visible discolorations where the surfactant had solidified. It was determined that this waxy residue cannot be avoided by changing the formula.

Several attempts were made to wash the remaining surfactant out of the fabric using polar and nonpolar solvents. Additional methods made use of higher temperature, length of wash time, and sonication. On a small scale (10-cm squares), the best results were obtained using nonpolar solvents. Larger fabrics (9 × 1.5 yd) were washed using the method that produced the best results on a small scale. When the large fabrics were washed, the waxy texture remained. All fabric samples tested, whether they had a waxy residue or not, demonstrated CAs with *n*-hexadecane of 130° or greater. Getting rid of this residue is an aesthetic desire.

The large-scale technology demonstration at NCSU was completed in June. With the help of Jeff Krauss (NCSU), scientists from Alexium and AFRL were able to treat 120 yd of Defender-M® woven and 100 yd of Defender-M® knit with BA-1, Quat and FS, and treat an additional 150 yd of cotton and 50 yd of NyCo with FS only. We successfully treated all fabrics with the aqueous-based formula and washed out the surfactant to achieve repellent, residue-free fabrics (Figure 45).

Following the successful tech demo, experiments were performed that focused on applying the currently used textile treatments to alternative materials. A solution of FS in IPA applied to nylon

and leather portions of boots (intact boot, ABU style) was microwaved with positive results. This required defeating certain problems presented by the rubber soles, mainly their absorption of most of the applied microwave energy, which left the other parts of the boots unheated. To address this issue, the soles of the boots were wrapped in aluminum foil tape before microwaving. Shielding the lossy soles allowed other portions of the boots to absorb microwave radiation. After treatment, the leather and Nylon materials repelled *n*-hexadecane for more than 24 h.



Figure 45. Samples Taken from the Tech Demo at NCSU Demonstrating Repellency against Hydraulic Fluid and Kerosene

Other materials were then treated with FS, which included glass, stainless steel, polypropylene, Nylon (non-textile) and PET (polyethylene terephthalate). Results from the repellency testing on these materials are displayed in Figure 46. Three samples of each material were treated with a solution of FS in IPA, except for the steel, which was treated in both IPA and an aqueous surfactant formula. CA data are reported as percent improvement versus the untreated sample.

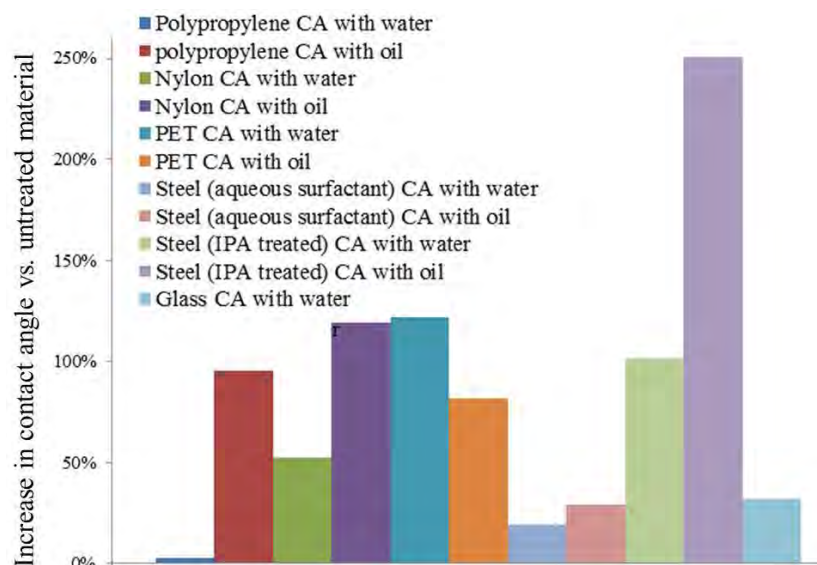


Figure 46. Repellency Data for Several Materials Treated with FS (Data Are Given As Percent Improvement Versus the Untreated Controls)

After the successful demonstration of large-scale microwave textile treatment, the focus of the work at AFRL shifted to the development and evaluation of new biocidal textiles. Experiments were performed with alternative antimicrobial compounds as well as existing compounds that have biocidal potential and that could be attached to fabrics using microwave technology. Ten different polyphenolic compounds were sprinkled on Luria agar as powders and tested against *B. atrophaeus* and *Ps. Fluorescens* using AATCC 147 as a guideline. The results are shown in Table 21 along with some representative pictures (Figure 47 and Figure 48). A “yes” result indicates that there was a zone of inhibition in which the bacteria did not grow around the powder.

Table 21. Biocidal Properties of Candidate Phenols; “Yes” Indicates a Zone of Inhibition

	<i>B. atrophaeus</i> 20100811	<i>Ps. fluorescens</i> 20100811
Gallic acid	yes	yes
8-Hydroxyquinoline	yes	yes
Phloroglucinol	yes	yes
Pyridoxal+HCl	yes	yes
Pyridoxine	yes	yes
Resveratrol*	yes	no
Salicylaldoxime	yes	inconclusive
Tannic acid	no	no
Tetrabromobisphenol A	no	inconclusive
Xanthurenic acid	yes	inconclusive

*See Figures 47 and 48.

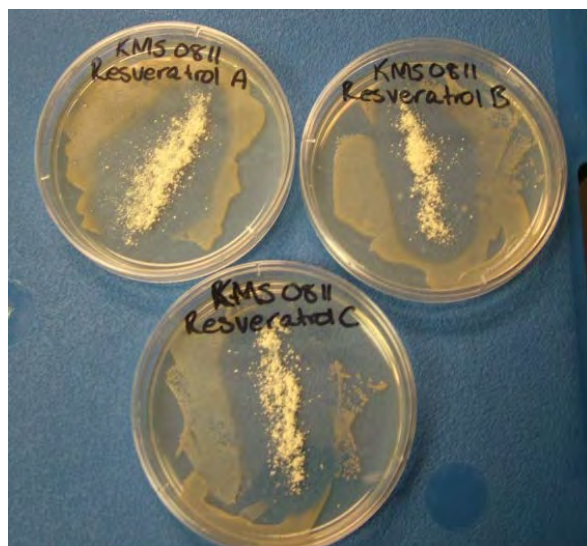


Figure 47. Resveratrol Powder Plated with *B. atrophaeus* Showing a Zone of Inhibition

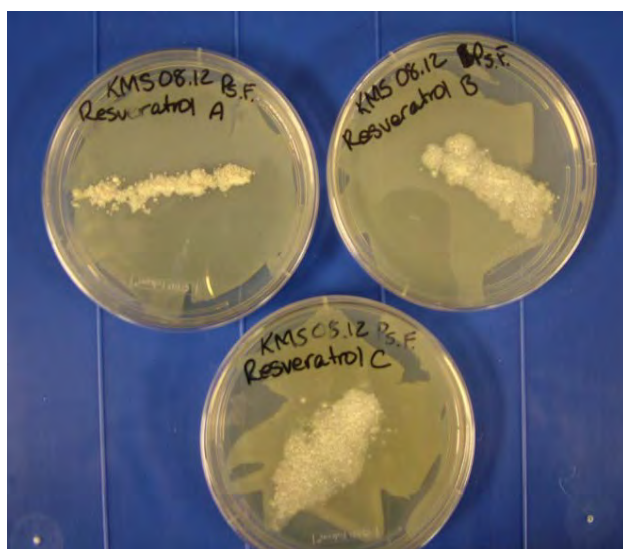


Figure 48. Resveratrol Plated with *Ps. fluorescens* Showing No Zone of Inhibition

Promising phenols were attached to NyCo fabric using MP addition with (3-glycidoxypentyl)-trimethoxysilane (GPTMS). Swatches of the treated textile were washed and dried before plating. The results are shown in Table 22 and Figures 49 and 50. The width of the zone of inhibition around the fabric indicates that the polyphenol compounds leached into the agar. Durability tests were performed to determine if the compound would remain on the fabric after five washes. Test results are displayed in Table 23.

Table 22. Biocidal Properties of Phenols Attached to NyCo with (3-Glycidoxypentyl)trimethoxysilane; “Yes” Indicates a Zone of Inhibition

	<i>B.</i> <i>atrophaeus</i>	<i>Ps.</i> <i>fluorescens</i>
Gallic acid	yes	no
Hydroxyquinoline*	yes	yes
Phloroglucinol	yes	no
Pyridoxal+HCl	yes	no
Pyridoxine	yes	no
Resveratrol	yes	no
Salicylaldehyde	yes	yes

*see Figures 2.13 and 2.14

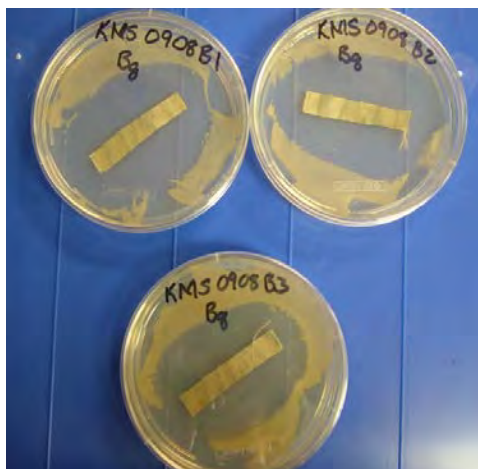


Figure 49. 8-Hydroxyquinoline Crosslinked to Fabric by (3-Glycidoxypentyl)trimethoxysilane Plated with *B. atrophaeus* Showing a Strong Zone of Inhibition

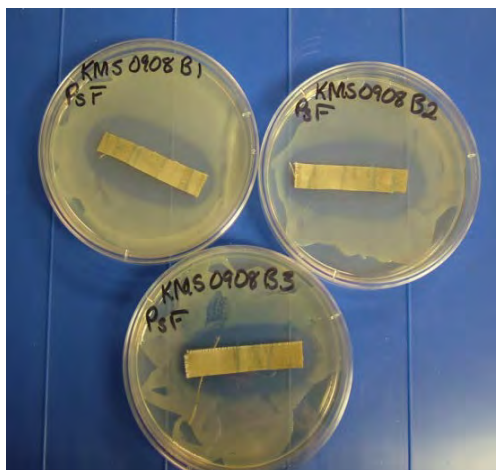


Figure 50. Same Sample Plated with *Ps. fluorescens* Showing Zone of Inhibition

In summary, none of the polyphenolic compounds attached with GPTMS was durable enough to kill *Ps. fluorescens* after five washes. 8-Hydroxyquinoline (8HQ) and salicylaldehyde were the strongest performers since they were the only candidates that killed Gram-positive and Gram-negative bacteria; however, the salicylaldehyde treatment was not durable. 8HQ demonstrated the largest zone of inhibition either because it has the greatest tendency to leach into the agar or because it has the strongest antimicrobial nature.

Table 23. Durability Test Results for Candidate Biocidal Textiles after Five Washes; “Yes” Indicates a Zone of Inhibition

	<i>B. atrophaeus</i>	<i>Ps. fluorescens</i>
Gallic acid	no	no
Hydroxyquinoline	yes	no
Phloroglucinol	no	no
Pyridoxal+HCl	no	no
Pyridoxine	no	no
Resveratrol	slight	no
Salicylaldehyde	no	no

Resveratrol was retained for future studies since it showed selective efficacy against the Gram-positive organism. It is possible that the antimicrobial nature of these compounds is derived from the acidity of the phenol. Cross-linking the phenolic compound with the epoxide by forming an ether bond ties up one or more phenol reactive sites. This technique was compared to the traditional attachment method of applying compounds to fabric by covalently bonding with tetraethyl orthosilicate (TEOS). Results shown in Table 24 were similar to those seen using GPTMS.

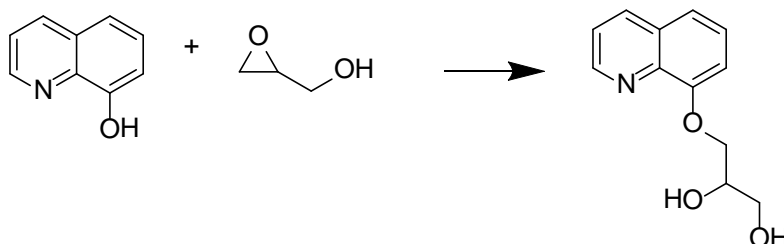
Table 24. Biocidal Tests Results for Phenols Attached to NyCo via TEOS

	<i>B. atrophaeus</i>	<i>Ps. fluorescens</i>
Gallic acid	yes	no
Hydroxyquinoline	yes	yes
Phloroglucinol	yes	no
Pyridoxal+HCl	yes	no
Pyridoxine	inconclusive	no
Resveratrol	yes	no
Salicylaldehyde	no	no

Due to its efficacy and durability, 8HQ and several derivatives of 8HQ were investigated to determine the method of antimicrobial activity as well as different ways to attach it to fabric. This and several other 8HQ derivatives were tested in powder form against *B. atrophaeus* and *Ps. florescens* and are shown in Table 25. Figure 51 is a representative reaction converting 8HQ into a diol derivative via reaction with glycidol.

Table 25. Biocidal Efficacy of 8-Hydroxyquinoline and Derivatives

Alternate quinoline powders	<i>B. atrophaeus</i>	<i>Ps. fluorescens</i>
8-(2,3-Dihydroxypropoxy)quinoline	yes	Yes
5-Amino-8-hydroxyquinoline Dihydrochloride	yes	Yes
5,7-Diiodo-8-hydroxyquinoline	slight	No
8-Hydroxy-5-quinolinesulfonic Acid	yes	Yes

**Figure 51. 8-(2,3-Dihydroxypropoxy)quinoline, a Derivative of 8HQ Prepared from Glycidol**

It is suspected that 5,7-diiodohydroxyquinoline did not perform as well as the other compounds because it has very low water solubility. The compounds in Table 25 were attached to fabric by three different methods: 1) the compound was combined in solution with TEOS and attached to the fabric using MP addition, 2) the 8HQ compounds were combined in solution with GPTMS and microwaved onto the fabric to test whether or not the epoxy ring would open and bind to the 8HQ derivative (then allowing the silane moiety to polymerize and form a coating around the fibers), or 3) the GPTMS was microwaved onto the fabric and the solutions of 8HQ derivatives were added in a second step. Results are shown below in Table 26.

Table 26. Biocidal Efficacy of 8-Hydroxyquinoline Derivatives Attached to NyCo by Three Different Methods

	TEOS crosslinker		GPTMS crosslinker			
			1 step		2 steps	
Quinoline Derivatives	<i>Bg</i>	<i>Psf</i>	<i>Bg</i>	<i>Psf</i>	<i>Bg</i>	<i>Psf</i>
8-(2,3-Dihydroxypropoxy)quinoline	yes	no	yes	no	slight	no
5-Amino-8-hydroxyquinoline Dihydrochloride	no	no	yes	no	yes	yes
5,7-Diiodo-8-hydroxyquinoline	slight	no	yes	no	yes	no
8-Hydroxyquinoline-5-sulfonic acid	yes	no	yes	no	yes	slight

To probe 8HQ's mechanism of biocidal activity, we explored other Schiff bases that are not quinolines. 3-Aminopropyltrimethoxysilane (APTS) was microwaved onto cotton and NyCo in a preliminary step, and salicylaldehyde and, separately, pyridoxal were added to the primary amine to allow the Schiff base to form as seen in Figure 52 and Figure 53.

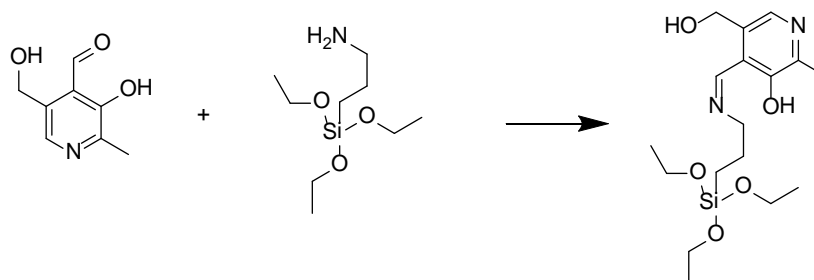


Figure 52. Reaction of Pyridoxal with APTS to Form a Schiff Base

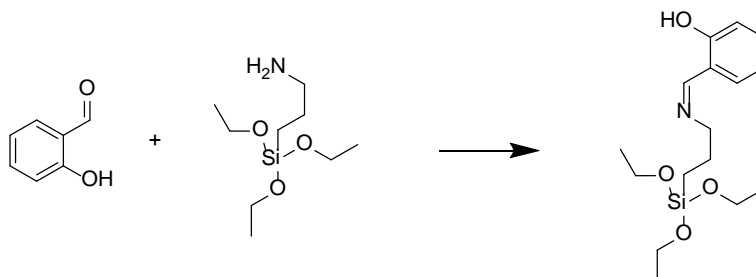


Figure 53. Reaction of Salicylaldehyde with APTS to Form a Schiff Base

These fabrics were parallel streak tested using AATCC 247 against *B. atrophaeus* and *Ps. fluorescens*. The fabric prepared with salicylaldehyde killed both species of bacteria but the fabric prepared with pyridoxal failed to kill either.

Again probing the biocidal mechanism of 8HQ, an experiment was performed to determine if binding 8HQ to the fabric by alternative (non-siloxane) means would preserve the antimicrobial nature of the material. Diiodo-8HQ was combined with cotton that had been treated with sodium hydroxide. An 8-in² piece of cotton was stirred with 200 mL of a 1 M NaOH solution. The fabric was rinsed, dried and treated with the diiodo-8HQ under anhydrous conditions in dimethyl sulfoxide and left overnight (Figure 54).

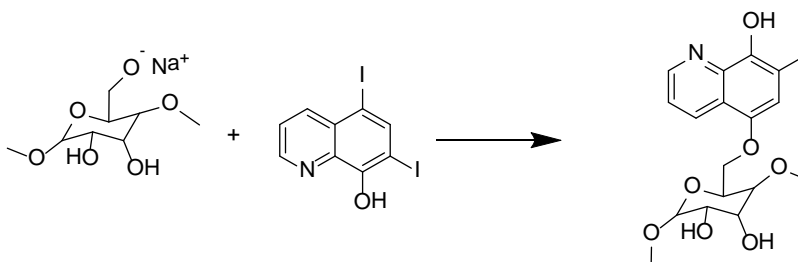


Figure 54. Proposed Reaction of Sodium Hydroxide and Cotton with Diiodo-8HQ

The treated cotton failed to kill *B. atrophaeus* or *Ps. fluorescens*. This is most likely due to failure of the 8HQ derivative to attach to the cotton.

An experiment was performed to determine if making a Schiff base by means of combining a carboxaldehyde with a primary amine is a viable way of covalently binding the Schiff base to the fabric. This method also allows for binding a copper cation or a silver cation, which may demonstrate secondary antimicrobial functionality. The cotton was treated with APTS and then

with 8-hydroxyquinoline-2-carboxaldehyde (8HQ2CA) (Figure 55). As the imine bond is known to hydrolyze in the presence of water, the fabric was submerged for a week in a beaker of water that was replenished with fresh liquid three times during the test. The fabric was then tested against *B. atrophaeus* and *Ps. fluorescens* using AATCC 147. The fabric did not show any activity against *Ps. fluorescens*, but did kill—with a zone of inhibition—*B. atrophaeus* (Figure 56).

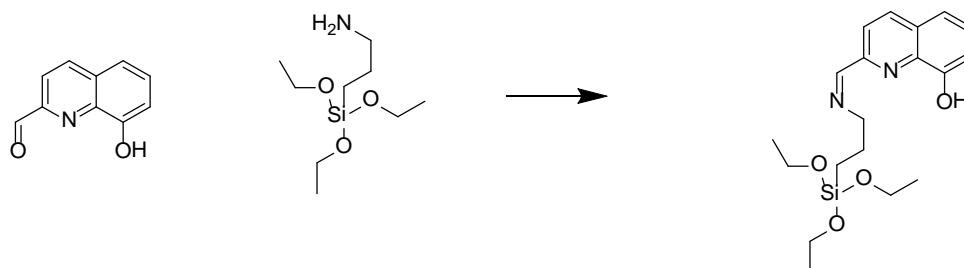


Figure 55. Cotton Treated with APTS, Then 8-Hydroxyquinoline-2-carboxaldehyde

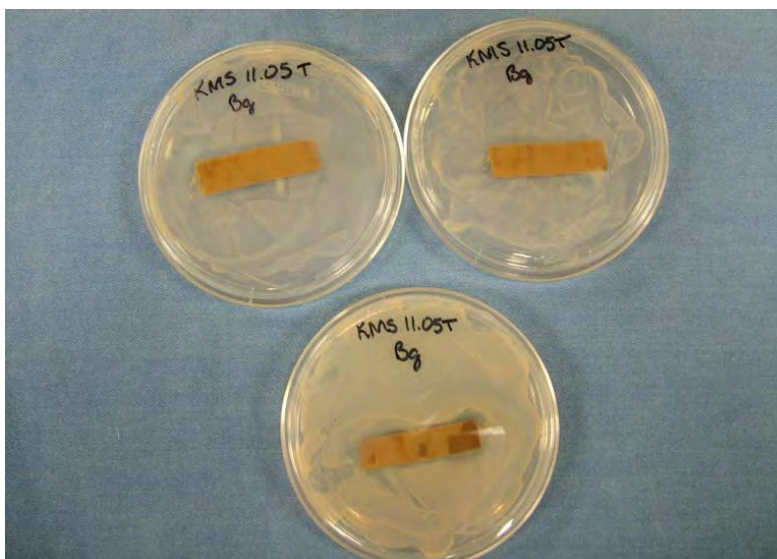


Figure 56. *B. atrophaeus* Killed by 8-Hydroxyquinoline-2-carboxaldimine-treated Cotton

Another experiment was performed to determine if the antimicrobial effect of 8HQ bound to fabric was due to an enzymatic pathway or simple lysing of the cell. Fabric treated with APTS and 8HQ2CA was tested against two enzymes, laccase and lysozyme, that act outside the cell. The laccase enzyme assay is based on UV-visible absorbance by syringaldazine. The treated substrate reacts with any enzyme left after reaction with the indicator is completed. The treated fabric reduced the amount of laccase enzyme as observed by the remaining syringaldazine. The enzyme laccase is a copper-containing molecule, and Schiff-base antimicrobials are known to complex with copper. The binding energy between copper and the Schiff base may be higher than the binding energy between the laccase enzyme and copper. The enzyme assay conducted with lysozyme failed to show any reaction with the fabric treated with APTS and 8HQ2CA.

The antimicrobial activity of phenols and Schiff bases was explored to measure the effect of complexing these chemicals with copper has on their antimicrobial activity. Tannic acid, 8HQ and 8HQ hemisulfate were allowed to dissolve in water, to which two molar equivalents of cupric sulfate was added. Cotton fabric was placed in the solution, which was heated to 60 °C for 30 min to allow the cotton fibers to swell with the solution. The cotton was then microwaved until just damp and further dried in a vacuum desiccator. The samples were cut in half, and half of the fabric was microwaved with a solution of TEOS in IPA. This was done to determine if intercalating the chelating agent with silanes will bind the compound to the fabric and give better durability for repeated washing. The fabric was tested for antimicrobial efficacy using AATCC 147, washed five times, and tested again for antimicrobial efficacy before an assay was performed with laccase enzyme. All of the treatments tested (Table 27) killed *B. atrophaeus*, but none killed *Ps. fluorescens*. Whether the fabric was treated with TEOS or not, durability after five washes was good enough to retain efficacy against *B. atrophaeus*.

Table 27. Biocidal Efficacy of Cotton Fabric Treated with Either Schiff Base or Phenol, and Complexed with CuSO₄

Sample	Chelating Agent	TEOS	<i>Ps. fluorescens</i> after 1 wash	<i>B. atrophaeus</i>	
				1 wash	5 washes
Blank	none		-	- ^a	-
KMS20101130A	Tannic Acid	TEOS	-	+	+
KMS20101130B			-	+	+
KMS20101130C	8-Hydroxyquinoline	TEOS	-	+	+
KMS20101130D			-	+	+
KMS20101130E	8-Hydroxyquinoline Hemisulfate	TEOS	-	+	+
KMS20101130F			-	+	+
KMS20101130G	none	TEOS	-	+	+
KMS20101130H			-	+	barely +

^a See Table 12.

An enzyme assay (Figure 57) was done on three fabrics to look for an effect of chelated cupric sulfate on the action of laccase. The three fabrics chosen were treated with cupric sulfate, tannic acid, and TEOS; 8HQ; and cupric sulfate with TEOS (with no chelating agent). A sample with just cupric sulfate was run as a control to see if it would react by itself or if the chelating agents, which are known antimicrobials, are responsible for the decrease in enzyme activity.

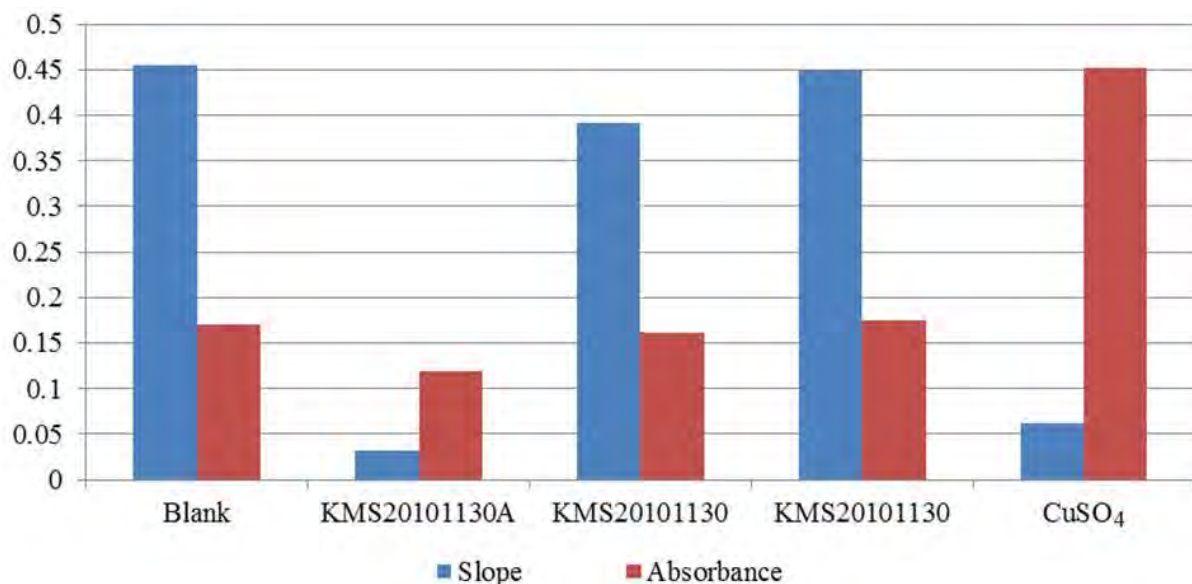


Figure 57. Laccase Enzyme Assay Showing Absorbance at 2 Min and Slope of Absorbance between 0.07 and 0.14 s

It should be noted that the control sample with cupric sulfate did not turn pink; it stayed blue and turned cloudy. A pink color indicates that laccase has reacted with syringaldazine. The high absorbance may be due to the turbidity of undissolved copper salts. Sample KMS20101130A, the only fabric sample to react with the laccase enzyme, did not turn pink and had the lowest absorbance. Sample A was treated with tannic acid and TEOS. Tannic acid was the only chelating agent tested that had available binding sites able to pull copper out of the enzyme.

4.2.4. Conclusions

A scaled-up demonstration for MP textile treatment was conducted in two phases: 1) Two 15-m lengths of fabric (Defender-M® and Kernel®) were treated at AFRL. The biocidal compounds were added successfully; however, the second treatment incorporating the hydro/oleophobic component did not work due to regioselective heating from the surfactant. 2) A second demonstration at NCSU realized the successful treatment of 120 yd of Defender-M® woven and 100 yd of Defender-M® knit with BA-1, Quat and FS, and an additional 150 yd of cotton and 50 yd of NyCo with FS only. This was done using surfactant solutions, which ultimately left no residue on the finished materials. Aqueous-based FS formulations were identified that allow textiles to be treated without the use of flammable organic solvents. ABU boots and several non-textile materials were treated with FS and displayed excellent hydro/oleophobicity vs. control materials. Later in the year, biocidal efficacy and durability of several phenolic and polyphenolic compounds attached to textiles were investigated. 8HQ and several of its derivatives have been effective against both Gram-positive and Gram-negative organisms. An enzyme assay was conducted- to determine the biocidal mechanism of the phenols and Schiff bases attached to textiles; however, the results were inconclusive. Investigations with these compounds are ongoing.

4.2.5. Follow-on Work

The direction of this effort is decided year-to-year by Drs. Schreuder–Gibson and Owens, based on the overall needs of the project and available funding. Therefore, some questions that arose during the past year (and years before) may not make the statement of work for successive years. The task to scale up a microwave treatment process was successfully completed, and future work in this area will be the responsibility of the textile industry. AFRL should continue to research novel biocidal textiles, while determining which new formulations or combinations of older compounds are most suitable for general or specific use. A liquid deposition test is suggested to give a more definitive answer about what concentration of Quat is most efficient as a biocide. Formulations to attach FS and BA-1 to textiles are now complete; however, due to durability problems with some inherently FR textiles such as Defender-M®, it may be worthwhile to revisit processes to create FR materials. The team should also continue to investigate the biocidal mechanism for 8HQ and its derivatives, as these compounds have proven themselves to be both effective and durable.

4.3. Chemical Agent Resistant Coating

4.3.1. Technical Introduction

The CARC project has made great strides in the past year, developing several superhydrophobic and superoleophobic coating formulations. Work at AFRL, the Army Research Lab (ARL), the Naval Research Labs (NRL), and ECBC has culminated with the development of four coatings based on the MIL-PRF-85285 specification, which demonstrate repellency against HD, VX and other agents for up to two weeks.

The motivation for this work is improved chemical defense for military assets. As most CWAs are oil-based, decontamination is extremely difficult if these agents contact and leach into a paint surface. CARCs are used on many military assets; however, they are particularly important in protecting aircraft and ground vehicles from the threat and use of CWAs. The Department of Defense policy for CWA-contaminated assets is that they are not allowed to return to the United States or any NATO country until the assets are thoroughly decontaminated (CWA undetectable by analysis). This presents a serious strategic problem, for example, contamination of a large number of cargo aircraft (i.e., C-130s or C-17s) by a persistent CWA could greatly affect military movement and supply chains. Additionally, the cost of some of these assets exceeds \$150 M, making replacement impractical or unlikely. If a repellent coating can be developed that would prevent sorption of CWAs, decontamination becomes a much simpler process.

Technical efforts at AFRL initially consisted of attempts to modify metal oxides for incorporation into CARC. Modifications included both repellent and reactive moieties. In addition to modifying particles, neat additives were also explored as potential modifiers for coating systems; for example, FS was sometimes used as a neat additive to impart repellency in a coating. Catalytic additives received from NRL were incorporated into CARC and investigated using both repellency and reactivity studies. Reactivity studies generally included challenges of 2-chloroethyl ethyl sulfide (CEES), 2-chloroethyl phenyl sulfide (CEPS), and demeton-S (DS). Repellency studies challenged coatings against the physical simulants TBP and MeS.

This project is currently in transition, and some of the effort has centered on identifying a contractor, DoD sponsor, and system program office to assist with a technology demonstration. Over the past year, the direction of research began to focus on developing a super repellent MIL-PRF-85285 APC (Advanced Performance Coating), rather than further researching potential reactive additives. Because of this, the technical work at AFRL changed from formulating in-house coatings to performing CA and surface energy analyses of the coatings developed by ARL. This work was largely carried out by 1Lt. Eileen Shannon, AFRL/RXQL. The role played by the ARA contract staff was largely administrative, and far less involved than in the two previous years of this project.

4.3.2. Methods

Static CA and surface energy measurements were made on a Krüss DSA 100 goniometer. In all studies unless otherwise noted, CAs were performed five times, to gain a reliable average for every sample. In some cases, simulant CAs were required. In these instances, TBP was used as a physical simulant for VX and MeS was used as a physical simulant for HD. To determine surface energies, CAs of diiodomethane and ethylene glycol were performed. Surface energy measurements were calculated using the DSA-100 software using both the Owens–Wendt and Extended Fowkes algorithms.

Coatings were purchased from PPG, Inc., or Deft, Inc., in two separate systems: a base resin and an activator resin. These components were mixed in a 1:1 (w/w) ratio. Additives were typically incorporated in a 3% (w/w) ratio versus the total metal oxide content. If neat additives were being used, they were added in various amounts after the addition of the metal oxides. Methyl ethyl ketone/methyl amyl ketone (MEK/MAK) 50/50 (v/v) (~1.0 mL) was added dropwise until the viscosity of the coating was comparable to room-temperature maple syrup. A curing catalyst, dibutyl tin dilaurate (5.0 μ L), was added last. The solution was mixed using a hand-held electric homogenizer. The coatings were applied to aluminum panels using a 0.020-in drawdown bar. Coatings were usually synthesized in pairs, making both PPG and Deft versions for testing. Punches (1.0 cm²) of the cured panels were made using a manual punch press. Repellency of coatings was tested by measuring the amount of simulant that absorbed into the coating. Circular punches (1.0 cm²) of each coating were cut and then weighed to the nearest 0.1 μ g on a microbalance. A 1.0- μ L droplet of simulant was deposited in the center of each punch, and the punches were weighed again. The punches sat exposed to air at ambient temperature (~21 °C) for 24 h, at which point they were re-weighed. The punches were then washed with 10 mL of flowing water dispensed from an electronic autopipette. Punches were blotted dry using lint-free cellulosic wipes. The samples were weighed a final time to determine the amount of simulant left in the coating.

The reactivity study procedure was developed in 2009, but underwent modification in CY10. To study reactivity, a 2-h and a 48-h study was typically completed. The 2-h studies challenged the coatings with CEES and DS, and the 48-h studies used CEPS and DS as reactive simulants. The lower vapor pressure of CEPS (vs. CEES) makes this simulant more useful when droplet must lie exposed for long intervals. Simulant droplets (1 μ L) were placed on a 1-cm² aluminum-backed punch. The coating was allowed to react for the predetermined time period, after which the sample was extracted in 10 mL of methylene chloride (MC) for 1 h. The extract was diluted 1:10 with MC and placed in a GC vial. The vials were vortexed and analyzed by GC-MS. The

reactive coatings were compared to control coatings to determine the percent reduction in simulant concentration due to the reactive additive.

MC is an aggressive, wide-spectrum, organic solvent, which makes it excellent for extracting CWA simulants; however, it also has the ability to extract other compounds within the coating. This can complicate chromatograms and foul components of both the GC and MS. To avoid complicating data analyses, MC was avoided in the past; however, the need for identification of reaction products with low vapor pressures necessitates the use of this solvent.

If no simulant was detected in any of the samples or blanks in the 2-h study, it was determined that the dilution factor was too great. To combat this issue, studies conducted with the 48-h interval were not diluted; 2 mL of the 10 mL extracted sample was placed directly in GC vials for analysis.

4.3.3. Results and Discussion

The following new PPG and Deft coatings were synthesized:

ETS20091222A: Deft formulation + polyoxometalate (POM) additive

ETS20091222B: PPG formulation + POM additive

ETS20091222C: PPG formulation + FC-43 (perfluorinated additive)

Reactivity studies were performed on several AFRL synthesized coatings:

ETS20091202A: Deft + fullerene additive

ETS20091202B: Deft + β -cyclodextrin (Ti) additive

ETS20091202C: Deft + β -cyclodextrin (Co) additive

ETS20091210H: PPG + dichlorodimethylhydantoin additive

ETS20091222A: Deft + POM additive

ETS20091222B: PPG + POM additive

Results of 2- and 24-h repellency testing of these coatings are shown in Tables 28 and 29.

Table 28. Two-hour Reactivity Data

Challenge	CEES		Demeton-S	
Coating	Average Count	% Reduction	Average Count	% Reduction
Blank	11423891	0%	36086269	0%
ETS20091202A	9708962	15%	34041764	5.6%
ETS20091202B	12536023	-9.7%	33982400	5.8%
ETS20091202C	15618169	-36.7%	34968776	3%
ETS20091210H	8021716	29.8%	16517069	54%
ETS20091222A	15216825	-33%	34623087	4%
ETS20091222B	17083076	-49.5%	40880736	-13%

Table 29. Twenty-four-hour Reactivity Data

Challenge	CEPS		Demeton-S	
Coating	Average Count	% Reduction	Average Count	% Reduction
Blank	51239218	0%	28145254	0%
ETS20091202A	58668093	-14.5%	32961467	-17%
ETS20091202B	58240102	-13.7%	33157018	-17.8%
ETS20091202C	51182933	0.1%	31641125	-12.4%
ETS20091210H	37603011	26.6%	11661828	58%
ETS20091222A	58015868	-13.2%	27658695	1.7%
ETS20091222B	50851810	0.8%	47785464	-69.7%

The data showed improvement in chromatographic precision and resolution versus previous reactivity studies. The AFRL-synthesized coating ETS20091210H, a PPG formulation with a dichlorodimethylhydantoin additive, performed the best of the six coatings studied. Consistent reduction was observed against both simulants over both time regimes. All other coatings performed poorly.

Repellency studies were performed on the coating ETS20091222C, a PPG + FC-43 formulation. The challenge consisted of a 1- μ L droplet of TBP on a coated aluminum coupon. Testing was conducted by measuring the change in mass of the coating after exposure to the challenge. The results from this experiment are shown in Table 30.

Table 30. Average Repellency Study using TBP (n=3)

Coating	Description	% mass change after 24 h	% simulant absorbed
ETS20091210H	PPG + FC-43	17.14	12.96
RAH20091124A	PPG Control	19.99	25.30
ETS20091210FC	Deft FC-43	37.44	51.04

FC-43, a possible FS alternative, performed poorly in the past when incorporated into a Deft formulation. When incorporated into a PPG coating, however, repellency was improved. This reinforced the belief that fluorinated additives do not perform well in Deft coatings, but can be effective in other paint formulations. ETS20091210H allowed only 12.96% of the challenge to absorb over a 24-h time period compared to a control, which absorbed 25.30%.

Repellency studies against MeS were also performed. Because MeS evaporates so quickly, the duration of the test was limited to 4 h. Results from this experiment are shown in Table 31. Since the control lost so much mass in just 4 h, it was determined that a repellency study of this duration is not effective for MeS.

Table 31. Average Repellency Study MeS (n=3)

Coating	Description	% mass change after 24 h	% simulant absorbed
ETS20091210H	PPG + FC-43	45.41	13.60
RAH20091124A	PPG Control	50.56	12.00

Repellency studies were performed on a series of coatings prepared by ARL (Table 32) and subjected to 2000-h weathering. The challenge consisted of a 1- μ L droplet of TBP on a coated aluminum coupon. Testing was conducted by measuring the change in mass of the coating after exposure to the challenge. The results from this experiment are shown in Table 33.

Table 32. Aircraft Protective Coatings Modified by ARL

ARL Coating	2 wt-% Additive to APC	Comments
JAE105A	None	Unpigmented Aircraft Protective Coating; Control
JAE115A	Lauric Acid	C ₁₁ H ₂₃ CO ₂ H
JAE115B	Myristic Acid	C ₁₃ H ₂₇ CO ₂ H
JAE115C	MHB 153-6B	Bolthorn H50 (0.9 eq oleic acid chain ends)
JAE115D	AAW 5-10	H50 (0.45 PEG-360, 0.45 behenic acid chain ends)
JAE117B	Boehmite nanofibers	Untreated nanofibers
JAE118B	Boehmite nanofibers	Fluorinated nanofibers
APC Grey	None	Untreated Deft coating; Control

Table 33. Average Repellency of Weathered Coatings on Al Coupons (*n*=1*)

ARL Coating	% Mass Change after 24 h		% Challenge Absorbed	
	TBP	MeS	TBP	MeS
JAE105A	5	1	1	-5
JAE115A	7	-1	14	-1
JAE115B	11	0	16	-1
JAE115C	12	0	15	0
JAE115D	13	-1	37	0
JAE117B	36	0	19	-1
JAE118B	40	-21	50	19
APC Grey	27	-11	28	10
Blank	6	0	0	0

*Due to limited amount of sample material, replicates were not performed

The CARC surrogate performed the best of all the coatings, absorbing almost no simulant. This was unexpected, as 105A contained no repellent additives. The 118B coating performed the worst, allowing 50% absorption. These data continued the trend that fluorinated additives perform poorly in Deft formulations. The difference between 115C and 115D was also unexpected, given the similarities of their formulations. This may be due to the number of samples tested in the analysis; that is, had more replicates been compared, the differences might have been less pronounced. The 117B and 115A–C coatings performed moderately with absorptions of 14–19% of the simulant challenge. It is of interest to note that the two coatings with nanofiber additives (117B and 118B) promoted the most evaporation of TBP. Repellency studies against MeS were also performed. Table 33 also shows the results from this experiment.

CAs of four separate liquids were measured on each coating. The results from this experiment are shown in Table 34.

Table 34. Average Contact Angle ($n=5$)

ARL Coating	Water	<i>n</i> -Hexadecane	Ethylene Glycol	Diiodomethane
JAE105A	67.42°	15.33°	38.47°	42.80°
JAE115A	72.74°	15.33°	57.60°	40.98°
JAE115B	76.58°	12.43°	58.10°	47.52°
JAE115C	73.34°	12.97°	68.92°	44.57°
JAE115D	96.68°	31.80°	84.86°	44.87°
JAE117B	72.52°	14.02°	55.77°	43.97°
JAE118B	97.40°	<1°	84.02°	36.30°
APC Grey	92.46°	17.07°	68.93°	39.85°

The 115D coating consistently showed some of the highest CAs. The other 115 series coatings also demonstrated relatively high CAs for all four liquids. These formulations consistently gave better results than the 105A control. The 118B coating gave the lowest CA for non-polar liquids, but performed better against the polar liquids. The opposite was true of the 105A CARC surrogate. Using the average CAs reported in Table 34, surface energy measurements were calculated for each sample. The results are shown in Table 35.

Table 35. Surface Energy (mN/m)

Coating	Extended Fowkes	Owens–Wendt
JAE105A	52.41	47.74
JAE115A	42.56	42.81
JAE115B	39.94	40.39
JAE115C	39.43	40.11
JAE115D	29.43	28.21
JAE117B	42.98	42.91
JAE118B	33.62	30.61
APC Grey	32.65	34.36

Surface energy measurements were recorded previously, before the coatings entered the weathering chamber. The 115D coating had the lowest surface energy using either of the two algorithms. All surface energy measurements increased after the 2000-h UV exposure except 115D. This surface energy decreased from 38.05 and 41.63 to 29.43 and 28.21 mN/m (Extended Fowkes and Owens–Wendt, respectively).

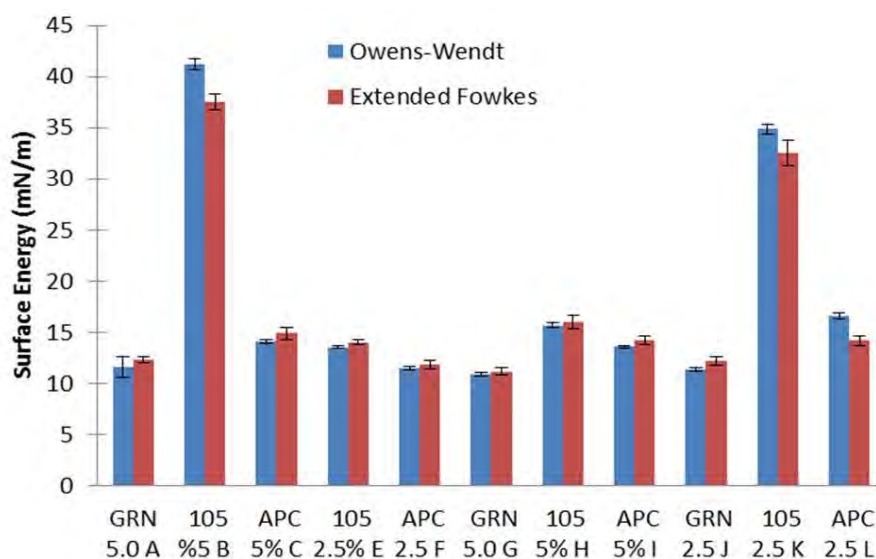
CAs of MeS and TBP were measured for each of the previous ARL coatings. The results are shown in Table 36. Although all coatings generated poor CAs against the simulants, 118B was by far the poorest performer. An actual value was not recorded because the droplet immediately absorbed into the coating. This result agrees with the absorption data in Table 36.

Table 36. Average Contact Angle ($n=5$)

ARL Coating	MeS	TBP
JAE105A	15.80°	30.10°
JAE115A	16.76°	30.63°
JAE115B	19.10°	24.26°
JAE115C	20.06°	27.86°
JAE115D	18.50°	32.86°
JAE117B	17.93°	28.22°
JAE118B	<1°	<1°
APC Grey	19.30°	20.30°

CAs of water, ethylene glycol, diiodomethane, and *n*-hexadecane were measured on another set of coatings supplied by ARL (data not shown). Each sample was rinsed with acetone after exposure to each of the test liquids. CAs on the 105 series coatings consistently showed the lowest values along with the greatest standard error. This is possibly due to the acetone rinse degrading the 105 series coatings (a very thin transparent film peeled away from the sample after the rinse). Because the film did not peel away entirely, some droplets touched the exposed sample surface while some droplets touched the film surface. This is likely the cause of the large standard error.

From the average CAs of a series of coatings prepared by addition of alumina nanowhiskers, surface energies were calculated for each sample, using both the Extended Fowkes and Owens–Wendt algorithms. The results are displayed in Figure 58. The 105 series coatings gave the highest surface energies, consistent with the low CAs observed against the test liquids. The modified GRN (MIL-DTL-64159) and APC (MIL-PRF-85285) series coatings gave similar results, although GRN surface energies were consistently the lowest.

**Figure 58. Surface Energies for 11 Modified Coatings**

Alumina nanowhiskers were added to A–F; fluorinated nanowhiskers were added to G–L

CAs of MeS, 3-hepten-2-one and TBP were taken on each coating. The results are shown in Figures 59–61

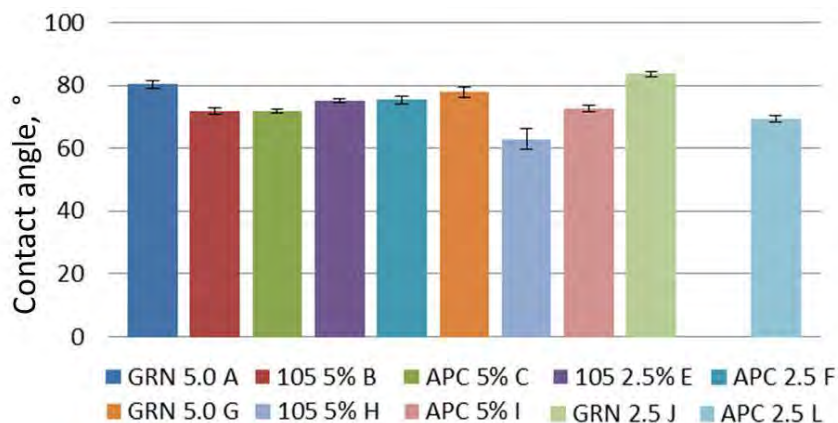


Figure 59. Average Contact Angle for Methyl Salicylate ($n=5$)

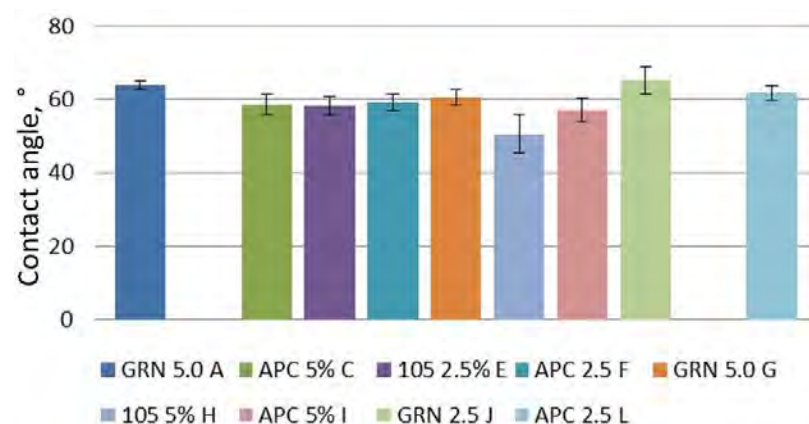


Figure 60. Average Contact Angle for 3-Hepten-2-one ($n=5$)

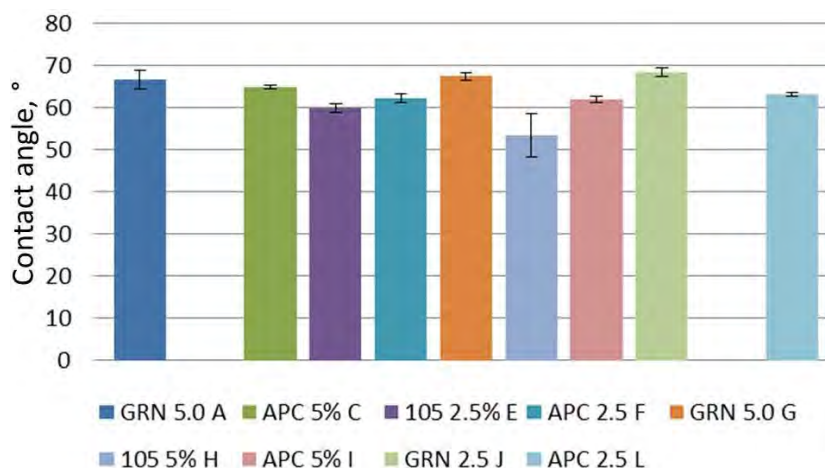


Figure 61. Average Contact Angle for Tributyl Phosphate ($n=5$)

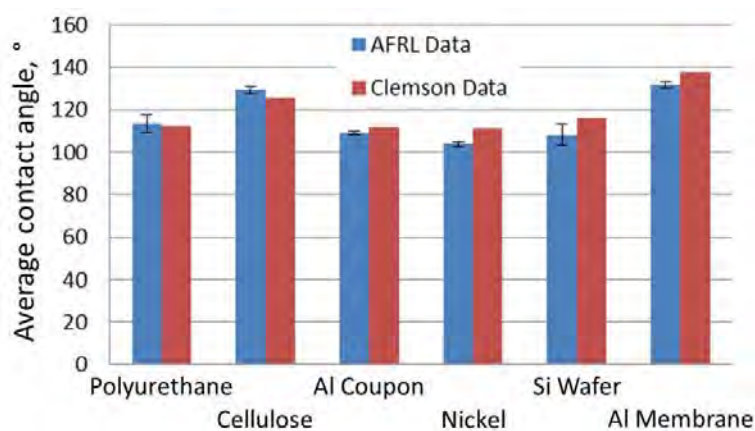
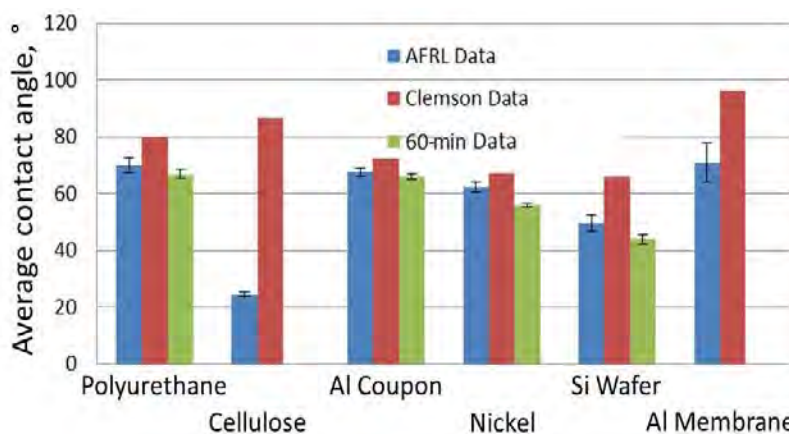
CAs of water, *n*-hexadecane, and TBP were measured on coatings sent from Clemson. Measurements were taken upon initial droplet deposition and again after 60 min. The results from this experiment are shown in Table 37.

Table 37. Average Contact Angles ($n=5$)

Surface	Water $t = 0$ min	n -Hexadecane		TBP	
		$t = 0$ min	$t = 60$ min	$t = 0$ min	$t = 60$ min
Polyurethane	113.6°	81.4°	68.9°	69.9°	66.9°
Cellulose Membrane	129.4°	95.5°	47.9°	24.3°	-
Al Coupon	109.2°	62.54°	62.5°	67.5°	65.8°
Nickel	104.0°	-	-	62.4°	55.9°
Si Wafer	108.2°	58.5°	46.3°	49.5°	43.9°
Al Membrane	131.7°	90.1°	-	70.9°	-

Due to lack of sample, not all measurements were carried out for the cellulose membrane, nickel, and the Al membrane coatings. The water droplets completely evaporated after the 60-min time limit, so no CAs were measured. Significant TBP absorption was seen on the cellulose and Al membrane samples so the 60-min data were not recorded.

CAs obtained at AFRL were then compared to values taken at Clemson. Data comparisons can be found in Figure 62–Figure 64.

**Figure 62. Comparison of Average Water Contact Angles ($n=5$)****Figure 63. Comparison of Average Tributyl Phosphate Contact Angles ($n=5$); for 60-min Cellulose and Si Wafer 60-min Data, $n=3$**

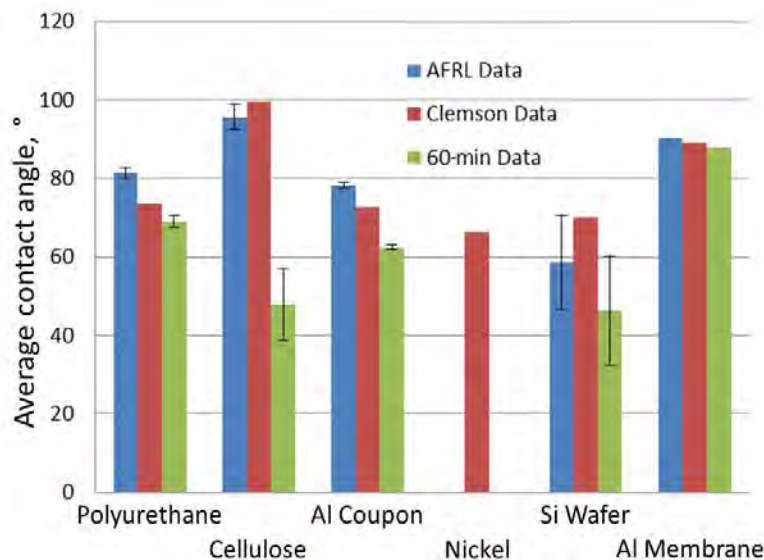


Figure 64. Comparison of Average Contact *n*-Hexadecane Contact Angles ($n=5$); for 60-min Cellulose and Si Wafer 60-min Data, $n=3$

The water and *n*-hexadecane CAs in the Clemson and AFRL data were comparable. TBP challenges revealed major differences between AFRL and Clemson data, most notably on the cellulose sample. The CAs of *n*-hexadecane consistently showed lower values after the 60-min time period due to droplet spreading on the surface. CAs of MeS, 3-hepten-2-one, and DMSO were evaluated for each coating. Measurements were taken upon initial droplet deposition and again after 60 min. The results are shown in Table 38.

Table 38. Average Contact Angles ($n=5$)

Surface	MeS		3-Hepten-2-one		DMSO	
		60 min		60 min		60 min
Polyurethane	76.88°	71.06°	62.10°	22.00°	79.50°	75.70°
Cellulose Membrane	74.10°	60.40°	56.60°	23.50°	110.7°	113.5°
Al Coupon	79.50°	75.80°	58.90°	18.00°	77.30°	75.70°
Ni	73.70°	69.60°	51.40°	13.50°	71.50°	59.70°
Si	75.20°	67.60°	58.30°	20.80°	72.20°	75.20°
Al Membrane	128.0°	122.0°	43.00°	-	94.10°	91.40°

Due to the fragility of the Al membrane coating, 60-min data were not obtained and there was not enough sample to repeat that portion of the experiment. The data are represented graphically in Figure 65–Figure 67. The CA of MeS consistently decreased after the 60-min time point. This is most likely due to evaporation at constant footprint. CAs of 3-hepten-2-one were dramatically lower after the 60-min time period, primarily due to droplet spreading.

Overall, no single coating performed best. The cellulose coating demonstrated the highest CA for DMSO and *n*-hexadecane; the polyurethane coating gave the highest CA for 3-hepten-2-one; the Al membrane coating gave the highest CAs for water, TBP, and MeS.

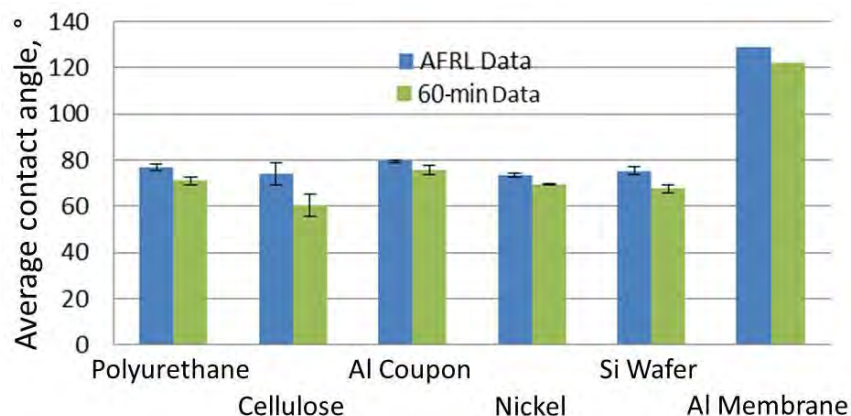


Figure 65. Average Contact Angles ($n=5$); for Methyl Salicylate on Al Membrane, AFRL Data, and 60-min Data, ($n=1$)

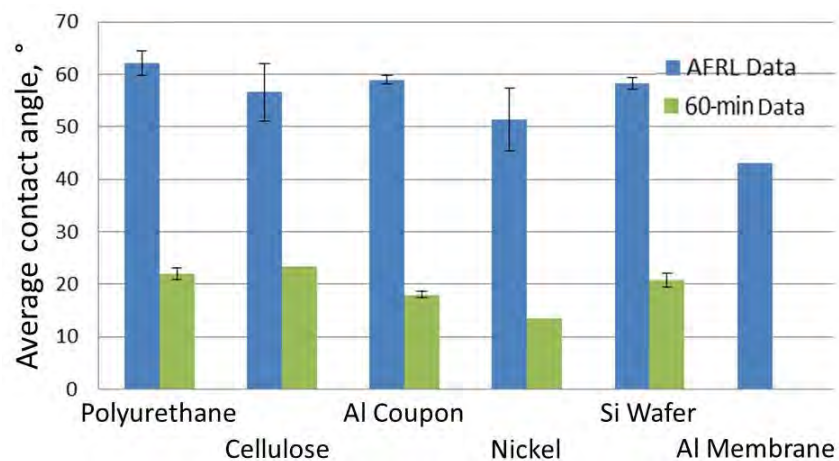


Figure 66. Average Contact Angles ($n=5$); for 3-Hepten-2-one; Cellulose and Nickel 60-min Data and Al Membrane Data, ($n=1$); Al Coupon 60-min Data and Nickel AFRL Data ($n=4$); Si Wafer Data ($n=3$)

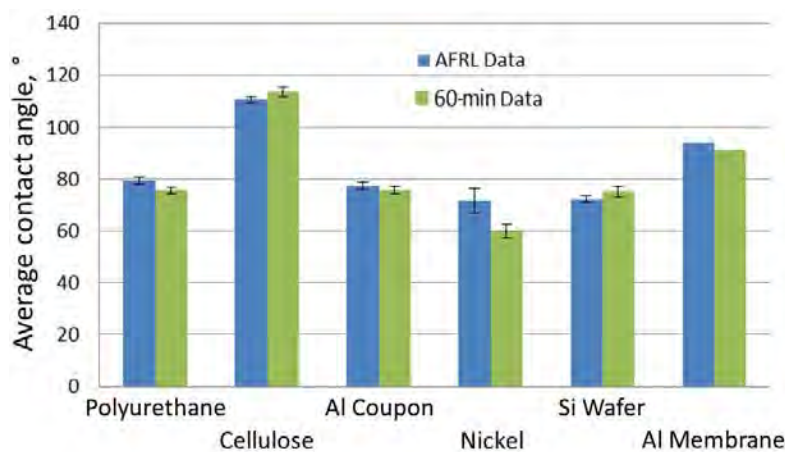


Figure 67. Average Immediate and 60-min Contact Angles for DMSO on Cellulose ($n=5$), Nickel ($n=3$), Si Wafer ($n=4$), and Al Membrane ($n=1$)

Roll-off angles were determined for water and *n*-hexadecane for each Clemson sample. The roll-off angle or dynamic CA is the angle of the sample table at which a droplet of liquid rolls off the sample. The data for roll-off angles can be found in Table 39. This gives information about how readily droplets can be shed from a surface, which is informative when evaluating a material's ability to mitigate hazardous substances.

Table 39. Average Roll-Off Angles for 50- μ L Droplets, ($n=3$)

Coating	Water	<i>n</i> -Hexadecane
Polyurethane	83.3°	21.7°
Cellulose Membrane	76.7°	13.3°
Al Coupon	60.0°	15.0°
Ni	31.7°	15.0°
Si	51.7°	45.0°*

* $n=1$ due to lack of sample

Roll-off angles were not determined for the Al membrane sample because there was not enough material available. Roll-off angle data are represented graphically in Figure 68.

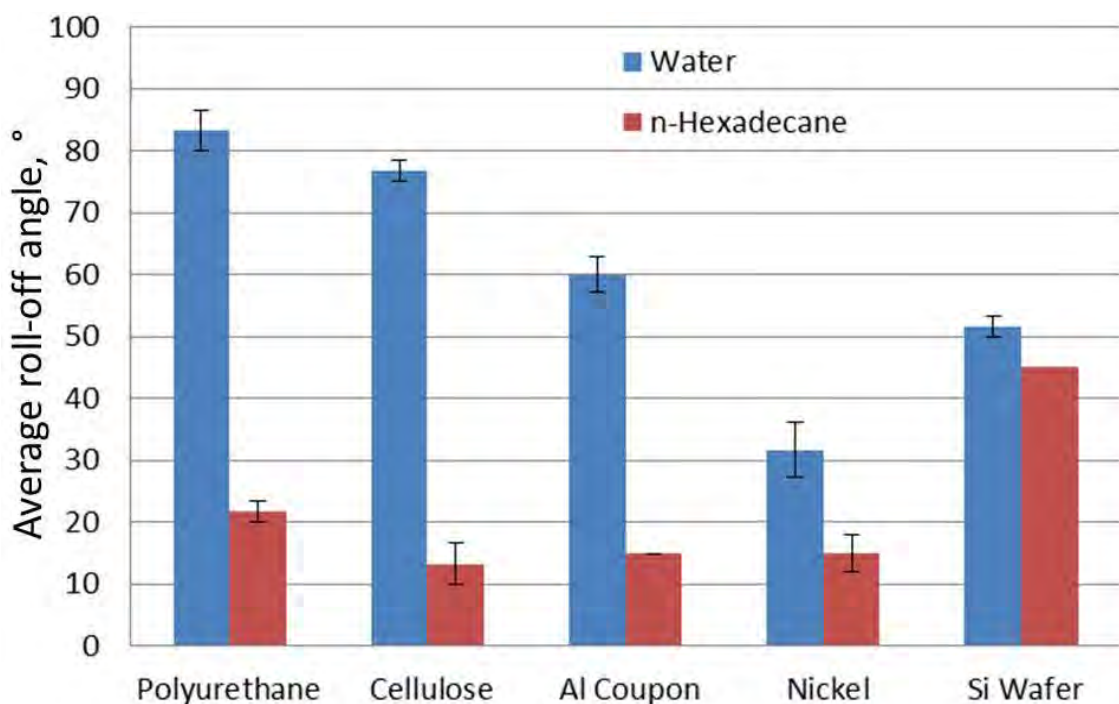


Figure 68. Average Roll-Off Angle ($n=3$)

Seven new reactive coatings formulated and synthesized at NRL were sent to AFRL for CA and surface energy analysis. The coatings were labeled Quat with Co Nano, P. Scrub, α -Ni CD, Oxime CARC, Co Nano in Latex, N85285 and N53022. CAs of four separate liquids were measured on each coating. The N85285 and α -Ni CD formulations performed the best, both having surface energies below 30 mN/m. These data are in agreement with the consistently high CAs for all liquids. The Quat with Co Nano-formulation performed poorly, with surface energy greater than 59 mN/m. The results from this experiment are shown in Table 40.

Table 40. Average Contact Angle ($n=5$)

Coating	Description	Water	<i>n</i> -Hexadecane	Ethylene Glycol	Diiodomethane
1	Quat w/Co Nano	18.86°	26.00°	18.40°	30.26°
2	P. Scrub	55.94°	0.00°	52.24°	0.00°
3	α -Ni CD	85.31°	32.60°	74.14°	40.20°
4	Oxime CARC	74.94°	16.12°	60.82°	34.96°
5	Co Nano in Latex	104.85°	35.72°	65.14°	32.64°
6	N85285	94.84°	35.46°	85.77°	54.32°
7	N53022	79.50°	24.12°	65.43°	37.94°

Using the average CAs reported in Table 42, surface energy measurements were calculated for each sample, using both the Extended Fowkes and Owens–Wendt method. The results are shown in Table 41.

Table 41. Calculated Surface Energies (mN/m)

Coating	Description	Extended Fowkes	Owens–Wendt
1	Quat w/Co Nano	59.41	64.76
2	P. Scrub	42.94	46.09
3	α -Ni CD	28.94	29.90
4	Oxime CARC	34.74	36.01
5	Co Nano in Latex	29.19	32.34
6	N85285	24.67	24.60
7	N53022	32.27	33.38

The N85285 and α -Ni CD formulations performed the best, both having surface energies below 30 mN/m. These data are in agreement with the consistently high CAs for all liquids, shown in Table 43. The Quat with Co nano-formulation performed poorly with a surface energy greater than 59 mN/m.

A coating was also formulated incorporating a reactive additive (hexadecyl(2-methoxyethyl)-dimethylammonium bromide) supplied by NRL. Once cured, the coating was tested for reactivity against CEPS and DS. The coating appeared to reduce simulant concentration after a 24-h challenge, however, not consistently. The additive worked significantly better in the PPG coating than in the Deft coating, as was observed in other coatings systems. AFRL synthesized modified reactive and repellent coatings incorporating the quaternary amine additive from NRL, FS, and FS modified nanofibers. These coatings represented a combination of the best repellent and most reactive additives to date. These coatings were tested for repellency, and surprisingly, the coatings with the repellent additives performed worse than the controls. Following those results, new formulations were made that incorporated slightly higher weight percentages of repellent additives. These coatings were then tested for reactivity. Unfortunately, the data were inconclusive, because the GC-MS results were imprecise.

4.3.4. Conclusions

Research at AFRL focused on the attachment of reactive and repellent functionalities to metal oxide particles. These modified particles were incorporated into both Deft and PPG coating systems and analyzed for reactivity and repellency against chemical simulants. The most successful of these in-house formulations were a hydantoin PPG coating and a PPG coating with

neat FS addition. As success was realized with perfluorinated coatings made at ARL, work at AFRL focused on performing analyses of these coatings.

Overall, no single ARL coating performed best, but the 105 series coatings performed decidedly the worst. CAs were not recorded against both TBP and 3-hepten-2-one for the 105 5% B and 105 2.5 K coatings because the droplets spread too quickly for a calculation to be performed. The same was true for 105 2.5 K against MeS and DMSO.

Repellency studies were performed on the 2000-h weathered ARL JAE series coatings. The challenge consisted of a 1- μ L droplet of TBP on a coated aluminum coupon. The CARC surrogate (105A) performed the best of all the coatings, allowing almost no simulant absorption. This is surprising because 105A contained no repellent additives. The 118B coating (APC modified with AFRL FS-nanofiber) performed the worst, allowing 50% absorption of TBP. These data continue to confirm the trend that fluorinated additives do not perform well in Deft formulations. It is of interest to note that the two coatings with nanofiber additives (117B and 118B) effectively promoted the evaporation of TBP. Almost all coatings showed excellent MeS repellency; however, this is due in part to the fact that nearly all of the MeS evaporated during the 24-h challenge time. Both Deft formulations (JAE118B and APC Grey) showed the lowest degree of MeS evaporation, thus greatest amount of simulant absorption.

Using the average CAs, surface energies were calculated for each ARL sample. All surface energies increased after the 2000-h exposure except 115D. This value decreased from 38.05 and 41.63 to 29.43 and 28.21 mN/m (Extended Fowkes and Owens–Wendt, respectively). CAs of MeS and TBP were taken on each coating. All coatings demonstrated poor CAs against the simulants (<33°).

Several perfluorinated coatings were received from ARL and CA and surface energy calculations were performed. CAs on the 105 series coatings consistently revealed the lowest values for both CA and surface energy. The GRN and APC series coatings gave similar results, although GRN surface energies were consistently the lowest. Overall, no single coating performed best, but the 105 series coatings performed decidedly the worst. CAs were not recorded for both TBP and 3-hepten-2-one on the 105 5% B and 105 2.5 K coatings because the droplets spread too quickly for a calculation to be performed. The same was true for MeS and DMSO on 105 2.5 K.

Reactivity studies were also performed on all of these coatings. Results showed improvements in chromatographic precision and resolution versus previous reactivity studies. AFRL-synthesized coating ETS20091210H, a PPG formulation with dichlorodimethylhydantoin, performed the best of the six coatings studied. Consistent reduction was observed against both HD and VX simulants over both time regimes. All other coatings performed poorly. ETS20091210H also performed well in a repellency study, allowing only 12.9% of the simulant to absorb over a 24-h time period vs. a control, which absorbed 25.3%.

More Deft and PPG coatings were formulated with additional NRL additives. These additives included fullerene, a β -cyclodextrin titanium, and a β -cyclodextrin cobalt. A Deft and PPG coating with neat FS was also synthesized. In an attempt to maximize coating repellency, a coating consisting of 90% FS-treated TiO₂, 10% FS-treated nanofibers, and 10% neat FS was

formulated. A replicate of a previously synthesized successful hydantoin coating was made, and a new perfluorinated compound, FC-43, was investigated as a potential FS alternative. Repellency studies were performed on all of these coatings; results further supported the idea that fluorinated particles are not well incorporated into Deft coating systems. Both Deft and PPG controls did better than most of the modified coatings, with the exception of RAH20091124C1, the PPG formulation with added FS, which demonstrated the highest degree of repellency. The FC-43-modified coatings were ineffective.

Following these results, new coatings were synthesized that incorporated another NRL additive, a polyoxometalate. Both Deft and PPG versions were formulated. In addition, a PPG coating was made with the FC-43 additive. Although it performed poorly in the past when incorporated into a Deft formulation, when FC-43 was incorporated into a PPG coating, repellency was improved. This reinforces the belief that fluorinated additives do not perform well in the Deft coatings tested, but can be effective in other paint formulations.

4.3.5. Follow-on Work

The next steps in the technical effort will be modification of another coating specification. Likely candidates could include MIL-DTL-64159 or MIL-DTL-53039B. Future exploratory research should focus on maximizing the reactivity of the coatings using *N*-chloramides, primary amines, quaternary amines, metal complexes, or other decontaminants. The most effective coating systems as determined by preliminary tests should undergo weathering, gloss, IR, permeation, abrasion and chemical agent testing. The CARC team will also be involved with the technology demonstration for the repellent MIL-PRF-85285 coating.

4.4. Directed Energy Enhanced Coatings

4.4.1. Introduction

The objective of this project is to evaluate the use of microwave heating as an alternative decontamination method for CWAs, on nominal CARCs. CARCs are used on many military assets; however, they are particularly important in protecting aircraft and ground vehicles from the threat and use of CWAs, as noted in Section 4.3.1.

CARCs doped with microwave susceptors are capable of coupling with microwave radiation at certain frequencies; thus, heating the coating and any sorbed contaminants to temperatures that can facilitate thermal decomposition, desorption, or vaporization. Additionally, microwave radiation generates strong electric currents at metal surfaces, causing resistive heating at the surface of the metals. Consequently, any sorbed agent will be influenced from within the coating, including CWA molecules at the polymer-metal interface—traditionally the most difficult region to decontaminate. This should provide a thorough level of decontamination without the use of harsh chemicals or bulky apparatus and without damaging relevant military equipment. Electronics and mechanical components within the airframe should be unaffected because military aircraft and other vehicles are typically hardened against electromagnetic radiation. The eventual goal is to use currently fielded military radar systems as the radiation source to facilitate decontamination; that is, radar offering readily available directed energy to act on enhanced coatings (DEEC).

During CY10, the original approach to achieve electromagnetic heating via thermal runaway of dielectric fillers was changed. The fillers, comprising metal oxide dopants, do not couple well with microwave radiation except at very high temperatures (and high values of the dielectric constant). Instead we elected to incorporate ferromagnetic metals and conductive polymers, which couple extremely well with microwaves at any temperatures that could reasonably be expected (but not near absolute zero). It was also determined that pristine CARC (MIL-PRF-85285) is heated by the application of microwave radiation; therefore, the original concept requiring microwave active dopants was no longer valid. At the end of CY10 there were still plans to research microwave susceptors that will enhance coupling to allow for faster heating, more-thorough decontamination, and less energy consumption.

4.4.2. Methods

The MIL-PRF 85285-compliant APC was formulated by first mixing TiO_2 particles with polyols at a 1:1 w/w ratio. The two components were mixed together with a homogenizer in a 50-mL conical vial until a thick slurry formed. Next, aliphatic diisocyanates were added to the slurry in a 10% excess and the solution was homogenized again. Approximately 1 mL of MEK/MAK was added to the new mixture to reduce the slurry to a high-viscosity solution. Figure 69 shows the reaction forming the polyurethane coating matrix from aliphatic diisocyanates and polyols.

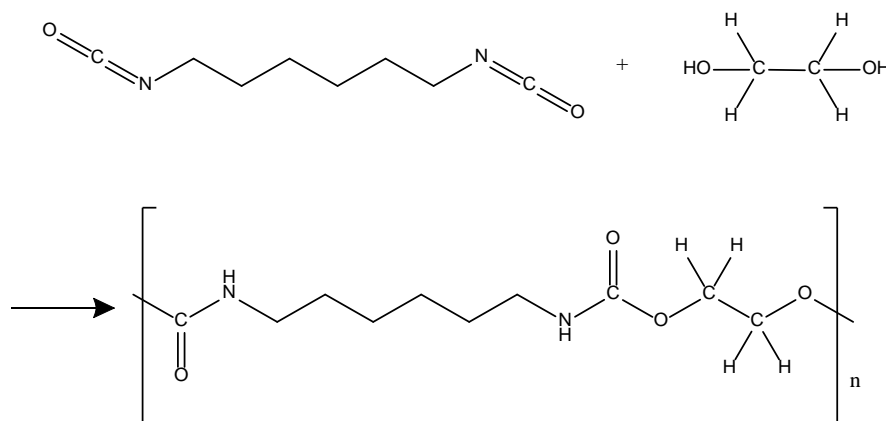


Figure 69. Step-Growth Polymerization to Form Polyurethane from Aliphatic Diisocyanates and Polyols

Polypyrrole (PPy) was synthesized via ferric chloride oxidation based on a published method (Omastova, Trchova, et al., 2003). The reaction (Figure 70) was carried out by adding 80.9 g of $\text{FeCl}_3 \cdot 6\text{H}_2\text{O}$ to 600 mL of distilled water and stirring. Next, 10.35 mL of pyrrole was added to 150 mL of distilled water and stirred. The pyrrole solution was then added dropwise to the FeCl_3 solution, immediately forming a black precipitate. The mixture was allowed to stir for 4 h. The precipitate was vacuum filtered and washed with distilled water three times. The product (~10 g) was then placed in a vacuum desiccator to remove excess water.

The synthesis of polyaniline (PAni) (Figure 71) was conducted using an interfacial polymerization method (Huang and Kaner, 2004). Aniline (1.6 mol) was added to 200 mL of MC in a 2-L beaker. Next, 0.32 mol of ammonium peroxydisulfate was added to 1 L of 600 mM hydrochloric acid and stirred until it was completely dissolved. The aqueous solution was carefully layered on top of the organic layer in the 2-L beaker, and the reaction was allowed to proceed

overnight. The next day, the solution was filtered twice through 0.20- μm filters, washed, and filtered a third time. The resulting PANi was dried in a vacuum desiccator, ground to a powder, and further dried.

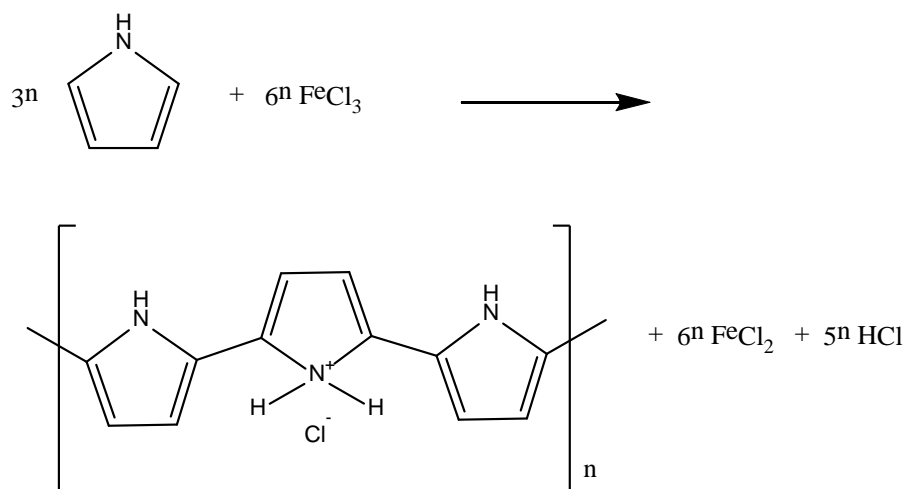


Figure 70. Synthesis of Polypyrrole from Pyrrole by Ferric Chloride Oxidation
According to the literature, this reaction typically produces polymers of $n \sim 10$ subunits.

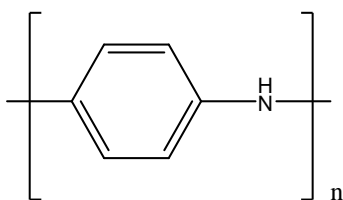


Figure 71. Polyaniline Chemical Structure

Microwave testing was conducted with a custom, variable-power system purchased from Gerling Applied Engineering, Inc. (GAE) and assembled by onsite staff. The system (Figure 72) contains a 3.5-kW water-cooled magnetron, a directional coupler, three-stub tuner, water-cooled dummy load, and sliding short circuit. Two cavities were available; 1) a cylindrical multimode cavity fabricated in-house using a stainless steel pipe, and 2) a water-cooled cavity with ceramic insulators and two cut-off tubes allowing samples to be inserted directly into the field without opening or closing the cavity. The microwave was manually and automatically controlled using LabVIEW with code written in-house. Much of the evolution of this effort involved development of appropriate test equipment, some of which required trial and error. This is all reported below in the *Results and Discussion* section.



Figure 72. Variable-power Microwave Test System

4.4.3. Results and Discussion

Before any work could be performed using actual radar systems, it was necessary to demonstrate proof of concept on the laboratory scale. This involved using the bench-top microwave to determine first that the coatings (modified or unmodified) could be heated, and second the actual power requirements to produce a temperature sufficient for thorough decontamination. Using the synthesis mentioned above, 85285-type coatings were synthesized with 0 (control), 3, and 5% w/w carbonyl iron, and coated on aluminum coupons. The 85285 topcoat contains TiO_2 , which was expected to demonstrate some activity under microwave irradiation based on its dielectric properties. Initially control coupons of 85285 that were tested at 300–3500 W did not absorb microwaves or demonstrate an increase in temperature. At the time this was thought to be because TiO_2 was not interacting with the applied field; however, the successes of later experiments suggested that perhaps the cavity had not been properly tuned.

Samples tested were mounted on a flat-faced ceramic puck using double-sided tape to attach the CARC coupon and trap a thermocouple between the sample and the puck. This first-generation sample holder was entirely covered by the coated aluminum CARC panel. Its major faults were that it required an adhesive—which is microwave active—and also that it was difficult to position the sample and thermocouple in the cavity. Arcing also occurred where the aluminum coupon contacted the sides of the stainless steel cylindrical cavity.

To improve upon this design, a second-generation sample holder (Figure 73) was made, also from a ceramic disk, but this time a slight recess was cut into the face of the disk so that sample coupons could rest on ceramic without the assistance of adhesives and without touching the sides of the cavity. A 0.125-in hole was drilled through the side of the disk allowing a thermocouple to be placed directly against the back of the sample coupon as it rested within the recess. After testing several 85285 control coatings and method blanks (sample holder only), it became evident that the coatings were being heated primarily by conduction from the sample holder instead of the field. Defects in the lattice of the ceramics are prone to absorb energy, and as the

face of the coupon no longer covered the entire disk, it began to couple with the applied field (Figure 73 and Figure 74).



Figure 73. Ceramic with 85285 control (left) and Teflon (right) sample holders
The sample holder rests on its side in the cylindrical cavity with the coated coupon facing the direction of the applied field. The thermocouple is inserted along the horizontal axis and slides behind the sample. A small hole drilled through each piece (in the z-direction) can be used to remove samples that become lodged.

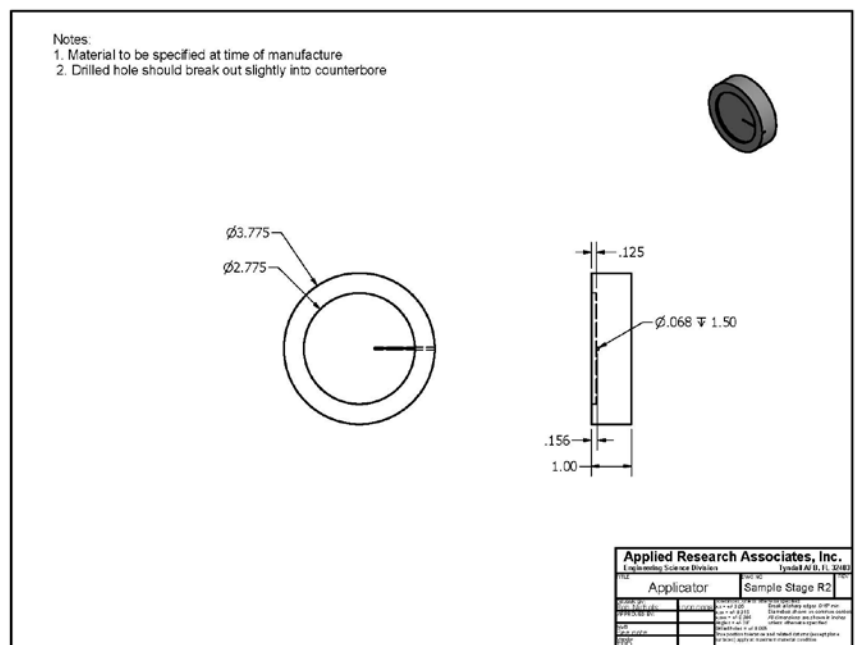


Figure 74. Schematic for the Ceramic and Teflon Sample Holders

This effect was tested by placing the empty sample holder in the cavity and irradiating at 300 W until the cavity felt hot. The microwave was then turned off and the thermocouple was inserted into the sample holder via a side access port in the cavity (the thermocouple could not be used while the microwave was on because without an aluminum coupon there would be nothing to shield it from the field). The sample holder attained a temperature of $\sim 330^{\circ}\text{C}$ in roughly 30 min.

Knowing that ceramic disks are susceptible to dielectric heating revealed that analysis of samples in this cavity would require a new material. Virgin electrical-grade Teflon was selected because it is a nonconductive material, functional up to ~260 °C, that can easily be machined. Because the only known flaw in the second-generation sample holder was the material that it was constructed from, the new Teflon sample holder was fabricated in an identical fashion.

The Teflon sample holder was tested at 300 W using a control coupon to cover the thermocouple. The sample could not be impedance-matched to the applied field, so no heating occurred. This was somewhat encouraging because although it suggested that the control coating may not be active at low fields, it showed that the Teflon sample holder did not absorb microwave radiation.

The 85285 APCs earlier formulated were tested using the new Teflon sample holder. Samples that contained 3 and 5% carbonyl iron were irradiated at 300 W in the cavity #1 described above. Although the new sample holder performed as desired—no arcing from panel or thermocouple contacts—it was difficult to achieve coupling between the sample and the applied field. At first this was believed to be due to interference from a newly added quartz pressure/vacuum window; however, removal of this component showed that it was not related. A possible explanation was that by introducing a transparent object (the sample holder) into the cavity, that the sample could be $\lambda/4$ out of phase with the applied field, thus not matched. Due to the design of the sample holder, the sample could not be moved within the cavity while a thermocouple was in use. Infrared (IR) temperature measurement was pursued as a possible remedy.

While IR temperature measurement was researched, a selection of candidate dopants (additives) were tested for possible incorporation into the next coating formulation. Approximately 100 mg of nickel, multi-walled carbon nanotubes (MWCNTs), boron nitride, 1- μ m mean diameter γ -alumina particles, nanoscale iron oxide, and carbonyl iron were placed in conical vials filled with paraffin wax and placed in a commercial microwave oven for 30 s at full power. Materials were determined to be microwave active if they attained sufficient temperature to melt/diffuse into the paraffin wax. Paraffin itself is microwave transparent, and will be heated only by conduction from the other material. Table 42 below gives a summary of the results of the candidate dopant test.

Table 42. Candidate Dopants for Incorporation into DEECs

Material	Activity at 1 kW 2.45 GHz	Arcing
Nickel	Yes	Yes
MWCNTs	Yes	No
Boron nitride	No	No
γ -Alumina	No	No
Nanoscale iron oxide	No	No
Carbonyl iron	Yes	No

Activity is qualitatively established as “yes” if the dopant diffused into the paraffin wax. The samples were also visually observed in the microwave to determine if the material arced under the applied radiation.

It was surprising that neither carbonyl iron nor MWCNTs arced in the microwave, because both samples are highly conductive and possess high surface areas. This knowledge is beneficial because while the overarching concept requires heating the doped coatings, arcing could damage a surface’s finish by the formation of local hot spots. However, the fact that the nickel sample

arced does not necessarily discount the use of this metal in a future coating. If the dopant is sufficiently dispersed at a low concentration then it may be heated without arcing. Both nickel and iron are ferromagnetic; thus, they are predictably very active in the microwave.

To alleviate the difficulties of temperature measurement inside a microwave cavity, an IR thermometer was purchased from Omega Engineering, Inc. Upon its arrival, work began to incorporate the new device into the already established test apparatus. This included modifying the stainless steel cylindrical end cap on cavity #1 and the Teflon sample holder by cutting a concentric hole in each piece. The end cap was fitted with a stainless steel cutoff tube (1.5 cm, (id) \times 8 cm), to attenuate microwave radiation while still allowing the IR beam to interact with samples inside the cavity. The IR sensor, which is encased in a metal shell, was mounted on an optical bench, without physically contacting the cavity; thus, no electrical interference could occur between the sensor and the cavity. The IR thermometer was connected to a power supply and interfaced to the LabVIEW virtual instrument already in use with the microwave system.

While upgrades to the test system were underway, a new coating component, PPy, was investigated. PPy is a widely used conductive polymer that has many applications in chemistry, biology, physics, materials science and engineering to name a few areas. It is a unique polymer because although it is completely organic it behaves much like a metal. This made PPy appealing because it has possibilities to be used as either a coating additive to facilitate microwave hybrid heating or even as a replacement for pigment metal oxides.

Once a sample had been synthesized, the finished PPy was placed in a conical vial containing paraffin wax and heated in a microwave oven as described above. Within 30 s the PPy diffused into the wax, demonstrating that the material is highly susceptible to microwave radiation. While this result was promising, the usefulness of PPy may be limited due to its spectral signature. As the polymer is black it is expected to absorb the entire visible light spectrum; therefore, it would be inappropriate at a high concentration for an 85285 coating. However, it is more likely that PPy could be used in Army coatings that require black and dark green pigments.

Difficulties such as arcing and extreme power reflectance while testing metal coupons continued, eventually prompting development of an alternate method to test the coatings. Previously synthesized 85285 coatings containing 1% PPy were stripped from the glass beaker in which they were mixed and cut into roughly equal-sized pieces. Samples were placed in conical polypropylene vials and irradiated in the water-cooled microwave cavity (cavity #2) at 300 W. Temperature and power absorption data were acquired every second by the LabVIEW software. The temperature profile of an empty polypropylene vial was also recorded as a negative control. As it is well known that polypropylene is transparent to microwave radiation, it was expected that no increase in temperature would be observed. The data were analyzed to determine the time required to reach a temperature of approximately 92 °C—chosen for safety reasons and to prevent melting of the polypropylene vials—and for the power absorption of the sample as a function of temperature. The vial containing 1% PPy reached the target temperature in approximately 60 s, while the temperature of the empty vial did not change over the course of 100 s.

Given these encouraging results, new coatings were formulated with 0 (positive control) and 1% nickel powder. The coatings were drawn onto Teflon sheets and cured. After curing, they were stripped from the Teflon and cut into 4.0 x 5.0-cm rectangles. These dimensions allowed them to

fit into a polypropylene sample vial without overlap and with sufficient surface area to ensure accurate readings from the IR thermometer. These samples were irradiated in the same manner described above, and temperature and power absorption data were recorded every second by the LabVIEW software (Figure 75 and Figure 76).

It should be noted that within the tolerances of the equipment, none of the doped samples was heated faster than the positive control. The tolerance of the power coupler interfaces (PCIs) at a power output of 300 W is ± 150 W. The tolerance of the IR thermometer is dependent on the emissivity of the sample, the exact value which is unknown; however, at an emissivity of 0.91 (generic value for a white pigmented finish) the specified tolerance of the thermometer is 2.2 °C.

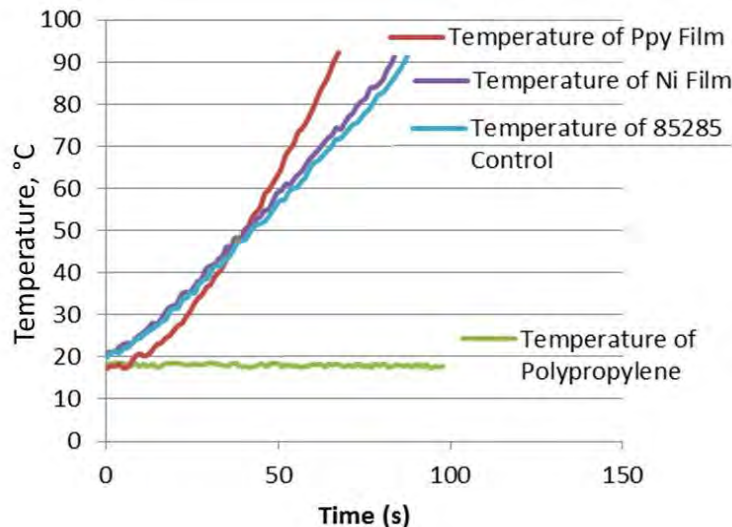


Figure 75. A Comparison of the Temperature Profiles of Various Coatings Exposed to Microwave Radiation (2.45 GHz) In Cavity #2

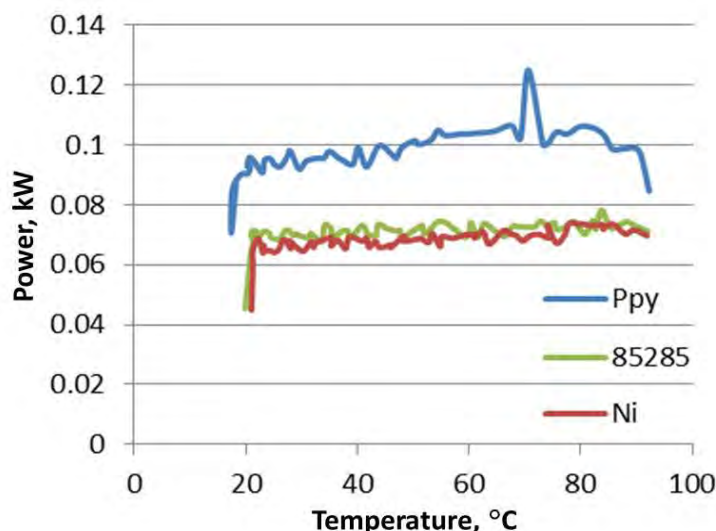


Figure 76. Comparison of the Power Absorption by a Control (85285) and Two Doped CARC Coatings as a Function of Temperature

It was also noted that the samples were of inconsistent thicknesses, even though a draw-down tool was used to apply them. As one might expect, the mass-to-surface-area ratio is a factor that determines how quickly the coatings are heated by irradiation; however, that relationship was not examined at this time.

Data in the two previous figures reveal that doping with 1% PPY or 1% nickel produces little to no discernable difference in the rate of heating or in power absorbed. There was a slight increase in power absorption with temperature, which is not unexpected—dielectric constants are directly proportional to temperature. The apparently greater power absorption of the PPY-doped film is well within the error of the PCIs, and is a result of our inability to manually tune the cavity in the short amount of time the films take to heat. It can be inferred that the unmodified 85285 coating itself couples strongly with microwave radiation at 2.45 GHz. The two major components of the coatings are polyurethane and titanium dioxide (TiO₂), the latter of which is not particularly active in microwave fields at temperatures below 200 °C. To verify this, a small amount of TiO₂ was placed in a conical vial filled with paraffin wax and irradiated for 60 s at 1.0 kW. The TiO₂ did not diffuse into the wax; therefore, the temperature of the material remained below ~55 °C.

Polyurethane, however, is known to be active in microwave fields (Jullien and Valot, 1985) (Karabanova, et al., 2009). The chemical structure of polyurethane (Figure 69) reveals several moieties that contribute large dipole moments, which will facilitate microwave coupling. The data indicate that the coatings are not significantly heated by microwave interactions with the additives or TiO₂, but are primarily heated by interaction with the polyurethane.

Upon retesting the samples of the 85285 controls, it was determined that curing time also made a significant difference in the rate of heating. Uncured samples couple more effectively than fully cured samples with an applied microwave field; however, the cured sample is still heated in a microwave field. After researching coating methods and standards, it was determined that a minimum of 14 days of cure time was required before testing.

Following this determination of curing time, 85285 coatings were formulated with 1, 5, and 10% PPY; 1, 5, and 10% Fe; and 5 and 10% Ni. The masses of the 4.0 x 5.0-cm coatings were inconsistent, and it was believed that the coatings were stretched when stripped off the Teflon sheet. Parafilm was selected as a replacement for Teflon because its mechanical properties are closer to that of the coatings. This proved partially successful, as the stretching problem was resolved (sample masses were more consistent). However, variability between coating batches was not resolved. It is believed that there are many variations that appear in small, handmade batches of coatings, which are either averaged out or not expressed in large industrial-scale batches.

Control samples and the 1% Ni samples were retested, and the 1 and 5% PPY, 1 and 5% Fe, and 5% Ni samples were also tested after a cure time of 14 days (data shown only for 1% PPY). These samples were irradiated at 300 W, and temperature and power absorption data were recorded every second by the LabVIEW software (Figure 77). These time data were analyzed for how quickly the samples reached a temperature of 140 °C, (approximate melting point of polypropylenes) and for the power absorption of the sample as a function of temperature. As can be seen in Figure 77, even small differences in mass resulted in noticeable differences in heating time. The more massive the sample, the shorter the time to reach the maximum temperature. As

can be seen, Sample 2, which had the lowest mass, did not reach 140 °C. Water-cooling the cavity also competed with microwave heating of the sample, which was more pronounced in the less massive samples. The difference in the time to heat of Samples 1 and 4 to the target temperature was approximately 201 s for a mass difference of 117 mg.

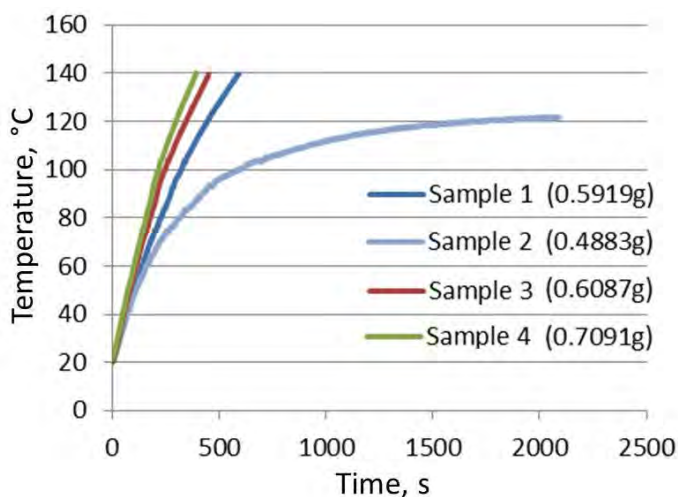


Figure 77. Heating rate to 140 °C for Four 1% PPy Samples of Differing Masses

The results are not conclusive and, until more samples are synthesized and tested, it is impossible to completely separate the contributions of heating due to the dopant versus the heating due to the mass of polyurethane.

Using experimental and theoretical results from collaborators at Clemson, and data collected by AFRL, we determined that semiconductors may actually be more active in a microwave field than ferromagnetic materials. Literature searches suggested the use of electrically conductive polymers that would also exhibit strong dielectric heating in the microwave field. Poly(3,4-ethylenedioxythiophene) or PEDOT has long been used in making LCDs and solar cells, and is transparent to visible light, which would be an obvious advantage if it were used in MILSPEC coatings. Unfortunately, PEDOT is very expensive in its pure form, so it was not pursued. As an alternative another highly conductive polymer, PANi, was selected as a test material. PANi is synthesized from low-cost starting materials, and the literature reports it to be highly conductive, especially in the nanofiber morphology (Thomas et al. 2009).

A small amount of PANi was placed in a conical vial with paraffin wax and irradiated in a microwave oven for 30 s. Melting of the paraffin indicated that PANi is active in a microwave field.

New 85285 coatings were fabricated with substitutions for TiO₂ incorporating 1, 5 and 10% Ni; 1, 5 and 10% Fe; 1 and 5% MWCNTs; 1% PPy, and 1% PANi, in quantities sufficient to prepare approximately 150 samples of each type as 4.0- x 5.0-cm coupons. The samples were sorted by mass, and samples of approximately 1.1, 1.2, and 1.3 g were selected for analysis. It was also determined that cure time could be reduced to 2 days at room temperature followed by 3 days of curing at 60 °C to obtain similar results to samples cured for 14 days at room temperature.

To remove the temperature constraints from using polypropylene vials, quartz glass, which has a very low loss factor ($\tan \delta = 0.0001$ at 25 °C) and softens at 1665 °C, was used as the container for coating samples. One quartz test tube was heated in the microwave cavity, and it was found that the time to elevate the temperature by 4 °C was over 20 min using the conditions mentioned previously. Therefore, quartz is not completely transparent to microwave radiation; however, any heating is negligible compared to that of the samples.

85285 samples chosen for analysis were heated in the microwave cavity. These samples were irradiated at 300 W, and temperature and power absorption data were recorded every second by the LabVIEW software. The data were analyzed to measure how quickly the samples reached a temperature of 200 °C, (chosen as the likely temperature for thermal decomposition, evaporation, and/or desorption of chemical agents and simulants) and for the power absorption of the sample as a function of temperature. Figure 78 shows the time required for several candidate coatings of mass, ~1.3 g respectively, to reach 200 °C.

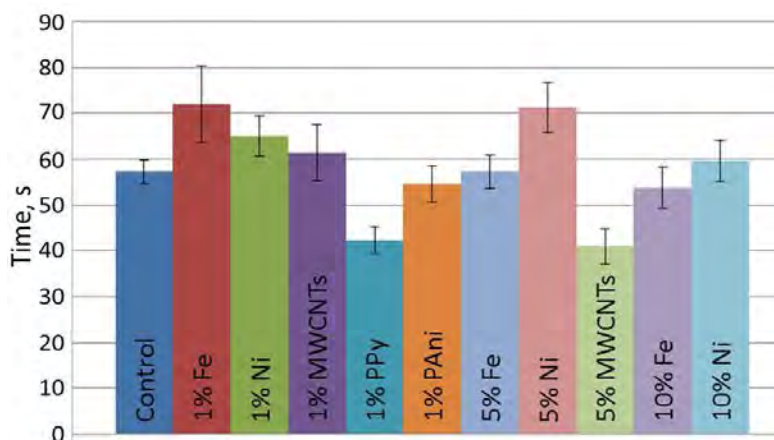


Figure 78. Time for Microwave Heating to Warm 11 Coating Samples to 200 °C; Average Sample Mass 1.3 g ($n=3$)

The data reveal that all of the samples tested are active in the microwave field. There were no noticeable trends with respect to sample mass within the limits of uncertainty (data not shown for 1.1- and 1.2-g samples). The tests consistently showed that 1% PPy and 5% MWCNTs heated the fastest, and 1% Fe and 5% Ni require the longest times (and most energy) to reach 200 °C.

In an effort to elucidate the exact relationship between sample mass and absorbed radiation, we began to retest all of the previously tested coatings and compile a complete data set. For the first 44 control samples, the cavity was tuned such that final absorbed power averaged 60 W ($\sigma = 30$) for samples averaging 1.14 g ($\sigma = 0.02$). This gave an average heating time of 143 s ($\sigma = 30.3$). For the remaining 73 samples the cavity was tuned such that the final absorbed power averaged to 90 W ($\sigma = 30$) for samples averaging 1.14 g ($\sigma = 0.09$). This gave an average heating time of 42.1 s ($\sigma = 8.2$). Due to the nature of the microwave, tuning the cavity is a delicate and highly variable process. The second set of control samples were tuned more effectively than the first. The large standard deviations of the absorbed power are due to the large tolerances of the power coupler. Another source of error arises from measuring temperature, as the infrared beam reads the surface temperature of the quartz test tubes and not the actual coatings. As quartz is low loss in a microwave, the temperature of the coating inside may be much higher than the temperature

on the surface of the test tube. The temperature of the quartz tube also depends on the temperature of the water cooling the universal waveguide applicator (cavity #2), which is subject to seasonal changes as the water is piped from a nearby water tower. To mediate some of these effects, the quartz tubes and coating samples were cooled to 20 °C before being irradiated. This test was eventually abandoned after a more effective method was determined.

The data, while showing clear trends, have large standard deviations for heating times and absorbed power. In an attempt to alleviate some of this variability, a calorimetry experiment was suggested. In this experiment, the coatings were placed in a quartz test tube, and a known amount of a low-loss liquid (light mineral oil) was added. The samples were then heated with a 15-s burst of microwave radiation at 300 W, and the equilibrium temperature of the oil was measured with a mercury thermometer. The process was repeated until the equilibrium temperature of the oil calorimeter reached approximately 150 °C. This temperature was chosen because defects on the inner surface of the quartz test tube and/or the coating sample would initiate nucleation near this temperature and the oil would begin to bubble. Control data were also taken with an empty quartz test tube and a test tube containing only mineral oil.

From the data collected, and using the gray body variation on the Stefan–Boltzmann Law,

$$Q = \varepsilon\sigma(T_h^4 - T_c^4)A \quad (6)$$

to determine how much energy is being radiated away from the calorimeter, one can determine how much energy is needed to heat a coating sample of known mass to 200 °C. For Equation 6, Q is the energy in Joules, ε is the emissivity of the object, σ is the Stefan–Boltzmann constant, T_h is the temperature of the object in Kelvin, T_c is the ambient temperature, and A is the surface area of the object. Figure 79 shows the energy required to heat 85285 coatings modified by the addition of 1% PPy for five ~1.25-g samples. Figure 80 and Figure 81 are control runs.

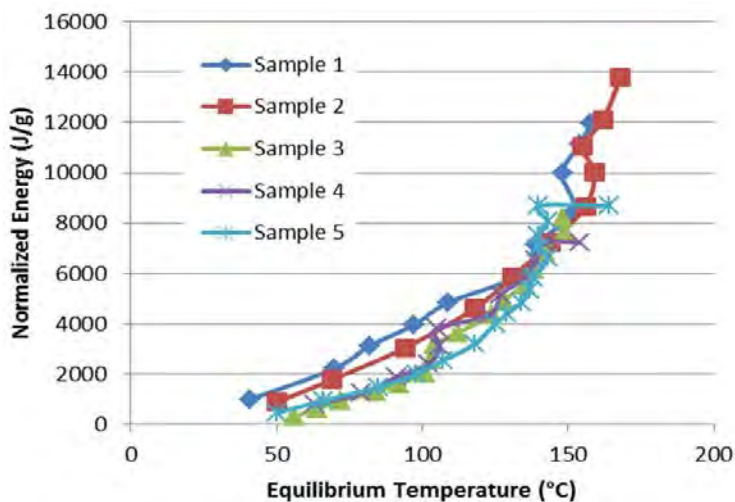


Figure 79. Energy per Gram of 85285 PPy Coating Necessary to Reach Various Temperatures in the Coating–Mineral Oil–Quartz Calorimeter ($n=3$)
Samples 1–5 were of nominally equal mass, ~1.25 g.

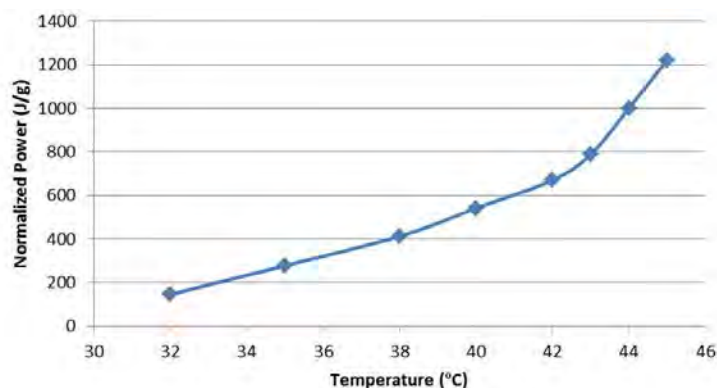


Figure 80. Energy Per Gram of Mineral Oil Necessary to Reach Temperatures in the Mineral Oil–Quartz Calorimeter ($n=3$)

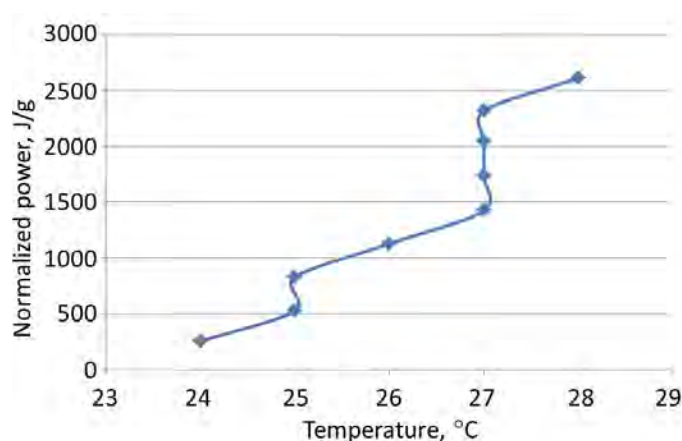


Figure 81. Temperature of Mineral Oil in Quartz Tubes vs. Energy per Gram ($n=1$)

As stated before, the microwave cavity is difficult to tune in the short amount of time the samples take to heat. To resolve this issue, two approaches for optimization of the cavity were taken. First, a vector network analyzer (VNA) was purchased to facilitate rapid impedance matching. Delivery was confirmed in early 2011. Another method to optimize heating within the cavity is to map the electric field of the unloaded cavity. This can yield information about the specific position(s) the sample would need to occupy to attain maximum interaction with the applied field. To do this, vertical layers of polystyrene foam separated by pieces of damp thermal paper, were placed in the cavity. After 10 s at 300 W, the magnetron was turned off, and the thermal papers were removed and examined. Loading the cavity is a time-consuming process, so only a few repetitions of this experiment have been completed. Once the entire data set has been collected, results will be reported (Chow, Ting, et al. 2009).

In an effort to expand the knowledge base and incorporate other coatings, commercial-off-the-shelf anti-graffiti coatings were researched. Since these are typically aliphatic polyurethane coatings, experiments were also conducted with a water-based anti-graffiti coating from Ecological Coatings (EC), in addition to the traditional 85285 coatings. The new anti-graffiti coatings were prepared with four parts by volume of a polyurethane component, one part by volume of an aliphatic diisocyanate component, and varying amounts of additives. We

originally planned to add the same fraction of TiO_2 that was used in the original 85285 coatings (the anti-graffiti coatings are unpigmented), but after adding TiO_2 in varying amounts from 10–50%, we discovered that the TiO_2 made the coatings very brittle. This is believed to be caused by the fact that TiO_2 is hygroscopic. Instead, a control coating was formulated with no additives at all, and coatings doped with 1, 3, and 5% PPy were synthesized. The 5% PPy was brittle, but the other doped coatings were flexible. The PPy also agglomerated within the coating, probably due to the fact that the polar character of the water-based coatings is greater than that of the previous 85285 versions.

In an effort to resolve the agglomeration of PPy in water-based coatings, small amounts of common organic solvents were tested for their ability to disperse the PPy in the coating. A 3:4 ratio of methanol to PPy worked best, but became problematic with large amounts of the polymer as the coating's viscosity was reduced. Also, adding large quantities of organic solvents is counterproductive because it defeats the purpose of using an aqueous system. A Deft coating included a proprietary dispersant added to their water-based coatings to allow pigmentation of the coatings (the EC coating was clear), and this dispersant allowed up to 5% PPy to be added to the coating, though it did alter the texture of the coating.

As an early technology demonstration, the 53rd Weapons Evaluation Group (WEG) at Tyndall Air Force Base, FL, agreed to allow the members of the DEEC team to conduct experiments using external electronic attack pods, which are used on the F-4 target drones. These drones were used to challenge F-22 pilots and were formerly used to expose F-15 pilots to tactically difficult situations that they might face in aerial combat. The pods operate on a higher frequency than the 2.45 GHz used in the laboratory test system, and the unattenuated output power is roughly four times what was previously used in the lab; therefore, it was believed that a coating could be heated by one of these pods if it was used to free irradiate the coating in close proximity.

Aluminum coupons (~6 in x 6 in) were coated with either 0 or 5% PPy-doped Deft coating or 0 or 1% PPy anti-graffiti coating, and allowed to cure for one week at ambient temperatures and for one week at 60 °C. Upon curing, the coupons were weighed, and half of the coupons were spiked with approximately 2 mL of phosphoric acid, a physical simulant for VX that possesses a dipole moment similar to many of the organophosphorus nerve agents. The coupons were allowed to sit overnight at room temperature to allow the phosphoric acid to adsorb into the CARC. The next morning, the excess acid was rinsed off with distilled water (~10 mL), and the coupons were weighed to determine the mass of simulant adsorbed.

Upon arrival at the WEG, an unspiked Deft control coupon was set up ~ 70 cm from the emitter of the pod. The output of the pod was set at the maximum of 50 dBmW (decibel milliwatts) with an 11 dB antenna gain—which converts to ~1200 W—and a 15° cone. No heating was observed. The coupon was moved closer, approximately 10 cm from the emitter, and again no heating was observed. It was noted that some antennas have dead zones near the emitter, so it was decided to test a coupon that would be more susceptible to the radiation. A phosphoric acid-spiked Deft coupon with 5% PPy was placed approximately 150 cm from the active pod. Again no heating was observed. As both the coating and PPy are known to heat in the laboratory test system, this was unexpected. It was not anticipated that the coatings would heat as efficiently with low-power radar travelling across free space, but some heating was expected.

Following these tests, a debriefing was held at AFRL consisting of members of the DEEC team and the 53rd WEG (MSgt Donald Rouse and Maj Robert Cocke). The failures from the test were discussed, as well as possible solutions and a schedule to retest the coatings. According to the WEG team, the drone that was used was likely not the best choice. The possibility that the drone was ineffective at close distances due to a protective feedback mechanism was considered. The WEG plans to have a new full-scale drone in early 2011, which could correct this problem, and the DEEC team is planning to conduct the test again at that time.

In the meantime, commercially available equipment that produces broadband, high-powered microwaves was researched. Both klystron generators and traveling wave tube amplifiers (TWTAs) were investigated as possible options to achieve this capability. A klystron is a specialized linear-beam vacuum tube that is used as an amplifier at microwave and radio frequencies to produce both low-power reference signals for radar receivers and to produce high-power carrier waves for communications. Klystron amplifiers have the advantage (over the magnetron) of coherently amplifying a reference signal so its output may be precisely controlled in amplitude, frequency and phase. Klystrons can emit high power (up to several kW), but tend to have narrow frequency bands generally less than 0.5 GHz. A TWT, which is also used to amplify microwave frequencies, consists of an elongated vacuum tube with an electron gun (a heated cathode that emits electrons) at one end. A magnetic containment field around the tube focuses the electrons into a beam, which then passes down the middle of a wire helix that stretches from RF input to output. The focused electron beam strikes a collector at the other end of the vacuum tube. A TWT can have one or two octaves of bandwidth, but tends to produce lower power than a klystron. Typical bandwidths for a TWT are 1–2.5 GHz, 2.5–7.5 GHz and 7.5–12 or 18 GHz.

TWTAs from three companies, HD Communications Corp, AR Microwave Instrumentation and Advanced Test Equipment, were evaluated in anticipation of purchasing a system in early 2011. TWTAs being evaluated all have a frequency range of 7.5–18 GHz and maximum output power of 500 W. In addition, all have multiple output connections including coaxial and WRD750 waveguide, which allows the user flexibility in choosing the frequency and mode for the application.

4.4.4. Conclusions

The most significant finding during this effort was that the unmodified MIL-PRF-85285 APC can be heated by 2.45-GHz electromagnetic radiation at powers as low as 150 W. Heating coatings to 200 °C—deemed the maximum safe temperature for the coating still likely to facilitate thermal desorption, decomposition, or vaporization—occurred in times as short as 60 s. This was of course carried out inside a resonant cavity and was not proven to occur in free space. Coatings modified with ferromagnetic materials or conductive polymers showed promise as well, with some reaching the target temperature in ~40 s. Candidates containing 1% PPy and 5% MWCNTs showed the most promise, while the ferromagnetics, nickel and carbonyl iron, did not perform as well and sometimes arced. Tests conducted at the WEG using live EA pods did not provide the desired results; however, it is highly likely that this was due to a frequency matching problem or negative feedback from the emitter. The WEG has offered to allow the team to conduct more tests using a better-suited EA pod once they acquire it. Preliminary results from calorimetry experiments using the gray-body variation of the Stefan–Boltzmann Law suggest that the energy required to heat coatings to 150 °C is approximately 7–10 kJ/g of coating irradiated. A VNA was purchased in 2010 and arrived 3 January 2011. This will be used for rapid impedance matching with the cavity and load, and will greatly increase the efficiency of

microwave testing in the laboratory. A TWTA was also selected, but not ordered due to financial restrictions placed on AFRL. Down-selection of coating additives should now be complete. It is evident that the conductive polymers and carbon nanotubes are the best performers, and offer the greatest advantages to increase heating efficiency and reduce energy requirements.

4.4.5. Follow-on Work

We recommend making more coatings for irradiation by a microwave and TWTA, using the new fluorinated and Deft coatings on Eccosorb (lossy substrate). The group should also continue to refine experiments to quantify the heating profiles of various coatings to provide power requirements for decontamination. The VNA will need to be installed and tested, and it will require some time for the staff to become fully comfortable using it to tune the cavities. A TWTA was selected but not purchased; therefore, we recommend that the government begin making plans to purchase this on a Form 9. The WEG needs to be contacted to inquire about testing with their new EA pod. In addition we recommend refining the calorimetry method of determining the power necessary to heat a given mass of coating. Specific formulations for coatings containing microwave susceptors need to be developed; for example, while it is known that both 1 and 5% PPy-doped coatings are heated more efficiently than controls, the optimal weight percent of the additive has yet to be determined. Depending on the success of the field demonstrations at the WEG, the team may need to begin thinking about a full-scale technology demonstration. This will require increased funding for FY12 and should be requested in the next SOW as early as June 2011.

4.5. Summary

A scaled-up demonstration for MP textile treatment was conducted in two phases: 1) Two 15-m lengths of fabric (NyCo and Kermel®) were treated at Tyndall AFB. The biocidal compounds were added successfully; however, the second treatment incorporating the hydro/oleophobic component did not work due to regioselective heating from the surfactant. 2) A second demonstration at NCSU realized the successful treatment of 120 yd of Defender-M® woven and 100 yd of Defender-M® knit with BA-1, Quat, and FS, and an additional 150 yd of cotton and 50 yd of NyCo with FS only. This was done using surfactant solutions, which ultimately left no residue on the finished materials. Aqueous-based FS formulations were elucidated, allowing the textiles to be treated without the use of flammable organic solvents. ABU boots as well as several non-textile materials were treated with FS and displayed excellent hydro/oleophobicity vs. control materials. Later in the year, several polyphenolic compounds were investigated for biocidal efficacy and durability when attached to textiles. 8HQ and several of its derivatives have been effective against both Gram-positive and Gram-negative bacteria. An enzyme assay was conducted to determine the biocidal mechanism of the polyphenols and Schiff bases attached to textiles; however, the results were inconclusive.

CARC research at AFRL focused on the attachment of reactive and repellent functionalities to metal oxide particles. These modified particles were incorporated into both Deft and PPG coating systems and analyzed for reactivity and repellency against chemical simulants. The most successful of these in-house formulations were a hydantoin-PPG coating and a PPG coating with neat FS addition. As success was realized with perfluorinated coatings made at ARL, work at AFRL focused on analysis of these coatings. The CARC surrogate 105A performed the best of all the coatings, allowing almost no simulant absorption—surprising, as 105A contained no repellent additives. The 118B coating (APC modified with AFRL FS-nanofiber) performed the

worst, allowing 50% absorption of TBP. These data continue to confirm the trend that fluorinated additives do not perform well in Deft formulations. It is of interest to note that the two coatings with nanofiber additives (117B and 118B) effectively promoted the evaporation of TBP. Almost all coatings showed excellent MeS repellency; however, this is due to the fact that nearly all of the MeS evaporated during the 24-h challenge time. Both Deft formulations (JAE118B and APC Grey) showed the lowest degree of MeS evaporation, thus greatest amount of simulant absorption.

CA and surface energy measurements were performed on several perfluorinated coatings received from ARL. CAs of the 105 series coatings consistently revealed the lowest values for both CA and surface energy. The GRN and APC series coatings gave similar results, although GRN surface energies were consistently the lowest. Overall, no single coating performed best, but the 105 series coatings performed decidedly the worst.

More Deft and PPG coatings were formulated with additional NRL additives. These additives included fullerene, a β -cyclodextrin titanium, and a β -cyclodextrin cobalt. Both Deft and PPG coatings with neat FS were also synthesized in an effort to compare repellent formulations created from the base components of the two manufacturers. In an attempt to maximize coating repellency, a coating consisting of 90% FS-treated TiO_2 , 10% FS-treated nanofibers, and 10% neat FS was formulated. A replicate of a previously synthesized successful hydantoin coating was made, and a new perfluorinated compound, FC-43, was investigated as a potential FS alternative. Repellency studies were performed on all of these coatings; results further supported the idea that fluorinated particles are not well incorporated into Deft coating systems. Both Deft and PPG controls did better than most of the modified coatings, with the exception of RAH20091124C1, the PPG formulation with added FS, which demonstrated the highest degree of repellency. The FC-43-modified coatings were ineffective.

Seven coatings formulated and synthesized at NRL were sent to AFRL for CA and surface energy analysis. The coatings were labeled Quat with Co Nano, P. Scrub, α -Ni CD, Oxime CARC, Co Nano in Latex, N85285 and N53022. The N85285 and α -Ni CD formulations performed the best, both having surface energies below 30 mN/m. These data are in agreement with the consistently high CAs for all liquids. The Quat with Co nano-formulation performed poorly with a surface energy greater than 59 mN/m.

The most significant finding from the DEEC effort was that the unmodified MIL-PRF-85285 APC can be heated by 2.45-GHz electromagnetic radiation at powers as low as 150 W. Heating coatings to 200 °C—deemed as the maximum safe temperature for the coating still likely to facilitate thermal desorption, decomposition, or vaporization—occurred in times as short as 60 s. This was of course carried out inside a resonant cavity and was not proven to occur in free space. Coatings modified with ferromagnetic materials or conductive polymers showed promise as well, with some reaching the target temperature in ~40 s. Candidates containing 1% PPy and 5% MWCNTs showed the most promise, whereas the ferromagnetics, nickel and carbonyl iron, did not perform as well and sometimes arced. Tests conducted at the WEG using live EA pods did not provide the desired results; however, it is highly likely that this was due to a frequency matching problem or negative feedback from the emitter. The WEG has offered to allow the team to conduct more tests using a better-suited EA pod once they acquire it. Preliminary results from calorimetry experiments using the gray-body variation of the Stefan—Boltzmann Law

suggest that the energy required to heat coatings to 150 °C is approximately 7–10 kJ/g of coating irradiated. A VNA purchased in 2010 arrived 3 January 2011. This will be used for rapid impedance matching with the cavity and load, and will greatly increase the efficiency of microwave testing in the laboratory. A TWTA was also selected; however, it was not ordered due to financial restrictions placed on AFRL. Down-selection of coating additives should now be complete. It is evident that the conductive polymers and carbon nanotubes are the best performers, offering the greatest advantages to increase heating efficiency and reducing energy requirements.

- In 2010 ARA staff continued their excellence in support of the Reactive/Responsive Materials team. Ms. Shelle McDonald travelled to the American Association for Aerosol Research (AAAR) conference in Portland, OR, where she presented her MS thesis work involving “Live-Animal Infectivity Study of a Viable Pathogen Penetrating through a Reactive Medium.” She also presented some of the same work at ARA’s Engineering and Science Symposium held in Orlando, FL. Mr. Bruce Salter presented research from the DEEC effort at the International Microwave Power Institute (IMPI) symposium held in Denver, CO. The presentation was titled, “Development and Evaluation of Enhanced Coatings for Directed-Energy Decontamination.”
- Ms. McDonald was co-author on a paper with former ARA employee Mr. Ryan Hayn, titled “Preparation of highly hydrophobic and oleophobic textile surfaces using microwave-promoted silane coupling” (Hayn, Owens, et al. 2010). Mr. Salter was an author on a paper published as a collaborative effort between Reactive/Responsive Materials and the Bioaerosol group (Salter et al. 2010)
- Due to the success of the CARC effort, many other government agencies became interested in this work, mainly, AFSOC, US Special Operations Command (SOCOM), and the Joint Program Managers office for Decontamination (JPM Decon). DTRA had already elected to fund this program for \$1.2M in FY 11. JPM Decon (Vic Murphy) visited AFRL Tyndall in May to learn about some of the new Air Force and DoD capabilities, and on the strength of a technical briefing on the CARC and DEEC efforts by Mr. Salter, they elected to fund the CARC effort for an additional \$800k in FY11. Ultimately, DTRA decided to further fund the same project by \$200k, bringing the total award to \$2.2M.
- Mr. Salter wrote a DTRA funding proposal for AFRL titled “Aqueous-Based Transport of Organophosphates and Organophosphonic Acids through Porous Substrates.” Ms. McDonald wrote another proposal titled “Self-Decontaminating Ocular Prophylaxis and Hemostatic Bandages for Wounds Exposed to CWAs,” which was invited to participate in DTRA’s final selection phase.

5. TOXIC AND PATHOGENIC AEROSOLS

5.1. Introduction

The toxic and pathogenic biological aerosol research area focused primarily on three major projects in CY 2010: 1) Biomedical Advanced Research and Development Authority (BARDA) H1N1 influenza project, 2) U.S. Army Natick Soldier Systems Center spore biological aerosol method development, and 3) Food and Drug Administration (FDA) filtering facepiece respirator (FFR) cleaning project. ARA personnel also provided support to maintain the functionality of the Biological Safety Level (BSL) II facility and new space allocated in the Fire lab. Although significant resources and time are expended to perform these functions, which include building manager duties, fire safety, tool kit compliance, environmental safety, hazardous waste disposal, instrument maintenance and recordkeeping, and chemical inventory, none of these tasks will be discussed in the report. Rather, the report will focus only on the technical progress made in the three defined areas in CY2010.

5.2. H1N1 Filtration and Total Inward Leakage Study

5.2.1. Technical Introduction

The recent H1N1 influenza pandemic spotlighted the urgent need to establish effective infection control methods to mitigate the pandemic. H1N1 is an airborne communicable disease that is readily spread from person to person. The primary device for protecting individuals from pathogenic aerosols is the National Institute for Occupational Safety and Health (NIOSH)-approved N95 FFR. The Occupational Safety and Health Administration (OSHA) and The Centers for Disease Control (CDC) recommend healthcare workers wear a properly fitted, NIOSH-approved FFR when attending to patients with influenza symptoms (OSHA 2007, CDC 2007). While it has been shown that FFRs are effective at removing fine inert particles (Heinz 1999) and many microorganisms from the air stream (Gardner *et al* 2006, Heimbuch *et al* 2007), we could find no data unequivocally proving that FFRs remove H1N1 influenza from the air stream. The purpose of this study was to determine if N95 FFRs remove viable H1N1 influenza with the same efficiency as inert particles of the same size.

5.2.2. Methods

5.2.2.1. Preparation of H1N1 Virus

Influenza A/PR/8/34 VR-1469 (ATCC VR-95) was propagated in embryonic chicken eggs using standard protocols (WHO 2002). Virus titers were determined using a tissue culture infectious dose assay (TCID₅₀) in Madin–Darby canine kidney cells (MDCK; ATCC CCL-34) with cell culture techniques approved by the World Health Organization (WHO 2002).

5.2.2.2. Aerosol Test Conditions

Three aerosol test conditions were used to challenge the FFRs with influenza virus (Table 43). Conditions 1 and 3 are based on the NIOSH standard flow rate (85 L/min (LPM)) for certification of FFRs and only vary in the particle size used. Condition 2 uses a flow rate of 170 LPM to provide a more rigorous challenge.

Table 43. Conditions for Challenging FFRs with H1N1**Common Conditions**

Method guidance	ATEC method for challenging air purification devices with viable aerosols
Viral strain	Influenza A/PR/8/34 VR-1469 (ATCC VR-95) ~23 °C
Temperature	
Humidity	35% – 50% RH
Aerosolization device	Laboratory-Scale Aerosol Tunnel (LSAT)
Atomizer	Collison nebulizer
Viable collector	AGI-30
Collection buffer	Serum-free EMEM (may contain neutralizers for antimicrobial FFRs)
Viable assay	TCID ₅₀ assay in MDCK cells
Replicate measurements	3 FFRs and three upstream and downstream measurements for each FFR
Duration of viable sampling	5 min per impinger
Quality control	Leak check FFRs, background check on LSAT, stable aerosol check, pressure drop

Condition #1

Flow rate	85 LPM
Particle size	0.85 µm count median diameter
Aerosolization media	Artificial saliva

Condition #2

Flow rate	170 LPM
Particle size	0.85 µm count median diameter
Aerosolization media	Artificial saliva

Condition #3

Flow rate	85 LPM
Particle size	~0.1 µm count median diameter
Aerosolization media	0.5% mucin

5.2.2.3. Laboratory-Scale Aerosol Tunnel (LSAT)

The LSAT was designed to challenge air purification systems with viable microbial aerosols and is ideally suited for this study (Figure 82). A complete description, operation instructions, validation report, and accompanying test protocols have been previously described (Foarde 2010). Briefly, the LSAT is composed of 10-cm diameter stainless steel sanitary fittings; a 15-cm diameter filter holder is used to accommodate the FFR. The biological aerosol is generated using a six-jet Collison nebulizer (BGI Inc., Waltham, MA). Dilution air, which is conditioned by passing the air through a humidifier, is added through two porous tube diluters (Mott Corporation, Farmington, CT), one located upstream and the other downstream of the charge neutralizer. The Kr-85 charge neutralizer (TSI Inc., Shoreview, MN) is required to counteract charges created on particles during aerosolization. To divert aerosol away from the test specimen, overflow valves

are located upstream of the expansion chamber. The expansion duct contains three mixing screens that create turbulent flow and allow the aerosol to mix prior to being exposed to the test specimen. Isokinetic sampling ports located upstream and downstream of the sample allow for viable sampling of microbial agents from the airstream and can also be used with traditional particle counters.

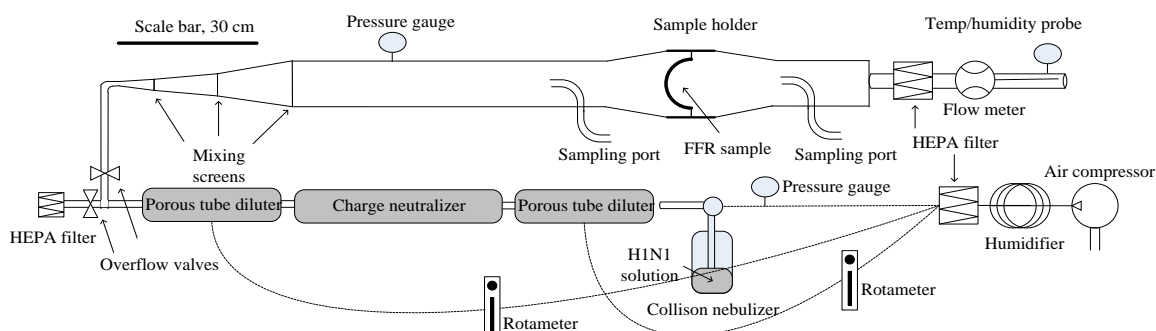


Figure 82. Laboratory-Scale Aerosol Tunnel (LSAT)

A critical mechanical operational element of the LSAT is to ensure the upstream and downstream sampling ports collect the same volume of particles. To validate the performance of the sampling ports for Condition #1, 30 mL of artificial saliva buffer (Aps 2005) (0.42 g NaHCO_3 , 0.04 g $\text{MgCl}_2 \cdot 7 \text{H}_2\text{O}$, 0.13 g $\text{CaCl}_2 \cdot \text{H}_2\text{O}$, 7.70 mL 0.2 M KH_2PO_4 , 12.3 mL 0.2 M K_2HPO_4 , 0.11 g NH_4Cl , 0.19 g KSCN , 0.12 g $(\text{NH}_2)_2\text{CO}$, 0.88 g NaCl , 1.04 g KCl , 3.00 g mucin (Sigma Aldrich, St. Louis, MO, M1778), 1 L deionized water, pH 7, was placed in a six-jet Collison nebulizer (BGI Inc., Waltham, MA) and attached to the LSAT. Compressed air (20 psi) was added to the Collison nebulizer to start the aerosol flow. Dilution air was added to both porous tube diluters to produce a total flow of 85 LPM. For Condition #2, the total flow was adjusted to 170 LPM. For Condition #3, 0.5% mucin was used rather than artificial saliva.

The LSAT was run for 10 min (30 min for Condition #2), then samples were taken alternately from the upstream and downstream ports using the Aerodynamic Particle Sizer (APS, TSI Inc., Shoreview, MN). Three upstream and three downstream measurements were collected. The port correlation was repeated three additional times using an aerosol of 0.8- μm PSL beads (Thermo Scientific, Waltham, MA).

5.2.2.4. Preparation of Filtering Facepiece Respirators

Three surgical FFRs common to hospital settings were selected for the study: 3M 1860S, 3M 1870, and Kimberly Clark PFR. Also selected were two FFRs that contain an antimicrobial coating: Triosyn T5000 and the Glaxo Smith–Kline Actiprotect face mask. Three replicate samples of each FFR were glue-sealed into 15-cm sample holders. The filters were leak checked by challenging each filter with an aerosol composed of either 0.8- μm (Conditions #1 and #2, Figure 83) or 0.1- μm (Condition #3) PSL beads as previously described.

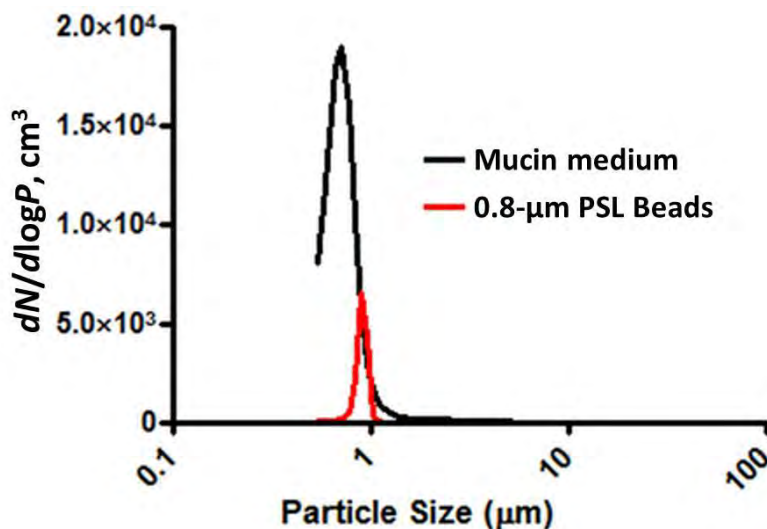


Figure 83. Comparison of Mucin PSD to 0.8- μm PSL Bead PSD

5.2.2.5. H1N1 Filtration Studies

Prior to each test, the LSAT was flushed with HEPA-purified air for 30 min, after which a minimum of three APS measurements were taken on the upstream and downstream port. A leak-checked FFR was loaded into the LSAT using sanitary compression seal fittings. The six-jet Collison nebulizer, containing 1 mL of H1N1 influenza virus ($8.6 \log_{10} \text{TCID}_{50}$ per mL) suspension diluted into 30 mL of mucin buffer, was attached to the LSAT. The LSAT was configured to direct the aerosol to the overflow and not to the FFR. Compressed air (20 psi) was applied to the Collison nebulizer, and dilution air was added to both porous tube diluters to bring the total flow to 85 LPM. The system operated for 10 min to bring the nebulizer to steady state, whereupon the LSAT overflow valves were reconfigured to direct the viral aerosol to the FFR sample for an additional 5 min. Viable sampling of the aerosol via upstream and downstream ports was initiated by connecting all-glass impingers (AGI-30, Ace Glass, Vineland, NJ), containing 20 mL of serum-free Eagle's Minimum Essential Medium (sf-EMEM; Hyclone Laboratories Inc, Logan, UT) supplemented with 1% penicillin/streptomycin (Sigma Aldrich, St. Louis, MO) and 1% L-glutamine (BioWhittaker, Walkersville, MD), to the LSAT. The AGI-30s were directly attached to the isokinetic sampling ports on the LSAT to minimize particle loss. Sampling was started by opening the valve on the isokinetic sampling port, while simultaneously applying vacuum to the AGI-30, which sampled at ~ 12.5 LPM. After 5 min, the isokinetic sampling port was closed and the vacuum was deactivated. The AGI-30 samples were transferred to 50-mL centrifuge tubes and placed on ice until viable plating was performed. A total of six samples (three upstream and three downstream, alternately sampled) were collected for each FFR.

5.2.2.6. Viable Plating of H1N1 Influenza Virus

The sf-EMEM buffer from the AGI-30s was evaluated for viable H1N1 using a TCID₅₀ assay in MDCK cells as described previously. The upstream samples were serially diluted 1/10 to 10⁻⁶. The 10⁻² through 10⁻⁶ dilutions were plated in quadruplicate into 24-well tissue culture plates containing a confluent lawn of MDCK cells. The downstream samples for the N95 FFR were serially diluted to 10⁻⁴, and all stages of the dilutions were plated in quadruplicate. The downstream Triosyn T5000 samples were serially diluted to 10⁻², and the 10⁻¹ and 10⁻² samples were plated in quadruplicate. In addition, the entire volume of the neat sample for the Triosyn T5000 FFRs was also plated to maximize sensitivity. The plates were incubated for 4 days at 5% CO₂/37 °C prior to reading cytopathic effects and crystal violet–glutaraldehyde staining.

5.2.3. Data Analysis

5.2.3.1. Sampling Port Correlation Factor (CF)

Port correlation of 0.8-μm bead studies (Conditions #1 and #2) used APS particle size bins ranging from 0.723–0.925 μm; the 0.1-μm bead studies (Condition #3) used the Scanning Mobility Particle Sizer (SMPS; TSI Inc., Shoreview, MN) particle bins ranging in size from 0.0947–0.1094 μm. Each port was sampled in triplicate, alternating between upstream and downstream. Counts for these bin ranges were summed to yield a representative particle concentration that included the CMD of the particle size distribution (PSD). The port correlation, calculated as the ratio of the average downstream counts to the average upstream counts, was required to be >96%.

5.2.3.2. Filtration Efficiency

Upstream and downstream measurements for the 0.8-μm bead study were collected using the 0.723–0.925 μm bins on the APS as described previously. In a similar fashion, the concentration of the 0.1-μm bead aerosol was determined using the 0.0947–0.1094 μm size bins on the SMPS. Viable virus collected in the upstream and downstream AGI-30s (viable virus per mL of extract) were determined using the Spearman–Kärber formula (Finney 1964). Equation 7 was used to determine the total amount of virus recovered from each sample (L_s), in which L is the amount of viable H1N1 expressed in units of log₁₀TCID₅₀/mL, and V is the sample volume (20-mL impinger volume). Viable filtration efficiency (VFE) of the FFRs was determined using Equation 8, in which DLs and ULs are the downstream and upstream log₁₀TCID₅₀ values, respectively, CF is the correlation factor, and n is the number of determinations. Particle filtration efficiency (PFE) of the sample was determined using Equation 9, in which U is the upstream particle concentration, and D is the downstream particle concentration. Prism 5 software (GraphPad Inc., La Jolla, CA) was used to determine 95% confidence intervals for the filtration efficiency.

$$L_s = 10^{[L+\log(V)]} \quad (7)$$

$$VFE = \left(\sum_{n=1}^i [1 - (DLs/ULs)/CF] (100\%) \right) / n \quad (8)$$

$$PFE = \left(\sum_{n=1}^i [1 - (D/U)/CF] (100\%) \right) / n \quad (9)$$

5.2.3.3. Statistical Analysis of Penetration Data

A two-tailed, unpaired *t*-test was used to compare the non-viable (beads) and viable (H1N1 influenza) filtration data for the three replicates of each N95 FFR. The average PFE and VFE values for each FFR were loaded into Prism 5 software to perform the *t*-test at 95% confidence intervals.

5.2.4. Results

5.2.4.1. Condition #1: 0.8- μ m bead, 85-LPM flow rate

The filtration efficiency for all FFRs challenged with 0.8- μ m beads, with the exception of the Triosyn T5000, ranged from 99.53% to 99.99% (Table 44). The Triosyn T5000 provided one to two orders of magnitude higher filtration performance and meets the NIOSH rating for a P100 FFR. The VFE for the FFRs challenged with H1N1 influenza also ranged from 98.51% to 99.94% for the four N95 FFRs (Table 45).

**Table 44. Challenge of N95 Filtering Facepiece Respirators with PSL Beads
—Percent Reduction Using Condition #1 (85 LPM, 0.8- μ m particles)**

3M 1860S	Average	L 95% CI	U 95% CI
FFR #1	99.89%	99.78%	99.99%
FFR #2	99.74%	99.66%	99.81%
FFR #3	99.91%	99.90%	99.93%
3M 1870	Average	L 95% CI	U 95% CI
FFR #1	99.92%	99.85%	99.99%
FFR #2	99.80%	99.65%	99.96%
FFR #3	99.94%	99.99%	99.99%
Kimberly Clark	Average	L 95% CI	U 95% CI
FFR #1	99.53%	99.23%	99.84%
FFR #2	99.79%	99.67%	99.90%
FFR #3	99.83%	99.75%	99.91%
Triosyn T5000	Average	L 95% CI	U 95% CI
FFR #1	99.9995%	99.9990%	99.9990%
FFR #2	99.9977%	99.9940%	100.0000%
FFR #3	99.9997%	99.9990%	99.9990%
GSK Actiprotect	Average	L 95% CI	U 95% CI
FFR #1	99.99%	99.99%	99.99%
FFR #2	99.96%	99.85%	100.06%
FFR #3	99.88%	ND	ND

The Triosyn T5000 FFR gave slightly higher removal efficiencies, but not at the level observed for the inert beads. A comparison of the inert PFE and the VFE using statistical methods shows that for all FFRs, with the exception of the Kimberly Clark, the differences are not significant ($P > .05$; Table 46). The actual difference in inert filtration efficiency and VFE was $< 1\%$ for the Kimberly Clark, so the difference between the two data sets is not practically meaningful.

**Table 45. Challenge of N95 Filtering Facepiece Respirators with H1N1 Influenza—
Percent Reduction Using Condition #1 (85 LPM, 0.8-µm particles)**

3M 1860S	Average	L 95% CI	U 95% CI
FFR #1	99.15%	98.52%	99.77%
FFR #2	98.97%	97.15%	99.99%
FFR #3	99.69%	99.17%	99.99%
3M 1870	Average	L 95% CI	U 95% CI
FFR #1	99.94%	99.85%	100.00%
FFR #2	99.90%	99.90%	99.90%
FFR #3	99.94%	94.46%	100.70%
Kimberly Clark	Average	L 95% CI	U 95% CI
FFR #1	98.51%	94.82%	102.20%
FFR #2	99.11%	97.17%	101.10%
FFR #3	99.16%	97.08%	101.20%
Triosyn T5000	Average	L 95% CI	U 95% CI
FFR #1	99.9570%	99.9910%	100.0000%
FFR #2	99.9937%	99.9850%	100.0000%
FFR #3	99.9570%	99.9900%	100.0000%
GSK Actiprotect	Average	L 95% CI	U 95% CI
FFR #1	99.94%	99.85%	100.00%
FFR #2	99.19%	98.12%	100.30%
FFR #3	98.55%	ND	ND

Table 46. Average Removal Efficiencies for Condition #1 (85 LPM, 0.8-µm particles)

FFR Model	H1N1 influenza	0.8-µm Bead	P-value
3M 1860S	99.27%	99.85%	0.061
3M 1870	99.13%	99.90%	0.384
Kimberly Clark	98.93%	99.72%	0.026
Triosyn T5000	99.9825%	99.9990%	0.274
GSK Actiprotect	99.23%	99.94%	0.150

5.2.4.2. Condition #2: 0.8-µm bead, 170-LPM flow rate

The filtration efficiency for all FFRs challenged with the 0.8-µm beads, with the exception of the Triosyn T5000, ranged from 98.29% to 99.97% (Table 47). The Triosyn T5000 provided one to two orders of magnitude higher filtration performance as was seen in Condition #1. The VFE for the FFRs challenged with H1N1 influenza ranged from 95.66% to 99.83% for the four N95 FFRs (Table 48). The Triosyn T5000 FFR gave slightly higher removal efficiencies, but not at the level observed for the inert beads. The statistical comparison of the inert and viable data sets showed that only the Kimberly Clark PFR was significantly different ($P = 0.005$; Table 49). One additional FFR for the GSK Antiprotect FFR remains to be tested to complete the data set.

Table 47. Challenge of N95 Filtering Facepiece Respirators with PSL Beads—Percent Reduction Using Condition #2 (170 LPM, 0.8- μ m Particles)

3M 1860S	Average	L 95% CI	U 95% CI
FFR #1	99.79%	98.59%	100.20%
FFR #2	99.31%	98.28%	98.22%
FFR #3	99.01%	100.50%	100.50%
3M 1870	Average	L 95% CI	U 95% CI
FFR #1	99.97%	99.89%	100.00%
FFR #2	99.93%	99.91%	99.95%
FFR #3	99.99%	99.99%	99.99%
Kimberly Clark	Average	L 95% CI	U 95% CI
FFR #1	98.29%	96.57%	100.00%
FFR #2	98.73%	98.46%	98.99%
FFR #3	98.09%	97.59%	98.60%
Triosyn T5000	Average	L 95% CI	U 95% CI
FFR #1	99.999%	100.000%	100.000%
FFR #2	99.999%	100.000%	100.000%
FFR #3	99.984%	99.970%	100.000%
GSK Actiprotect	Average	L 95% CI	U 95% CI
FFR #1	99.29%	99.10%	99.48%
FFR #2	99.33%	99.22%	99.45%
FFR #3	Not Determined Yet		

5.2.4.3. Condition #3: 0.3- μ m bead, 85-LPM flow rate

Technical difficulties from a variety of problems did not allow this testing to be completed for Condition #3. Near the end of the Condition #2 work, TCID₅₀ analyses indicated that H1N1 infectivity was below detection limit. New H1N1 virus was propagated in hopes of increasing viral stability due to possible degradation in cryofreezer storage over time. The new virus stocks were determined to have a titer of 8.10 log TCID₅₀ per mL which is an acceptable level. During the propagation process, a substantial amount of residue was discovered within the LSAT, as a result of previously used nebulization fluids. To eliminate as much residue as possible, the LSAT was disassembled, sterilized, and cleaned. Follow-up testing indicated that the LSAT functioned properly. All the problems were sorted out during the last quarter of CY 2010 (data not shown), and Condition #3 filtration work was anticipated to be completed in January 2011. However, the contracting dilemma prevented any progress. Preliminary data were collected by challenging the 3M 1860 and 3M 1870 with the 100-nm PSL beads. The filtration efficiencies for these masks were shown to be 94% (Table 50).

Table 48. Challenge of N95 Filtering Facepiece Respirators with H1N1 Influenza—Percent Reduction in 0.8- μ m Particles at 170 LPM

3M 1860S	Average	L 95% CI	U 95% CI
FFR #1	99.15%	98.52%	99.78%
FFR #2	99.00%	99.00%	99.00%
FFR #3	97.56%	94.46%	100.70%

3M 1870	Average	L 95% CI	U 95% CI
FFR #1	99.29%	96.99%	101.60%
FFR #2	99.65%	99.17%	100.10%
FFR #3	99.83%	99.51%	100.10%

Kimberly Clark	Average	L 95% CI	U 95% CI
FFR #1	96.74%	91.00%	102.50%
FFR #2	96.48%	91.35%	101.30%
FFR #3	95.66%	90.15%	101.20%

Triosyn T5000	Average	L 95% CI	U 95% CI
FFR #1	99.975%	99.910%	100.000%
FFR #2	99.901%	99.700%	100.100%
FFR #3	99.446%	98.330%	100.600%

GSK Actiprotect	Average	L 95% CI	U 95% CI
FFR #1	98.43%	94.97%	101.90%
FFR #2	98.43%	94.97%	101.90%
FFR #3	ND	ND	ND

Table 49. Average Removal Efficiencies of 0.8- μ m Particles at 85 LPM and at 170 LPM

0.8-μm Bead				H1N1 Influenza		
Removal Efficiency at				Removal Efficiency at		
FFR Model	85 LPM	170 LPM	<i>P</i>-value	85 LPM	170 LPM	<i>P</i>-value
3M 1860S	99.85%	99.37%	0.11	99.27%	98.57%	0.27
3M 1870	99.90%	99.96%	0.36	99.13%	99.59%	0.60
Kimberly Clark	99.72%	98.37%	0.003	98.93%	96.29%	0.002
Triosyn T5000	99.999%	99.994%	0.38	99.982%	99.94%	0.25
GSK Actiprotect	99.943%	99.31%*	N/A**	99.23%	98.43%*	N/A**

*Only two replicates have been challenged to date; ** Unable to determine *P*-value

Table 50. Filtration Efficiencies of 3M 1860S and 3M 1870 Challenged with Different Beads

Particle Size (nm)	3M 1860S	3M 1870
800	99.9%	99.9%
250	99%	99%
100	94%	94%

5.2.5. Discussion

The data in this study clearly show that all five models of N95 FFRs are effective at removing viable H1N1 particles from the air stream. The filtration efficiency for all FFRs exceeded their rating, as expected for the particle size used for this study—the FFR rating is based on penetration by the nominal most-penetrating particle size (~0.3 μ m). CMD of particles used for this study centered near 0.8 μ m, so the measured filtration efficiency was higher than the rated value.

Condition #2 (170 LPM) provided a slight decrease in both VFE and inert particle removal efficiency for all FFRs (Table 49); however, the result was statistically significant (compared to the 85 LPM flow rate) for only the Kimberly Clark FFR ($P = 0.003$). The N95 FFR allowed significant penetration of H1N1 influenza, but this does not suggest the device is inadequate for protecting users from airborne transmission of influenza. To perform the aerosol test, the challenge concentration of influenza is intentionally increased to levels higher than would be expected in a normal infectious disease setting—the average of $3.76 \log_{10} \text{TCID}_{50}$ per liter of air used in this study far exceeds values recorded for airborne influenza concentrations in hospital settings (Blachere *et al.* 2009).

Because the environment in which the test is performed influences the removal efficiency of the FFR, conditions were carefully selected based on the guidance in a Department of Defense (DoD) test method for evaluating air purification devices with viable aerosols (Foarde *et al.* 2010). The critical conditions are flow rate and particle size. The NIOSH standard test rate of 85 LPM was used as the flow rate for Conditions #1 and #3; for Condition #2, the flow rate was increased to 170 LPM to provide a more rigorous challenge. The $0.8\text{-}\mu\text{m}$ particle size was selected to simulate the size of particles generated by a human cough. This was a compromise among the varying particle sizes reported to be exhaled by humans (Hall 2007, Tang 2006, Tellier 2006, Knight 1980, Papieneni 1997, Riley 1961, Zhao 2005, Zhu 2006). We chose to focus on particles produced during coughing, as this is a clinical symptom of influenza. Yang *et al.* studied the PSD produced by coughs from healthy human volunteers and determined that 82% of droplet nuclei generated by coughs fell inside the particle size window of $0.74\text{--}2.12 \mu\text{m}$. The PSD used for Conditions #1 and #3 had CMDs centered on $\sim 0.8 \mu\text{m}$, which was produced by delivering the virus in artificial saliva. A smaller particle size, $0.1 \mu\text{m}$, was also selected, as it provides a more rigorous challenge; for electret media used in production of FFRs, the most penetrating particle size is $30\text{--}70 \text{ nm}$ (Balazy 2006). While it can be argued that other particle sizes and/or solutions could be used, we consider these particles representative of human respiratory secretions. The same particle size is also used in an ASTM method developed to load surfaces with H1N1 particles that are representative of human respiratory secretions (ASTM 2010).

A comparison of the viable H1N1 penetration and the non-viable bead penetration demonstrated that four of the five models of FFRs evaluated provide equivalent filtration efficiency. The Kimberly Clark FFR produced statistically different results for VFE and inert beads, but the actual difference in penetration was only 1–2%, making the practical significance of this finding moot. Thus, it can be concluded that the presence of infectious microorganisms does not influence filtration efficiency of the FFR. This same phenomenon has been demonstrated by other researchers using different microbial agents (Gardner *et al.* 2006, Heimbuch *et al.* 2007). We have yet to collect data for Condition #3, but we expect similar results.

Another caveat of these data that must be considered is that the performance of only the filtration media was evaluated. To achieve expected levels of respiratory protection by a device, a good fit must also be achieved. It is imperative that an OSHA-regulated FFR fit test program be implemented by any organization with a respiratory protection program.

5.2.6. Conclusions

The primary focus of this study was to determine experimentally that N95 FFRs do or do not remove H1N1 influenza particles equally efficiently as inert particles of the same size. To date, all five FFR types have demonstrated filtration performances that meet their benchmark N95 rating for both inert PSL bead and H1N1 influenza aerosols. The data analysis indicates that filtration efficiency is not dependent on a particle's nature of origin, but more on the PSD of the aerosol challenge.

5.3. Biological Aerosol Test Method Study

5.3.1. Technical Introduction

The goal of this project is to develop an aerosol method for applying *Bacillus* spores to surfaces. Protocols developed for this method will make an effort to mimic *Bacillus* spore aerosols that are representative of a state-sponsored biological warfare agent. The method will describe all required steps beginning with preparation of the spores and ending with data analysis (Figure 84). The value of this method is far-reaching and will provide solutions for scientists performing a variety of research. The primary initiative for developing the studies is to evaluate the utility of self-sanitizing/reactive materials. Self-sanitizing materials are more active in the presence of water (Heimbuch unpublished results, Prugh and Calomiris 2006) and, thus, standard test methods using water-based inoculums may provide misleading results. The aerosol method will mimic aerosol deposition of spores onto surfaces and will provide data that are representative of a real-world biological attack. These data are critically important at the early development stage (6.1 and 6.2) so that value of materials can be properly assessed. The method will also be valuable in the evaluation of sporicidal compounds. The method will call for an agglomeration of spores, which is more difficult to inactivate than single spores. Reaerosolization studies can also make use of this method, as the techniques used to apply spores to surfaces will influence how the spores interact with the surface and ultimately how they are released from the surface.

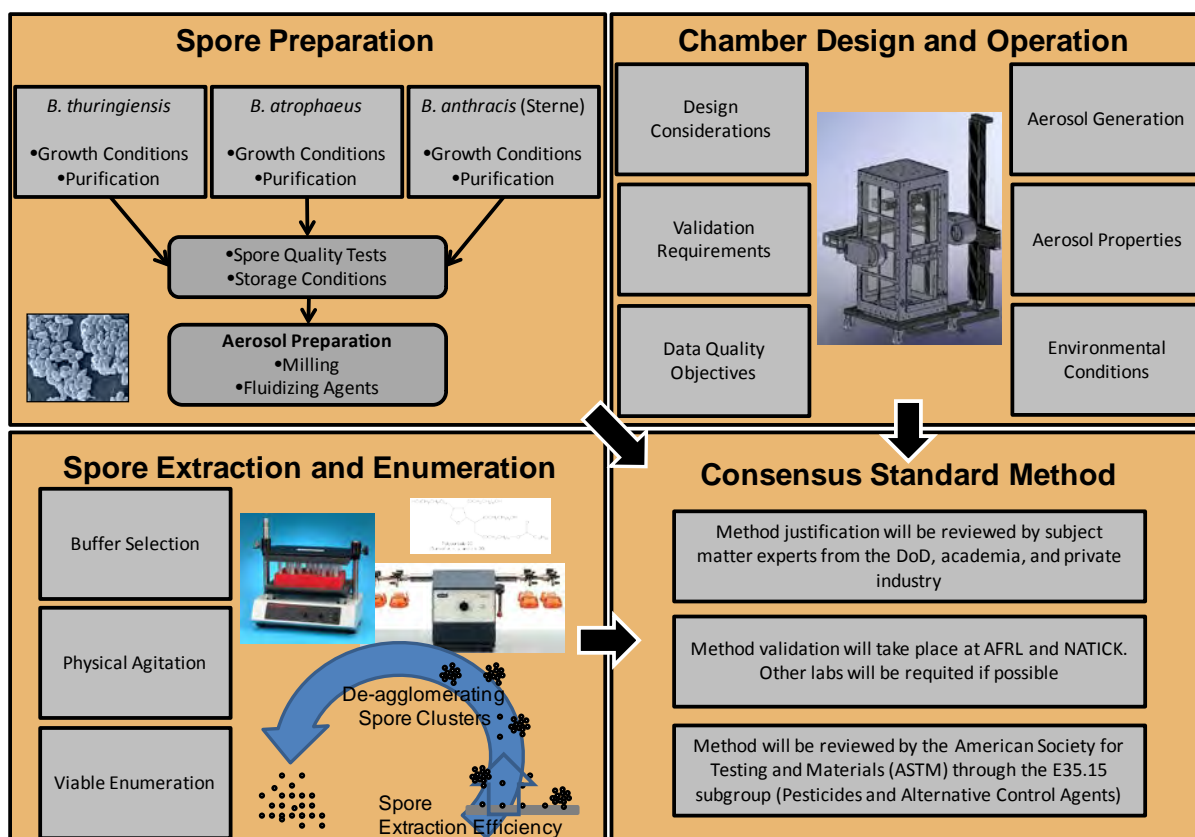


Figure 84. *Bacillus* Spore Aerosol Project Overview

The process of developing methods for depositing “threat-representative” *Bacillus* spores onto surfaces began with an extensive literature review to find common practices among researchers. We identified six critical method parameters that provided the foundation for developing the method (Table 51). Over 100 peer-reviewed journal articles and Department of Defense (DoD) technical reports were mined for information related to the six critical method elements.

Table 51. Critical Method Elements

Selection of a <i>Bacillus</i> spore suitable as an anthrax simulant
Procedures for preparation and purification of spores
Design and operation of Biological Dispersing System (BDS)
Aerosol characteristics and treatment
Extraction of spores from surfaces and viable enumeration
Data quality and data analysis

Based on findings in the literature, a method justification was developed to outline initial research plans for each parameter derived from common practices (detailed in the section to follow). The plan was only a starting point and it was anticipated the steps would change based on experimental research, and, as expected, the plan evolved. The method justification was also reviewed by several *Bacillus* spore experts within the United States Government, who provided invaluable input into shaping the methods (Table 52). Their comments will be discussed where applicable in the following sections. The end goal of this project is to publish the method as a

consensus standard that will be available to researchers around the world. To that end, the effort was registered as a work item with the American Society for Testing and Materials (ASTM), WK28501, under the purview of the E35.15 subcommittee that specializes in antimicrobials and microbiology. What follows is a description of the research performed at both AFRL/RXQL and Natick Soldier Systems Center to meet the objectives set forth in the method justification.

Table 52. Reviewers for the Method Justification

Reviewer Name	Organization
Tony Buhr, PhD	NSWC, Dahlgren, VA
Jose–Luis Sagripanti, PhD	ECBC
Jonathan Kiel, PhD	AFRL
Ed Fisher, M.Sc.	NIOSH-NPPTL
Vipin Rastogi, PhD	ECBC

5.3.2. Results and Discussion

5.3.2.1. Spore Selection, Production, and Quality Control

The most divergent areas we encountered in the literature review and among the reviewers were which spores to use, how to grow the spores and how to assess their quality. Our initial plan called for using three *Bacillus* species: *B. thuringiensis* (Bt), *B. atrophaeus* (Bg; formerly *B. globigii*), and *B. anthracis* (Sterne strain) (Ba(S)). Both Bt and Ba(S) are closely related to fully virulent *B. anthracis* and all three fall within the *B. cereus* family (Ash *et al.* 1991). These three are generally differentiated only by their plasmid contents, and some bacterial taxonomists suggest that they are all the same species (Ash *et al.* 1991, Helgason *et al.* 2004, Rasko *et al.* 2005). Both Bt and Ba(S) also produce an exosporium, which is a feature of fully virulent *B. anthracis* (Steichen *et al.* 2003). Bg was selected for this method because it is a historical strain used by the DoD and maintains a bridge to historical data. Several reviewers took exception to the use of Bg, which they consider unrepresentative of *B. anthracis*. Drs. Buhr, Kiel, and Rastogi recommended using *B. thuringiensis* Al Hakam (Bt-AH) strain because it is known to be highly environmentally stable. Dr. Rastogi recommended the use of *B. anthracis* ΔSterne (ΔS), which lacks both virulent plasmids and is a BSL-1 microorganism. Drs. Buhr and Rastogi, respectively, generously provided these strains, which were the focus of our spore production, purification, and quality control experimental plan. We performed some work with Bg and greatly broadened our work on the ΔS and Bt-AH strains.

Data quality objectives (DQOs) for spore purity and quality are critical to ensure the validity of subsequent tests using those spores. Poor-quality spores will yield poor data and likely produce inconsistent test results among laboratories. The primary DQO described in the literature is purity $\geq 95\%$ phase-bright spores. There are many tests for spore quality, but the commonest is heat resistance. Heating times and temperatures varied widely, and we settled on a treatment of 65 °C for 30 min. This was incorporated into the purification step, so a firm DQO was not set. However, only spores that survived the test would be used. Another data quality assessment of the spores is to test acid resistance. Dr. Sagripanti strongly recommended that the spores be acid resistant. The commonest test in the literature was to suspend spores in 2.5 N HCl for 10 min, neutralize to pH 7, then assess viability by dilution plating (Carrera *et al.* 2007, Sagripanti and Bonifacino 1996). A survival rate of $> 88\%$ is the objective of the test. Dr. Rastogi suggested using bleach tolerance as a quality control test for the spores, but we could find no references to this test in the literature. Also, Dr. Rastogi did not provide a firm DQO (survival rate after treatment with a specified

concentration of bleach for a given time), so we decided not to use this as a measure of quality for spore preps. The final DQO is concentration of the spores. We arbitrarily set an objective for the spore concentration to be 10^{11} spores/g of lyophilized material. Data quality of spores we produced as part of this method is discussed in the following paragraphs.

Growth conditions for producing spores (media, phase, time, agitation) diverged so widely that we were unable to justify the selection of a single media type based on best practices in the literature. We set an initial goal to select a common method and see if it would achieve the DQOs for spore purification and quality control. The method is a two-stage production in which spores are incubated in brain–heart infusion (BHI) broth (25 mL/250-mL flask) on a rotary shaker at 220 rpm and 37°C until the culture reaches log-phase growth (~2.5 h). In later experiments TSB was used instead of BHI broth. One mL of the inoculum is then transferred into 99 mL of Difco sporulation medium (Galeano *et al.* 2003; Lai *et al.* 2003)—identical to Schaeffer’s medium (Nicholson and Setlow 2000)—in a 1-L baffled flask. The flask is then incubated in a rotary shaker (300 rpm at 37°C) for 5 d or until it contains > 90% phase-bright spores. A common theme among many researchers is that a flask-to-liquid-volume ratio ≥ 10 is required for optimal sporulation. With this ratio, sufficient oxygen—vital for sporulation—is allowed to penetrate the medium.

Initial results using Bg were very favorable following this method, as it produced a large number of liberated phase-bright spores (Figure 85a). The same result was not observed using Bt (but *not* Bt-AH), as many of the spores were not released from the mother cell (Figure 85b). We were initially surprised by the Bt result, but apparently it is quite common. Drs. Buhr and Kiel reported having experienced the same phenomenon when preparing Bt spores. We considered treating the Bt spores with enzymatic or other methods to liberate the spores, but Dr. Sagripanti discouraged the idea, citing concerns over damaging the spore crop and reducing their overall resistance. Dr. Buhr suggested that the problem can be overcome by using a medium developed by his laboratory (Buhr *et al.* 2008), which contains 200 mM L-glutamate and trace salts that should allow the spore to mature and be released from the mother cells. We tried this medium with the Bt-AH culture and had better success but could not achieve high-quality preparations. Dr. Kiel recommended using blood agar plates (BAPs) to prepare the spores and we found this to produce free spores for both Bt-AH and ΔS (Figure 86). However, Bt-AH formed massive clumps that we could not disaggregate using normal methods and buffers. Drs. Kiel and Buhr acknowledged this problem and suggested that clumping was caused by the extremely hydrophobic surface of the spores. Dr. Kiel proposed using an ionic detergent to dissociate the spores but noted that the detergent would have to be removed prior to using the spores for testing, which would likely result in their re-aggregation. We viewed the clumping as a major limitation that would cause problems with the method and elected to focus solely on ΔS for the method.

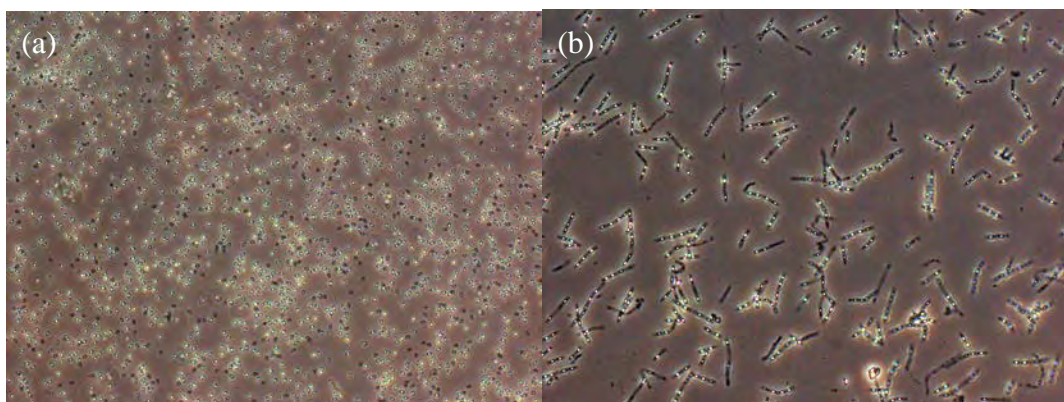


Figure 85. Spore Preparations Using Difco Sporulation Medium. (a) Bg Spores (Phase-dark Bodies Are Out-of-focus Phase-bright Spores), (b) Bt Spores

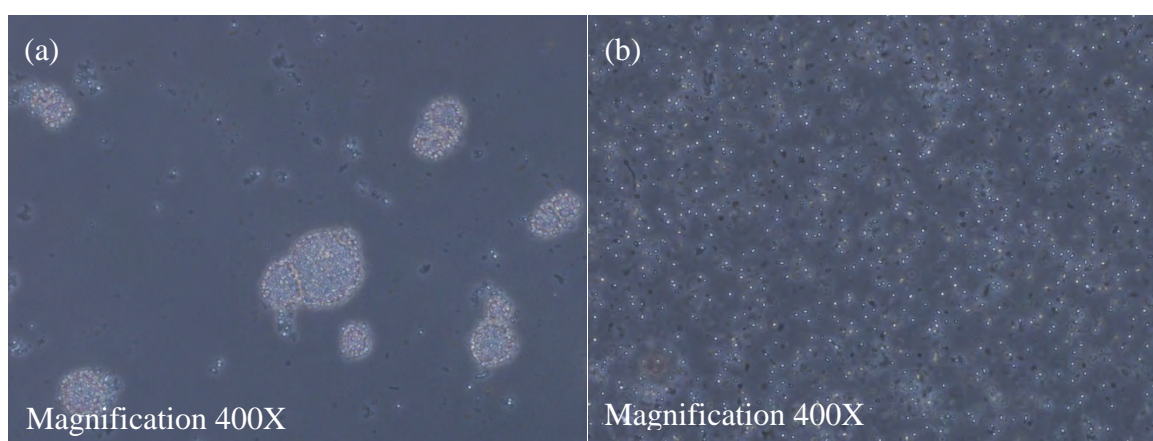


Figure 86. Spore Preparations Using Blood Agar Plates. (a) *B. thuringiensis* Al Hakam, (b) *B. anthracis* Δ Sterne

Two media for production of Δ S spores were compared: solid, BAP (20 petri plates); and liquid, 2.5% nutrient broth medium plus 200 mM L-glutamate and salts defined in the casein-hydrolysate media (CCY, Stewart *et al.* 1981) salts (900 mL of medium) using the shaking conditions described previously. Initially, we had some concerns over the quality of spores produced in solid vs. liquid cultures, but Dr. Kiel provided data showing that both spore preps behaved similarly when exposed to disinfectants. Our results (Table 53) indicated that the two methods produced similar amounts of spores.

Table 53. Comparison of Titters of *B. anthracis* Δ Sterne Grown on Blood Agar Plates with Spores Grown in Liquid Medium

Titer (Spores/g)				
Liquid medium			Blood agar plates	
Flask 1	Flask 2	Flask 3	Plate Set 1	Plate Set 2
2.00×10^9	1.20×10^9	2.30×10^9	2.20×10^9	2.45×10^9

However, when observed following six water washes liquid sporulation yields fewer phase-dark particles than those grown on BAP (Figure 87). The liquid sporulation medium is also a much easier protocol to use, so it was selected for production of spores. Note, however, that not all

replicate flasks gave the same sporulation efficiency. The reason for this is unclear, but the result illustrates clearly that spore quality must be tracked and documented.

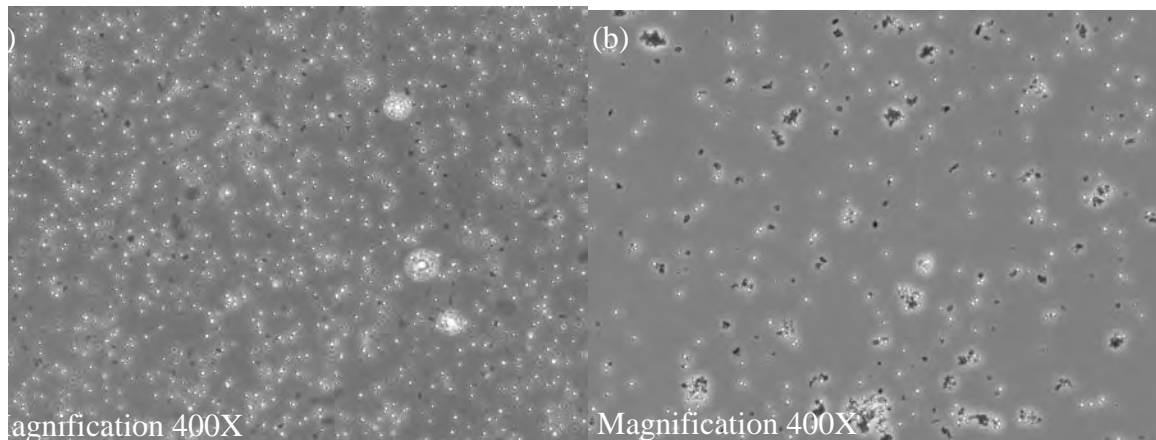


Figure 87. Preparations of *B. anthracis* Δ Sterne Spores from (a) Nutrient Agar with 200 mM L-Glutamate and CCY Salts, (b) Blood Agar Plates

Purification of Δ S was accomplished by water washings of the spores. As mentioned above, poor-quality spore preparations can be produced with the method, which will yield a lower percentage of phase-bright spores. Those preparations were discarded. We experimented with density gradient purification protocols using Histodenz (Sigma, St. Louis, MO), which does improve the quality of spore preparations (Figure 88); however, significant spore loss occurs. Also, if the reagents are not thoroughly removed by the water washes, they remain as a contaminating substance that can compete for antimicrobial compounds, adding another element that can complicate the method, *e.g.*, by consuming hypochlorite. The goal for the purification was $\geq 95\%$ phase-bright spores. Histodenz let us achieve this concentration—but with two-log loss in spore quantity (from 4.00×10^{10} to 2.40×10^8 spores/g) and inclusion of a contaminant that could compete with/for disinfectants. For these reasons, the spore DQO may have to be lowered.

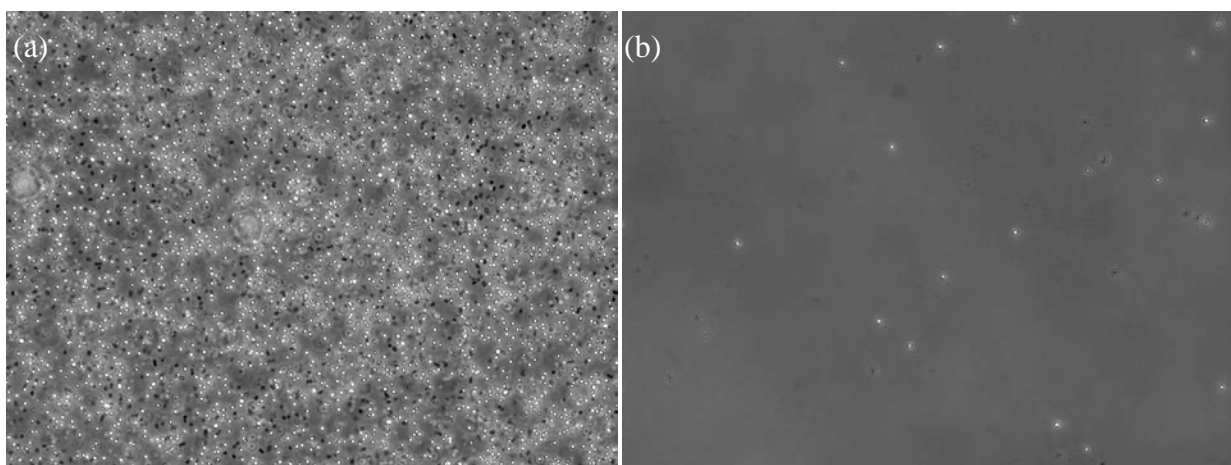


Figure 88. Preparation of *B. anthracis* Δ Sterne Spores (a) before Treatment with Histodenz, (b) after Treatment with Histodenz

Δ S spores were tested for acid resistance using the standard protocol described in the method justification. Our data determined that only $27 \pm 4\%$ of the spores were viable following treatment with 2.5 *N* HCl, one-third of the criterion of an 88% survival rate. The result was puzzling so we tested the *pH* of the solution following neutralization and measured *pH* 1. The neutralization step obviously did not succeed, consequently resulting in a longer treatment time. We have revised the neutralization step and will repeat the test. However, if the spores still show a low survival rate in acid, we will lower the acceptability standard. Δ S spores are clearly the spores of choice—they are closely related to the fully virulent strain *and* a BSL-1 microorganism. It is possible that alternate growth conditions will produce more-acid-resistant spores, so research will continue to investigate this further.

Optimal storage conditions for the spores are as a lyophilized powder (Nicholson and Setlow 1990), which is also used for aerosolization of the spores. Purified Δ S spore preps were lyophilized after being washed free of nonionic detergents, other salts, and amino acids. Four 900-mL lots of spores were grown using the liquid sporulation medium described above, yielding after lyophilization an average spore concentration of $2.0 \times 10^{11} \pm 5.84 \times 10^9$ spores/g, which meets the DQO set for the method.

Conditions for plating the spores are critical to achieving accurate plate counts. Clumping or poor extraction of spores from surfaces will provide variable results. Many viable plating tests were performed to generate the data described above. Each plating test used a defined buffer and agitation protocol to attempt to disaggregate the spores. The buffer was composed of 1X phosphate buffered saline (PBS), 0.05% Tween 20, and 250 mM glycine. PBS and Tween were common components found in many buffers in the literature. We added glycine because it improved removal efficiency of MS2 coli phage from porous surfaces in previous studies in our laboratory. Glycine is a small molecule and a zwitterion that competes with charge interactions that cause spores to stick to surfaces or themselves. The only concern for using glycine was that it might prematurely germinate the spores—some amino acids are known to cause germination. However, we demonstrated that glycine does not germinate any of the spore species we tested over the 24-h duration of the test. Agitation conditions selected for our tests require 5 min of swirling using a vortex mixer, followed by a 1-min sonication period using a standard sonicator.

5.3.2.2. Biological Dispersing System

Two identical chambers were constructed based on best practices found in the literature (Figure 89). The chambers will be operated at both AFRL/RXQL and Natick so the aerosol methods can be validated. A third chamber will also be constructed and sent to ECBC so they can participate in the validation as well. The chamber is a 0.6-m² base by 1.2-m high enclosure with six panels composed of 316 stainless steel and glass. Glass is typically not included in aerosol chambers as it is a nonconductive surface; it was needed to allow the chamber to be compatible with the Spraytec (Malvern Instruments Ltd, Worcestershire, UK) laser particle analyzer (Figure 89m). If the glass proves problematic, it can be replaced with conductive materials. The six panels are removable to allow unlimited modifications to the chamber. Easy access for cleaning and processing samples is available through two doors included on the chamber. The left door opens the entire side and the right door provides access to the lower portion of the chamber.

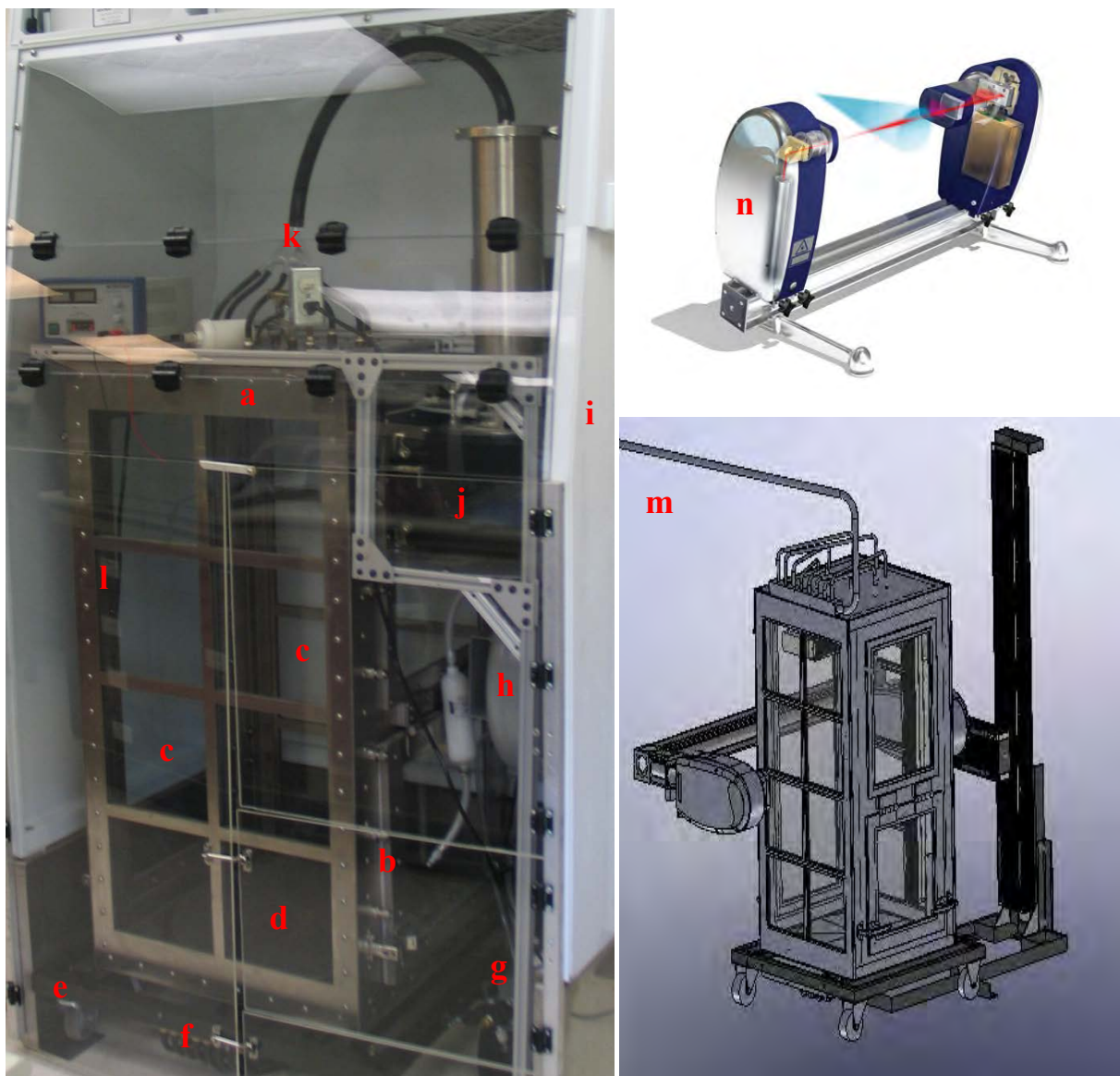


Figure 89. Biological Aerosol Dispensing System (BDS): (a) Chamber (b) Sample Access Door, (c) Optically Clear Glass Panels, (d) Rotating Table, (e) Rolling Cart, (f) Air Exit Manifold, (g) Air Compressor, (h) Air Buffer Tank, (i) Type I Biological Safety Cabinet, (j) Pitt-3 Powdered Aerosol Dispenser, (k) Six-Way Diffuser, (l) Large Access Door, (m) Biological Dispersing System, (n) Malvern Spraytec

The interior floor is a turntable for holding test samples; its variable-speed control allows rotational speeds up to 7 rpm. The turntable is not expected to be needed for this project, but experiments that utilize large droplets or droplet nuclei may require rotation of the samples to permit uniform distribution of particles/droplets onto the samples themselves. The top and bottom of the chamber have particle distribution manifolds that provide eight inlet and discharge ports for even distribution of the particles. The chamber is mounted on a wheeled cart for easy transport.

The aerosol generation system selected for this application is the Pitt-3 aerosol generator (Alburty Lab, Drexel, MO), which supports particles on a latex diaphragm that drives them using an audio speaker mounted below the diaphragm. The speaker is excited by the audio output of a computer sound card, which is controlled using “Sigjenny,” a software package that generates an audio signal. Audio signal frequency, amplitude, and wave form of the speaker can be adjusted to provide different aerosol characteristics. Compressed air lifts the suspended particles vertically into a 10-cm diameter stainless steel tube, then into 1.87-cm interior diameter conductive tubing. The conductive tubing is attached to a six-port glass diffuser that feeds the spores into the BDS. Air from the BDS is supplied to the aerosol generator using a diaphragm air compressor, regulator, and accumulator tank to eliminate pressure pulses from the compressor (Figure 90). HEPA filters are included at the compressor inlet and the aerosol generator inlet to assure that spores are not introduced into the compressor and that clean air is supplied to the aerosol generator. An additional HEPA filter is installed on a vent port located on the top of the BDS to assure that the enclosure is not pressurized. The system is a closed loop, assuring that the masses of air entering and leaving the chamber are equal, and guaranteeing the system remains at atmospheric pressure.

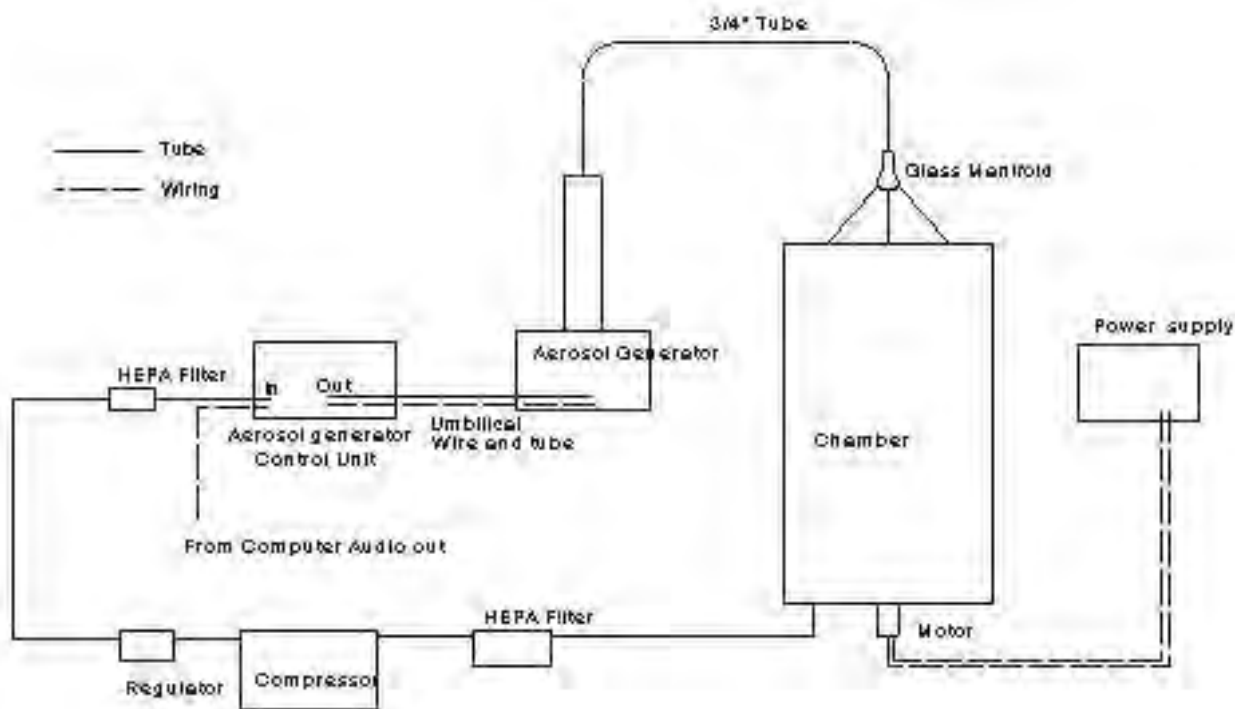


Figure 90. Plumbing Schematic Detailing Airflow in the Biological Dispersing System

5.3.2.3. Biological Aerosol Studies

The goal is for aerosolization conditions to mimic an operational threat. The preparation of spores for aerosolization may be considered sensitive information; however, the principles for causing spores to persist in the air are well known and exist in the open literature. The primary parameters of interest for our application are particle size and addition of fluidizing agents. The size range used by most researchers ranged from 1–5 μm , deeply respirable particles. The fluidization agent is commonly amorphous silica and we found researchers use it at a loading of 10–20% by weight

(Baron *et al.* 2008, Buttner *et al.* 2001). There are many types of amorphous silica and only one researcher identified a manufacturer. Brown *et al.* (2007, 2008) used Aerosil R812S (Evonik Degussa Corp., Parsippany, NJ), which we selected for our study. One area that was not detailed in any of the literature was the actual milling process to yield particles in the desired particle size range. We will experimentally determine those conditions using a commercial ball mill. The DQO for the aerosol is to create a fluidized spore preparation that results in an aerosol with a CMD of $\sim 2\ \mu\text{m}$. The DQO for aerosol concentration of spores will be experimentally determined based on the aerosol concentration required to meet the surface-loading objectives of $10^5\ \text{CFU}/\text{cm}^2$.

The first step in validating the chamber was to better understand the operation of the Pitt-3 aerosol generator. Speaker frequency, speaker amplitude, and airflow can all be adjusted independently and which condition produces the optimum output and size distribution is unknown. As the chamber was not complete at the time of the experiment, the Pitt-3 was coupled with an Aerodynamic Particle Sizer (TSI Inc., Shoreview, MN), as shown in Figure 91, to measure the particle output. We also had not prepared lyophilized spores yet, so we used a commercially available insecticide, Dipel® dust (Voluntary Purchasing Group, Bonham, TX) that contains Bt spores. Twenty-seven experiments were performed that varied each of the parameters. Three-factor interactions were assumed to be zero, making the data set large enough to obtain confidence levels. At a 95% or greater confidence level, flow and amplitude were shown to increase the number of particles (Figure 92). Amplitude also caused a slight increase in particle size, but flow had no effect on particle size (Figure 93). Frequency did not affect the number or the size of the particles (data not shown). In addition, none of the two-level interactions were significant, which supports the assumption that the three-level interaction was near zero.

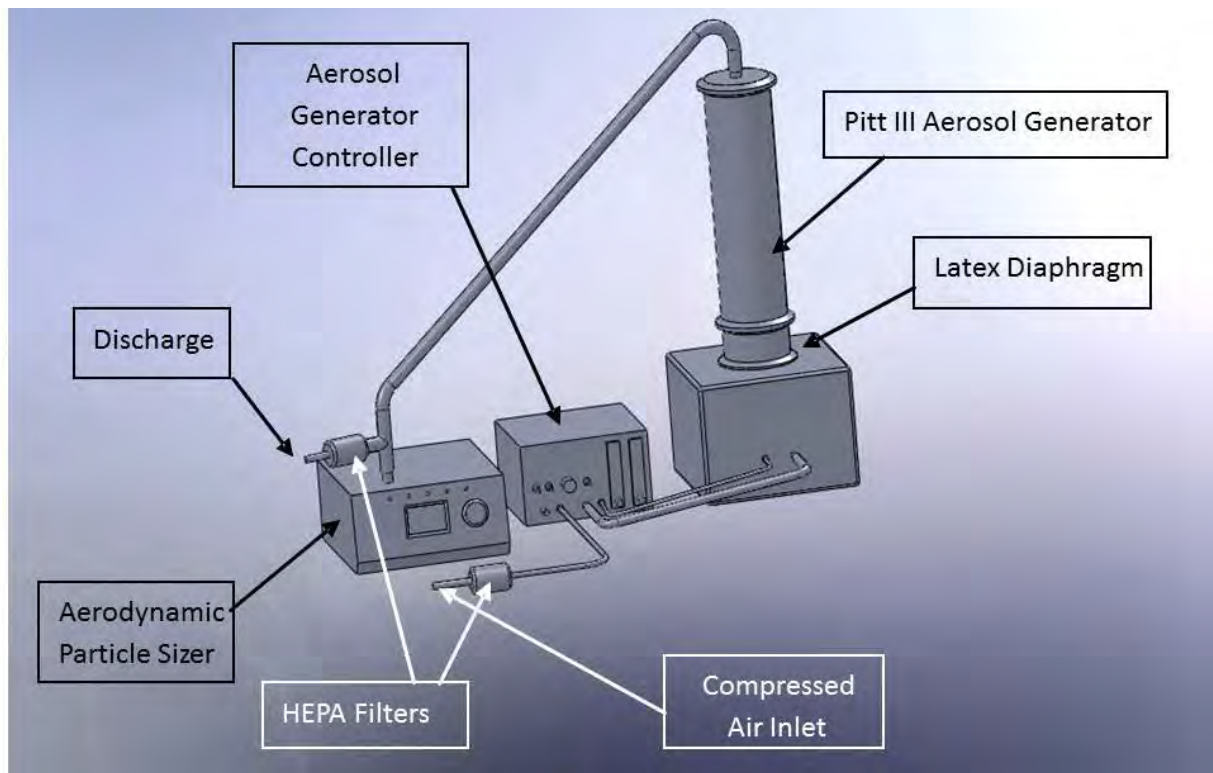


Figure 91. Test Setup for Analyzing Pitt-3 Aerosol Generator

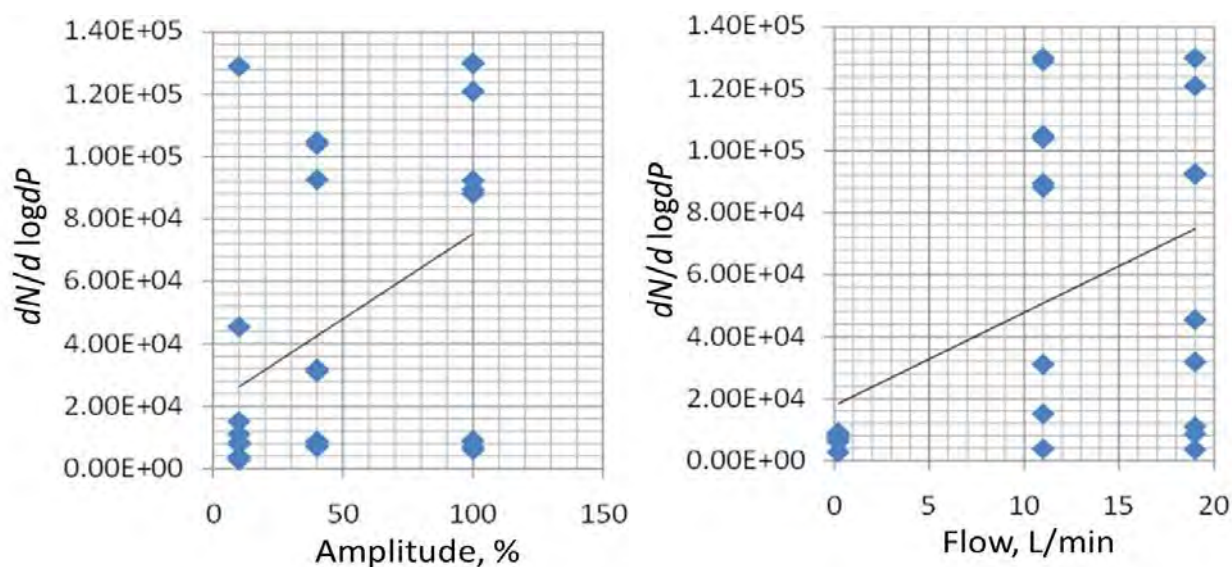


Figure 92. Particle Quantities as Functions of Speaker Amplitude and Flow

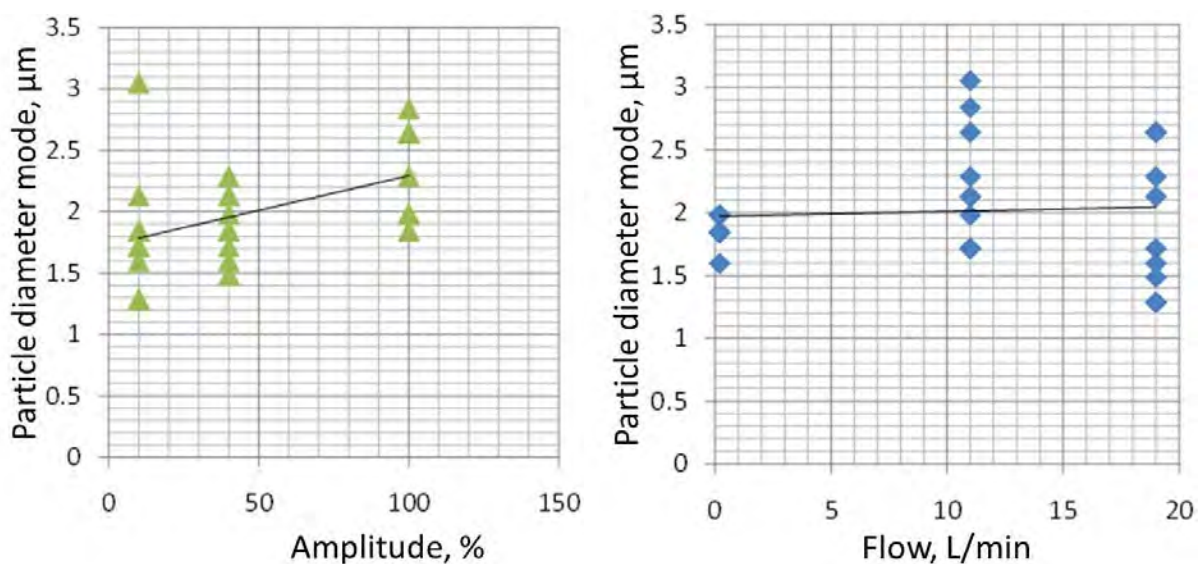


Figure 93. Particle Size as a Function of Amplitude and Flow

The optimal operational conditions selected for the Pitt-3 generator were 100-Hz speaker frequency using a sine wave input, 80% speaker amplitude (volume), and 20 L/min airflow.

We anticipated that the amount of spore powder we can prepare will be limited, so we also wanted to determine the minimum amount of powder required to create the aerosols. Three experiments were performed using the optimal conditions and varying powder amounts: 50, 100, and 250 mg. The data show that the 100-mg charge produced the same concentration of 2- μm CMD particles as the 250-mg charge, and only slightly more than the 50-mg charge (Figure 94). The 250-mg charge produced a higher concentration of larger particles, but that is not the goal of this study and, in practice, could be considered a liability. Hence, we selected 100 mg as the powder charge to aerosolize in subsequent experiments with Dipel®. These data also demonstrate that 10 min of aerosolization time yields a maximum concentration of spores in the size range of interest.

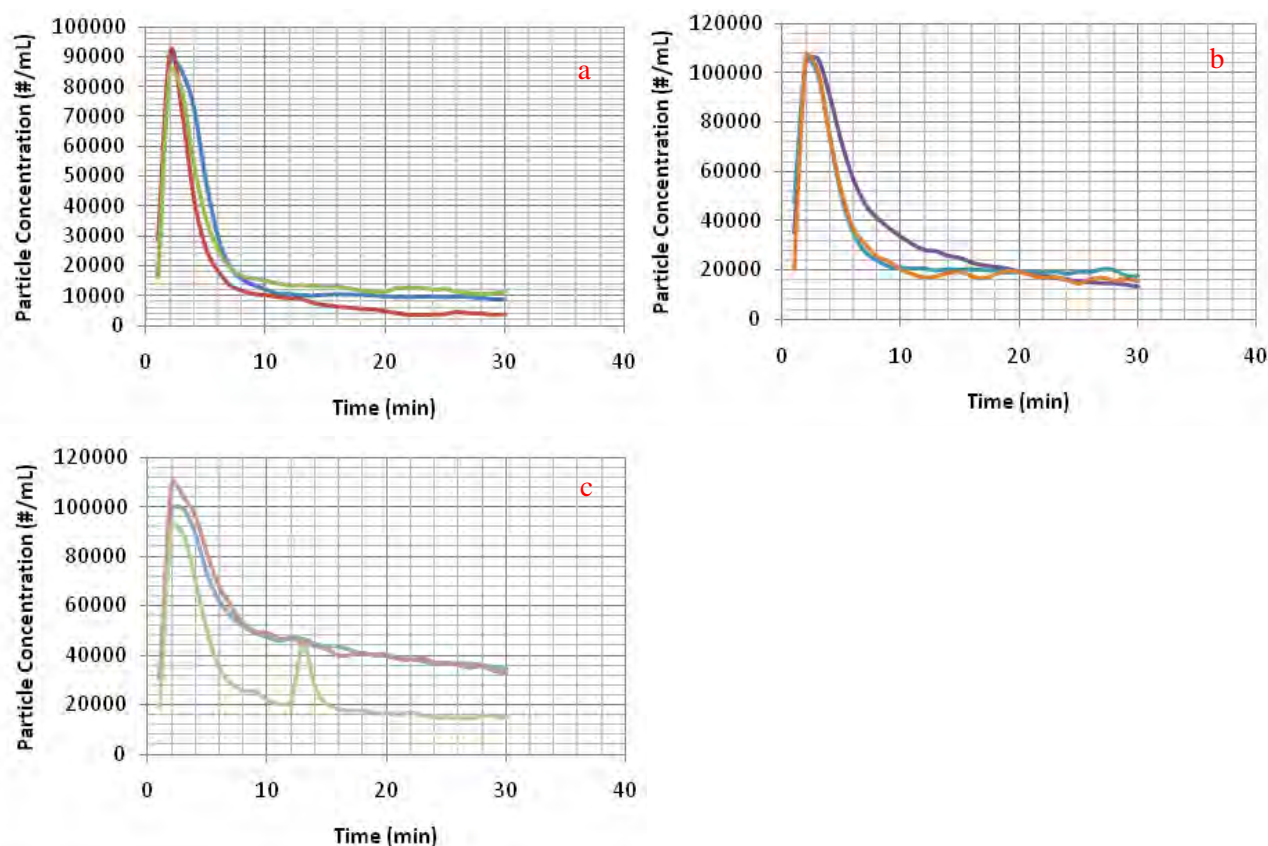


Figure 94. Particle Concentration Produced in the Pitt-3 Aerosol Generator Using Different Starting Weights of Dipel® Dust: (a) 50 mg, (b) 100 mg, (c) 250 mg.

5.3.2.4. Chamber Studies

The first test performed in the BDS used the parameters derived above with unmilled Bg spore powders. ΔS spores would have been preferred, but those spores were not available at the time of the study. However, the purpose of this test was only to determine particle size distribution in air, and loading concentration and distribution of spores onto surfaces, for which any spore would suffice. The Pitt-3 was loaded with 100 mg of Bg spores produced using standard methods described previously. It was operated for 10 min at a flow rate of 20 L/min, while the speaker delivered a 100-Hz sine wave at 80% amplitude. The APS detected two distinct peaks in the aerosol, at $<1 \mu\text{m}$ and $\sim 2.84 \mu\text{m}$, which comprise single spores and small agglomerates (Figure 95). The DQOs for the study call for a CMD of $2.5 \mu\text{m}$, so we appear to have shown that the specification will need to be restated.

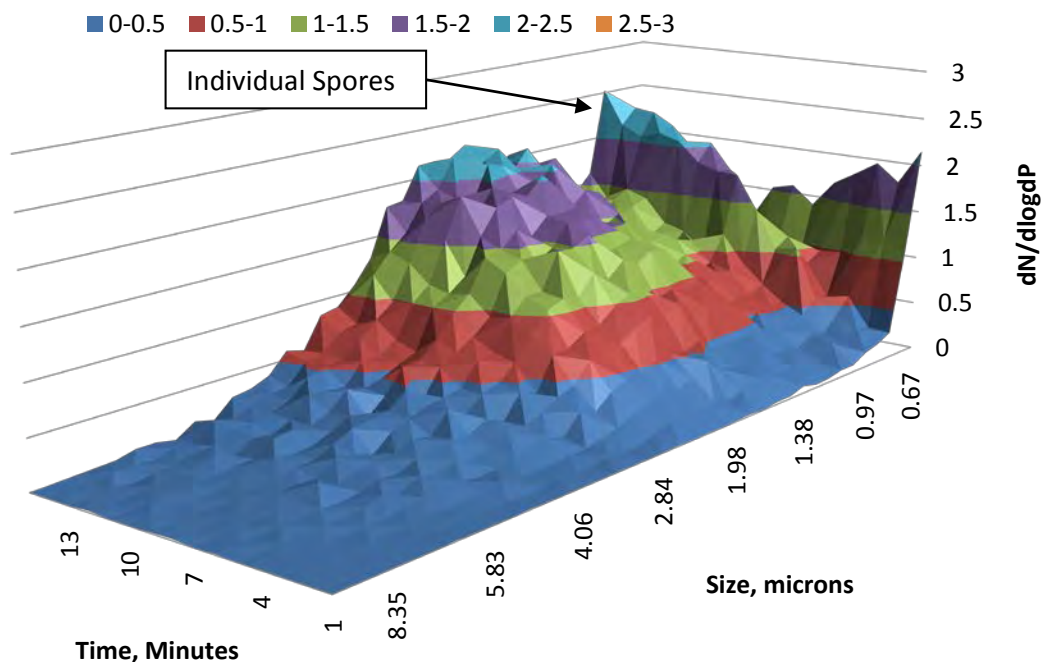


Figure 95. Particle Size as a Function of Amplitude and Flow

To evaluate spore loading, nine samples of four representative materials (Table 54) were loaded on the BDS turntable (Figure 96). To correlate direct colony counts, trypticase soy agar (TSA) plates and reservoirs that had a similar outside diameter as the test samples were also loaded. The liquid reservoirs were filled with 3 mL of the extraction buffer, which will be used to evaluate extraction efficiency from samples. The presumption is that spores will load equally onto a given surface area and thus a comparison of the total spores that settled on the liquid reservoirs and test samples will provide information on how difficult the spores are to remove from the surfaces. Following loading, spores were allowed to settle onto the substrates overnight (~18 h). Samples were then collected and placed into 50-mL conical tubes containing 10 mL of extraction buffer. For the reservoir samples, the 3 mL of fluid was added to 7 mL of extraction buffer in a 50-mL conical tube. The TSA plates were directly removed from the chamber and incubated at 37 °C. The remaining samples were extracted and viable plating was performed as described above. The following day, colonies were counted and CFUs/cm² were determined for each spore surface.

Table 54. Material List and Dimensions of Sample Used to Evaluate Spore Loading in the Biological Dispersing System

Material	Diameter (in)	Height (in)
Liquid reservoir	1.25	0.4375
Butyl rubber	1.0	0.25
COLPRO tent	1.0	~0.03
Polycarbonate	1.0	0.25
Stainless steel	1.00	0.25

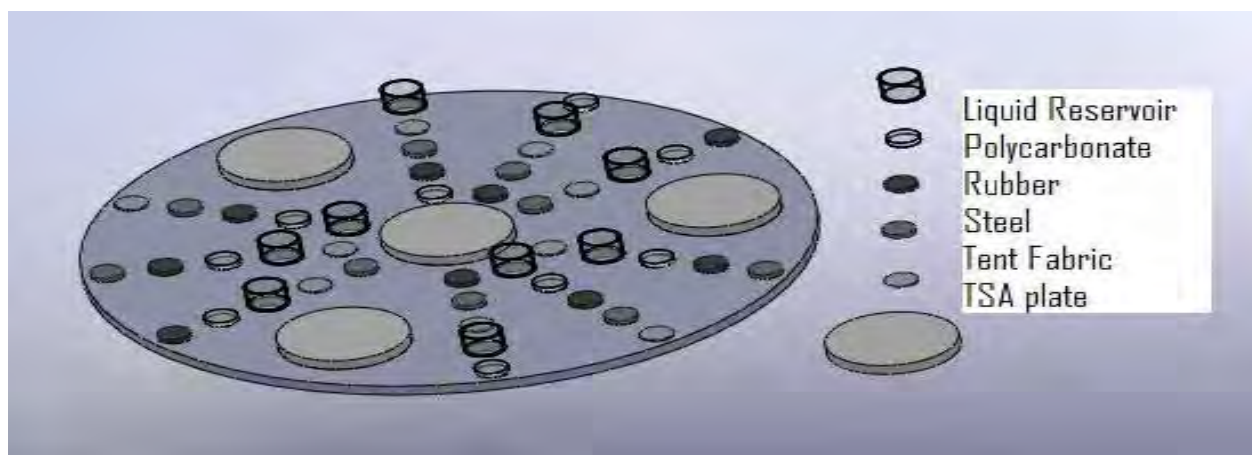


Figure 96. Sample Loading Pattern in the Biological Dispersing System

All samples provided a loading concentration exceeding the DQO of 10^5 CFU/cm² (Table 55.).

Table 55. Data Compiled from the *Bacillus atrophaeus* Spore Aerosol Run in the Biological Dispersing System

Samples	Average CFUs/ cm ²	STDEV	CV	Extraction Efficiency
Liquid reservoir samples	1.46×10^5	1.08×10^4	7.4%	-----
Butyl rubber	2.02×10^5	2.87×10^4	14.2%	138%
COLPRO tent	1.93×10^5	1.88×10^4	9.7%	132%
Polycarbonate	4.30×10^5	1.41×10^5	32.7%	295%
Stainless steel	1.86×10^5	2.75×10^4	14.8%	127%

The coefficient of variation (CV) among the nine samples was also within specification for three of the four samples and the liquid reservoirs (CV < 20%). This not only demonstrates that each sample loads evenly, but that the spores are also evenly distributed throughout the chamber. The nine samples were intentionally distributed across the chamber (Figure 96) to support this evaluation. The polycarbonate samples anomalously load >2x higher than the rest, but at a CV of only 32.7%. The moderate CV suggests that the test is reliable and that a systematic bias is acting, possibly a static charge on the polycarbonate attracting spores through some charge effect. Grounding the polycarbonate vessel or adding a fluidization agent to the spores may diminish this effect. Measurements of extraction efficiency showed recoveries exceeding 100% for all samples, which we can't explain yet. Recovering the liquid from the reservoirs was a challenge and incomplete recovery would bias the extraction efficiency. A weak trend of loading nonconductive surfaces more heavily might indicate attraction to weakly charged aerosol surfaces. New reservoirs have been added that we hope will alleviate this problem. It may also be possible that the spores don't load onto liquid or porous surfaces with the same efficiency as solid surfaces. We consider this unlikely, but substitution of the new reservoirs will be the next step in evaluating this question.

5.3.3. Conclusions

A great deal of progress was made during FY2010 towards the end goal of developing an ASTM method for applying threat-representative *Bacillus* spores onto surfaces. The method justification provided the framework for the effort and, along with the review from the spore experts, laid the groundwork for the experimental effort. The spore production, purification, and quality control

measures proved to be more time consuming and more difficult than expected. In hindsight, we should have expected more delays in this area, as we have been frustrated many times by trying to repeat methods in the literature. The nuances and difficulties are simply not reported by the authors. However, even with the delays, we still managed to finalize the steps for growing and purifying the spores. It is likely however that a large-scale fermentation (30-L fermenter) may be needed to produce enough spores to perform multiple aerosol experiments. The current protocol generates roughly 100 mg of spores per 900 mL of starting medium, so an adequate supply of spores could in principle be so prepared, yet the task would consume many labor hours.

The chamber development was a challenging process, as the goal was to develop a chamber that meets the requirements of this project but can be easily modified to meet the needs of future projects. This was accomplished by making all six sides removable. There were also some engineering challenges to mate the system with the Malvern Robotics system, but they were overcome. Currently, there are two chambers: Natick and AFRL each own one. A third chamber is being constructed for ECBC that will allow for a three-lab validation of the methods. Understanding the operational characteristics of the Pitt-3 generator provided the framework for determining the conditions for aerosolizing the spores. The literature involving the Pitt-3 indicated significant changes in particle size and concentration could be achieved by varying three parameters. We found that adjusting only sound amplitude (volume) and flow rate made a difference. Essentially, both were roughly maximized for net output of particles around 2.5 μm . It appears very little can be done to affect particle size distribution which, under such delicate aerosolization conditions, can be expected to be determined by the initial size of the particles.

The experimental plan focused entirely on reaching DQOs. The spore purity and acid test won't meet the initial DQOs. We can meet spore purity objectives but only by sacrificing yield and adding a potential interferent to the mix. We can't justify the tradeoff to reach the DQO for purity at this stage of investigation. Acid resistance is a function of the spore and we don't think much can be done to influence this without changing spore type and, as we are using the most appropriate strain, *B. anthracis* ΔSterne , we don't see changing strains to accommodate an acid test as reasonable. There also seems to be little justification for including acid resistance as a criterion. DQOs for aerosol properties of the spores and for loading and distribution of the spores were achieved using Bg spores. We don't anticipate that ΔS spores will behave differently. This test was performed with non-fluidized spores, but we think the addition of the fluidizing agent will only enhance spore dispersion and may decrease some of the charge effects that appear to have acted in the loading of the polycarbonate collector.

Our goal was to have all the spore loading studies completed in CY10 and the only limitation is producing an adequate amount of spores to do the experiments. Preliminary studies of milling indicate a significant loss of spores that was not initially accounted for. We are in the process of scaling up spore production and hopeful that these tests will be completed in CY10. If not, they will be completed in early CY11. Validation of the methods also remains to be completed. Spore production methods have taken many turns that prevented a formal validation. We anticipate the spore production to be validated at both Natick and AFRL in early CY11. Validation of the spore deposition methods should also occur at Natick, ECBC, and AFRL in early 2011. Natick has their chamber and we have received quotes to have the ECBC chamber constructed and delivered to them. Once the validation is complete, we will be able to write and deliver the formal ASTM method to the E35.15 committee. Unfortunately, that is just the starting point and it will take

some time to get the method officially approved. ASTM meets only twice annually and all negative ballots must be rectified and reballoted. We hope that our experience in gaining approval for two other ASTM methods will expedite the process.

5.4. FFR Hospital FFR Wear Assessment and Cleaning Study

5.4.1. Technical Introduction

Pandemic influenza outbreaks historically occur every 40 to 50 years and have caused millions of deaths worldwide (Kilbourne 2006, Oxford 2000). Before the turn of the century, the Hong Kong Flu of 1968 was the most recent pandemic and experts feared another epidemic was imminent. Their fears were realized in the spring of 2009, with the onset of the H1N1 swine flu (Dawood *et al.* 2009, Naffakh 2009). On 11 June 2009, the World Health Organization (WHO) raised the pandemic alert level to Phase 6, announcing that a pandemic was underway and alerting the need for global response and mitigation. The WHO reported H1N1 infections in more than 214 countries and attributed over 18,449 deaths to H1N1 infections in their August 2010 update (WHO 2010). While this outbreak was less severe than earlier pandemics, it was sufficiently similar to previous pandemics to merit concern. Although it is not certain that the current H1N1 strain will mutate into a more virulent strain, healthcare workers are taking the possibility very seriously (Morens *et al.* 2010).

A primary barrier for protecting healthcare workers from airborne infections is the National Institute for Occupational Safety and Health (NIOSH)-approved FFR. Although many types of these devices are available, the focus of this report is N95 FFRs. N95 FFRs are rated to capture $\geq 95\%$ of airborne particles $\sim 0.3 \mu\text{m}$ in diameter and have been demonstrated to remove infectious microorganisms from the atmosphere (Balazy *et al.* 2006, Heimbuch *et al.* 2006). The modes for human transmission of influenza are actively debated (Bridges *et al.* 2003, Tellier 2006), but data exist that support aerosol transmission (Tellier 2006). This information led the Occupational Safety and Health Administration (OSHA) and the Centers for Disease Control (CDC) to recommend that healthcare workers wear a properly fitted, NIOSH-approved FFR when treating patients with influenza symptoms (CDC 2007, OSHA 2007). During a pandemic lasting 42 days, the CDC estimates that healthcare workers will require over 90 million FFRs (Bailar *et al.* 2006). These projections indicate that a shortage of FFRs is likely to occur, leaving healthcare workers exposed and possibly aggravating the severity of the pandemic. A solution proposed for alleviating a shortage is to decontaminate and reuse FFRs (Bailar *et al.* 2006).

FFRs are labeled as “single-use” devices and have not been approved for reuse. Consequently, scarce data are available to describe how FFRs behave following decontamination/cleaning. Many properties require evaluation before FFR decontamination and reuse would be appropriate: biocidal efficacy, filtration efficiency, pressure drop, fit, residual toxicity, and overall durability. Studies performed by NIOSH indicate that some decontamination technologies did not degrade the performance of FFRs; however, other technologies (e.g., autoclaving) render FFRs unusable (Viscusi *et al.* 2007, 2009, Bergman 2010). NIOSH also has data to support that fit is not significantly altered following decontamination via three energetic decontamination methods (ultraviolet germicidal irradiation, microwave-generated steam, and low-temperature moist heat; R. Shaffer, personal communication). AFRL has demonstrated that six commonly distributed FFRs treated with a diverse range of decontaminants do not leave toxic residues on the FFR (Salter *et al.* 2010). Furthermore, it was shown that the three energetic decontamination methods

mentioned above provide > 4-log reduction in viable H1N1 influenza applied to FFRs as droplets or droplet nuclei that are representative of human respiratory secretions (Heimbuch *et al.* 2010a).

While there are data to support the possibility of FFR reuse and decontamination, more research is needed before the procedures could be implemented. One criterion lacking from the initial study was the ability to clean the FFRs. FDA policies for reuse of medical devices dictate that cleaning is required before the device can be returned to service. Cleaning FFRs is a challenging task and must meet the same acceptance criteria described for decontamination. The porous outer surfaces of FFRs do not lend themselves to efficient cleaning. To address the ability to clean N95 FFRs, AFRL performed a study that evaluated three contaminants (*S. aureus*, mucin protein, and synthetic sebum) and their removal efficiency from three N95 FFR models (Heimbuch *et al.* 2010b). AFRL selected three commercially available wipe products for the evaluation: 3M 504/07065 respirator cleaning wipe with active ingredient, benzyl alkyl chloride (3M MSDS); Current Technology, Inc., Hype-wipe with active ingredient, 0.9% hypochlorite (Current Technologies MSDS); and Pampers baby wipe, no active ingredients (Proctor and Gamble MSDS). The study evaluated three FDA-approved, NIOSH-certified N95 FFRs: 3M 1860S, 3M 1870, and Kimberly Clark PFR. The 3M and Hype-wipe products both contain an antimicrobial compound, and the combination of both cleaning (removal of *S. aureus*) and the disinfection (inactivation of *S. aureus*) contributed to a microbial removal efficiency of > 99% on the external and internal surfaces of the FFRs. The baby wipe removed > 85% of the *S. aureus* applied to the three models of FFRs. The baby wipe does not contain an antimicrobial and, thus, the difference in *S. aureus* recovery can be contributed to removal. The addition of the disinfectants in the Hype-wipe and 3M respirator cleaning wipe appear to provide an advantage over the baby wipe. However, concerns of residual chemicals and toxicity to the user are present with both technologies. Hypochlorite discolors the respirator and leaves a chlorine odor. Moreover, the 3M respirator cleaning wipe caused a slight reduction in particle performance after one cleaning. For these reasons and until more research can be performed, it was determined the only suitable wipe product was the baby wipe.

A potential drawback to the cleaning study was that it focused on new FFRs. It is not clear that used FFRs will be cleaned with the same efficiency as new FFRs. Also, high concentrations of contaminants were used to measure high-log reductions. It is not likely these concentrations will be achieved during normal use, and the evaluation of a “normal” loading concentration is a data gap that requires more research. Our current study is aimed at determining the microbial loading of FFRs during typical use in a healthcare facility, the diversity of microorganisms collected, and how effectively these FFRs can be cleaned.



5.4.2. Materials and Methods

5.4.2.1. Collection of FFRs

FFRs were treated with ultraviolet germicidal irradiation (UVGI) to reduce the normal microbial flora on new FFRs. An XX-405 UV Bench Lamp (UVP, LLC Upland, CA), containing a bulb producing UV-C (254 nm) light, was configured so that new FFRs could be placed 2 in from the bulb and exposed for 30 min. The dose of UV-C irradiation was 20 mW/cm², measured using a calibrated UVX Radiometer (UVP, LLC Upland, CA). The UVGI-treated FFRs selected for this study (Table 56) were provided to the environmental staff at Bay Medical Center (Panama City, FL), who donned the FFRs during their normal cleaning routines of rooms of discharged patients.

The environmental staff documented the duration of time the FFR was worn and the room location. Upon completion of cleaning duties, each staff member doffed the respirator and placed it in a sterile plastic bag, preloaded with a sterile cotton plug saturated with 5 mL of sterile water to maintain a humid environment. The bag was placed in a cooler containing ice for ~18 h.

Table 56. Filtering Facepiece Respirators (FFRs) Selected for the Study

<u>Image</u>		
<u>Model</u>	3M 1860S	3M 1870

In an attempt to avoid hand contact with the areas targeted for extraction and analysis, respirator training was provided to the environmental staff, focusing on proper donning and doffing of the new FFR. Prior to donning the respirator, the environmental staff was instructed to wear two pairs of clean gloves. Once the room was cleaned, staff members were instructed to remove the outside set of gloves and doff the used FFR with a clean glove, avoiding the central areas, and place the FFR into the sterile bag. The respirators were worn for ~30 min.

5.4.2.2. Cleaning of FFRs with Wipes

Sterile bags containing the FFRs were placed into a biological safety cabinet (BSC) and the FFRs were removed for cleaning. On a typical day, 4–6 respirators were collected from the environmental staff. Half of the FFRs were wiped with a Pampers baby wipe (Procter & Gamble, Cincinnati, OH), as previously described (Heimbuch *et al.* 2010b), and the remainder were not cleaned.

5.4.2.3. Extraction of Microbial Contaminants from FFRs

Each respirator was placed on a sterile Teflon® cutting board and cut with a 38-mm circular hammered punch to produce three coupons per FFR (total surface area evaluated was 34 cm²). The coupons were dismantled to separate the filtering layer (middle layer) from the external layer (exposed to the hospital air). The internal layer was discarded. The like samples from each FFR (filtering or external layer) were placed in a 50-mL polypropylene centrifuge tube containing 10 mL of extraction buffer [250 mM glycine, 0.01% Tween 80, 50 mM phosphate buffer and PBS (potassium phosphate [monobasic] 0.18 g/L, potassium phosphate [dibasic] 1.52 g/L, sodium chloride 8.5g/L at pH 7.0)]. The samples were mixed for 5 min using a multitube vortex mixer (Fisher Scientific, Pittsburgh, PA). A 2-mL portion of the extract was placed in sterile cryovials and frozen at -80 °C. A 5-mL aliquot of the extraction fluid was filtered through a sterile (0.45 µm, 47 mm) GN-6 Metrical® MCE membrane disc filter (Pall Corporation, Ann Arbor, MI). The filter was placed, loaded-side-up, on the surface of a trypticase soy agar plate (TSA, Fisher Scientific, Pittsburgh, PA) and incubated at 37 °C for 48 h. Following incubation,

the colonies were counted and recorded. Microbial loading (microorganisms/cm² of FFR) was determined using Equation 10, in which VB is viable bacteria extracted per cm² of FFR, and n is the number of bacteria on the filter. The cleaning efficiency of the wipe for each FFR was determined using Equation 11, in which CE is the cleaning efficiency, and VB is the count of viable bacteria extracted per cm² of FFR.

$$VB = n \times 2 \div 34 \quad (10)$$

$$CE = \frac{\overline{VB}_{uncleaned}}{\overline{VB}_{cleaned}} \times 100\% \quad (11)$$

5.4.2.3. Quantitation and Selection of Representative Microorganisms Extracted from FFRs

Too many bacterial colonies were growing on the surface of membrane disc filters in TSA plates to select all of the isolates; therefore, a representative population was chosen based on colony color, size, and morphology. Representatives of each colony type were transferred from the isolation plates and streaked for isolation onto TSA plates. Additional purification was performed as needed to obtain pure isolates. Isolates were then suspended in 10% glycerol and frozen at -80 °C.

5.4.2.4. Biochemical Analysis and Antimicrobial Resistance Testing of Bacterial Isolates

Purified isolates were characterized by Gram staining to determine Gram reaction and cell morphology. Each bacterial isolate was then tested on MacConkey's mannitol salt medium and bile esculin agar, both acting as selective/differential media. According to manufacturing procedures, Gram-negative microorganisms were tested with the 20E API® system; Gram-positive microorganisms were tested with the API® Staph test system; and Gram-variable microorganisms were tested with both systems (bioMérieux Clinical Diagnostics, Marcy l'Etoile, France). Bacterial control microorganisms, *Ps. aeruginosa*, *E. coli*, and *S. aureus*, were routinely tested to ensure the process and reagents were performing as necessary.

Antibiotics were purchased from Sigma–Aldrich (St. Louis, MO) and added to sterile TSA, cooled to 58 °C. Vancomycin was added at a concentration of 64 µg/mL and oxacillin was added at 4 µg/mL. Bacterial isolates were T-streaked onto TSA-antibiotic plates and incubated at 35 °C. Resistance was determined by growth at 24 and 48 h. Strong, uninhibited growth was designated full positive (high); partial growth, one-half positive (low); and absence of growth, negative.

5.4.2.5. Tracer Microorganism Loading onto FFRs (*S. aureus*)

This portion of the effort has not been completed due to equipment allocation issues. Protocols for performing this work were previously described (Heimbuch *et al.* 2010b).

5.4.3. Results

5.4.3.1. Quantitation of Microbial Load from FFRs

For the 3M 1860 respirators, 50 FFRs worn by the environmental staff at Bay Medical Center were evaluated: 25 were cleaned with baby wipes and 25 served as uncleaned controls. The uncleaned, external section yielded a mean of 24.15 CFU/cm² of respirator (Figure 97); thus, a typical 200 cm² respirator would yield ~4830 CFU on the full surface of the used FFR. The filtering layer yielded a mean of 0.6 CFU/cm² of respirator (Figure 97); therefore, a typical 200-cm² respirator would yield 120 CFUs. For the 3M 1870 respirators, 53 were donned by the Bay Medical environmental staff and evaluated: 26 were cleaned with baby wipes and 27 were not

cleaned and served as controls for the experiment. The uncleaned, external sections of the FFR donned by the staff yielded a mean of 3.11 CFU/cm² of respirator (Figure 98); hence, a typical 200 cm² respirator would yield ~622 CFU on the total external surface of a used FFR. The internal layer of the uncleaned FFRs had a mean of 0.1 CFU/cm² of respirator (Figure 98), indicating a typical 200-cm² respirator would yield 20 CFUs. Analysis of microbial loading on the external and filtering layers of the 3M 1860 FFR showed that 97.5% of viable microorganisms were deposited on the external layer and 2.5% were found in the filtering element. An unpaired, two-tailed *t*-test found the two populations to be statistically significant ($P=0.0004$) at 95% confidence intervals (CI). Similar data were found for the 3M 1870 FFR where 96.9% of viable microorganisms were deposited on the external layer and only 3.1% were deposited on the internal filtering layer. An unpaired, two-tailed *t*-test revealed the two populations to be statistically significant ($P=0.011$) at 95% CI.

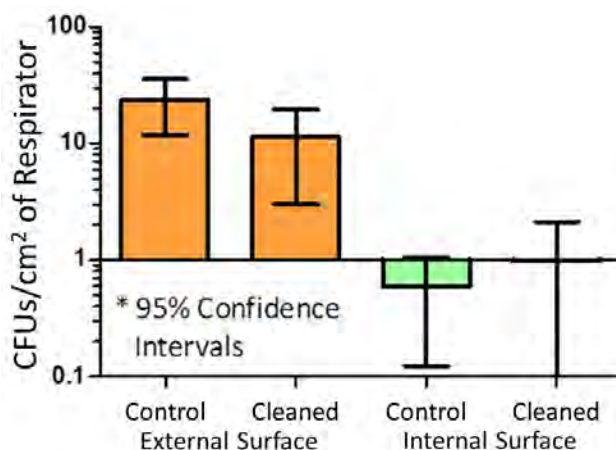


Figure 97. Cleaning Efficiency for the 3M 1860 FFR

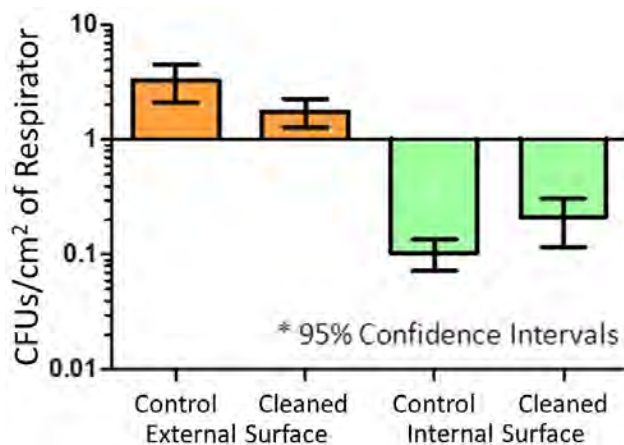


Figure 98. Cleaning Efficiency for the 3M 1870 FFR

5.4.3.2. Cleaning Efficiency of Baby Wipes on FFRs

The external sections of the cleaned 3M 1860 respirators resulted in an average of 11.26 CFU/cm² of respirator, a 52.5% reduction (Figure 97) in viable bacteria. However, the data were not statistically significant ($P=0.0888$) at the 95% CI, as indicated by an unpaired, two-tailed *t*-test. The external layer of 26 cleaned 3M 1870 respirators resulted in an average of 1.75 CFU/cm² of respirator, showing a 44.0% reduction in bacteria that were present on the uncleaned FFR (Figure

98). Using an unpaired, two-tailed *t*-test, a statistical comparison of the cleaned and uncleaned data for the 3M 1870 FFR demonstrated the two populations were not statistically significant ($P = 0.2779$) at the 95% CI. The external layer of 13 unused, UVGI-treated 3M 1860 FFR controls was examined, resulting in a mean of 0.09 CFU/cm² (standard deviation ± 0.191). Additionally, the external layer of 13 unused, UVGI-treated 3M 1870 FFRs were observed, averaging 0.05 CFU/cm² (standard deviation ± 0.0673).

Using an unpaired, two-tailed *t*-test, a comparison of the cleaned and uncleaned data (0.98 and 0.6 CFU/cm², respectively, Figure 97) for the filtering layer of the 3M 1860 FFR demonstrated the two populations were not statistically significant ($P = 0.5258$) at the 95% CI. Testing the internal layer of 14 unused, UVGI-treated 3M 1860 FFRs found a mean of 0.0672 CFU/cm² (standard deviation ± 0.159). Evaluation of the filtering layer of 25 cleaned 3M 1870 FFRs demonstrated a mean of 0.18 CFU/cm² vs. the uncleaned filtering layer, which contained 0.10 CFU/cm². Statistical analysis using an unpaired, two-tailed *t*-test, showed the two populations were not significant ($P = 0.2791$) at the 95% CI. The internal layer of 13 unused, UVGI-treated 3M 1870 FFR controls yielded a mean of 0.1447 CFU/cm² (standard deviation ± 0.283).

5.4.3.3. Colony Morphology and API Analysis

Initial selection of bacterial isolates based on colony size, color, and morphology aided in the selection of representative colonies of each bacterial type extracted from the FFRs and minimized duplication. A total of 550 isolates were selected; however, some cultures did not grow during purification, and several isolates did not recover from the -80 °C freezer stocks. A total of 498 isolates were Gram-stained and screened by API analysis. API analysis provided a means for separation of bacterial isolates into groups with varying degrees of confidence (Table 57).

5.4.3.4. Differential/Selective Media and Antibiotic Resistance.

Bile esculin is the recommended differential/selective medium for growth and identification of *Enterococci*. Accordingly, 81.3% of bacterial isolates from both FFRs grew in the presence of the 4% bile salts. In addition, 23.3% of the isolates expressed ability to metabolize esculin to glucose and esculetin, which combines with ferric ions to produce a black color on the agar (Table 58). For *Staphylococcus* identification, mannitol salt agar uses 5% salt concentration to inhibit growth of other bacterial types. Results showed that 78.1% of the isolates grew in this particular medium. Isolates capable of metabolizing mannitol to lactic acid, producing a yellow color, accounted for 21.5% of the isolates (Table 58). Eleven isolates were identified as *S. aureus* by API analysis; all of these isolates grew on mannitol salt agar, and nine isolates produced the yellow color.

Numerous isolates distributed among many API identification species demonstrated antibiotic resistance to both vancomycin and oxacillin: 29.1% and 59.6%, respectively (Table 59). Only a fraction of these isolates were highly resistant: 16.5% vancomycin and 12.9% oxacillin.

5.4.3.5. Tracer Microorganism Loading of FFRs (*S. aureus*).

This portion of the effort was not completed due to equipment allocation issues.

5.4.4. Discussion

The initial purpose of this study was to determine if FFRs contaminated with microorganisms in a hospital setting could be effectively cleaned using a standard wipe product. However, the data collected afford a great deal of insight into many other issues surrounding decontamination and

reuse of FFRs. A significant data gap exists regarding the level of microbial contamination found on FFRs. This study demonstrated that, for a 20-min FFR wear time, the level of contamination varied from 3–24 CFU/cm². For a typical FFR (200 cm²), the level of loading would be 600–4800 CFUs. It is uncertain that this level of loading would cause concern for FFR wearers. FFRs are not labeled as a sterile product, and it is unclear what the allowable bioburden is for new devices. The wide differences in microbial contamination between the 3M 1860 and 3M 1870 cannot be clearly discerned. When the 3M 1860 FFR was introduced into the study, the environmental staff wearing the FFRs had turned over. It is possible that the new staff was less careful in handling the FFRs. However, the second team also worked in different areas of the hospital, which could have contained more contamination. A third possibility is that microbes are recovered more easily from the 3M 1870 than the 3M 1860. However, for the high concentration of *S. aureus* applied to both models, recovery efficiencies were similar (Heimbuch *et al.* 2010b). As this was a field study, we expected a certain amount of variability and the inability to account for all variables.

FFRs contain multiple layers that provide various functions. FDA-approved surgical FFRs, like those used in this study, have a hydrophobic outer scrim and an internal layer to protect the filtering layer that is sandwiched between the two. For this study, only the external and filtering layers were evaluated to determine the location of the microorganisms contaminating the FFR. The internal layer would have contained a high microbial load due to contamination with respiratory secretions from the user of the device. Our data indicate that > 96% of the microbial contamination existed on the external layer of the FFR. This was surprising, given that most experts believe the filtering layer is responsible for removing airborne particles from the air stream. These data suggest that a majority of the particles that come in contact with the FFR are quite large and are trapped on the external membrane. The filtration efficiency of the external membrane is not defined, but is likely very low; otherwise, it would contribute significantly to the breathing resistance of the device. The FFRs for this study were worn by environmental staff, and significantly different data could be found if healthcare workers with direct patient contact were utilized; this certainly deserves further examination. If the results were the same, it could indicate the N95 is over-protective and that a lower level of protection may be adequate. Using a device with a lower level of protection would confer some benefits: user comfort, better sealing capacity, lower pressure drop, etc. While the data collected here are compelling, there is concern that FFR contamination may have occurred by contact transmission, rather than airborne transmission due to improper handling techniques. The staff was trained not to touch the FFRs, but not observed during respirator use; therefore, we cannot rule out this possibility. A study with a higher level of control, including sampling observation, would eliminate this concern.

Table 57. API Analysis of Bacterial Isolates from FFRs 3M 1860 and 3M 1870

*Genus and species	API Identification Match							Total
	99.9 - 90%	90 - 80%	80-70%	70-60%	60-50%	50-40%	40-30%	
<i>Micococcus spp</i>	95	5	1	2	0	0	0	103
<i>Staphylococcus epidermidis</i>	32	15	8	1	6	2	0	64
<i>Staphylococcus hominis</i>	7	5	8	8	3	9	3	43
<i>Staphylococcus haemolyticus</i>	1	1	2	1	3	9	0	17
<i>Staphylococcus capitis</i>	1	2	4	5	3	0	1	16
<i>Staphylococcus cohnii ssp cohnii</i>	5	2	0	1	1	0	4	13
<i>Staphylococcus sciuri</i>	2	2	4	2	0	1	1	12
<i>Staphylococcus lentus</i>	11	0	0	0	0	0	0	11
<i>Staphylococcus aureus</i>	4	2	0	5	0	0	0	11
<i>Staphylococcus saprophyticus</i>	1	3	2	2	1	1	0	10
<i>Kocuria varians/rosea</i>	1	4	0	1	0	2	0	8
<i>Kocuria kristinae</i>	3	1	2	0	0	1	0	7
<i>Staphylococcus lugdunensis</i>	1	2	1	2	0	1	0	7
<i>Staphylococcus chromogenes</i>	0	3	1	0	0	2	1	7
<i>Staphylococcus warneri</i>	0	2	0	3	0	0	0	5
<i>Pseudomonas fluorescens/putida</i>	0	4	0	0	0	0	0	4
<i>Staphylococcus xylosus</i>	2	0	0	1	0	0	0	3
<i>Ochrobactrum anthropi</i>	0	0	0	2	1	0	0	3
<i>Staphylococcus caprae</i>	1	0	0	1	0	0	0	2
<i>Staphylococcus auricularis</i>	0	0	0	1	1	0	0	2
<i>non-fermenter spp</i>	0	0	0	0	0	0	2	2
<i>Acinetobacter baumannii/calcoaceticus</i>	1	0	0	0	0	0	0	1
<i>Pasteurella pneumotropica/Mannheimia</i>	0	1	0	0	0	0	0	1
<i>Rahnella aquatilis</i>	0	1	0	0	0	0	0	1
<i>Stenotrophomonas maltophilia</i>	0	0	1	0	0	0	0	1
<i>Staphylococcus schleiferi</i>	0	0	0	0	0	0	1	1

*146 isolates unacceptable identification

Table 58. Growth Properties of Bacterial Isolates on Differential and Selective Media

Genus and species	Totals	Bile Esculin		Mannitol salts	
		Growth	Color	Growth	Color
<i>Micococcus spp</i>	102	92	14	87	9
<i>Staphylococcus epidermidis</i>	66	58	3	61	3
<i>Staphylococcus hominis</i>	42	34	7	39	6
<i>Staphylococcus haemolyticus</i>	17	17	7	16	10
<i>Staphylococcus capitis</i>	16	16	4	16	6
<i>Staphylococcus cohnii ssp cohnii</i>	12	11	8	11	5
<i>Staphylococcus sciuri</i>	12	11	8	11	5
<i>Staphylococcus lentus</i>	11	8	7	8	5
<i>Staphylococcus aureus</i>	11	10	1	11	9
<i>Staphylococcus saprophyticus</i>	9	9	1	9	6
<i>Kocuria varians/rosea</i>	8	8	1	8	1
<i>Kocuria kristinae</i>	7	5	2	7	1
<i>Staphylococcus lugdunensis</i>	6	6	2	6	0
<i>Staphylococcus chromogenes</i>	7	6	0	7	2
<i>Staphylococcus warneri</i>	5	5	0	5	0
<i>Pseudomonas fluorescens/putida</i>	4	3	0	0	0
<i>Staphylococcus xylosus</i>	3	3	1	2	2
<i>Ochrobactrum anthropi</i>	3	3	2	2	0
<i>Staphylococcus caprae</i>	2	1	0	2	2
<i>Staphylococcus auricularis</i>	2	2	0	2	1
<i>non-fermenter spp</i>	2	1	1	1	0
<i>Acinetobacter baumannii/calcoaceticus</i>	1	0	0	0	0
<i>Pasteurella pneumotropica/Mannheimia</i>	1	1	0	1	0
<i>Rahnella aquatilis</i>	1	1	1	1	1
<i>Stenotrophomonas maltophilia</i>	1	1	0	1	0
<i>Staphylococcus schleiferi</i>	1	1	0	1	1
*146 isolates unacceptable identification	146	92	46	74	32
Total	498	405	116	389	107
Percent of Total	-----	81.3%	23.3%	78.1%	21.5%

*API cut off for identification is < 30%

Table 59. Vancomycin and Oxaicillin Resistance of Bacterial Isolates from FFRs

Genus and species	Totals	Vancomycin Resistance		Oxacillin Resistance	
		High	Total	High	Total
<i>Micococcus spp</i>	102	10	41	78	85
<i>Staphylococcus epidermidis</i>	66	5	17	20	25
<i>Staphylococcus hominis</i>	42	3	8	22	30
<i>Staphylococcus haemolyticus</i>	17	4	6	10	14
<i>Staphylococcus capitis</i>	16	2	3	2	3
<i>Staphylococcus cohnii ssp cohnii</i>	12	1	2	4	7
<i>Staphylococcus sciuri</i>	12	0	0	6	7
<i>Staphylococcus lentus</i>	11	1	1	7	8
<i>Staphylococcus aureus</i>	11	0	4	3	7
<i>Staphylococcus saprophyticus</i>	9	0	4	2	3
<i>Kocuria varians/rosea</i>	8	1	2	3	4
<i>Kocuria kristinae</i>	7	0	0	4	4
<i>Staphylococcus lugdunensis</i>	6	0	1	0	0
<i>Staphylococcus chromogenes</i>	7	0	3	0	1
<i>Staphylococcus warneri</i>	5	0	2	1	1
<i>Pseudomonas fluorescens/putida</i>	4	3	3	3	4
<i>Staphylococcus xylosus</i>	3	1	1	2	2
<i>Ochrobactrum anthropi</i>	3	1	1	3	3
<i>Staphylococcus caprae</i>	2	0	1	1	1
<i>Staphylococcus auricularis</i>	2	1	1	2	2
<i>non-fermenter spp</i>	2	2	2	2	2
<i>Acinetobacter baumannii/calcoaceticus</i>	1	1	1	1	1
<i>Pasteurella pneumotropica/Mannheimia</i>	1	0	0	0	0
<i>Rahnella aquatilis</i>	1	1	1	0	1
<i>Stenotrophomonas maltophilia</i>	1	0	0	0	0
<i>Staphylococcus schleiferi</i>	1	0	0	0	0
*146 isolates unacceptable identification	146	27	41	57	82
Total	498	64	146	233	297
Percent of Total	-----	12.9%	29.3%	46.8%	59.6%

*API cut off for identification is < 30%

Cleaning efficiency of the FFRs was demonstrated to be 52.5% and 44% for the external layer of the 3M 1860 and 3M 1870 FFRs, respectively. Cleaning of the filtering layers was ineffective, as would be expected. In fact, bacterial loads isolated from the filtering layers of the cleaned FFRs are actually higher than those obtained from the uncleaned FFRs, implying that wiping may have pushed some bacteria through the external membrane onto the filtering layer. However, all data for both the external and internal cleaning of both models of FFRs were not statistically significant compared to the control population. This indicates high variability in the data, easily observed in Figures 97 and 98. Large variability was expected, as this was a field study with multiple factors affecting loading on any given day: don/doff technique of the staffer, room cleaned, duration between previous cleanings, cleaning techniques, thoroughness, etc. Had a larger population of FFRs been collected, differences between the cleaned and uncleaned population might have proven to be significant. However, a larger data set would likely not have changed the 40~50% cleaning efficiency. FFRs have porous surfaces and were not designed to be cleaned. If cleaning becomes a requirement for decontamination and reuse, it is likely that development of a new FFR with an easily cleaned surface will be necessary.

To determine the threat posed to healthcare workers, identification of the microbial population recovered was of interest. The process of identification is quite laborious and costly; thus, not all microbes could be evaluated. A directed approach, based on colony morphology, was used to identify isolates for further identification. It is important to note that no attempt was made to group isolates based on colony morphology or to speculate on the quantity of specific types of microbes found throughout the study. Instead, we undertook a directed/random sampling of the population to provide some insight on the types of microorganisms collected on FFRs. API tests (Table 57) provided identifications for 77% of the isolates; the remainder fell below the 30% threshold. We grouped the isolates into brackets comprising percentage ranges, but the significance is unclear of, for example, an identification of 40–50%. Our discussion with an API representative elicited no clarity about what the percent match means or why 30% is the cutoff for rejecting an identification of an isolate. Clearly, higher percentage matches should correlate to higher levels of confidence in the match. Twenty-six species were identified with a majority of the isolates falling in the *Micrococcus* and *Staphylococcus* genera. Of notable interest, there was an identification of *Acinetobacter baumannii/caccae*, which is a known problem in hospitals. Only one isolate was identified, but was in the 90–99% confidence bracket. There were also eleven *S. aureus* strains, all having an identification > 60%. Many of the other matches are benign organisms, some of which are commonly found on human skin (*S. epidermidis*, *Kocuria*), lending credence to the possibility that some of the FFR contamination may have been contact transfer from the environmental staff. Interestingly, no *Enterococcus* species was identified as vancomycin-resistant. *Enterococcus* is a common problem in hospitals.

The bile esculin and mannitol salts biochemical tests support that there would be numerous *Enterococcus* and *Staphylococcus aureus* species identified (Table 58). Bile esculin agar supported growth and color change for 23.3% of the isolates, but as mentioned above, no *Enterococcus* was identified using the API biochemical strips. Equally perplexing is the bile esculin results that are positive for both growth and color change for microbes identified as non-*Enterococcus* bacteria by the API strips. More work is needed to sort out the discrepancies. The mannitol salts medium supported growth and color change for 21.5% of the isolates and properly identified nine of the eleven *S. aureus* strains identified by API analysis. As with the bile esculin results, it not clear why positive results were found for other genera identified by the API strips.

The antibiotic resistance data shows a large number of isolates resistant to both vancomycin and oxacillin (Table 63). This is not surprising given the amount of methicillin-resistant *S. aureus* (MRSA) and vancomycin-resistant *Enterococcus* (VRE) found in hospitals. However, only eleven *S. aureus* isolates were identified (seven were resistant to oxacillin) and 297 additional isolates were shown to have some resistance to oxacillin. The same phenomenon was found for vancomycin resistance, in which 146 isolates displayed some resistance, but none were identified as *Enterococcus*. This indicates the antibiotic resistance is prevalent in species other than MRSA and VRE. Many of these organisms are not human pathogens, but are present on the skin where they may have been exposed to the antibiotics. They are unlikely to cause any harm unless they develop other virulence factors. They may also act a reservoir for the antibiotic-resistant genes and transfer them to more virulent strains. More work should be done on this subgroup of antibiotic-resistant, but non-pathogenic group of microorganisms to see what role they play in the incidence of nosocomial infections.

5.4.5. Study Limitations

We acknowledge that the study presented in this report is not perfect and as with any study, additional funding, time, resources, and capabilities would have added value and answered some of the lingering questions. Each of the study limitations is explained in the following paragraphs:

- Ideally, this study would have been performed with healthcare workers wearing FFRs when treating patients. This may have significantly changed the number and types of microbes found on the FFRs. However, one cannot say that the number of microbes loaded onto the FFRs would have increased or decreased. Modification in the study, however, would not have affected cleanability of the FFRs, the primary focus of the study.
- As mentioned previously, the limited number of FFRs collected and the use of only two FFR models provide a degree of uncertainty in the cleaning data. Significantly increasing the sample size may cause the difference between the cleaned and uncleaned populations to be significant. However, it is improbable that there would be a change in the 40~50% removal efficiency of the viable contamination from the surface of FFRs. Other models may also provide a different result; however, we consider this unlikely, as many FFRs have a porous outer surface, which may be the primary impediment to cleaning.
- The isolation strategy for collecting viable populations was not ideal, and changes in the media used might provide a different outcome. Ideally, multiple media should be used; as microbial populations found on the FFRs were so small, a filtration technique had to be used to concentrate the extracts so that the population could be properly enumerated. This limited the study to using only one medium. TSA was selected for this study because it is

common and supports the growth of many types of aerobic heterotrophic bacteria. Use of more-selective media for facilitating the growth of fastidious microbes may have yielded more unique microorganisms, but it would have involved isolating the vast majority of microorganisms; both methods could not be performed

- The use of molecular biology methods would have improved the study. Not all microorganisms are culturable, and analysis with molecular identification techniques would have added value. As the microorganisms present on the FFRs are essentially unknown, the standard method for performing this type of research would be to create 16s rRNA libraries. This research is very expensive and timely; hence, it was not available as part of this effort. Also, while these techniques would have provided a better understanding of the diversity of microbes present, it would not have provided additional information about the cleanability of FFRs.

5.4.6. Summary

The primary objective of this study was to evaluate the cleaning efficiency of FFRs worn in a hospital setting. It is unlikely that the 40~50% reduction in viable bacteria observed in this study will be satisfactory to meet regulatory requirements for cleaning. That result, however, does not diminish the importance of this study. At the very least, cleanability of current FFRs on the market was addressed. The results of this study, as well as a previous cleaning study (Heimbuch *et al.* 2010b), point to several aspects of the FFR that could be improved to yield a cleanable device. Additionally, much needed data on several issues were provided by the study. The load of viable microorganisms on FFRs was approximated at 100s to 1000s for a typical 20-min wear time. We are unaware of other data that estimate the microbial load applied to FFRs during use. The location of the contamination on the external membrane, rather than the filtering membrane, not only has significant implications for evaluating the threat posed to the user, but also can be employed for advanced development of FFRs. More-appropriate devices can be developed to better meet the needs of healthcare workers. Finally, the diversity of microbes found and their antibiotic resistance patterns are also noteworthy. The data suggest that numerous non-pathogenic microbes are resistant to vancomycin and oxacillin. Research conducted to better understand their role in nosocomial infections would be invaluable. We acknowledge the study has drawbacks and limitations, but it provides some reasonable estimates for previous data gaps, and credence for future research.

5.5. Summary/Intangibles

Considerable achievements were made under this task for all three technical projects: spore deposition method development, FFR soiling and decontamination, and H1N1 challenge of FFRs. Valuable information was obtained about microorganisms that exist in a hospital environment and the hazards that may be faced by healthcare workers. The presence of antibiotic-resistant microorganisms should motivate industry to develop products that are antimicrobial in nature and offer better protection to healthcare workers. The realization that the FFR external layer shields the majority of microorganisms from contact with the filtering layer was an important discovery that will aid in developing a more user-friendly FFR that lends itself to cleaning. Furthermore, flow rate and particle size challenges to the FFRs confirmed the N95 FFRs consistently provides competent protection. Alterations can be made to the FFR that allow

for manufacturing a less expensive FFR, while still affording adequate protection to the user. Additionally, we discovered that there is no consensus in the scientific literature on methods for spore preparation. The research we conducted on *B. anthracis* Δ Sterne spore preparation, as well as the BDS deposition studies looking at loading density and distribution on various substrates, will lead to publishing an ASTM International standard that emphasizes data quality objectives for other researchers to follow, ultimately leading to advanced quality research. Defining these criteria for researchers will be helpful in future investigations addressing reaerosolization properties of spores. In addition to these technical accomplishments, ARA also provided support for proposals, presentations, and publications that are summarized below.

5.5.1. Proposals

- A quad chart and white paper titled “Fate, Virulence and Transport of Microorganisms Co-Aerosolized with Environmental Contaminants” was submitted to the Defense Threat Reduction Agency in response to the services call for Phase I research. DTRA notified us that the idea was accepted for Phase II.
 - Four white papers were submitted to BARDA.
 - “Measurement of Respiratory Secretions Produced by Humans”
 - “Need for Multiple Sizes of Articulated Respirator Test Headforms”
 - “Novel Designs for Filtering Facepiece Respirators”
 - “Advanced Development of Respiratory Protection Devices”

5.5.2. Meetings/Presentations

- A lecture titled “A Pandemic Influenza Preparedness Study: Decontamination of Filtering Facepiece Respirators in the Event of a Shortage Caused by Pandemic Influenza” was presented by Mr. Brian Heimbuch at the Biothreat Agents Workshop in Charlotte, ND. The workshop focused on strategies to counter biothreats and enhance national preparedness in the event of a threat.
- A lecture titled “Respiratory Protection Goes beyond Pandemic Influenza” presented by Mr. Brian Heimbuch at the Technical Support Working Group December meeting in Fort Lauderdale, FL.
- An lecture titled “Pandemic Influenza Preparedness” was presented in April by Mr. Brian Heimbuch at the ARA Engineering and Science Symposium in Orlando, FL.
- A lecture titled “Evaluation and Cleaning of Filtering Facepiece Respirators Worn in a Hospital Setting” was presented by Dr. William Wallace at the American Association for Aerosol Research’s October meeting in Portland, OR.
- A lecture titled “Deposition of *Bacillus* Spores on Zero-Volume Airlock Materials” was presented in April by Dr. William Wallace at the ARA Engineering and Science Symposium.
- A lecture titled “Live-Animal Infectivity Study of a Viable Pathogen Penetrating through a Reactive Filter Medium” was prepared and presented by Ms. Rashelle McDonald at the ARA Engineering and Science Symposium; a poster on the same topic was presented to the American Association for Aerosol Research in October.
- A poster titled “Standard Method for Applying Threat Representative *Bacillus* Spores to Surfaces” was presented by Ms. Kimberly Kinney and Mr. McDonald at the Florida

branch meeting of American Society for Microbiology and also at the American Association for Aerosol Research annual meeting, both held in October.

- A poster presentation titled “Challenge of Filtering Facepiece Respirators with Viable H1N1 Influenza Aerosols” was prepared and presented by Mr. Del Harnish at the Florida branch meeting of American Society for Microbiology and also, the American Association for Aerosol Research, both held in October.

5.5.3. Publications and Standards

- Heimbuch BK, WH Wallace, K Kinney, AE Lumley, C-Y Wu , M-H Woo, J. D. Wander, A Pandemic Influenza Preparedness Study: Use of Energetic Methods to Decontaminate Filtering Facepiece Respirators Contaminated with H1N1 Aerosols and Droplets , *American Journal of Infection Control*, 2010;38(1):3–8
- Salter WB, Kinney K, Wallace WH, Lumley AE, Heimbuch BK, Wander JD. Analysis of Residual Chemicals on Filtering Facepiece Respirators after Decontamination. *Journal of Environmental and Occupational Health*. 2010;7(8):437–445
- Bergman M.S., D.J. Viscusi, B. K. Heimbuch, J.D. Wander, A.R. Sambol, R.E. Shaffer, Evaluation of Multiple (3-Cycle) Decontamination Processing for Filtering Facepiece Respirators, *Journal of Engineered Fibers and Fabrics*. 2010; 5(4):34-41
- ASTM 2720-10: Standard test method for effectiveness of decontamination of air-permeable materials challenged with biological aerosols containing human pathogenic viruses. American Society for Testing and Materials (ASTM) International, 100 Barr Harbor Drive, West Conshohocken (PA) 19428-2959. 2010 *in press*.
- ASTM 2721-10: Standard test method of evaluating of the effectiveness of decontamination procedures for surfaces when challenged with droplets containing human pathogenic viruses. American Society for Testing and Materials (ASTM) International, 100 Barr Harbor Drive, West Conshohocken (PA) 19428-2959. 2010 *in press*.

6. PROGRAM SUPPORT

6.1. Background/Overview

The Airbase Sciences Branch employed approximately 50 personnel consisting of a mix of government civilians, military officers, academic researchers, and support contractors performing under several contracts. Each year, the branch typically had 10 – 25 active projects, a similar number of research contracts and/or academic grants, and an \$8–12M budget from multiple funding sources. Skilled program and financial management, project reporting, and engineering/administrative support was needed to assist RXQL in managing at the individual project level as well as looking at the “big picture–long term” needs of the branch. ARA has a long history of providing this program and financial management, project reporting, and engineering/administrative support to RXQL. ARA proposed providing this support in a task identified as Laboratory/Logistics Support and Program, Financial Management, Reporting and Administrative Support and was awarded a task identified as Technical Area 5. Simply stated, this team provided the behind the scenes skills and labor to relieve the government project officers and contractor research staff of the necessary, routine, but often tedious and burdensome duties required to run the laboratory. The program support team enabled the researchers to focus their time and talent on RXQL’s technical mission.

6.2. Laboratory/Logistics Support

This task provided AFRL/RXQL with critical, skilled support personnel; Laboratory Apparatus Fabricator/CAD Design Specialist Mr. Bob Nichols and Engineering Assistant/Admin Specialist Ms. Kathy Kirby. Both of these employees had a long history supporting AFRL. Mr. Nichols made extensive modifications to the design and structure of nearly every item of equipment in Dr. Owens’ microwave research laboratory, making it possible for his team to produce a prototype run of treated textiles. After proof of concept was established, Mr. Nichols disassembled the equipment and prepared it for shipment to Alexium International, the transition agent. He troubleshooted, repaired, modified, and fabricated numerous items of laboratory apparatus and equipment enabling Dr. Johnson’s Applied Biochemistry research and Mr. Henley’s development of novel geopolymers for airfield pavements. His skills include, but are not limited to, glass blower, machinist, electrician, draftsman, and CAD artist. He is AFRL/RXQ’s corporate memory on the building 1117 physical plant, and served as AFRL’s liaison with the 325th Civil Engineer Squadron. Without exception, Mr. Nichols’ unique and diverse skill set supported every one of the branch’s researchers and projects throughout the course of this contract.

Ms. Kirby, as engineering assistant/admin specialist, supported all of the branch’s project officers with day-to-day functions such as ordering and tracking supplies (555 purchases totaling \$487.4K), assisting with R&D case file management, status report preparation, preparation of briefings, technical report processing and other general administrative functions. She built and maintained a spreadsheet tool dubbed “the checkbook,” which she used to track supply purchases and contractor travel in real-time (Figure 99). Given the sometimes months-long lag time between ordering, receipt, invoicing, and payment, Kathy’s ledger style records provided a running balance of remaining funds available for purchases and travel. This function was particularly important given the structure of this contract, which unlike previous AFRL contracts, required managing the funding for each project separately. She assisted in putting together the

	Name of Vendor	Serial Port/Device	IP Address	Host Name	Status	Comments
		Serial	192.168.1.1	192.168.1.1	OK	
		Serial	192.168.1.2	192.168.1.2	OK	
		Serial	192.168.1.3	192.168.1.3	OK	
		Serial	192.168.1.4	192.168.1.4	OK	
		Serial	192.168.1.5	192.168.1.5	OK	
		Serial	192.168.1.6	192.168.1.6	OK	
		Serial	192.168.1.7	192.168.1.7	OK	
		Serial	192.168.1.8	192.168.1.8	OK	
		Serial	192.168.1.9	192.168.1.9	OK	
		Serial	192.168.1.10	192.168.1.10	OK	
		Serial	192.168.1.11	192.168.1.11	OK	
		Serial	192.168.1.12	192.168.1.12	OK	
		Serial	192.168.1.13	192.168.1.13	OK	
		Serial	192.168.1.14	192.168.1.14	OK	
		Serial	192.168.1.15	192.168.1.15	OK	
		Serial	192.168.1.16	192.168.1.16	OK	
		Serial	192.168.1.17	192.168.1.17	OK	
		Serial	192.168.1.18	192.168.1.18	OK	
		Serial	192.168.1.19	192.168.1.19	OK	
		Serial	192.168.1.20	192.168.1.20	OK	
		Serial	192.168.1.21	192.168.1.21	OK	
		Serial	192.168.1.22	192.168.1.22	OK	
		Serial	192.168.1.23	192.168.1.23	OK	
		Serial	192.168.1.24	192.168.1.24	OK	
		Serial	192.168.1.25	192.168.1.25	OK	
		Serial	192.168.1.26	192.168.1.26	OK	
		Serial	192.168.1.27	192.168.1.27	OK	
		Serial	192.168.1.28	192.168.1.28	OK	
		Serial	192.168.1.29	192.168.1.29	OK	
		Serial	192.168.1.30	192.168.1.30	OK	
		Serial	192.168.1.31	192.168.1.31	OK	
		Serial	192.168.1.32	192.168.1.32	OK	
		Serial	192.168.1.33	192.168.1.33	OK	
		Serial	192.168.1.34	192.168.1.34	OK	
		Serial	192.168.1.35	192.168.1.35	OK	
		Serial	192.168.1.36	192.168.1.36	OK	
		Serial	192.168.1.37	192.168.1.37	OK	
		Serial	192.168.1.38	192.168.1.38	OK	
		Serial	192.168.1.39	192.168.1.39	OK	
		Serial	192.168.1.40	192.168.1.40	OK	
		Serial	192.168.1.41	192.168.1.41	OK	
		Serial	192.168.1.42	192.168.1.42	OK	
		Serial	192.168.1.43	192.168.1.43	OK	
		Serial	192.168.1.44	192.168.1.44	OK	
		Serial	192.168.1.45	192.168.1.45	OK	
		Serial	192.168.1.46	192.168.1.46	OK	
		Serial	192.168.1.47	192.168.1.47	OK	
		Serial	192.168.1.48	192.168.1.48	OK	
		Serial	192.168.1.49	192.168.1.49	OK	
		Serial	192.168.1.50	192.168.1.50	OK	
		Serial	192.168.1.51	192.168.1.51	OK	
		Serial	192.168.1.52	192.168.1.52	OK	
		Serial	192.168.1.53	192.168.1.53	OK	
		Serial	192.168.1.54	192.168.1.54	OK	
		Serial	192.168.1.55	192.168.1.55	OK	
		Serial	192.168.1.56	192.168.1.56	OK	
		Serial	192.168.1.57	192.168.1.57	OK	
		Serial	192.168.1.58	192.168.1.58	OK	
		Serial	192.168.1.59	192.168.1.59	OK	
		Serial	192.168.1.60	192.168.1.60	OK	
		Serial	192.168.1.61	192.168.1.61	OK	
		Serial	192.168.1.62	192.168.1.62	OK	
		Serial	192.168.1.63	192.168.1.63	OK	
		Serial</				

Q226.7AD - INSP Obligation and Execution Plan													
End	Start	Funds Received	Planned Obligations	Actual Obligations	Roll-up of Planned Obligations	Cumulative Roll-up of Actual Obligations	Monthly Roll-up of Actual Obligations	Tyntal In-House Contractor Expenditures	Tyntal In-House Contractor Expenditures	Tyntal In-House Contractor Expenditures	Contractor 3 M. Costs	Gelling Agency Reimbursement	Total Outside Contractor
Dec-08	\$ 400,000				\$ -	\$ -	\$ -	\$ -	\$ -	\$ -	\$ -	\$ -	\$ -
Jan-09	\$ 400,000	\$ 43,873	\$ 43,873		\$ -	\$ -	\$ -	\$ -	\$ -	\$ -	\$ -	\$ -	\$ -
Feb-09	\$ 400,000	\$ 43,873	\$ 43,873		\$ -	\$ -	\$ -	\$ -	\$ -	\$ -	\$ -	\$ -	\$ -
Mar-09	\$ 400,000	\$ 43,873	\$ 43,873		\$ -	\$ -	\$ -	\$ -	\$ -	\$ -	\$ -	\$ -	\$ -
Apr-09	\$ 400,000	\$ 250,922	\$ 250,922	\$ 66,800	\$ 1,632	\$ 1,632	\$ 1,632	\$ 442	\$ 442	\$ -	\$ -	\$ 1,629	\$ -
May-09	\$ 400,000	\$ 250,922	\$ 250,922	\$ 33,200	\$ 2,176	\$ 2,176	\$ 2,176	\$ 544	\$ 544	\$ -	\$ -	\$ 2,05	\$ -
Jun-09	\$ 400,000	\$ 283,827	\$ 283,827	\$ 100,200	\$ 2,720	\$ 2,720	\$ 2,720	\$ 544	\$ 544	\$ -	\$ -	\$ 371	\$ -
Jul-09	\$ 400,000	\$ 283,827	\$ 283,827	\$ 100,200	\$ 3,841	\$ 3,841	\$ 3,841	\$ 1,121	\$ 1,121	\$ -	\$ -	\$ 325	\$ -
Aug-09	\$ 400,000	\$ 381,197	\$ 381,197	\$ 301,000	\$ 7,308	\$ 7,308	\$ 7,308	\$ 2,664	\$ 2,664	\$ -	\$ -	\$ 4,645	\$ 14,255
Sep-09	\$ 400,000	\$ 342,500	\$ 342,500	\$ 200,400	\$ 21,412	\$ 45,307	\$ 14,307	\$ 14,307	\$ 14,307	\$ -	\$ -	\$ 4,080	\$ 40,800
Oct-09	\$ 400,000	\$ 342,500	\$ 342,500	\$ 218,800	\$ 66,742	\$ 115,020	\$ 13,222	\$ 13,222	\$ 13,222	\$ 13,222	\$ 13,222	\$ 4,080	\$ 40,800
Nov-09	\$ 400,000	\$ 342,500	\$ 342,500	\$ 207,200	\$ 92,318	\$ 25,376	\$ 11,322	\$ 11,322	\$ 11,322	\$ 11,322	\$ 11,322	\$ 4,080	\$ 40,800
Dec-09	\$ 400,000	\$ 450,000	\$ 400,000	\$ 300,000	\$ 117,894	\$ 25,376	\$ 11,322	\$ 11,322	\$ 11,322	\$ 11,322	\$ 11,322	\$ 738	\$ 7,254
Jan-10	\$ 400,000	\$ 400,000	\$ 400,000	\$ 334,000	\$ 141,493	\$ 23,599	\$ 13,222	\$ 13,222	\$ 13,222	\$ 13,222	\$ 13,222	\$ 738	\$ 7,254
Feb-10	\$ 400,000	\$ 400,000	\$ 400,000	\$ 356,000	\$ 156,691	\$ 15,508	\$ 13,222	\$ 13,222	\$ 13,222	\$ 13,222	\$ 13,222	\$ 738	\$ 7,254
Mar-10	\$ 400,000	\$ 400,000	\$ 400,000	\$ 400,000	\$ 177,762	\$ 19,570	\$ 13,837	\$ 13,837	\$ 13,837	\$ 13,837	\$ 13,837	\$ 738	\$ 7,254
Apr-10	\$ 400,000	\$ 400,000	\$ 400,000	\$ 400,000	\$ 188,126	\$ 18,864	\$ 18,864	\$ 18,864	\$ 18,864	\$ 18,864	\$ 18,864	\$ 738	\$ 7,254
May-10	\$ 400,000	\$ 400,000	\$ 400,000	\$ 400,000	\$ 188,963	\$ 2,903	\$ 13,837	\$ 13,837	\$ 13,837	\$ 13,837	\$ 13,837	\$ 738	\$ 7,254
Jun-10	\$ 400,000	\$ 400,000	\$ 400,000	\$ 400,000	\$ 231,408	\$ 42,475	\$ 2,735	\$ 2,735	\$ 2,735	\$ 2,735	\$ 2,735	\$ 738	\$ 7,254
Jul-10	\$ 400,000	\$ 400,000	\$ 400,000	\$ 400,000	\$ 332,345	\$ 103,887	\$ 3,784	\$ 37,845	\$ 37,845	\$ 37,845	\$ 37,845	\$ 738	\$ 7,254
Aug-10	\$ 400,000	\$ 400,000	\$ 400,000	\$ 400,000	\$ 374,513	\$ 14,968	\$ 6,896	\$ 7,474	\$ 7,474	\$ 7,474	\$ 7,474	\$ 738	\$ 7,254
Sep-10	\$ 400,000	\$ 400,000	\$ 400,000	\$ 400,000	\$ 380,122	\$ 12,809	\$ 9,275	\$ 9,275	\$ 9,275	\$ 9,275	\$ 9,275	\$ 738	\$ 7,254
Oct-10	\$ 400,000	\$ 400,000	\$ 400,000	\$ 400,000	\$ 374,043	\$ 14,281	\$ 8,321	\$ 8,321	\$ 8,321	\$ 8,321	\$ 8,321	\$ 738	\$ 7

6.3. Program/Financial Management, Reporting and Administrative Support

140

Ms. Wright performed a variety of administrative support tasks. She supported all of the project officers with drafting, editing, and coordinating test plans, technical reports, visit requests, clearance documents, non-disclosure agreements, and other products. She received training to maintain LiveLink electronic inboxes and Material Safety Data Sheet (MSDS) electronic files. She completed records and case file management training in preparation for assuming the records custodian role. Her training enabled her to help Mr. Wayne Randall and the RXQL project officers collect the necessary forms and documents to update and maintain electronic project case files. She established and maintained the inventory for general lab supplies, and submitted government purchase card (GPC) purchase requests to replenish stock as needed. She helped maintain the contract modifications and deliverables in E-office, ARA's on-line project maintenance data system.

6.4. Notable Achievements

While many of the activities performed by the program support team are "routine," this section highlights contractor activities that were significant for their scope and complexity. The government project officers have specific responsibilities and requirements in areas in which the contractor support staff does not have signatory authority or custodial responsibility. However, while not responsible for these functions, the contractor staff did the "heavy lifting" involved in preparing these activities and programs for the responsible government project officers. While there are many instances of such activity, only two examples of the more notable contractor support achievements will be summarized; contractor support to the annual laboratory management review and maintenance of the RXQL equipment and TMDE accounts.

6.4.1. Laboratory Management Review (LMR)

The annual LMR is a labor-intensive annual tasking levied on the government project officers in accordance with AFRL Instruction 61-202. The LMR, consisting of initial, periodic, and final reviews is a detailed review of both the technical and financial progress/status of every open project. *Initial* reviews are required to start a work unit, establish its JON(s), and establish a work unit baseline; *Periodic* LMRs are conducted annually throughout the life of the work unit to measure progress and allow management the opportunity to make decisions regarding technical progress, adjust scope in response to decreased (or increased) funding, potential duplication of effort, cost overruns, and schedule slippages; *Final* LMRs are conducted when the technical effort is completed, the final report submitted, and the work unit is ready for close out. Briefing slides are prepared and presented, but the primary purpose of the LMR is to obtain signatures (which signify approval to start, continue, or stop a project) on an AFRL Form 2913 (Figure 102), which is used to summarize the project funding, objectives, and progress and rank the project as Excellent, Satisfactory, Marginal, or Unsatisfactory. The signed 2913 is a required item in the project case file and is filed after completion of the LMR.

The program support team relieved the government project officers of this crushing administrative burden by preparing the financial and technical briefing slides, and AFRL Forms 2913 and 21 (Figure 101) for each of the branch's 35 work units plus slides for an additional nine work breakdown structures (WBS) which are subsets of several of the larger, more complex work units. These documents were then forwarded to the project officers for review and addition or correction of technical details. The program support team expended 197 man-hours preparing and

finalizing the slides and documents for the project officers and was on hand to answer detailed questions throughout the LMR presentation during the week of 21 June 2010. This relieved six primary government project officers of nearly 25 man-days of administrative burden—freeing up over four days per project officer—time made available to their research or other duties.



Figure 101. LMR Products

6.4.2. Equipment Account Management

The RXQL branch possesses a large inventory of laboratory design, fabrication, test, and analytical equipment ranging from hand-held devices to mass spectrometers to a nuclear magnetic resonance spectrometer. This equipment was maintained under two equipment accounts: Account 881EC had 109 items with a value of \$2,598,206.10. Account 158CB had 50 items valued at \$1,088,756.16. Custodial responsibility for the equipment rests with a government person in a position of authority—typically the branch chief. Ms. Kirby, though not in a position of custodial responsibility, stepped forward and relieved the branch chief of the huge administrative burden of maintaining these accounts. She prepared all of the supply documents to add or remove items from the account, obtained the account labels, and conducted the annual inventory and labeled each item. The inventory is a labor-intensive project which normally takes 2+ weeks to accomplish. The branch chief then typically spot checked the account before signing the annual inventory. During the course of this contract, Ms. Kirby conducted an out-of-cycle inventory to facilitate Major Saucer's permanent change-of-station (PCS) move. The branch chief's trust in Ms. Kirby's diligence relieved him of a large administrative burden and garnered positive comments on the condition of the accounts from both the 325th Supply Squadron's equipment management section, and a Staff Assistance Visit (SAV) team from Wright Patterson AFB.

7. Report Summary

ARA provided world-class technical, program, and laboratory support to AFRL/RXQL for the period of performance (1 January 2010–30 December, 2010) for contract FA4819-10-C-0012. ARA supported three major technical programs for RXQL: chemical dynamics, reactive responsive materials, and toxic and pathogenic biological aerosols. To provide exemplary support for AFRL/RXQL, ARA went above and beyond contract deliverables by participating in proposal writing and oral presentations, representing AFRL research and gaining the respect of colleagues in similar research arenas. The dedication ARA's employees put into their individual projects laid the groundwork for future efforts supporting RXQL's technical mission. The exceptional program/financial management, project reporting, and engineering/administrative support provided to RXQL by ARA employees, coupled with ARA's talented laboratory staff that concentrated on the technical aspect of the individual projects, provided outstanding teamwork while further championing AFRL/RXQL's research ambitions.

8. REFERENCES

- (anon.) (2007). Determination of Inorganic Anions by Ion Chromatography, EPA Method 9056A.
- 3M. (2009). Material Safety Data Sheet. 504 Respirator Cleaning Wipe. <http://www.3M.com>. Accessed 25 May 2010.
- Alkan M, M Oktay, et al. (2005). "Solubility of chlorine in aqueous hydrochloric acid solutions," *Journal of Hazardous Materials*, 119(1–3):13–18.
- Aps JKM and LC Martens. (2005). "Review: The physiology of saliva and transfer of drugs into saliva," *Forensic Science International*, 150(2):119–131.
- Ash C, JAE Farrow, et al. (1991). "Comparative Analysis of *Bacillus anthracis*, *Bacillus cereus*, and Related Species on the Basis of Reverse Transcriptase Sequencing of 16S rRNA," *International Journal of Systematic Bacteriology*, 41(3):343–346.
- ASTM E2720-10: *Standard test method for effectiveness of decontamination of air-permeable materials challenged with biological aerosols containing human pathogenic viruses*, American Society for Testing and Materials (ASTM) International, 100 Barr Harbor Drive, West Conshohocken, PA 19428-2959. In press.
- Atkinson R (1997). "Gas-phase tropospheric chemistry of volatile organic compounds .1. Alkanes and alkenes," *Journal of Physical and Chemical Reference Data* 26(2):215–290.
- Bailar JC, DS Burke, LM Brosseau, HJ Cohen, EJ Gallagher, KF Gensheimer, et al. (2006). *Reusability of facemasks during an influenza pandemic*. Washington D.C.: Institute of Medicine, National Academies Press.
- Balazy A, M Toivola, A Adhikari, SK Sivasubramani, T Reponen, SA Grinshpun. (2006). "Do N95 respirators provide 95% protection level against airborne viruses, and how adequate are surgical masks?" *AJIC state of the science report*, 34(2):51–57.
- Balazy A, M Toivola, T Reponen, A Podorski, A Zimmer, S Grinshpun. (2006). "Manikin-Based Performance Evaluation of N95 Filtering-Facepiece Respirators Challenged with Nanoparticles," *Annals of Occupational Hygiene*, 50(3):259–269.
- Baron PA, CF Estill, et al. (2008). "Development of an Aerosol System for Uniformly Depositing *Bacillus Anthracis* Spore Particles on Surfaces," *Aerosol Science and Technology*, 42(3):159–172.
- Bergman MS, DJ Viscusi, BK Heimbuch, JD Wander, AR Sambol, RE Shaffer (2010). "Evaluation of Multiple (3-Cycle) Decontamination Processing for Filtering Facepiece Respirators," *Journal of Engineered Fibers and Fabrics*, 5(4):33–41.
- Blachere FM, WG Lindsley, TA Pearce, SE Anderson, M Fisher, R Khakoo, BJ Meade, O Lander, S Davis, RE Thewlis, I Celik, BT Chen, DH Beezhold (2009). "Measurement of Airborne Influenza Virus in a Hospital Emergency Department," *Clinical Infectious Diseases*; 48:438-440.
- Bridges CB, MJ Kuehnert, CB Hall (2003). "Transmission of influenza: Implications for control in health care settings," *Clinical Infectious Diseases*, 37(8):1094–1101.
- Brown GS, RG Betty, et al. (2007 (a)). "Evaluation of a Wipe Surface Sample Method for Collection of *Bacillus* Spores from Nonporous Surfaces," *Applied and Environmental Microbiology*, 73(3):706–710.
- Brown GS, RG Betty, et al. (2007 (b)). "Evaluation of vacuum filter sock surface sample collection method for *Bacillus* spores from porous and non-porous surfaces," *Journal of Environmental Monitoring*, 9:666–671.

- Buhr TL, DC McPherson, et al. (2008). "Analysis of broth-cultured *Bacillus atrophaeus* and *Bacillus cereus* spores," *Journal of Applied Microbiology* 105:1604–1613.
- Buttner MP, P Cruz–Perez, et al. (2001). "Enhanced Detection of Surface-Associated Bacteria in Indoor Environments by Quantitative PCR," *Applied and Environmental Microbiology*, 67(6):2564–2570
- Carrera M, RO Zandomeni, et al. (2007). "Difference between the spore sizes of *Bacillus anthracis* and other *Bacillus* species," *Journal of Applied Microbiology*, 102:303–312.
- Centers for Disease Control and Prevention (CDC) (2007). *Guideline for isolation precautions: preventing transmission of infectious agents in healthcare settings*. Ed.: JD Siegel and the Healthcare Infection Control Practices Advisory Committee.
http://www.cdc.gov/ncidod/dhqp/gl_isolation.html. Accessed 20 October 2008.
- Chow, TV, T Chan, HC Reader (2000). *Understanding Microwave Heating Cavities*. Artech House.
- Conder JR, CL Young (1979). *Physicochemical Measurement by Gas Chromatography*. New York, John Wiley & Sons.
- Current Technologies Inc. (2010). Materials Safety Data Sheet. Hype-wipe (Disinfecting Towel with Bleach). www.daigger.com/assets/pdf/msds/EF8482A.pdf. Accessed 25 May 2010.
- Dawood FS, S Jain, L Finelli, MW Shaw, S Lindstrom, RJ Garten, et al. (2009). "Emergence of a novel swine-origin influenza A (H1N1) virus in humans," *New England Journal of Medicine*, 360:2605–2615.
- Finlayson–Pitts, BJ and JNJ Pitts (2000). *Chemistry of the Upper and Lower Atmosphere*. San Diego, CA, Academic Press.
- Finney DJ (1964). *Statistical methods in biological assays*. 2nd ed. Hafner Publishing, New York.
- Foarde K, BK Heimbuch, A Maxwell, D VanOsdell (2009). *Method for evaluating air purification technologies for collective protection using viable microbial aerosols. Test Operating Procedure (TOP) under the Army Test and Evaluation Command (ATEC)*. Edgewood Chemical and Biological Center, Edgewood, Md. *in press*.
- Galeano B, E Korff, et al. (2003). "Inactivation of Vegetative Cells, but Not Spores, of *Bacillus anthracis*, *B. cereus*, and *B. subtilis* on Stainless Steel Surfaces Coated with an Antimicrobial Silver- and Zinc-Containing Zeolite Formulation," *Applied and Environmental Microbiology*, 69(7):4329–4331.
- Gardner PD, AW Richardson, JP Eshbaugh, KC Hofacre (2006). *Respirator Filter Efficiency Testing Against Particulate and Biological Aerosols Under Moderate to High Flow Rates*, ECBC-CR-085. Edgewood Chemical and Biological Center, U.S. Army Research Development and Engineering Command, Aberdeen Proving Ground, MD 21010-5423.
- Jullien H, H Valot (1985). "Polyurethane curing by a pulsed microwave field," *Polymer*. 26:506–510.
- Hair M (1977). "Heat of adsorption from spectroscopic measurements," *Journal of Colloid and Interface Science*. 59(3):532–540.
- Hall CB (2007). "The Spread of Influenza and Other Respiratory Viruses: Complexities and Conjectures," *Healthcare Epidemiology*. 45:353–359.
- Hanna S, J Chang (2008). "Gaps in Toxic Industrial Chemical (TIC) Model Systems," *12th Conference on Harmonisation within Atmospheric Dispersion Modelling for Regulatory Purposes*, Cavtat, Croatia.

- Hanna SR (2007). "Characteristics of liquified pressurized chlorine released from storage tanks." *GMU Conference*, Fairfax, VA.
- Hanna S, S Dharmavaram, et al. (2008). "Comparison of six widely-used dense gas dispersion models for three recent chlorine railcar accidents," *Process Safety Progress* 27(3):248–259.
- Heimbuch BK, JD Wander (2006). *Bioaerosol challenges to antimicrobial surface treatments: enhanced efficacy against MS2 coli phage of air filter media coated with polystyrene-4-methyltrimethylammonium triiodide*. ADA444909, Defense Technical Information Center (DTIC). AFRL-ML-TY-TP-2006-4527, Air Force Research Laboratory, Tyndall Air Force Base, FL.
- Heimbuch BK, JD Wander. *Cleaning of Filtering Facepiece Respirators with Commercially Available Wipe Products*. Defense Technical Information Center (DTIC). To be submitted, Air Force Research Laboratory, Tyndall Air Force Base, FL.
- Heimbuch BK, C-Y Wu, J Hodge, JD Wander (2007). *Viral Penetration of HEPA Filters*. Defense Technical Information Center (DTIC). Air Force Research Laboratories, Report number: AFRL-ML-TY-TP-2007-4512.
- Heimbuch BK, WH Wallace, K Kinney, AE Lumley, C-Y Wu, M-H Woo, Wander JD (2010a). "A Pandemic Influenza Preparedness Study: Use of Energetic Methods to Decontaminate Filtering Facepiece Respirators Contaminated with H1N1 Aerosols and Droplets," *American Journal of Infection Control*, *In press*.
- Helgason E, NJ Tourasse, et al. (2004). "Multilocus Sequence Typing Scheme for Bacteria of the *Bacillus cereus* Group," *Applied and Environmental Microbiology*, 70(1):191–201.
- Hill AC (1971). "Vegetation: A sink for atmospheric pollutants," *Journal of the Air Pollution Control Association*, 21(6):341–346.
- Hinds WC (1999). *Aerosol Technology Properties, Behavior, and Measurement of Airborne particles*, 2nd ed. John Wiley and Sons Inc., New York, New York.
- Hu, JH, Q Shi, et al. (1995). "Reactive Uptake of Cl₂(g) and Br₂(g) by Aqueous Surfaces as a Function of Br⁻ and I⁻ Ion Concentration: The Effect of Chemical Reaction at the Interface," *Journal of Physical Chemistry*, 99(21):8768–8776.
- Huang J, RB Kaner (2004). "A general chemical route to polyaniline nanofibers," *Journal of the American Chemical Society*, 126:851–855.
- Katz S, DG Gray (1981). "The adsorption of hydrocarbons on cellophane: I. Zero coverage limit," *Journal of Colloid and Interface Science*, 82(2):318–325.
- Kilbourne ED (2006). "Influenza pandemics of the 20th century," *Emerging Infectious Diseases*, 12:9–14.
- Knight V (1980). "Viruses as Agents of Airborne Contagion," *Annals of the New York Academy of Sciences*, 353:147–156.
- Karabanova LV, et al. (2009). "Semi-interpenetrating polymer networks based on polyurethane and poly(2-hydroxyethyl methacrylate): Dielectric study of relaxation behavior," *Journal of non-Crystalline Solids*, 355:1453–1460.
- Lai E-M, ND Phadke, et al. (2003). "Proteomic Analysis of the Spore Coats of *Bacillus subtilis* and *Bacillus anthracis*," *Journal of Bacteriology*, 185(4):1443–1454.
- Lee J, et al. (2002). "Adsorption Equilibria of CO₂ on Zeolite 13X and Zeolite X/Activated Carbon Composite," *Journal of Chemical and Engineering Data*, 47(5):1237–1242.
- Lide DR (1995). *CRC Handbook of Chemistry and Physics*. Boca Raton, FL, CRC Press, Inc.
- Ludwig HR, JJ Whalen, et al. (1994). *Documentation for Immediately Dangerous to Life or Health Concentrations (IDLH)*. HEWOSH, National Technical Information Service.

- Omastova M, M Trchova, J Kovářová, J Stejskal (2003). "Synthesis and structural study of polypyrroles prepared in the presence of surfactants," *Synthetic Metals* 138:447–455.
- Mochida M, J Hirokawa, et al. (1998). "Heterogeneous reactions of Cl₂ with sea salts at ambient temperature. Implications for halogen exchange in the atmosphere," *Geophysical Research Letters*, 25(21):3927–3930.
- Morens DJ, JK Taubenberger, H Harvey, M Memoli (2010). "The 1918 influenza pandemic: lessons for 2009 and the future," *Critical Care Medicine*, 38 (4 Suppl): E10–20.
- Naffakh N, S van der Werf (2009). "An outbreak of swine-origin influenza A (H1N1) Virus with Evidence for Human-to-Human Transmission," *Microbial Infection* 11(8–9):725–728.
- Nicholson, WL, P Setlow (1990). "Sporulation, Germination and Outgrowth," in *Molecular biological methods for Bacillus*, CR Harwood and SM Cutting, eds., pp. 391–450.
- Occupational Safety and Health Administration (OSHA) (2007). *Pandemic influenza preparedness and response guidance for healthcare workers and healthcare employers*. Pub. No. OSHA 3328-05.
- Oxford JS (2000). "Influenza A pandemics of the 20th century with special reference to 1918: virology, pathology and epidemiology," *Review of Medical Virology*, 10(2):119–133.
- Papieneni RS, FS Rosenthal (1997). The Size Distribution of Droplets in the Exhaled Breath of Healthy Human Subjects, *Journal of Aerosol Medicine*, 10:105–116.
- Pohanish RP (2008). *Sittig's Handbook of Toxic and Hazardous Chemicals and Carcinogens* (5th Edition), William Andrew Publishing.
- Procter & Gamble Company®. 2006. Materials Safety Data Sheet. Pampers Unscented Natural Aloe Wipes, www.whatsinproducts.com/msds/8519_16030117%20MSDS%20PG%20Pampers_wipes- CM MSDS.pdf?... Accessed 25 May 2010.
- Prugh A, JJ Calomiris (2006). *Inactivation of Bacillus anthracis Spores Delivered as Liquid Suspension or Aerosol to Self-Decontaminating Fabric*. Defense Technical Information Center (DTIC) AFRL-HE-WP-TP-2006-0060.
- Thomas RM, et al. (2009). "Optimization of preparation conditions on the dielectric properties of polyaniline," *Journal of Applied Polymer Science*, 112:2676–2682.
- Rasko DA, MR Altherr, et al. (2005). "Genomics of the *Bacillus cereus* group of organisms," *FEMS Microbiology Reviews* 29:303–329.
- Renard JJ, SE Calidonna, et al. (2004). "Fate of ammonia in the atmosphere—a review for applicability to hazardous releases," *Journal of Hazardous Materials*, 108(1–2):29–60.
- Riley RL (1961). "Droplets, Droplet Nuclei, and Dust," in F O'Grady (ed.), *Airborne infection: transmission and control*. Macmillan, New York, New York.
- Sagripanti J-L, A Bonifacino (1996). "Comparative Sporicidal Effects of Liquid Chemical Agents," *Applied and Environmental Microbiology*, 62(2):545–551.
- Salter W, K Kinney, W Wallace, A Lumley, BK Heimbuch, and JD Wander (2010). "Analysis of Residual Chemical on Filtering Facepiece Respirators after Decontamination," *Journal of Occupational and Environmental Hygiene*, 7:437–445.
- Schlyer, DF, AP Wolf, PP Gaspar (1978). "Rate constants for the reactions of atomic chlorine with group 4 and group 5 hydrides," *Journal of Physical Chemistry*. 82(25):2633–2637.
- Smith A, H Shirazi (2000). "Quartz Microbalance Microcalorimetry: A new method for studying polymer–solvent thermodynamics," *Journal of Thermal Analysis and Calorimetry*, 59(1):171–186.
- Standard Test Method for Determining of Dissolved Alkali and Alkaline Earth Cations and Ammonium in Water and Wastewater by Ion Chromatography, ASTM D6919-09.

- Stanley FA, GE Smith (1956). "Effect of Soil Moisture and Depth of Application on Retention of Anhydrous Ammonia," *Soil Science Society of America Journal*, 20(4):557–561.
- Steichen C, P Chen, et al. (2003). "Identification of the Immunodominant Protein and Other Proteins of the *Bacillus anthracis* Exosporium," *Journal of Bacteriology*, 185(6):1903–1910.
- Stewart GSAB, K Johnstone, E Hagelberg, DJ Ellar (1981). "Commitment of bacterial spores to germinate, A measure of the trigger reaction," *Biochemical Journal*, 198:101–106.
- Sykes I, SF Parker, et al. (1998). *PC-SCIPUFF Version 1.2PD Technical Documentation*. Princeton, NJ, Titan Corporation.
- Tang JW, Y Li, I Eames, PKS Chan, GL Ridgway (2006). "Factors involved in the aerosol transmission of infection and control of ventilation in healthcare premises," *Journal of Hospital Infection*, 64:110–114.
- Tellier R (2006). "Review of aerosol transmission of influenza A virus," *Emerging Infectious Diseases*, 12:1657–1662.
- Thielmann F (2004). "Introduction into the characterisation of porous materials by inverse gas chromatography," *Journal of Chromatography A*, 1037(1–2):115–123.
- Viscusi DJ, MS Bergman, BC Eimer, RE Shaffer (2009). Evaluation of five decontamination methods for filtering facepiece respirators," *Annals of Occupational Hygiene*, 53(8):815–827.
- Viscusi DJ, WP King, RE Shaffer (2007). "Effect of decontamination on the filtration efficiency of two filtering facepiece respirator models," *Journal of the International Society for Respiratory Protection*, 24:93–107.
- White GC (1972). *Handbook of Chlorination*. New York, Van Nostrand Reinhold.
- WHO manual on animal influenza diagnosis and surveillance (2002). World Health Organization http://www.who.int/vaccine_research/diseases/influenza/WHO_manual_on_animal-diagnosis_and_surveillance_2002_5.pdf/.
- World Health Organization (2010). Influenza A (H1N1) update 112. Available from: http://www.who.int/csr/don/2010_08_06/en/index.html. Accessed 2 November 2010.
- Xiang Q, Y Lee, et al. (2003). "Heterogeneous aspects of acid hydrolysis of α -cellulose," *Applied Biochemistry and Biotechnology*, 107(1):505–514.
- Yan Z, S Chen, et al. (2008). "Biosynthesis of bacterial cellulose/multi-walled carbon nanotubes in agitated culture," *Carbohydrate Polymers*, 74(3):659–665.
- Yang S, GWM Lee, C-M Chen, C-C Wu, K-P Yu (2007). "The Size and concentration of Droplets Generated by coughing in Human Subjects," *Journal of Aerosol Medicine* 20:484–494.
- Zhao B, Z Zhang, X Li (2005). "Numerical study of the transport of droplets or particles generated by respiratory system indoors," *Building Environment*, 40:1032–1039.
- Zhu S, S Kato, J-H Yang (2006). "Study on transport characteristics of saliva droplets produced by coughing in a calm indoor environment. *Building Environment*, 41:1691–1702.

LIST OF SYMBOLS, ABBREVIATIONS, AND ACRONYMS

8HQ	8-hydroxyquinoline
8HQ2CA	8-hydroxyquinoline-2-carboxaldehyde
AATCC	American Association of Textile Chemists and Colorists
ABU	Airman Battle Uniform
ACU	Army Combat Uniform
AFM	atomic force microscopy
AFRL/RXQL	Air Force Research Laboratory, Airbase Sciences Branch
APC	advanced performance coating
APTS	3-aminopropyltrimethoxysilane
ARA	Applied Research Associates, Inc.
ARL	Army Research Laboratory
ATCC	American Type Culture Collection
BARDA	Biomedical Advanced Research and Development Authority
BDS	Biological Dispersing System
BDU	Battle Dress Uniform
CA	contact angle
CARC	chemical agent resistant coatings
CB	chemical/biological
CBD	chemical/biological defense
CBWA	chemical/biological warfare agent
CDC	Centers for Disease Control
CEES	2-chloroethyl ethyl sulfide
CEPS	2-chloroethyl phenyl sulfide
CF	correlation factor
CI	confidence intervals
CMD	count medium diameter
CV	coefficient of variation
CWA	chemical warfare agent
DEEC	directed energy to act on enhanced coatings
DIFP	diisopropyl fluorophosphate
DMMP	dimethyl methylphosphonate
DMSO	dimethyl sulfoxide
DoD	Department of Defense
DQO	Data Quality Objective
DS	demeton-S
DTRA	Defense Threat Reduction Agency
EC	ecological coating
ECBC	Edgewood Chemical and Biological Center
FDA	Food and Drug Administration
FFR	filtering facepiece respirator
FID	flame ionization detection
FR	flame-retardant
FS	fluorosilane
FTE	full-time equivalent

GAE	Gerling Applied Engineering, Inc.
GC/FID	gas chromatograph/flame ionization detection
GC/MS	gas chromatograph/mass spectrometer
GPTMS	(3-glycidoxypropyl)trimethoxysilane
HD	mustard gas; sulfur mustard; bis(2-chloroethyl) sulfide
HDTA	hexadecyltrimethylammonium chloride
HPAC	Hazard Prediction and Assessment Capability
IGC	inverse gas chromatography
INDP or IP	Individual Protection
IPA	isopropyl alcohol
IR	infrared
LMR	Laboratory Management Review
LSAT	Laboratory-Scale Aerosol Tunnel
MC	methylene chloride
MDCK	Madin–Darby canine kidney cells
MEK/MAK	methyl ethyl ketone/methyl amyl ketone
MeS	methyl salicylate
MOPP	Mission Oriented Protective Posture
MP	microwave-promoted
MS	mass spectrometry
MWCNT	multi-walled carbon nanotube
NCSU	North Carolina State University
NIOSH	National Institute for Occupational Safety and Health
NKA	Nomex/Kevlar antistatic
NP	nanoparticle
NRL	Naval Research Laboratory
NWU	Navy working uniform
NyCo	50/50 nylon–cotton fabric
OSHA	Occupational Safety and Health Administration
PAni	polyaniline
PEG	poly(ethylene glycol)
PEDOT	poly(3,4-ethylenedioxythiophene)
PET	poly(ethylene terephthalate)
POM	polyoxometalate
PCI	power coupler interface
PCS	permanent change of station
PPM	parts per million
PPy	polypyrrole
PSD	particle size distribution
PSL	polystyrene latex
RH	relative humidity
RNA	ribonucleic acid
SAV	staff assistance visit
SCCM	standard cubic centimeters per minute
SERDP	Strategic Environmental Research and Development Program
SME	subject matter expert

SMPS	Scanning Mobility Particle Sizer
SPME	solid-phase microextraction
TBP	tributyl phosphate
TEOS	tetraethyl orthosilicate
TIC	toxic industrial chemical
TiO ₂	titanium dioxide
TMDE	test, measurement, and diagnostic equipment
TSA	trypticase soy agar
TWTA	traveling wave tube amplifier
UVGI	ultraviolet germicidal irradiation
VNA	vector network analyzer
VRE	vancomycin-resistant <i>Enterococcus</i>
VX	<i>O</i> -ethyl <i>S</i> -[2-(diisopropylamino)ethyl] methylphosphonothioate
WBS	work breakdown structure
WEG	Weapons Evaluation Group
WHO	World Health Organization
WUN	work unit number
XRD	X-ray diffraction